The Influence of Subpolar Gyre Dynamics on Centennial to Millennial Scale Holocene Climate Variability in the High-Latitude North Atlantic

by

Ursula Quillmann

B.A., University of Colorado, 2003

M.Sc., University of Colorado, 2006

A thesis submitted to the

Faculty of the Graduate School of the

University of Colorado in partial fulfillment

of the requirement for the degree of

Doctor of Philosophy

Department of Geological Sciences

2014

This thesis entitled:

The Influence of Subpolar Gyre Dynamics on Centennial to Millennial Scale Holocene Climate Variability in the High-Latitude North Atlantic

written by Ursula Quillmann

has been approved for the Department of Geological Sciences

_____

Dr. Thomas M. Marchitto

_____

Dr. Anne E. Jennings

Date: _____

The final copy of this thesis has been examined by the signatories, and we find that both the content and the form meet acceptable presentation standards of scholarly work in the above mentioned discipline.

In Memory of Danielle
11.07.1988-11.22.2012

I love you forever

Quillmann, Ursula (Ph.D., Geological Sciences)

The Influence of Subpolar Gyre Dynamics on Centennial to Millennial Scale Holocene Climate Variability in the High-Latitude North Atlantic

Thesis directed by Dr. Anne E. Jennings and Dr. Thomas M. Marchitto

Holocene paleoclimatic reconstructions provide longer time series than instrumental records, allowing us to examine climate variability under more extreme boundary conditions. I reconstructed temperature and $\delta^{18}O_{sw}$ using paired measurements of Mg/Ca ratios and $\delta^{18}O_{calcite}$ of planktonic and benthic foraminifera at sites in the subpolar North Atlantic that are sensitive to Subpolar Gyre (SPG) dynamics today. Glacial freshwater from the final stages of the decay of the Laurentide ice sheet influenced SPG dynamics and was routed via the SPG throughout the subpolar basin. Near Iceland we recorded the 8.2 ka cooling event and the freshwater spike from the catastrophic outburst flood of proglacial lakes Agassiz and Ojibway using paired Mg/Ca and $\delta^{18}O_{calcite}$ of the benthic foraminifer *Cibicides lobatulus*. This evidence for a brief cooling and freshening is supported by a coeval increase in arctic benthic foraminifera and a decrease in biogenic carbonate. Through the Holocene, the SPG warmed and the $\delta^{18}O_{sw}$ became heavier (saltier), suggesting a progression towards a contracted gyre. This is in sharp contrast to the established view of the rest of the North Atlantic, which was warmest during the early-mid Holocene. We attribute the SPG warming trend to a weakening of the NAO-like circulation in response to increasing winter insolation through the Holocene. Overlying this general trend were abrupt shifts that cannot be

explained by changes in insolation. Between 10,000 and 8,000 cal yr BP, my study sites recorded cold temperature and light $\delta^{18}O_{sw}$ values, suggesting an extended SPG. Between 8,000 and 6,000 cal yr BP, the SPG changed shape but was still extended. This change coincided with the onset of Labrador Sea water formation, which today is associated with intensified SPG circulation. Between ~6,000 and 3,800 cal yr BP, I see a strong influence of Atlantic water on the SW Iceland shelf, consistent with a contracted SPG. After 4,000 cal yr BP, freshwater from the Arctic Ocean appeared on the SW Iceland shelf. The water column as recorded in benthic and planktonic foraminiferal assemblages went from well mixed in the early Holocene to stratified in the late Holocene. Overall my records show that the SPG played an important and, in some ways, surprising role in the Holocene climate evolution of the North Atlantic.

Acknowledgments

First and foremost, I would like to thank my advisors, Tom Marchitto and Anne Jennings, for their continuous support and guidance throughout the course of my PhD research. Tom had his door always open and was ready to discuss my data. He was very supportive when the tephra contamination in my samples frustrated me beyond measure. Anne had an open door policy as well. She loves forams at least as much as I do and we spent countless hours discussing forams and their meanings. Tom and Anne are both excellent writers and I learned a lot from both of them.

I would also like to thank John Andrews. He was always involved in my research and always available to help me. Thanks for helping with the statistical analysis of my data. I am especially grateful to him for making a research cruise possible for me. The month I spent on the CCGS Hudson is unforgettable. Not only did I start to appreciate all the work and passion that goes into retrieving sediment cores from the ocean floor, but I am also left with many memories of incredible icebergs and landscapes very few people are lucky enough to see. Seeing a polar bear on an ice floe was spectacular. The experience of being at sea made me a strong advocate for protecting these precious arctic environments. I have shared my passion for arctic environments with my 2,067 students I have been teaching since the fall semester of 2011 at the Colorado State University in Fort Collins. Thanks, John.

After my daughter Danielle's death, Anne, Tom, and John set up biweekly meeting with me. These meetings helped me to get back into my research. They left me space to start healing, but nudged me gently into continuing my research and were

confident that I could finish my PhD. I could have not done it without their support and encouragement. I cannot thank them enough.

I would also like to thank my other committee members, James Syvitski and David Andersen. I was James' teaching assistant for several semesters. He was an excellent mentor on how to be a good teacher. My students at CSU are benefiting immensely from what I learned from him. Dave Andersen joined my PhD committee toward the end. He brought lots of enthusiasm and energy into the final stages of my thesis. Dave always helped me focus on the wider impact of my research. I will remember that there are ALWAYS "three things….."

I would also like to thank Hans Petter Sejrup and Walt Dean for being on my comprehensive exam committee.

Special thanks goes to Patrick Cappa for helping me in the ICP-MS laboratory and to Wendy Freeman for helping me in the core processing room. Thanks to all the undergraduate researchers involved in my project: Michelle Carlson, Stephen James, Daniel Giffitts, Vivian Underhill, and Christina Sheldon.

I had great technical support from Chad Stoffel and Tara Hess. Thanks for keeping me sane when my laptop acted up. Thanks to Shelly Sommer for finding the most obscure documents for me that I needed for my research. There are so many wonderful people at INSTAAR that I would like to thank, but the list would be too long. I especially want to acknowledge Jen Hall Bowman, Larry Bowlds, Shelly Sommer, and Anne Kelley for being good friends.

I liked that I had so many of the student and postdoc visitors from Europe share my office space. I was sad when they left. We had lots of conversations and became

friends, and thanks to Facebook we are still in touch. Thanks Saedis, Heidi, Steffen, Birgitte, Kirstin, Anders, Christine, and Kari.

I would also like to thank the Graduate School and Dean Stevenson for making special arrangements after Danielle's death and being supportive. Numerous travel grants came from the Graduate School and from the Department of Geological Sciences that supported attendance at international and national conferences. I would like to thank the Department of Geological Sciences, especially Lang Farmer, for supporting me through teaching assistantships, travel grants, a research grant award ($1,000), and undergraduate research help.

The last years were crazy but thanks to good friends I made it through. The list is long. Thanks for all the confidence you have had in me and for cheering me on. To Lance, Chuck, Jen, Anders, and Mary: Thanks for the formatting, proofreading, and printing help.

Finally, I would like to say thanks to my daughter Lena and my husband Volker. We are getting through hard times together. Lena and I encouraged each other to finish up our PhD work. Our research topics could have not been more different: German women writers in the 1800s and Holocene forams.

The funding for my research came from a research grant from the National Science Foundation (Grant No. 0823525), with the PIs: Anne, Tom, and John. Thank you. NSF also supported the help from undergraduate researchers.

Table of Contents

List of Tables

List of Figures

Chapter 1
Introduction

1.1 Modern Atmospheric and Oceanic Circulation in the Subpolar North Atlantic

The Fifth Assessment Report of the Intergovernmental Panel on Climate Change (IPCC) states, “Each of the [past] three decades has been warmer than all the previous decades in the instrumental record, and the decade of the 2000s has been the warmest”, with linearly increasing temperatures since the 1970s (Hartmann et al., 2013). Climate models predict that large temperature changes will occur in the high latitude North Atlantic region; in the twenty-first century, the ocean near the vicinity of the Greenland ice sheet is expected to warm by ~1.7 to 2.0°C, which is about twice the global mean (Yin et al., 2011). Large changes in the wind-driven ocean circulation have been observed in the high latitude North Atlantic Ocean over recent decades (Hakkinen and Rhines, 2009). At the same time more freshwater is being added to this region via melting of the Greenland ice sheet (Rignot and Kanagaratnam, 2006) and sea ice and fresh water export from the Arctic Ocean (Serreze et al., 2007), while more subtropical water is advecting northward (Hakkinen and Rhines, 2009). The high-latitude North Atlantic shows a trend toward longer seasonal stratification in surface water, which adversely affects biological productivity (Taboada and Anadon, 2012).

However, any multidecadal trend of increasing temperature in the subpolar North Atlantic is obscured because the climate is highly dynamic in this region and varies on the decadal and multidecadal timescales (Rhein et al., 2013). Longer time series are

needed to better predict future changes and to separate decadal internal variability from externally-forced trends (Zhang and Church, 2012). To provide context for present-day climate change, we can turn to paleoclimatic reconstructions to obtain longer time series during a period when climate variability was not influenced by human activity.

The dominant and recurrent pattern of the atmospheric circulation in the high latitude North Atlantic today is the North Atlantic Oscillation (NAO) (Hurrell et al., 2003). The NAO is the dominant mode of interannual wind variability in the North Atlantic. Its index describes the normalized sea surface atmospheric pressure between the Azores High and the Icelandic Low and switches between high and low phases (Hurrell, 1995). When the pressure gradient is high, and the NAO index is positive, the Icelandic low is deeper than normal with stronger than normal westerly surface winds (Westerlies) (Figure 1.1). The storm track crosses the North Atlantic at a more northerly position. When the NAO index is negative, the pressure gradient between the Azores high and the Icelandic low is weaker, the Westerlies are weaker and the storm track is shifted southward. The NAO pattern is most pronounced during the winter months. The NAO has been the principal force affecting the sea surface temperatures (SSTs) over the instrumental period (Sarafanov, 2009).

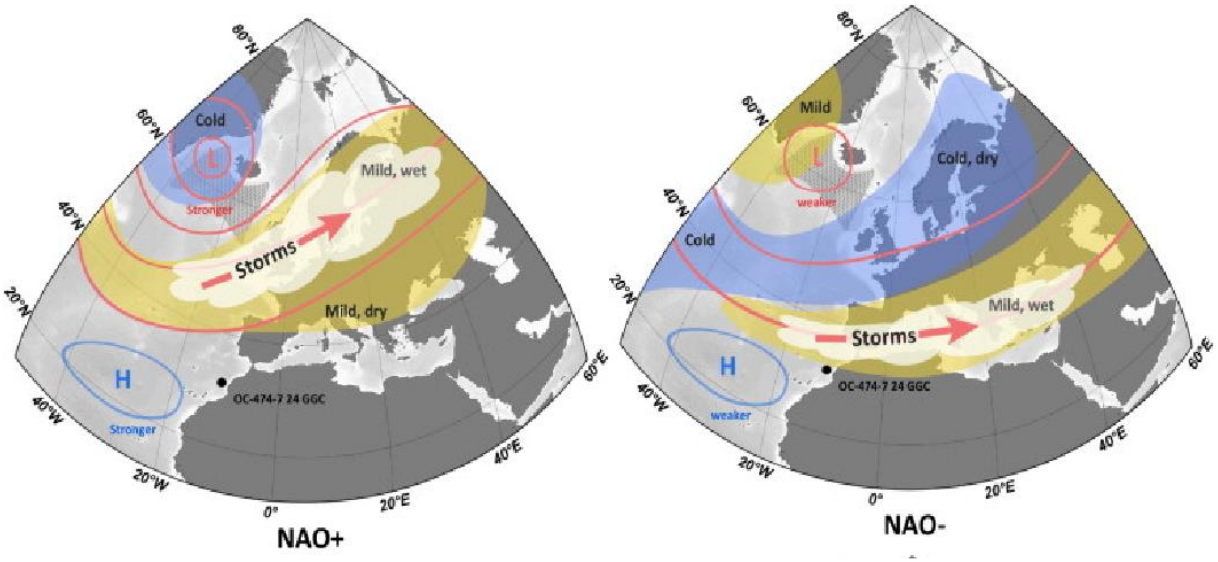

Figure 1.1 North Atlantic Oscillation (NAO). During a postive phase of the NAO (left image), the pressure gradient between the Azores high (H) and the Icelandic low (L) is larger than normal and the storm track of the Westerlies is at a more northern position. During a negative phase of the NAO (right image), the pressure gradient between the Azores high (H) and the Icelandic low (L) is weaker than normal and the storm track of the Westerlies is at a more southern position. (Figure after Morley et al. (2013); their Figure 5))

The ocean circulation in the subpolar North Atlantic is impacted by the convergence of warm, subtropical water with polar water, which is regulated by the subpolar gyre (SPG) on annual and interannual timescales (Yashayaev and Clarke, 2008). Over the past 50 years, the SPG oscillated between two extreme states: an extended mode (high-gyre index) typically associated with positive NAO, and a contracted mode (low-gyre index) typically associated with negative NAO (Sarafanov, 2009) (Figure 1.2). During the extended state, the subpolar front that delineates the boundary of the SPG extends into the Iceland Basin and the water in the eastern Atlantic becomes fresher and colder. During the contracted state, the SPG retreats into the western part of the subpolar Atlantic, and water masses from the subtropical gyre

(STG) advance into the Iceland Basin and the water in the south of Iceland becomes more saline and warmer.

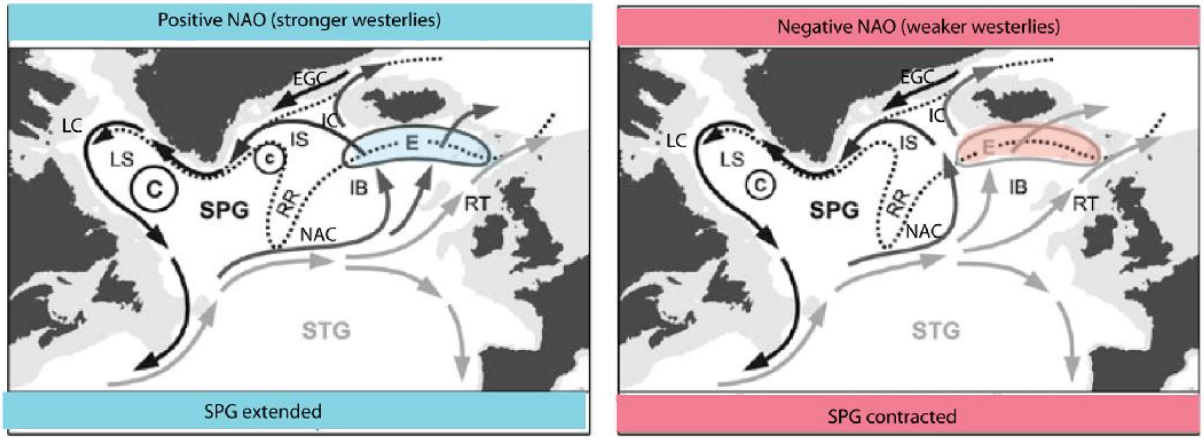

Figure 1.2 Subpolar Gyre (SPG) modes. When the NAO is positive, the SPG is extended (left image) and relatively more polar water is entrained (E) into the surface currents. When the NAO is negative, the SPG is contracted (right image) and relatively more subtropical water from the subtropical gyre (STG) is entrained (E) into the surface currents. The surface currents that demarcate the SPG are the North Atlantic Current (NAC), the Irminger Current (IC), the East Greenland Current (EGC), and the Labrador Current (LC). The ocean basins affected by the SPG are the Irminger Basin (IB), the Iceland Basin (IS), and the Labrador Sea (LS). Bathymetric features shown are the Reykjanes Ridge (RR) and the Rockall Trough (RT). The strength of LS convection depends on the SPG mode, shown as C in the images above. Larger circle indicates stronger convection. (Figure after Sarafonov et al (2008); their Figure 3)

Four main surface currents delineate the SPG and span three ocean basins (Figure 1.2). The surface currents are the North Atlantic Current (NAC), the Irminger Current (IC), the East Greenland Current (EGC), The West Greenland Current (WGC), and the Labrador Current (LC). The NAC is an extension of the Gulf Stream and carries warm saline waters to the high latitudes. The IC branches off the NAC and turns counterclockwise along the SW Iceland shelf before crossing the Irminger Sea. Here the denser waters of the IC subduct under the fresher, colder waters of the EGC. As the

EGC rounds the southern tip of Greenland, part of the current continues north as the West Greenland Current and part of the current turns counterclockwise south and meets the LC. The LC is a cold fresh current coming from Baffin Bay and joining the SPG. The SPG can occupy three ocean basins: the Irminger Basin at the eastern boundary, the Irminger Sea at the northern boundary, and the Labrador Sea at the western boundary.

The impact of the NAO on the SPG can be overridden by surface freshening over the Labrador Sea, as was the case during the Great Salinity Anomaly (GSA) of 1968-1971 (Dickson et al., 1988). Hydrographic conditions in the Labrador Sea strongly affect SPG dynamics. When the convection over the Labrador Sea is shut down, as for example during the GSA, the SPG weakens and contracts. The shutdown occurred when winters were mild associated with a negative NAO-index. It took a severe winter that caused a large surface heat flux to restart the convection in 1972 and the intensity of SPG strengthened and the SPG zonally expanded. Figure 1.3 illustrates the key components affecting the SPG and in turn how the SPG is affecting the global climate.

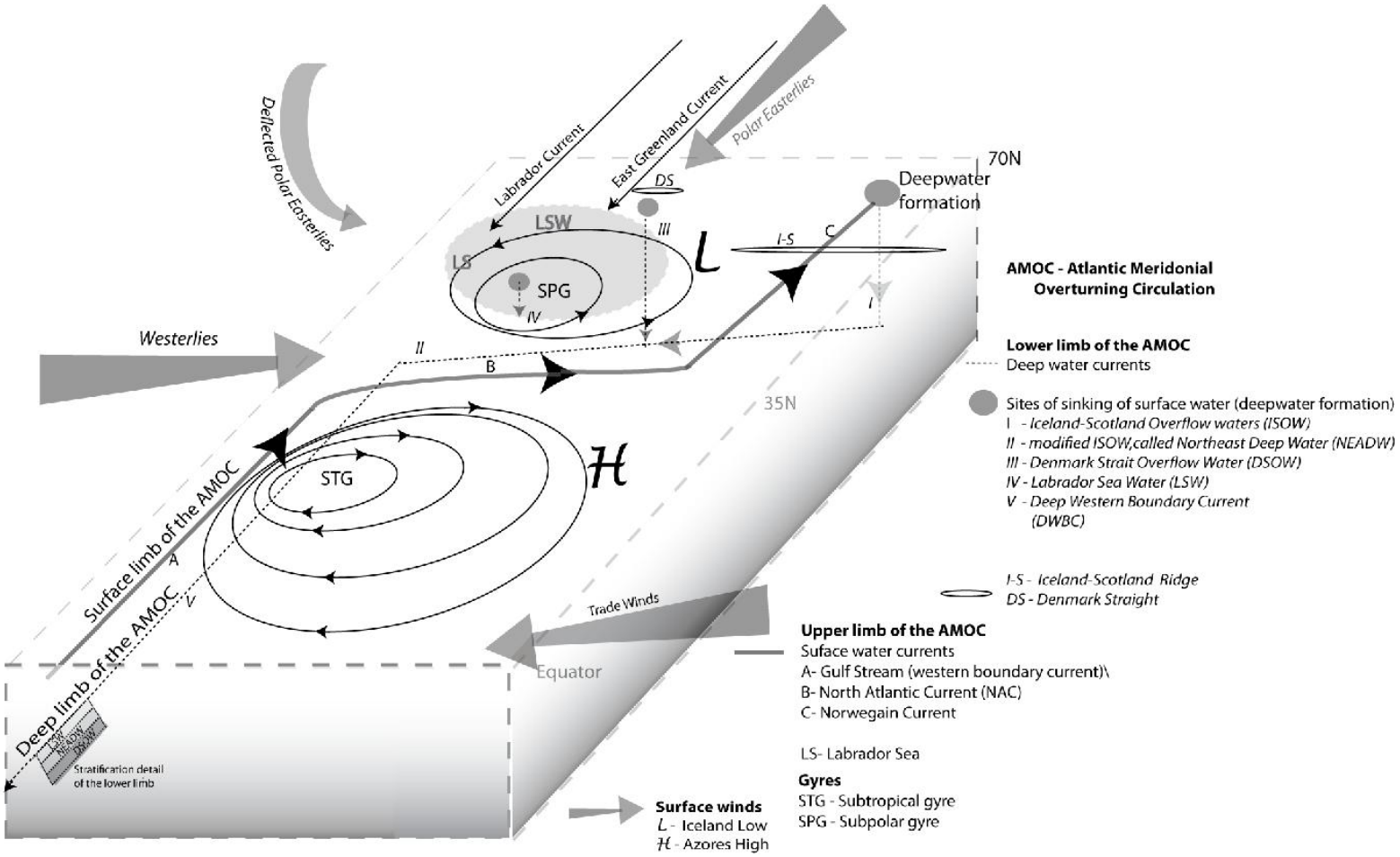

Figure 1.3 Schematic diagram of SPG dynamics. This diagram is illustrating Atlantic Meridonal Overturning Circulation (AMOC) and how the SPG influences the upper and lower limbs of the AMOC.

1.2 Research Questions

Changes in the Milankovitch forcing, the Earth's precession, obliquity, and eccentricity, have been commonly considered to be the ultimate forcing on Earth's climate changes in the Quaternary (Marchal et al., 2002). However, the emerging picture of Holocene climate in the North Atlantic region illustrates that the climate response to insolation forcing was not linear (Kaufman et al., 2004). High-latitude North Atlantic climate showed a delayed warming to maximum summer insolation at 65N, which peaked between 11,000 and 10,000 cal yr BP (Marchal et al., 2002). The onset of the Holocene Thermal Maximum (HTM) in the subpolar high latitude North Atlantic region was delayed because of the impact the final phases of the Laurentide Ice Sheet (LIS) deglaciation had on atmospheric and oceanic circulation (Carlson et al., 2008; Jennings et al., 2011; Kaufman et al., 2004). After the HTM, the climate deteriorated and became cooler during the Neoglaciation.

The role of SPG dynamics on Holocene climate has just started to be recognized (Thornalley et al., 2009), and the established view of the Holocene climate evolution might not hold true in the SPG region. A climate model by Rimbu et al (2003) predicted the SPG region to warm in response to an orbitally-forced weakening of the NAO through the Holocene (Figure 1.4).

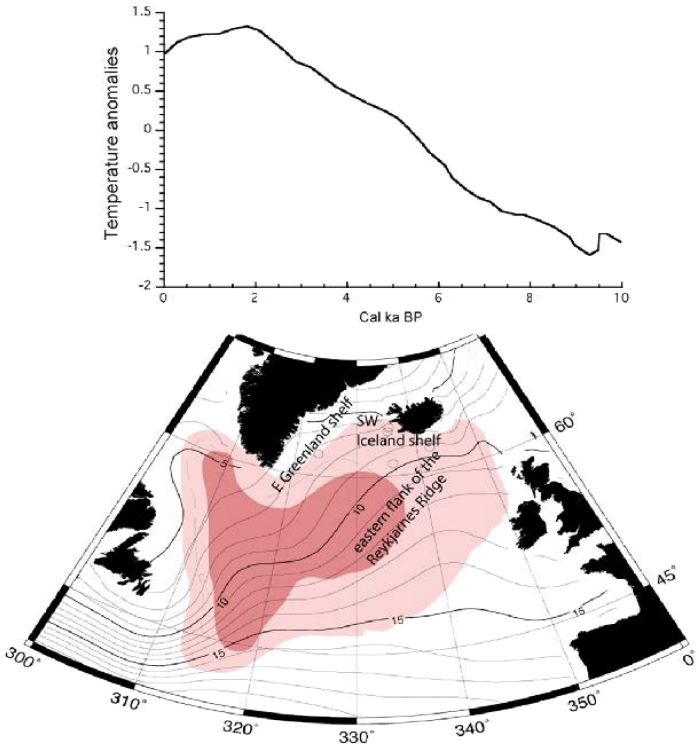

Figure 1.4 Warming in the SPG region through the Holocene. Climate modeling simulates warming in the SPG through the Holocene (Rimbu et al., 2003). The upper panel shows the temperature anomaly. The lower panel shows the areas modeled to warm (light pink). The red area highlights the regions that warmed the most.

The goal of this thesis research is to add to the understanding of the influence of SPG dynamics on the centennial to millenial Holocene climate variability in the high-latitude North Atlantic. We are concentrating on marine sediment cores from the Iceland shelf, the eastern flank of the Reykjanes Ridge, and the E. Greenland shelf (Table 1.1; Figure 1.5). These cores are within the SPG region and/or are affected by SPG dynamics. Given the sensitivity of the modern SPG to wind and freshwater forcing, and its relevance for heat transport and climate in the North Atlantic region, we are interested in its evolution through the Holocene as boundary conditions changed.

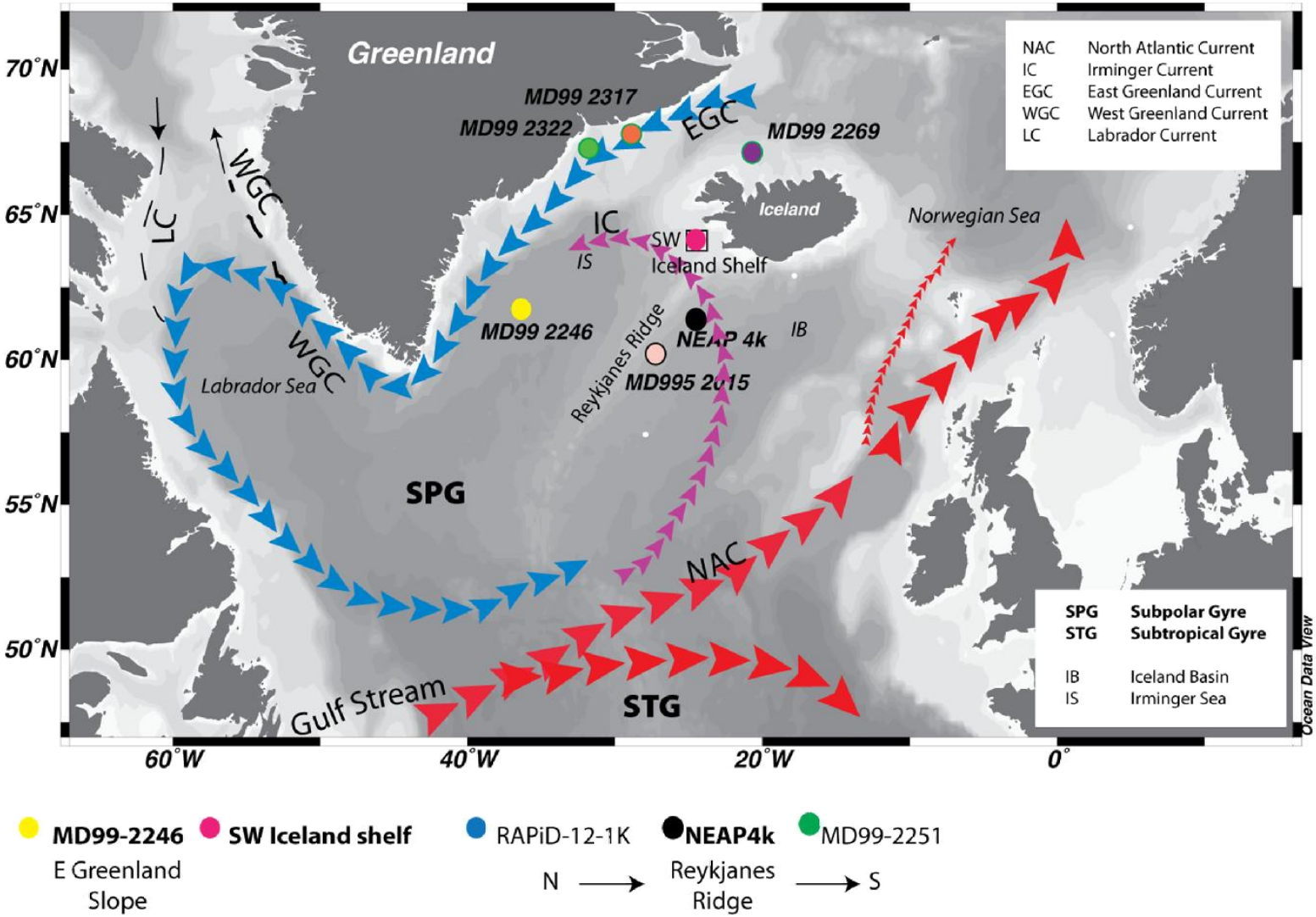

Figure 1.5 Location map of study sites and surface currents. Details for study sites are given in Table 1.1. Cold surface currents are indicated in blue arrows, warmer currents in red.

Table 1.1 Core locations. Cores with new Mg/Ca records in red font; previously published records that are being used in this thesis for comparison in blue font.

Core	Latitude (N)	Longitude (W)	Water depth [m]	Thesis Chapter	Published
MD99-2266	66.230	23.265	106	2	Quillmann et al., 2010
MD99-2256	64.303	24.207	246	3 & 4	Olafsdottir et al, 2010; Jennings et al., in press
MD99-2259	63.963	24.483	385	3 & 4	
NEAP4k	61.498	24.1726	1627	3	Hall et al., 2004
MD99-2246	61.912	36.358	2750	3	Hall, unpublished
RAPiD-12-1K	62.905	17.82	1938	3	Thornally et al., 2009
MD99-2251	57.433	27.912	2629	3	Farmer et al, 2008
MD99-2269	66.625	20.853	365	3	Giraudeau et al., 2004; Kristjansdottir et al., 2007; Stoner et al. 2007
MD99-2322	67.136	30.828	714	4	Jennings et al., 2011
MD99-2264	66.679	24.196	235	4	Olafsdottir et al, 2010

We take advantage of the entire spectrum of Holocene environmental and climate variability, aiming to answer the following questions:

- Do temperature reconstructions at our sites show a warming in the SPG gyre through the Holocene as predicted by Rimbu et al.'s (2003) simulation of NAO weakening?
- How did the meltwater from the last phases of the LIS glaciation affect SPG gyre dynamics?
- Did the SPG circulation provide a pathway for the meltwater from the catastrophic drainage of the proglacial lakes Agassiz and Ojibway 8,200 cal yr BP to reach the Icelandic shelf?

- By reconstructing SPG dynamics through the Holocene can we assess how NAO-like conditions evolved though the Holocene?
- How was the HTM expressed in the SPG?
- How does the freshwater from melting of the Greenland ice sheet and sea ice export from the Arctic Ocean during the Neoglaciation affect SPG dynamics?

The SW Iceland shelf is ideal to study Holocene climate variability because it lies at the intersection of two contrasting ocean currents: the IC, which transports relatively warm and saline waters northward; and the EGC, which transports relatively cold and fresh waters southward. The IC has received increased attention over the past years because of its role in the instability of the Greenland ice sheet (Holland et al., 2008; Straneo et al., 2011; Straneo et al., 2013; Sutherland and Straneo, 2012). The continued melting of the Greenland ice sheet can be anticipated to be a key factor in climate change over the next few centuries (Blaschek and Renssen, 2013a). The majority of the glaciers that have been accelerating in the past decades on the southeastern and western margin of the Greenland ice sheet are affected by the Atlantic waters in the IC (Holland et al., 2008; Straneo et al., 2013; Zweng and Munchow, 2006). The IC also plays a crucial role in Labrador Sea Water formation (Vage et al., 2011; Yashayaev et al., 2007). By monitoring the IC on the SW Iceland shelf, we also gain insights into climate forcings on the subpolar North Atlantic.

We are testing the following hypotheses on the SW Iceland shelf:

1. By the time the Atlantic water masses carried in the IC reach the SW Iceland shelf, these water masses have been transformed by their interaction with the atmosphere during their transit in the SPG.
2. In the early Holocene, the Atlantic water inflow was dampened by freshwater from the final decay of the LIS.
3. In the mid Holocene the IC influence was strongest, with minor freshwater forcing.
4. In the late Holocene the IC was influenced by northern source waters, e.g. freshwater and sea ice export from the Arctic Ocean and melt water of the Greenland ice sheet.

1.3 Foraminiferal Stable Isotopes and Mg/Ca Ratios

Geochemical analysis of foraminiferal carbonate yields information about the properties of the ambient seawater in which the foraminifer calcified. The temperature relationship of the oxygen isotopic composition ($\delta^{18}O_{calcite}$) in foraminiferal calcite has been utilized since the 1950s (e.g. (Emilliani, 1955)) for temperature reconstructions. Later the $\delta^{18}O_{calcite}$ was recognized to be a function of both temperature and the oxygen isotopic composition of the ambient seawater ($\delta^{18}O_{sw}$) (Shackelton, 1967).

During the calcification process, minor and trace elements can substitute for the calcium ion. The amount of magnesium incorporated into the calcite lattice is temperature dependent (Nurnberg et al., 1996; Rosenthal et al., 1997). By combining these two proxies the temperature and $\delta^{18}O_{sw}$ contributions to $\delta^{18}O_{calcite}$ can be

separated. In today's ocean a linear relationship between $\delta^{18}O_{sw}$ and salinity exists (LeGrande and Schmidt, 2008; Lynch-Stieglitz et al., 2002). However, in the early Holocene the $\delta^{18}O_{sw}$:salinity relationship was likely different, and is poorly constrained, because of the residual ice sheet, which had very light values. Hence $\delta^{18}O_{sw}$ provides some measure of relative salinity changes, but not quantitative paleosalinity values.

1.4 Thesis Organization

This dissertation is organized into the three "data" chapters. Each of these chapters was written for publication as a research article.

The motivation for the first article (Chapter 2), "Cooling and freshening at 8.2 ka on the NW Iceland Shelf recorded in paired $\delta^{18}O$ and Mg/Ca measurements of the benthic foraminifer *Cibicides lobatulus,*" was to show that the melt water from the catastrophic draining of proglacial lakes Agassiz and Ojibway at 8,200 cal yr BP was transported in the SPG and IC as far as the NW Iceland Shelf. This study was the first high-resolution record reconstructing near-surface (100m water depth) temperatures and $\delta^{18}O_{sw}$ by paired measurements of Mg/Ca and $\delta^{18}O$ of the benthic foraminifer *Cibicides lobatulus*. In addition to the geochemical proxies, we added biological and sedimentological proxies: benthic foraminiferal assemblages and calcium carbonate percent. We developed the first Mg/Ca temperature calibration for *Cibicides lobatulus*, a cosmopolitan species often used for paleoceanographic reconstructions. This article was published in *Quaternary Research* (78; 528-539) in 2012. This publication was co-authored by Thomas M. Marchitto, Anne E. Jennings, John T. Andrews, and Birgitte F. Friedstad.

The second article (Chapter 3), “The roles of winter insolation and ocean dynamics on the Holocene history of the North Atlantic Subpolar Gyre,” puts present day SPG dynamics into the context of longer time scales to understand the full spectrum of SPG variability. We reconstructed Holocene temperature and $\delta^{18}O_{sw}$ from paired measurement of $\delta^{18}O_{calcite}$ and Mg/Ca ratios of the planktonic foraminifer *Globigerina bulloides* from marine sediment cores at sites that are sensitive to SPG dynamics today. We show that the SPG contracted and warmed through the Holocene, consistent with an orbitally-forced weakening of the NAO. Our study is the first to explore the role of winter precession on SPG dynamics and adds to the understanding of oceanic and atmospheric circulation in this region.

The third article (Chapter 4), “The Implications of Freshwater Forcings on the Hydrography of the Irminger Current Through the Holocene,” takes an in-depth look at changes in the hydrography of the IC as it crosses the SW Iceland shelf. We show various freshwater forcing on the IC, e.g. freshwater from the decaying Laurentide ice sheet in the early Holocene and freshwater from sea ice export from the Arctic Ocean and possibly from melting of the Greenland ice sheet in the late Holocene. By monitoring the IC on the SW Iceland shelf, we also gain insights into climate forcings on the subpolar North Atlantic. Our proxies are suitable to detect changes in the strength of Atlantic waters, potential influences of polar waters, stratification of the water column, and variations in productivity, which are all key constituents for detecting environmental changes.

Chapter 5 summarizes the key findings and discusses avenues for further research. (*Work Cited* for Chapter 1 “Introduction” after Chapter 5). Data tables are presented in the appendices.

Chapter 2
Cooling and freshening at 8.2 ka on the NW Iceland Shelf recorded in paired $\delta^{18}O$ and Mg/Ca measurements of the benthic foraminifer *Cibicides lobatulus*

2.1 Abstract

A shallow marine sediment core from NW Iceland provides evidence for a brief cooling and freshening at ~8200 cal yr BP, consistent with the hypothesis that the catastrophic outburst flood of the proglacial lakes Oijbway and Agassiz caused the 8.2 ka event. This is the first high-resolution record reconstructing near-surface temperatures and $\delta^{18}O_{sw}$ by paired measurements of Mg/Ca and $\delta^{18}O_{calcite}$ of a benthic foraminifer. We developed a new Mg/Ca temperature calibration for *Cibicides lobatulus*. Our down-core Mg/Ca derived temperature reconstruction dates the 8.2 ka cooling event between ~8300 cal yr BP and ~8100 cal yr BP, which is similar to the timing and 160 year duration recorded in the Greenland ice cores. The near-surface temperature drop of ~3 to 5°C during the 8.2 ka event was accompanied by lighter $\delta^{18}O_{sw}$ values. Synchronously to the changes in the geochemicial proxies, the percentages of two Arctic benthic foraminifers increased and the percent calcium carbonate decreased. Our record, combined with several others from the region, suggests that the freshwater outburst spread far from the source, into the high latitude North Atlantic. This freshwater input could have directly caused substantial high latitude cooling, with reduced North Atlantic Deep Water formation amplifying the climatic impact.

2.2 Introduction

The high-latitude North Atlantic contains large, poorly understood feedbacks between ice, freshwater, deep water formation, and temperature that are believed to have played large roles in past abrupt climate changes, and that may be relevant for future climate change. Of particular interest is the so-called 8.2 ka event, because this short-lived climate excursion holds important information about potential causes of abrupt climate changes during the otherwise climatically stable Holocene epoch.

The 8.2 ka event was first documented in Greenland ice core records as a sudden drop in surface air temperatures, with a magnitude ranging from 3 to 8°C, depending on various reconstructions (Alley et al., 1997; Johnsen et al., 1992; Johnsen et al., 2001; Kobashi et al., 2007). Based on analysis of these ice cores the cooling anomaly during the 8.2 ka event was brief, lasting only 160.5±5.5 years with a defined cooling peak lasting only 69±2 years (Thomas et al., 2007). The cooling has been attributed to the catastrophic drainage of the proglacial lakes Agassiz and Ojibway into the North Atlantic during the final deglaciation of the Laurentide Ice Sheet (Barber et al., 1999) (Fig. 2.1). The timing of the outburst flood has been constrained to the interval between 8,040 to 8,490 cal yr BP (Lewis et al., in press), which is later but overlapping with the previously proposed timing between 8,160 and 8,740 cal yr BP (Barber et al., 1999). It has been hypothesized that the estimated 200,000 km^3 freshwater input from these proglacial lakes spread across the subpolar North Atlantic and suppressed the formation of North Atlantic Deep Water (NADW), thus reducing meridional heat transport and altering atmospheric circulation (Alley et al., 1997; Barber et al., 1999; Clark et al., 2001; Praetorius et al., 2008). The 8.2 ka cooling could have taken place, however, without changing the rate of northward transport of Atlantic Water, as model

results by Clarke et al. (2009) demonstrated. They showed that the freshwater could have promoted sea ice growth and altered atmospheric circulation, causing substantial cooling over Greenland. In contrast, Condron and Winsor (2011) illustrated in a model study that the proposed outburst flood may have been carried southward in a narrow coastal current to the subtropics, without ever having affected the surface or deep water regime in the subpolar North Atlantic. The oceanographic changes associated with the 8.2 ka event thus remain controversial.

Paleoceanographic data can help to constrain the potential cause and magnitude of the 8.2 ka event. The 8.2 ka event, in turn, provides a test bed for modeling changes in the density structure of the North Atlantic under near-interglacial boundary conditions. The freshwater input during the 8.2 event lends itself as an analogue for present-day freshwater input into the North Atlantic, both from the melting of the Greenland Ice Sheet and the export of sea ice from the Arctic Ocean.

Climate anomalies around 8,200 years ago have been tracked around the North Atlantic region (see review by Rohling and Palike, 2005). However, a number of these records show a multi-centennial-scale climate perturbation that started ~8,600 cal yr and ended ~8000 cal yr BP, onto which the 8.2 ka event cooling may have been superimposed. Rohling and Palike (2005) suggest that the multi-centennial-scale perturbation may be part of a repeating pattern throughout the Holocene, and hence not strictly related to the briefer 8.2 ka event. Here we follow Thomas et al. (2007) in applying the term “8.2 ka event” only to the brief interval between 8247 and 8086 cal yr BP as recorded in the Greenland ice core records. There is limited knowledge of how this brief 8.2 ka event is expressed in the ocean because open ocean sedimentation

rates are generally low and thus provide poor temporal resolution compared to the highly resolved Greenland ice core records. Even though the cause of the 8.2 ka event is believed to be known, unequivocal proof is lacking that the sudden and catastrophic freshwater input from the proglacial lakes Agassiz and Ojibway caused the 8.2 ka cooling via an impact on the North Atlantic. In contrast it has been suggested that the lake drainage caused cooling over Greenland because of an atmospheric response to the altered relative distributions of exposed land, water, and glacial ice in North America (Dean et al., 2002).

In this study, we focused our attention on a narrow time interval encompassing the 8.2 ka event as recorded in the Greenland ice core record. We aimed to determine the evolution and magnitude of ocean temperature change in the North Atlantic, and whether the cooling was accompanied by a freshening. This was accomplished by investigating sediment core MD99-2266 from the mouth of Ìsafjarðardjúp, a large and shallow fjord in NW Iceland (Figure 2.1 and Figure 2.2). Previous results on the Holocene paleoceanographic evolution at this site, including a comparison to inner fjord conditions, were published in Quillmann et al. (2010). In this new study, we performed a higher-resolution analysis on the interval from 8400 to 7600 cal yr BP that encompassed the 8.2 ka event.

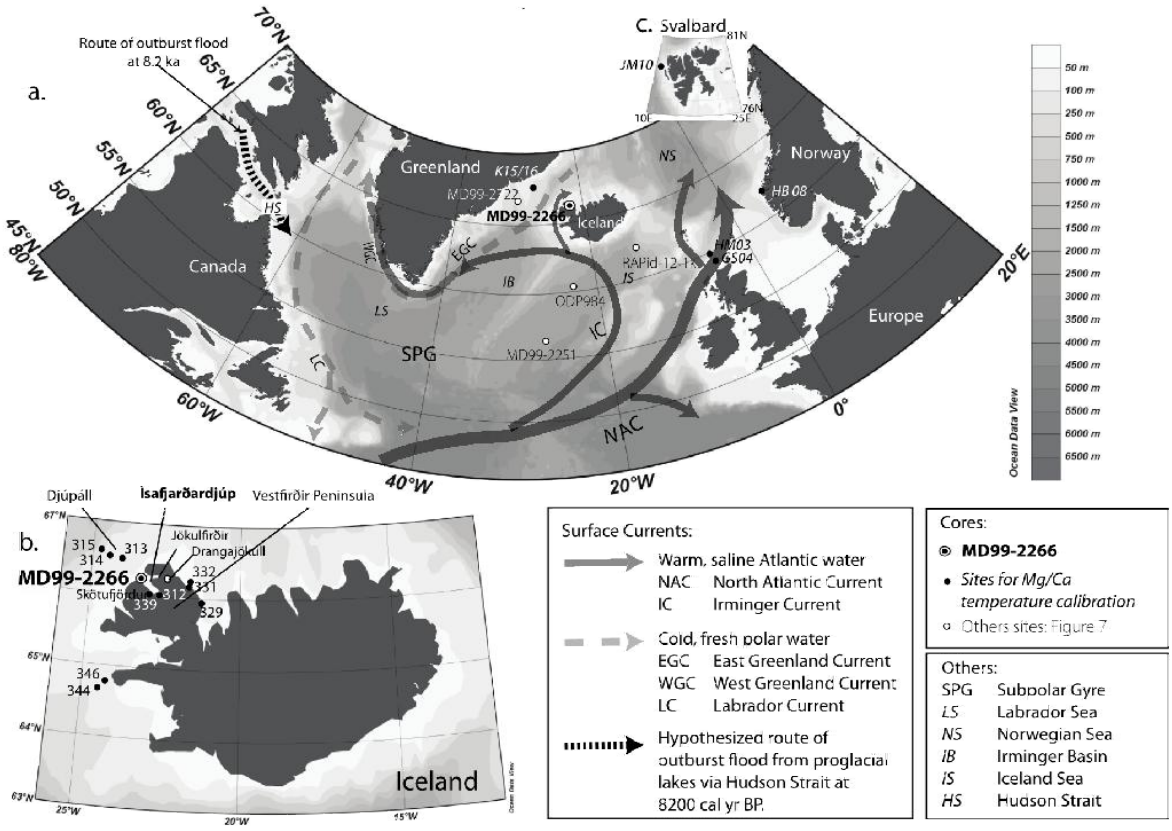

Figure 2.1 Location map. Panel A shows the high latitude North Atlantic with schematic surface current regime and the hypothesized route of the outburst flood of the proglacial lakes Agassiz and Ojibway at ~8200 cal yr BP. Also shown are Greenland, Faroe Island, and Norwegian sites for Mg/Ca temperature calibrations (black dots) and other regional temperature reconstructions shown in Fig. 7 (white dots). Panel B zooms in on Iceland and provides details about site MD99-2266 (this study). Also shown are the B997 sites for Mg/Ca temperature calibration (black dots). Inset C shows the Mg/Ca temperature calibration sites from Svalbard.

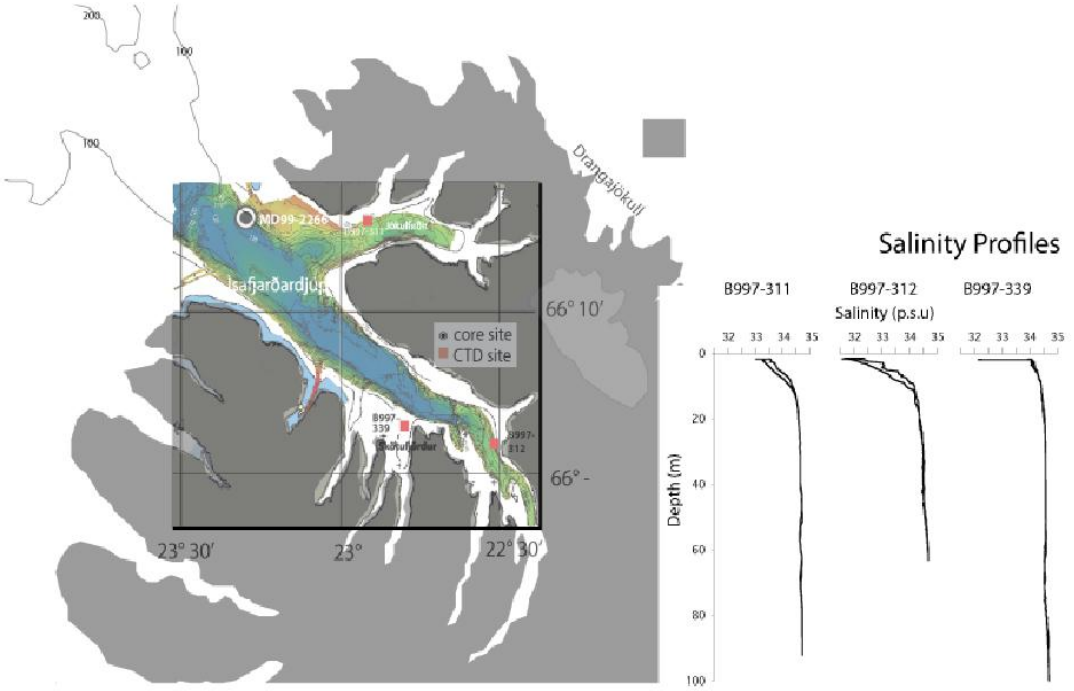

Figure 2.2 Bathymetry and CTD salinities. The multibeam bathymetry of the Ìsafjarðardjúp fjord system (courtesy of the Marine Research Institute of Iceland) is superimposed onto a map of the region. The depths (m) of various contours at the fjord entrance (pers. comm. Gudrun Helgadottir) are indicated in white font. The salinity profiles from three inner-fjord CTD casts taken during the summer of 1997 are shown, with locations plotted in red (Helgadottir, 1997).

2.3 Regional Setting and Oceanography

Our study site, MD99-2266 (66 °13.77'N, 23°15.93'W, 106 m water depth), is located at the mouth of Ìsafjarðardjúp (Figure 2.1 and Figure 2.2). Ìsafjarðardjúp continues beyond the fjord mouth onto the continental shelf as a shelf trough. The Ìsajarðardjúp trough is slightly shallower seaward of the fjord mouth, but the depth of this threshold is between 110 and 120 m in the center, as shown in the map generated by the Marine Research Institute of Iceland based on multibeam bathymetry data (Figure 2.2). The bathymetric map therefore shows no topographic barrier that would restrict open ocean inflow to our 106 m study site at the present.

Three CTD (conductivity, temperature, depth) casts were taken in the Ìsafjarðardjúp fjord system in the summer of 1997 during a research cruise conducted by the Icelandic Marine Research Institute on board the *Bjarni Saemundsson* (Helgadottir, 1997). All three CTD casts display similar characteristics with a thin lid of runoff-influenced low salinity water above 15 m (Figure 2.2). The lack of a discernable intra-fjord spatial pattern in the subsurface salinities suggests that the terrestrial influence is mainly limited to the <15 m layer. All three CTD locations are landward of MD99-2266, and the modern benthic foraminiferal fauna at the three sites are dominated by *C. reniforme* and *E. excavatum* f. *clavata* (Jennings et al., 2004) typical of Icelandic fjords, unlike the fauna at MD99-2266, which displays modern Icelandic shelf fauna. We therefore conclude that the seafloor at the MD99-2266 site is characteristic of open shelf conditions today.

The Vestfirðir Peninsula lies close to the marine polar front, where the northward flowing, warm and saline Atlantic Water of the Irminger Current (IC) meets the southward flowing, cold and fresh Arctic Water of the East Greenland Current (Figure 2.1). More precisely it is the eastern branch of the IC that is present off western Iceland, where it flows clockwise around the island and is known as the North Iceland Irminger Current (NIIC). Today the Atlantic Water in the NIIC occupies the upper ~200 m of the water column, capped by a ~10 to 20 m thick lid of fresher water from terrestrial runoff along the NW Icelandic shelf (www.hafro.is). The IC is a branch of the North Atlantic Current (NAC). The NAC is an extension of the Gulf Stream and flows northeastward across the North Atlantic along the southern and eastern boundary of the subpolar gyre, and constitutes the most northern upper limb of the ocean conveyor belt.

2.4 Material and Methods

2.4.1 MD99-2266

MD99-2266 is a 10 cm diameter Calypso piston core measuring 38.90 m in length, all of which is Holocene in age. It was raised during the 1999 IMAGES V cruise, Leg III, aboard the *R/V Marion Dusfresne* (Labeyrie et al., 2003)

2.4.2 Chronology

The chronology for MD99-2266 is based on 20 accelerator mass spectrometer (AMS) radiocarbon (^{14}C) dates and the depth of the 10,200±120 yr BP Saksunarvatn tephra, as discussed in Quillmann et al. (2010) (Figure 2.3). The dates were converted to calibrated years using the CALIB Radiocarbon Calibration online program, version 5.0.2. (Stuiver et al., 1998) with an ocean reservoir correction of 400 years ($\Delta R=0$) and an uncertainty of 50 years in ΔR. Recalibration using the latest version of CALIB (6.1) would change only one of the dates, by just 14 yr. Kristjansdottir et al. (2007) identified the 8019±277 cal yr BP Suduroy tephra (Wastegard, 2002) on the North Iceland shelf and used it to conclude that the central estimate of the local reservoir age was 430 years at that time. The interval investigated here, from 7600 to 8400 cal yr BP, is bracketed by dates at 1398-1399 cm (7314 ±105 cal yr BP) and at 2237-2238 cm (8816 ±170 cal yr BP) (Fig. 3). Four additional dates between 8101 and 8284 cal yr BP lie within this interval, but we omitted one date at 1784-1785 cm (8252 ±118 cal yr BP) (Figure 2.3B). Although this date falls well within the 2σ range of the underlying date, its inclusion would have introduced a slight age reversal. The combination of dense AMS dating and a reasonably well-constrained reservoir age lead us to estimate that our age

control at ~8200 cal yr BP is accurate to about one century. According to Channell et al. (2012), MD99 cores are severely stretched by more than 50% and caution is in order when interpreting sedimentation rates. Regardless of any stretching, our sampling interval of ~10 cm affords an average temporal resolution of ~18 yr.

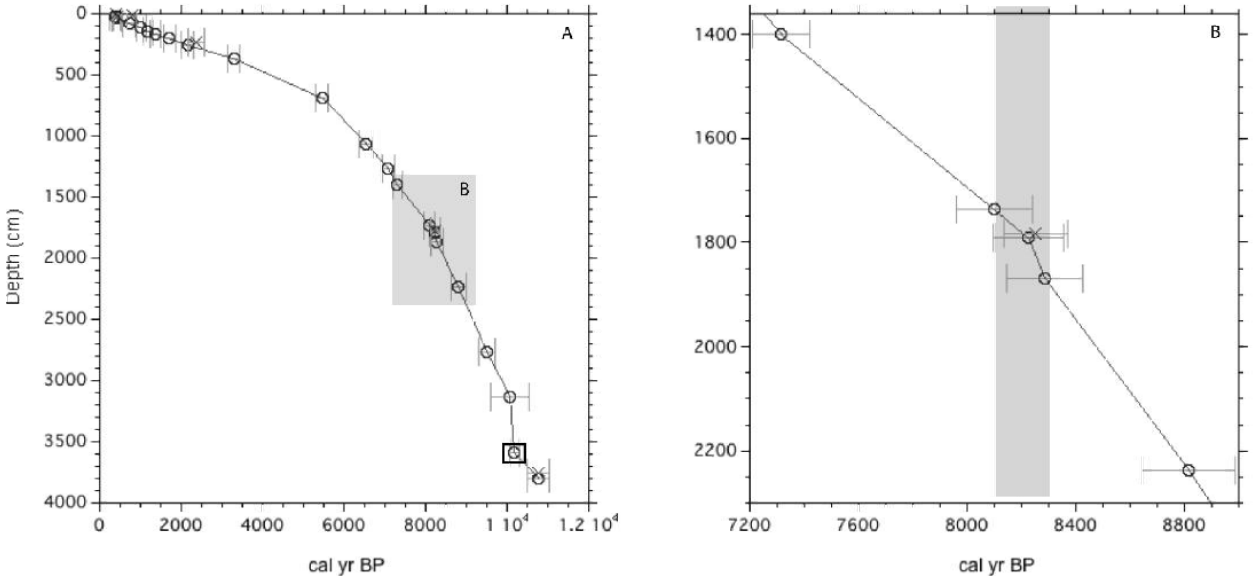

Figure 2.3 Chronology for MD99-2266 based on ^{14}C AMS dates and the depth of the Saksunarvatn tephra deposit. Dates with their ±2□ bars are shown. Dates incorporated into the age model are indicated by open, dark gray circles and omitted dates by a light gray x. The date of the Saksunarvatn tephra is indicated by a boxed open circle. A 0%-weighed curve fit was applied to the age-depth data to obtain the age model. In Panel A the age model for the entire core is shown, as published in *Quillmann et al*. [2010]. In Panel B the close up of the two dates bracketing study interval and the four dates falling within the study interval are shown. The vertical light gray band highlights the timing of the 200-yr climate perturbation found in this study.

2.4.3 Geochemical Proxies: $\delta^{18}O_{calcite}$ and Mg/Ca

C. lobatulus was chosen because this species is cosmopolitan and epifaunal, and comprised at least 10% of the foraminiferal assemblage in every sample. We added

40 samples between 7600 and 8400 cal yr BP to the already existing $\delta^{18}O_{calcite}$ record (Quillmann et al., 2010b). We submitted ~10 >150 µm *C. lobatulus* specimens per sample for isotope analysis to the Curry lab at the Woods Hole Oceanographic Institution. Measurements were made on a Finnigan MAT 252 mass spectrometer with a Kiel Carbonate Device. The results are given in conventional δ-notation in ‰ relative to the VPDB standard with precision better than 0.07‰.

For the Mg/Ca temperature calibration, ~25-35 >150 µm *C. lobatulus* specimens were picked from 31 surface sediment samples collected in the high-latitude North Atlantic. For the paleoceanographic reconstruction, ~40-50 >150 µm *C. lobatulus* specimens were picked from core samples in MD99-2266; abundances of *C. lobatulus* sufficient for Mg/Ca analysis were present in 21 MD99-2266 samples.

Mg/Ca ratios were measured on a Thermo-Finnigan Element2 magnetic-sector single-collector ICP-MS, following methods of Rosenthal et al. (1999) and Marchitto (2006). Crushed samples were cleaned reductively and oxidatively, in a Class-1000 clean lab, according to the cleaning protocol from Boyle and Keigwin (1985) as modified by Boyle and Rosenthal (1996). Long-term 1σ precisions for Mg/Ca are 0.5% (Marchitto, 2006)

It has been suggested that in addition to temperature, Mg/Ca ratios potentially are affected by partial dissolution and by the saturation state with respect to calcite (ΔCO_3^{2-}). Partial dissolution of foraminiferal calcite potentially could lower Mg/Ca ratios, thus mimicking a cooling in the reconstructed temperatures, as calcite formed in warmer waters (higher Mg/Ca ratios) is likely more susceptible to dissolution (Dekens et al., 2002; Rosenthal et al., 2000). However, benthic foraminifers spend their entire life cycle

in relatively constant water temperatures and thus are expected to be resistant to the partial dissolution effect. Bottom water ΔCO_3^{2-} seems to influence benthic Mg/Ca ratios during growth, but the effect is likely only significant in the deep sea where ΔCO_3^{2-} is low and varies much more than temperature does (Bryan and Marchitto, 2008; Elderfield et al., 2006; Marchitto et al., 2007). In shallow sites as in this study, ΔCO_3^{2-} is highly saturated and likely is not a major influence on the Mg/Ca ratios. We also note that recent field studies (Ferguson et al., 2008; Mathien-Blard and Bassinot, 2009) suggest that the positive effect of salinity on planktonic foraminiferal Mg/Ca may be larger than that determined from live culturing (Kisakurek et al., 2008; Lea et al., 1999), particularly in very saline waters. In the absence of observations supporting a salinity effect on benthic foraminiferal Mg/Ca, we interpret our *C. lobatulus* record solely in terms of temperature.

2.4.4 Biological Proxies

Jennings et al. (2004) and Rytter et al. (2002) have shown that changes in modern benthic foraminiferal assemblages on the Iceland shelf coincide with changes in oceanic currents and water masses. We present abundance results in the 106-1000 μm sand fraction for *C. reniforme* and *E. excavatum* f. *clavata*, both Arctic species, found today on the Icelandic shelf in Polar-dominated waters and in fjord environments with cold bottom water temperatures (Jennings et al., 2004).

2.4.5 Sedimentological Proxies

Total inorganic carbon (TIC) percentages were determined by coulometric titration of CO_2 following extraction from the sediment by acid volatilization (Engleman et al., 1985), at the USGS laboratories, Denver, Colorado. Weight percent TIC was converted to weight percent $CaCO_3$ by dividing by 0.12. The accuracy and precision for TIC, determined from hundreds of replicate standards, usually are better than 0.1 wt %.

2.5 Results

2.5.1 Mg/Ca Temperature Calibration for *C. lobatulus*

Because of its primarily epifaunal habitat *C. lobatulus* should be a good recorder for bottom water conditions, but it has not before been used for Mg/Ca-derived temperature reconstructions. We therefore developed a new Mg/Ca temperature calibration for *C. lobatulus* based on high-latitude North Atlantic surface sediment and core top samples. *C. lobatulus* can become detached after death and can be transported to deeper sites, so we limited our selection to samples taken from depths <700 m and chose only pristine, well-preserved looking individuals.

We measured 44 Mg/Ca ratios in surface sediment samples or core tops from 22 different locations in the high latitude North Atlantic: the west to north Icelandic shelf, the east Greenland shelf, the Norwegian shelf, Svalbard, and the

Faroe Islands (Table 2.1; Figure 2.1). The bottom water temperature at each site was estimated from the CTD cast taken at the time of core collection, ranging from 0.01-9.50°C. Since most of the cruises were performed during summer, we regress Mg/Ca

against summer temperature by default, which may make a difference at the shallowest sites.

Table 2.1 Site information for the *C. lobatulus* Mg/Ca temperature calibration. Four samples (indicated by °) were excluded from the final Mg/Ca temperature regressions because they were >2σ outliers relative to initial regression equations. Seven samples (indicated by *) were analyzed at the University of Cambridge using a different cleaning protocol (see text for details) and were also excluded. The Iceland shelf cores were collected during the 1997 joint Icelandic and US cruise aboard the *R/V Bjarni Saemundsson* (B997) (Helgadottir, 1997). The East Greenland cores were collected on the inner shelf off Nansen Fjord during the 1991 joint Icelandic and US cruise aboard *R/V Bjarni Saemundsson* (B1191) (Andrews et al., 1991). Cores from Svalbard were collected during the 2010 cruise aboard *A/S Jan Mayen* (JM10) (Husum, 2010). The core from the west Norwegian margin (HB08-BC) was collected during a 2005 cruise to Byforden, Salhusfjorden and Herdlefjorden aboard the *B/V Hans Brattstrøm* (Hjelstuen et al., 2008). Cores from the Faroe Islands were collected during a cruise in 2003 aboard *R/V Håkon Mosby* (HM03-133) and in 2004 aboard *R/V G.O. Sars* (GS04-138)

Core name	Location name	sample type	water depth (m)	Latitude °N	Longitude °W	BWT (°C)	BWS (psu)	Mg/Ca (mmol mol^{-1})
B997-312s	NW Iceland fjord	surface	72	65.98	-22.49	5.22	34.69	1.780
B997-312s	NW Iceland fjord	surface	72	65.98	-22.49	5.22	34.69	1.988
B997-339s	NW Iceland fjord	surface	104	66.02	-22.80	5.30	34.70	1.948
B997-313s	Djúpáll, NW Iceland shelf	surface	313	66.61	-23.93	5.87	35.00	1.809
B997-313s	Djúpáll, NW Iceland shelf	surface	313	66.61	-23.93	5.87	35.00	1.822
B997-314s	Djúpáll, NW Iceland shelf	surface	233	66.70	-24.18	6.03	35.05	1.734
B997-314s	Djúpáll, NW Iceland shelf	surface	233	66.70	-24.18	6.03	35.05	1.780
B997-315s	Djúpáll, NW Iceland shelf	surface	217	66.73	-24.33	6.04	35.05	2.050
B997-315s	Djúpáll, NW Iceland shelf	surface	217	66.73	-24.33	6.04	35.05	1.963
°B997-329s	N Iceland shelf	surface	110	65.96	-22.30	3.07	34.61	2.084
°B997-329s	N Iceland shelf	surface	110	65.96	-22.30	3.07	34.61	1.964
B997-331s	N Iceland shelf	surface	44	66.07	-21.64	6.71	34.26	1.896
B997-331s	N Iceland shelf	surface	44	66.07	-21.64	6.71	34.26	1.958
B997-332s	N Iceland shelf	surface	104	66.14	-21.59	5.54	34.49	1.937
B997-332s	N Iceland shelf	surface	104	66.14	-21.59	5.54	34.49	1.857

B997-344s	W Iceland shelf	surface	282	64.84	-24.37	6.90	35.12	1.884
B997-346s	W Iceland shelf	surface	320	64.93	-24.26	7.12	35.11	2.202
B1191-K15	East Greenland shelf	surface	455	68.10	-29.27	0.96	34.75	1.231
B1191-K16	East Greenland shelf	surface	100	68.11	-29.27	0.96	n/a	1.189
°JM10-181-MCG	Svalbard, Kongsfjorden	core top, 1-2	290	78.59	11.38	0.46	34.67	1.713
JM10-182-MCG	Svalbard, Kongsfjorden	core top, 0-0.5	287	78.98	11.51	0.35	34.71	1.265
JM10-182-MCC	Svalbard, Kongsfjorden	core top, 0.5-1	287	78.98	11.51	0.35	34.71	1.076
JM10-182-MCC	Svalbard, Kongsfjorden	core top, 1-2	287	78.98	11.51	0.35	34.71	1.241
JM10-183-MCD	Svalbard, Kongsfjorden	core top, 0-0.5	271	79.02	11.73	0.01	34.67	1.357
JM10-183-MCD	Svalbard, Kongsfjorden	core top, 1-2	271	79.02	11.73	0.01	34.67	1.317
°JM10-195-MCG	Svalbard, Kongsfjorden	core top, 0.5-1	360	79.18	11.70	1.14	34.67	1.030
JM10-195-MCG	Svalbard, Kongsfjorden	core top, 1-2	360	79.18	11.77	1.14	34.70	1.360
HB08-BC Gr 1	W Norway, Salhusfjorden	surface	344	79.00	5.16	8.20	34.70	1.982
HB08-BC Gr 2	W Norway, Byfjorden	surface	314	60.48	5.25	8.20	34.70	2.151
*HM03-133-13	Faroe Island, upper slope	surface	180	62.67	6.08	8.68	35.29	2.148
HM03-133-14	Faroe Island, shelf	surface	115	62.50	6.08	9.50	35.28	2.349
HM03-133-14	Faroe Island, shelf	surface	115	62.50	6.08	9.50	35.28	2.408
*HM03-133-14	Faroe Island, shelf	surface	115	62.50	6.08	9.50	35.28	2.411
*GS04-138-16	Faroe Island, slope	surface	416	62.80	6.06	3.39	34.96	1.718
*GS04-138-17	Faroe Island, slope	surface	462	62.80	6.15	2.88	34.95	1.652
*GS04-138-18	Faroe Island, slope	surface	498	62.80	6.15	1.00	34.90	1.509
*GS04-138-20	Faroe Island, slope	surface	614	62.85	6.13	-0.14	34.89	1.558
*GS04-138-21	Faroe Island, slope	surface	652	62.86	6.13	-0.33	34.89	1.614

Most of the samples (37) were analyzed at INSTAAR, following the procedure described earlier. Sample size was generally ~25-35 individuals per run, and no sample consisted of <10 individuals. The pooled standard deviation of the sample splits was 0.083 mmol mol^{-1} (6 degrees of freedom). We used Fe/Ca measurements to screen for detrital contamination (Barker et al., 2003), especially in the Icelandic shelf sites where contamination by high-Mg tephra potentially can be a problem. We rejected five samples with Fe/Ca >0.5 mmol mol^{-1}, and one sample that was an extreme Mg/Ca outlier. Four of the remaining 31 samples were excluded from the final Mg/Ca temperature calibrations because they were >2σ outliers relative to initial regression equations (gray crosses in Figure 2.4).

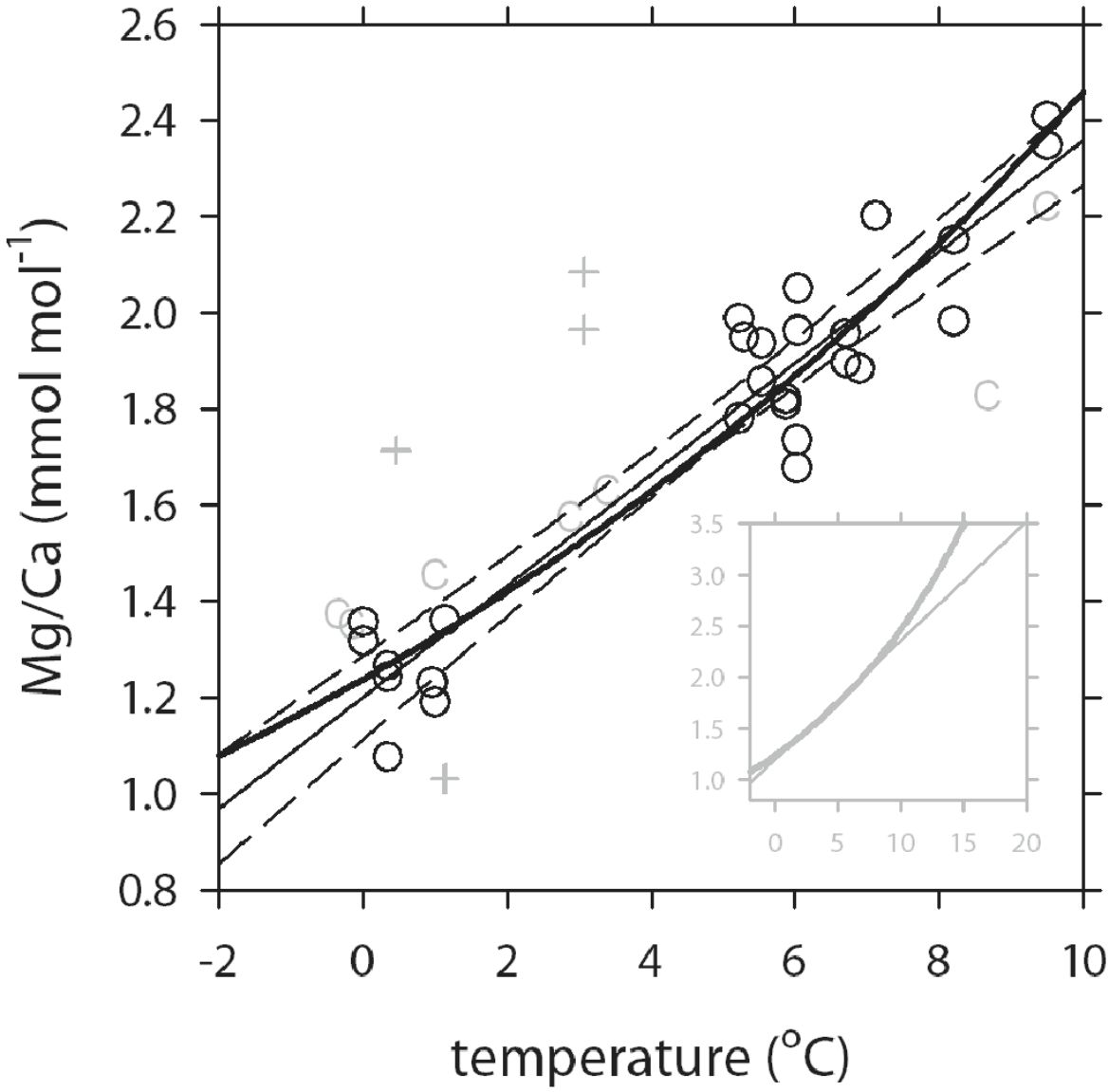

Figure 2.4 *C. lobatulus* Mg/Ca temperature calibration. High-latitude North Atlantic surface sediment *C. lobatulus* Mg/Ca plotted versus CTD bottom water temperature. Shown are the best fit linear regression (equation (1), fine solid line) with 95% confidence intervals (dashed lines) and best fit exponential regression (equation (2,) thick solid line). The + symbols were rejected because they were >2σ outliers relative to initial regression equations. The C symbols indicate samples analyzed at the University of Cambridge that did not include the reductive step, and a -15% correction is applied here; since this correction introduces additional uncertainty, we did not include these samples in the calibration equations. The gray inset shows the linear and exponential extrapolations to the highest Mg/Ca values measured in MD99-2266.

Seven samples were analyzed in the Cambridge University Laboratory (one previously published in (Elderfield et al., 2006)) and did not include the reductive step that we use at the INSTAAR ICP-MS lab. It has been proposed that the analytical offset between the two different cleaning protocols can be approximately corrected by subtracting 0.2 mmol mol^{-1} (Elderfield et al., 2006) or 15% (Barker et al., 2003; Rosenthal et al., 2004). Because this correction introduces additional uncertainty, we did not include these samples in the calibration equations. After subtraction of 15% (gray C's in Figure 2.4) they agree reasonably well with the INSTAAR data.

C. lobatulus Mg/Ca ratios correlate positively with bottom water temperature (Figure 2.4). Both a linear regression and an exponential regression fit the Mg/Ca measurements well.

Linear regression (±1□ errors): $Mg/Ca = 1.20\pm0.04 + 0.116\pm0.008\ T$ (Equation 2.1)

Exponential regression (±1□ errors): $Mg/Ca = 1.24\pm0.04\ e^{0.069\pm 0.005\ T}$ (Equation 2.2)

The linear equation has an r^2 value of 0.90 ($p < 0.0001$) and the exponential equation 0.89 ($p<0.0001$). The standard error of estimate for both regression fits is 0.12 mmol mol^{-1}, equivalent to 1.0°C using the linear slope.

From a thermodynamic point of view, the exponential regression fit is expected to capture the response of the Mg/Ca ratios to temperature and has traditionally been used for calibrations of planktonic foraminifera (Rosenthal et al., 1997). It has been proposed, however, that a linear response to temperature is a better approximation in

benthic foraminifera (Bryan and Marchitto, 2008; Marchitto et al., 2007). Physiological processes likely affect Mg incorporation into the shells and may mask the imprint of thermodynamics (Elderfield et al., 1996; Erez, 2003). We note that Equation (1) is identical to the linear calibration for *Cibicidoides pachyderma* based on multicore tops collected in the Florida Straits over a temperature range of 5.8-18.6 °C (Marchitto et al., 2007), and may support the assertion that neither the Florida data (Elderfield et al., 2006) nor the present data are significantly impacted by ΔCO_3^{2-}. Because this is an area of ongoing research, and because our linear and exponential fits are equally good, we apply both equations to our downcore reconstruction presented below.

2.5.2 Multi-proxy Evidence for a Climate Excursion in MD99-2266 at 8200 cal yr BP

All of our proxies show a prominent excursion overlapping temporally with the 8.2 ka event recorded in the GISP2 (Grootes and Stuiver, 1997) and NGRIP (Rasmussen et al., 2006) $\delta^{18}O_{ice}$ records (Figure 2.5). Although we cannot presently evaluate the uniqueness of this excursion in the context of the full Holocene record, we note that its timing and brief duration are fully consistent with the ice core record. The broadest excursion in MD99-2266, registered in the Mg/Ca record as a decrease of ~0.5 mmol mol^{-1}, lasted no more than ~200 years. In the Greenland ice cores the 8.2 ka event extends from 8247 to 8086 cal yr BP (Thomas et al., 2007), having lasted 160.5 ±5.5 years, with a peak cooling interval of 69 ±2 years.

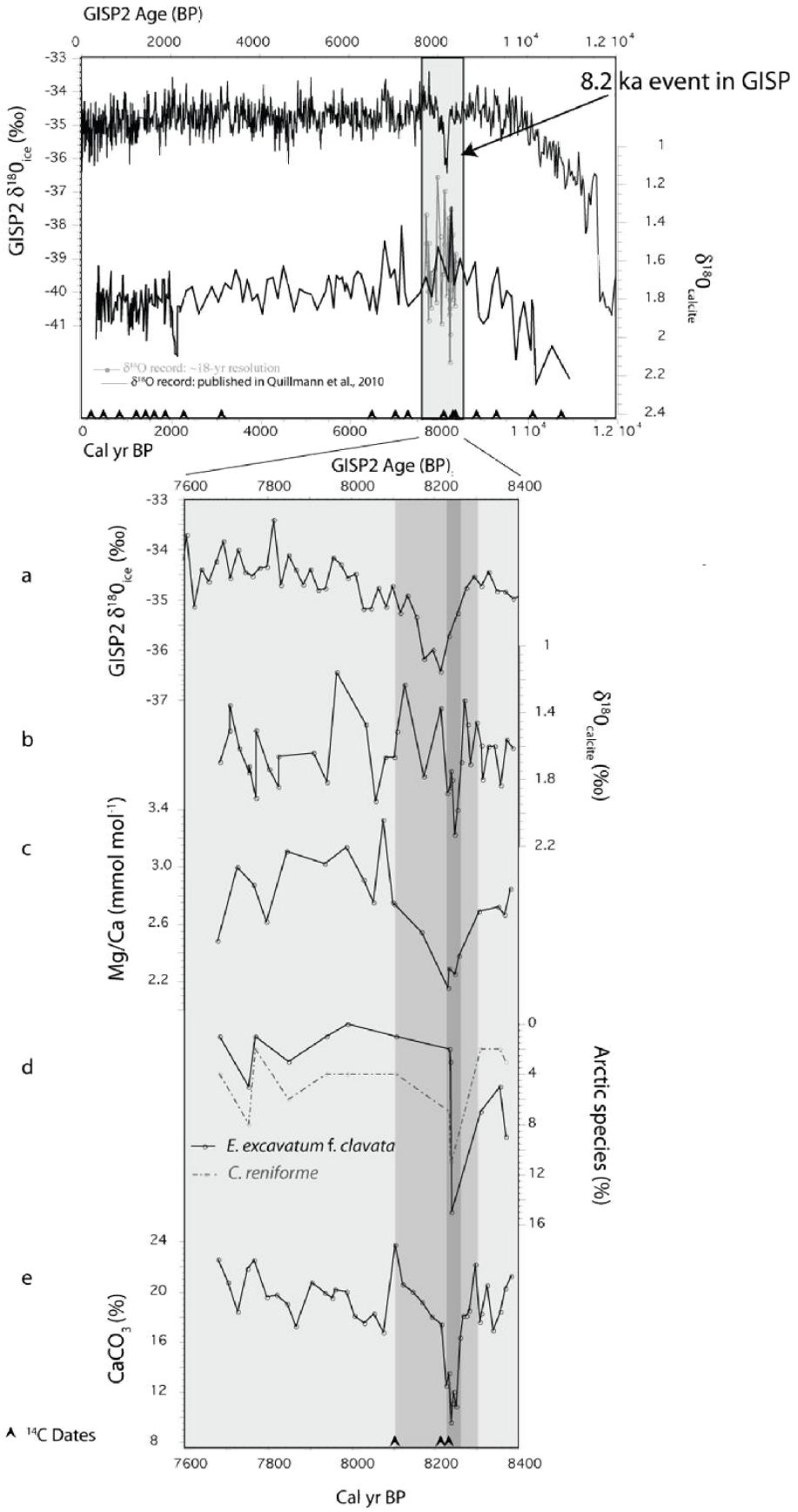
GISP2 Age (BP)
8.2 ka event in GISP
GISP2 δ18Oice (‰)
δ18Ocalcite
δ18O record: ~18-yr resolution
δ18O record: published in Quillmann et al., 2010
Cal yr BP
a
b
c
d
e
Mg/Ca (mmol mol-1)
CaCO3 (%)
Arctic species (%)
E. excavatum f. clavata
C. reniforme
14C Dates

Figure 2.5 Summary plot for MD99-2266 results. The upper panel shows the Holocene sections of the NGRIP (black, 20-yr mean: Rasmussen et al., 2006; Vinther et al., 2006) and GISP2 (gray, 2-m mean: Grootes and Stuiver, 1997) $\delta^{18}O_{ice}$ records, and the MD99-2266 *C. lobatulus* $\delta^{18}O_{calcite}$ record. The ages of the GICC05 chronology used for NGRIP were modified to a reference point of AD 1950. The black line in the MD99-2266 $\delta^{18}O_{calcite}$ record shows the published record from Quillmann et al. (2010), with ~50-yr resolution between 300 and 2700 cal yr BP and ~100-yr resolution between 2700 and 10,500 cal yr BP. The gray data show the samples that were added between 7600 and 8400 cal yr BP to improve the resolution to ~18 years (this study). The lower panels zoom in on the interval from 7600-8400 cal yr BP, showing (a) NGRIP (black) and GISP2 (gray) $\delta^{18}O_{ice}$, (b) *C. lobatulus* $\delta^{18}O_{calcite}$, (c) *C. lobatulus* Mg/Ca, (d) percentages of arctic benthic foraminifers *C. reniforme* (dashed line) and *E. excavatum* f. *clavata* (solid line) (note the reversed axis), and (e) percent $CaCO_3$. The medium gray vertical band highlights the low Mg/Ca ratio interval; the dark gray vertical band highlights the briefer interval of excursions in the other proxies. For both panels: arrowheads indicate radiocarbon dates in MD99-2266. Estimated age uncertainty in the 7600-8400 cal yr BP interval is shown by the horizontal bar.

All other proxies registered a briefer excursion, lasting ~40 years, and falling within the Mg/Ca excursion interval.

A *C. lobatulus* $\delta^{18}O_{calcite}$ positive excursion started at ~8260 cal yr BP and ended at ~8220 cal yr BP, during which the $\delta^{18}O_{calcite}$ became enriched by ~0.4‰. The heaviest $\delta^{18}O_{calcite}$ value of the past 10,000 yr, and the largest positive $\delta^{18}O_{calcite}$ excursion of the entire record (albeit with data resolution varying through the core) coincides with the Mg/Ca low at 8250 cal yr BP. Enrichment of $\delta^{18}O_{calcite}$ can be caused by colder temperatures, heavier $\delta^{18}O_{sw}$ values, or a combination of both.

To test if the foraminiferal assemblages register a change coinciding with the excursion registered in the Mg/Ca and $\delta^{18}O_{calcite}$, we selected samples from before, during, and after the excursion. The percentages of *C. reniforme* spiked from a mean of

4% to a high of 11% between ~8240 and 8235 cal yr BP; the percentages of *E. excavatum* f. *clavata* spiked from a mean of 2% to a high of 15% at ~8240 cal yr BP. Both are Arctic species, found today in Polar waters on the Icelandic shelf and in fjord environments with cold bottom water temperatures (Jennings et al., 2004). We therefore interpret the sudden increases of *C. reniforme* and *E. excavatum* f. *clavata* (albeit limited to one sample) as indicative of colder bottom waters.

An abrupt interval of low percent $CaCO_3$ started at ~8260 cal yr BP with a drop from ~ 18% to ~10% and ended at ~8220 cal yr BP, thus matching precisely the interval of the heavy $\delta^{18}O_{calcite}$ excursion. We interpret a drop in $CaCO_3$ as a decrease in bioproductivity. This may be consistent with a stronger halocline due to the outburst flood, since stratified waters become nutrient depleted quickly. Dilution by an abrupt increase of terrigenous (basaltic) material to the site is more difficult to rule out.

2.5.3 Temperature Reconstruction

Converting the Mg/Ca ratios into temperature posed a challenge, because most of the measured Mg/Ca ratios from the early Holocene lie outside the modern calibration range. Our temperature calibration is limited to the modern distribution of *C. lobatulus* in the high latitude North Atlantic, where bottom temperatures do not exceed ~10°C. However, the early Holocene is generally regarded as a warm period in the high latitude North Atlantic (Andersen et al., 2004a; Eiriksson et al., 2000; Jennings et al.; Justwan et al., 2008; Kaufman et al., 2004; Knudsen et al., 2004; Ólafsdóttir et al., 2010). *C. lobatulus* was apparently not displaced by this warmth, and indeed this species is known from as far south as the Georgia continental shelf today (Culver and Buzas, 1980). Our calibration data suggest that the relationship between *C. lobatulus*

Mg/Ca and temperature can be described as linear or exponential; neither regression fit is significantly better or worse than the other, but the choice of equation becomes important when applied outside of the calibration range (Figure 2.4 inset). Temperature reconstructions based on the linear regression fit yield not only higher overall temperatures but also give a greater temperature range than do the reconstructions based on the exponential regression fit (Figure 2.6), and therefore show the greatest discrepancy compared to other North Atlantic records (see Discussion below).

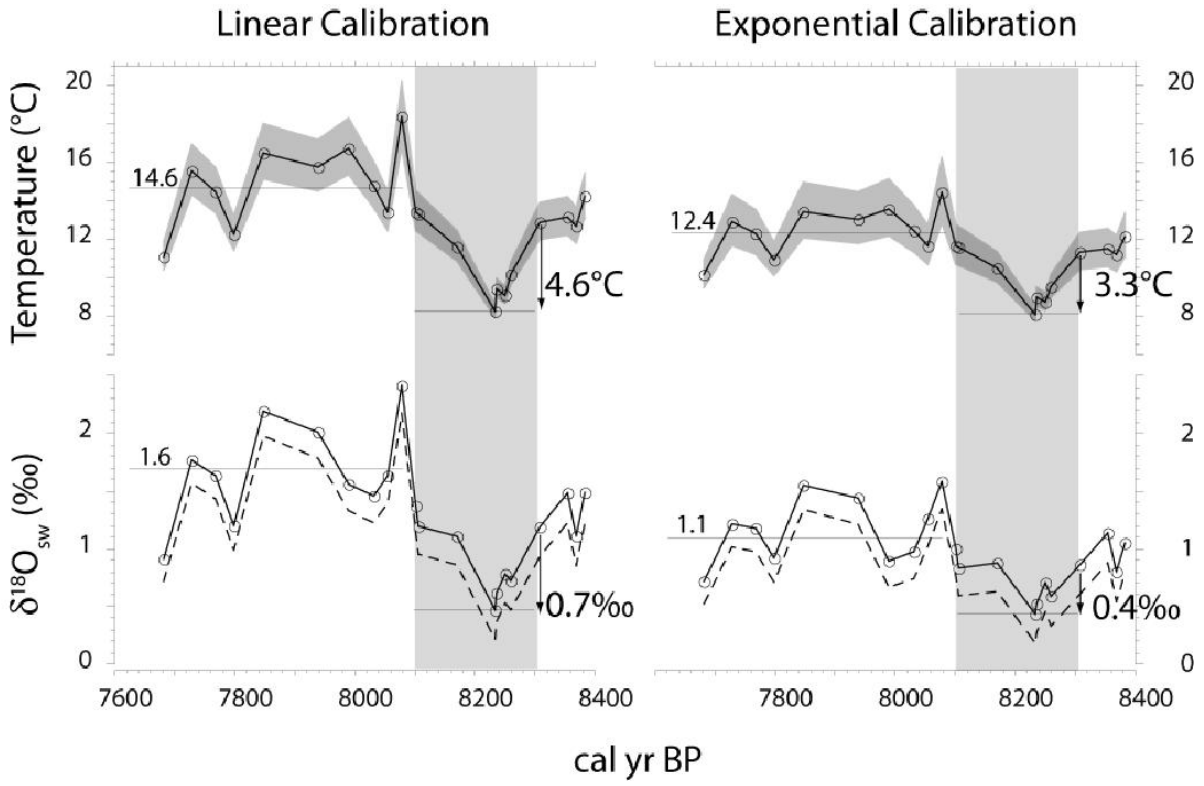

Figure 2.6 *C. lobatulus* temperature and $\delta^{18}O_{sw}$ reconstructions, based on the linear (left panels) and exponential (right panels) Mg/Ca temperature calibrations. The light gray vertical band highlights the 8.2 ka event interval, spanning from ~8300 to 8100 cal yr BP. The dark gray areas indicate the calculated ±2σ temperature uncertainty based on the linear regression fit. The dashed lines in the lower two panels show the $\delta^{18}O_{sw}$ corrected for global ice volume (Fairbanks, 1992).

Regardless of the temperature equation applied, during the 8.2 ka event we see a drop in Mg/Ca into the range of our calibration. Temperature dropped by ~5°C from ~13°C to 8°C (linear regression) or by ~3°C from ~11°C to 8°C (exponential regression). After recovery from the 8.2 ka event the temperature rose to an average of ~15°C (linear) or 12°C (exponential) over the subsequent 500 years.

C. lobatulus has been suggested to calcify in the peak summer months and therefore may reflect peak summer temperatures (Scourse et al., 2004). Comparison between our temperature reconstruction and present-day summer temperatures at 50 m water depth, as measured in August 2008 and 2009 during routine hydrographic surveys (www.hafro.is), shows that the average temperature during the immediately-post-8.2 ka interval in our record was warmer than today by ~7°C (linear equation) or ~4°C (exponential equation). The coldest reconstructed temperatures during the 8.2 ka event are the same as present-day summer water temperatures of ~8°C on the NW Iceland shelf.

2.5.4 Seawater $\delta^{18}O$ Reconstruction

C. lobatulus $\delta^{18}O_{calcite}$ hypothetically could have been influenced by both cooling and freshening during the 8.2 ka event. The outburst flood likely would have cooled the Atlantic Water transported by the IC, resulting in $\delta^{18}O_{calcite}$ enrichment. However the isotopically light floodwaters would have pushed $\delta^{18}O_{calcite}$ in the opposite direction, potentially dampening the $\delta^{18}O_{calcite}$ cooling signal. To separate the relative contributions of temperature and $\delta^{18}O_{sw}$ to the $\delta^{18}O_{calcite}$ signal we used the best-

constrained benthic foraminiferal calibration available, which is based on the genera *Planulina* and *Cibicidoides* from the Bahamas (Lynch-Stieglitz et al., 1999):

$$\delta^{18}O_{calcite} - \delta^{18}O_{sw} + 0.27 = 3.38 - 0.21T \qquad \text{Equation 2.3,}$$

where $\delta^{18}O_{calcite}$ is on the PDB scale and $\delta^{18}O_{sw}$ on the SMOW scale. The Mg/Ca-derived temperature was then used to extract the $\delta^{18}O_{sw}$ component captured in the $\delta^{18}O_{calcite}$ signal.

The lightest $\delta^{18}O_{sw}$ interval took place between ~8300 and 8100 cal yr BP, during which the $\delta^{18}O_{sw}$ values dropped by ~0.7 or 0.4‰, depending which temperature reconstruction is applied (linear or exponential, respectively) (Figure 2.6). The interval of lighter $\delta^{18}O_{sw}$ values coincides with the interval of cooler temperature as would be expected if the 8.2 ka event was caused by the outburst flood of proglacial lakes Agassiz and Ojibway. In Fig. 6 we show also the $\delta^{18}O_{sw}$ values corrected for global ice volume according to Fairbanks (1992).

In the modern surface ocean warmer than 5°C a linear relationship exists between $\delta^{18}O_{sw}$ and salinity (Lynch-Stieglitz et al., 1999):

$$\delta^{18}O_{sw} = -14.34 + 0.419S \qquad \text{Equation 2.4}$$

Using this relationship the lighter $\delta^{18}O_{sw}$ values would suggest a drop in salinity of ~1.8 or 1.3 p.s.u., depending on the temperature reconstruction used (linear or exponential, respectively). But likely the $\delta^{18}O_{sw}$ versus salinity relationship near Iceland differed from today during the 8.2 ka event because of the input of isotopically light meltwater from Lakes Agassiz and Ojibway (LeGrande and Schmidt, 2008). This

uncertainty precludes an accurate reconstruction of paleosalinity during the 8.2 ka event.

2.6 Discussion

2.6.1 Open Shelf Versus Local Icelandic Influences on MD99-2266

The high sedimentation rates at our site offer the advantage of high-resolution reconstruction of past marine environmental conditions. However, the close proximity to land potentially could overprint the regional marine signal with an influence from local fjord conditions, leading to the possibility that the cooling and freshening recorded in MD99-2266 is reflective of a local terrestrial signal and not a regional Atlantic signal.

As discussed earlier, the seafloor at site MD99-2266 today reflects open shelf conditions with negligible impact from runoff. At the time of our study interval, the eustatic sea level was ~15-20 m lower than today (Lambeck and Chappell, 2001). Postglacial isostatic rebound of Iceland was rapid, and the extensive ~8600 cal yr BP Þjórsárhraun lava flow met the sea at ~15 m below modern sea level, indicating that uplift was completed by that date (Norddahl and Einarsson, 2001). Hence we infer that relative sea level was ~15-20 m lower than today during our study interval, though we note that this is largely offset by the sediment column being ~18 m thinner at that time. Furthermore, since the slight threshold beyond the fjord mouth is ~10 m deeper than our core site today, its sediment sequence would only need to have been ~8 m thinner in order for the core site to have remained completely unrestricted from the open ocean. In total then the depth of our core site was approximately the same as it is today, and

bottom waters likely reflected open shelf conditions with relatively little impact from land, assuming that runoff was not drastically higher than modern.

At present, Drangajökull, an icecap of ~145 km^2, lies within the Ìsafjarðardjúp drainage system (Figure 2.2). There are no hydrographic data available from the rivers that drain Drangajökull (Andrews et al., 2008). But as indicated by the CTD data discussed earlier, modern runoff has no obvious impact on bottom waters near the mouth of Ìsafjarðardjúp. There is little known about the extent of the Drangajökull during the early Holocene, but the icecap was likely smaller than it is today if Drangajökull responded to the climatic optimum in a similar way as Langjökull in west central Iceland. Langjökull, the second largest ice cap on Iceland today, appears to have been much smaller during the early Holocene (Larsen et al., 2012). Larsen et al. (2012) showed a brief advance (~100 years) of Langjökull coinciding with the 8.2 ka event, but argued that even with this advance it was still much smaller than during the late Holocene and presently. Their findings agree with model results by Flowers et al. (2008) that simulate ice cap expansion of Langjökull during the 8.2 ka event, but still culminating in a much smaller size than today.

A paleoreconstruction in the tributary fjord Jökulfirðir (Core MD99-2265, water depth 43 m) showed that glacial and glacial river input from Drangajökull had ended by ~9800 cal yr BP, as suggested by a decrease in sedimentation rate (Olafsdottir, 2010a). However the same study pointed out the onset of unstable conditions at ~8600 cal yr BP punctuated by a bottom water cooling and organic carbon decline at ~8400 cal yr BP. This might represent an advance of Drangajökull, but we suggest that the 43 m

Jökulfirðir site would have been much more sensitive to such an event than our 106 m location at the mouth of Ìsafjarðardjúp (Fig. 2).

In summary, while we cannot completely rule out a terrestrial influence on MD99-2266 during the early Holocene and the 8.2 ka event, we have no reason to believe that our core location was significantly less representative of open shelf conditions than it is today.

2.6.2 Climate Perturbation in Iceland Around 8,200 cal yr BP

Geirsdottir et al. (2009), in a review paper on Holocene and Pleistocene climate fluctuations in Iceland, showed that many records from on and around Iceland show a climate perturbation near 8,200 cal yr BP. Multiple marine records from the west to north shelf show a temperature depression, documented in proxies including foraminiferal assemblages, oxygen isotopes, alkenones, and $CaCO_3$ percentages (e.g. Eiriksson et al. 2000; Andrews and Giraudeau, 2003; Castaneda et al. 2004). But, as Geirsdottir et al. (2009) point out, many of these climate and environmental perturbations do not exactly coincide with the timing of the 8.2 ka event in the Greenland ice core record. Rather they span a longer period, starting by at least 8,500 and lasting until ~8,000 cal yr BP. Several lacustrine records from Iceland (e.g. Caseldine et al. 2006) likewise show a broad cooling between ~8,500 and 8,000 cal yr BP.

The cooling of the Irminger Current around 8,200 cal yr BP was noted in a comparison study of a west Iceland site (246 m water depth from the Jökuldjúp trough) and a northwestern Iceland site (235 m water depth in the Djúpáll trough), the latter being close to MD99-2266 (Olafsdottir et al., 2010b). At the more southern location,

transfer functions of benthic foraminifera indicate that the cooling started around ~8740 cal yr BP and reached its lowest temperature around 8,200 cal yr BP. The same broad cooling interval is less pronounced at the northwestern site, with the bottom temperatures reaching a low of 6.4°C at ~8,200 cal yr BP. The temperature reconstruction by Olafsdottir et al. (2010b) is overall lower by several °C than our reconstruction, presumably because their site is deeper, and because they base their reconstructions on benthic foraminiferal transfer functions. As Olafsdottir et al. (2010b) pointed out, benthic assemblages reflect mean annual temperatures, whereas *C. lobatulus* has been suggested to calcify during peak summer months (Scourse et al., 2004) and we have calibrated Mg/Ca against summer temperatures.

In summary, multiple records from Iceland and the Iceland shelf show an excursion around 8,200 cal yr BP, but it seems that the 8.2 ka event is embedded within a longer lasting climate perturbation. While there is a general consensus that the cooling at 8,200 cal yr BP as recorded in Greenland ice cores was likely associated with a freshwater forcing, Geirsdottir et al. (2009) pointed out that causes for the longer period of climate perturbations in Iceland have not been resolved.

2.6.3 The 8.2 ka Event as a Regional Signal Dispersed in the North Atlantic

Although a climate anomaly has been tracked in a number of marine records from the North Atlantic region, the timing and duration of the observed anomalies are inconsistent ((Rohling and Palike, 2005) and references therein). These inconsistencies have been attributed, in part, to imprecise chronologies and to low resolution in marine sediment cores relative to the well-dated, highly resolved Greenland ice core records (Rohling and Palike, 2005).

Several regional near-surface records contain sufficient temporal resolution to potentially detect the 8.2 ka event. We can compare planktonic reconstructions with our benthic temperature reconstruction because our site is shallow (106 m today), so *C. lobatulus* records the same water conditions as many planktonic foraminiferal species that are commonly used in the subpolar North Atlantic to reconstruct surface or near surface water temperatures. A temporal expression of the 8.2 event that is comparable to that in MD99-2266 can be seen in high-resolution core MD99-2322 on the east Greenland shelf, which is also affected by a subsurface flow of Atlantic Water from the IC beneath Polar surface waters (Jennings et al.) (Figure 2.7a). Jennings et al. (2011) attributed the anomaly to a cooling in the Atlantic Water rather than an increased influence of Polar water to their site. The summer cooling at this site is estimated to be 1.8°C based on planktonic foraminiferal assemblages, compared to the ~3-5°C cooling recorded in MD99-2266 (Figure 2.7b). Although regressed against summer sea surface temperature, planktonic foraminiferal transfer functions integrate the signal of various growth seasons over the entire upper water column in which the various species calcified, from the mixed layer to below the thermocline (Andersson et al., 2010), potentially leading to a smaller 8.2 ka event excursion than the reconstruction based on *C. lobatulus* Mg/Ca at our site.

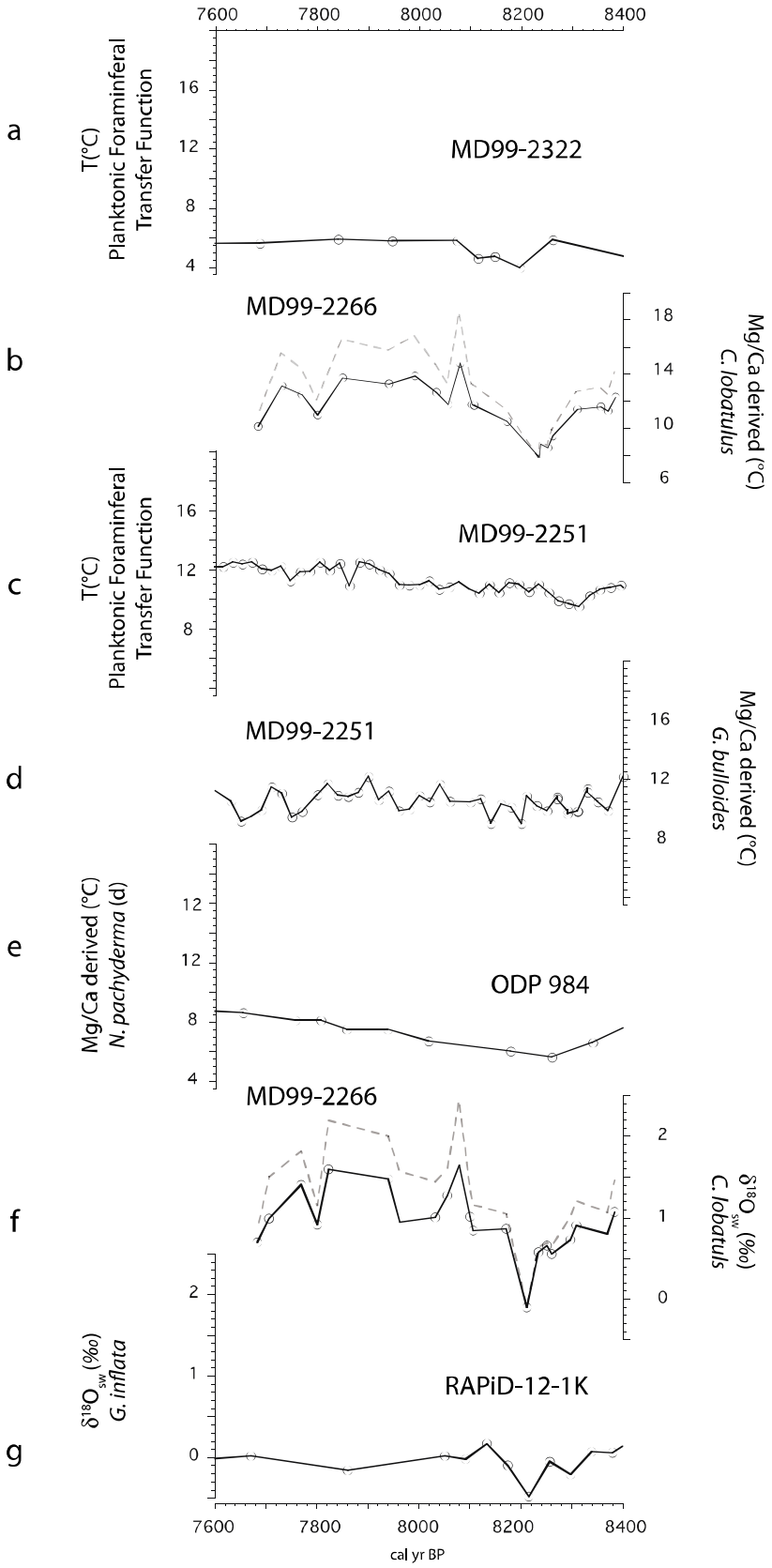
a
b
c
d
e
f
g
7600
7800
8000
8200
8400
cal yr BP
T(°C)
Planktonic Foraminferal
Transfer Function
MD99-2322
MD99-2266
MD99-2251
MD99-2251
ODP 984
MD99-2266
RAPiD-12-1K
Mg/Ca derived (°C)
C. lobatulus
Mg/Ca derived (°C)
G. bulloides
Mg/Ca derived (°C)
N. pachyderma (d)
δ18Osw (‰)
C. lobatuls
δ18Osw (‰)
G. inflata

Figure 2.7 Comparison of the temperature and $\delta^{18}O_{sw}$ reconstructions in MD99-2266 to other regional reconstructions, plotted on the same scale. Temperature reconstructions are based on: (a) planktonic foraminiferal assemblages in MD99-2322 from the Denmark Strait (Jennings et al. 2011); (b) this study, using both the linear (dashed) and exponential (solid) Mg/Ca calibrations; (c) planktonic foraminiferal assemblages in MD99-2251 from Gardar Drift south of Iceland (Ellison et al., 2006); (d) planktonic foraminiferal (*Globigerina bulloides*) Mg/Ca, on the same core (Farmer et al., 2008) as in (c); and (e) planktonic foraminiferal (*Neogloboquadrina pachyderma* (dextral) Mg/Ca in ODP984 on Björn Drift south of Iceland (Came et al., 2007). $\delta^{18}O_{sw}$ reconstructions are based on: (f) this study, using both the linear (dashed) and exponential (solid) Mg/Ca calibrations; and (g) *Globorotalia inflata* Mg/Ca and $\delta^{18}O$ in RAPiD-12-1K from the South Iceland Rise (Thornalley et al., 2009).

Using high-resolution core MD99-2251 from the Gardar Drift south of Iceland, Ellison et al. (2006) reconstructed Atlantic Water sea surface temperatures derived from planktonic foraminiferal transfer functions, and combined them with $\delta^{18}O_{calcite}$ of the planktonic foraminifer *Globigerina bulloides* to infer $\delta^{18}O_{sw}$. They found a cooling event with a magnitude of ~1.2°C and a minor freshening centered around 8290 cal yr BP (Figure 2.7c) (Ellison et al., 2006). The temperature depression is smaller than the cooling in our record, but the difference in the reconstruction methods might explain the discrepancy, as discussed above. However, Mg/Ca derived temperatures of *G. bulloides* from the same sample series (Farmer et al., 2008) did not record the same cooling interval as Ellison et al. (2006), but rather identified a series of small and rapid temperature fluctuations (Figure 2.7d).

At Björn Drift (ODP 984) on the eastern flank of the Reykjanes Ridge south of Iceland, Mg/Ca of the planktonic foraminifer *Neogloboquadrina pachyderma* (dextral) (aka *Neogloboquadrina incompta* (Darling et al., 2006)) showed an ~2°C cooling (Figure 2.7e) accompanied by a $\delta^{18}O_{sw}$ decrease of ~0.3‰ at ~8200 cal yr BP, but with lower temporal resolution than MD99-2266 (Came et al., 2007). A combined Mg/Ca-$\delta^{18}O$

record from the South Iceland Rise using the sub-thermocline planktonic foraminifer *Globorotalia inflata* showed a cooling of ~1°C and a $\delta^{18}O_{sw}$ drop of ~0.5‰ at ~8200 cal yr BP (Thornalley et al., 2009) (Fig. 7g). As was the case on Gardar Drift (Farmer et al., 2008), South Iceland Rise *G. bulloides* Mg/Ca did not record a cooling at this time (Thornalley et al., 2009).

Our record, combined with other high-resolution reconstructions discussed above, shows that the 8.2 ka event was associated with both a cooling and a freshening, and that the signal is seen far from the presumed source. The two most plausible scenarios are that the freshwater pulse from the proglacial lakes Agassiz and Ojibway entered the North Atlantic via the Hudson Strait and was entrained into the subpolar gyre where it cooled and freshened the Atlantic Water and the IC; and/or that the freshwater pulse dampened the formation of NADW and thus lessened the northward transport of warm, saline Atlantic Water to the high-latitude regions.

Clarke et al. (2009) modeled the Lake Agassiz and Ojibway outburst flood and concluded that it could have caused the cooling recorded in the Greenland ice cores by promoting sea ice growth and altering atmospheric circulation, without having altered the AMOC substantially. In this modeling study the sea surface temperature near our study site dropped by ~4-6°C during the first several decades of the 8.2 ka event, compared to our observed cooling of ~3-5°C. Furthermore Clarke et al. (2009) suggest an ~3.5-10 p.s.u. drop in salinity around Iceland, persisting for about 50 model years, which is considerably larger than our drop in $\delta^{18}O_{sw}$ suggests.

There is, however, convincing proxy evidence that changes in deep water circulation did occur during the 8.2 ka event. Sortable silt grain size decreased around

8.2 ka both in core MD99-2251 (Ellison et al., 2006) and ODP 984 (Praetorius et al., 2008), suggesting reduced flow speed of NADW. Kleiven et al. (2008) also inferred reduced NADW flow speed at site MD03-2665 south of Greenland on the basis of magnetic sediment grains, accompanied by a dramatic decrease in benthic $\delta^{13}C$.

Our observations challenge the results from a recent modeling study by Condron and Winsor (2011). They showed in a high-resolution global, ocean-ice circulation model that the freshwater from the outburst flood was likely confined in a narrow, buoyant coastal current, flowing southward along the continental shelf to the subtropical North Atlantic. According to the results of their modeling study, the freshwater from the outburst flood did not spread to the subpolar North Atlantic, and thus would not have reached the Iceland area nor the sites where deep water is formed. Our observations instead suggest that the freshwater was entrained into the subpolar gyre and spread toward Iceland, either via the Irminger Current or via an expanded gyre.

2.7 Conclusions

We aimed to determine if the brief 8.2 ka event as recorded in Greenland ice cores left a resolvable imprint in the marine realm, and if this imprint is consistent with the hypothesized catastrophic outburst flood of the proglacial lakes Oijbway and Agassiz. The high sedimentation rates at our site allowed for an ~18-yr sampling resolution, permitting us to assess the evolution of the 8.2 ka event at the mouth of Ìsafjarðardjúp in NW Iceland. We focused on the interval between 8400 and 7600 cal yr BP.

Our approach was novel as it is the first high resolution record that reconstructs near-surface temperatures and $\delta^{18}O_{sw}$ by paired measurements of Mg/Ca and $\delta^{18}O_{calcite}$

of a benthic foraminifer. We developed a new Mg/Ca temperature calibration for *C. lobatulus* based on 27 surface sediment and core top samples from the North Atlantic. We showed a cooling and freshening at 8.2 ka in accordance with the hypothesis that proglacial lakes drained into the North Atlantic via the Hudson Strait. We recorded the signal far from the source, implying a widespread impact on North Atlantic sea surface conditions. Such a large-scale influence could hypothetically have cooled the region on its own, with a resulting reduction in the AMOC amplifying the effect.

2.8 Acknowledgments

This project was funded by GSA graduate research grant No. 8111-05. Additional funding was provided by NSF grant 0823535 (PIs Jennings, Marchitto and Andrews). We thank the Department of Geological Sciences at CU Boulder for providing a mentorship grant that made it possible for undergraduate researcher Christopher Dodson to help us with sample preparation. We thank Walter Dean from the USGS in Lakewood, CO for making the carbonate measurements possible. We are grateful for the assistance of Patrick Cappa in the ICP-MS laboratory at INSTAAR and Josh Freeman in the sedimentology laboratory at the USGS in Lakewood, CO. Scott Lehman at the AMS Radiocarbon Preparation and Research Laboratory at INSTAAR provided additional radiocarbon dates for our project and we thank Jocelyn Turnbull for preparing the ^{14}C samples. We thank Gudrun Helgadottir from the Marine Research Institute of Iceland for providing the bathymetric map in Fig. 2. Special thanks to Katrina Husum and Steffen Aargaard Sørensen at the University of Tromsø for providing core top samples from Svalbard, and to Haflidi Haflidason, Hans Petter Sejrup, and Heidi Kjennbakken at the University of Bergen for providing surface samples from Norwegian

shelf. Our manuscript benefitted from the input of four anonymous reviewers, Garry Clarke, Rainer Zahn, and Jim Knox.

2.9 Work Cited

Alley, R. B., Mayewski, P. A., Sowers, T., Stuiver, M., Taylor, K. C., and Clark, P. U., 1997, Holocene climatic instability: a prominent, widespread event 8200 yr ago.: Geology, v. 25, no. 6, p. 483-486.

Andersen, C., Koc, N., Jennings, A., and Andrews, J. T., 2004, Nonuniform response of the major surface currents in the Nordic Seas to insolation forcing: Implications for the Holocene climate variability: Paleoceanography, v. 19, no. 2.

Andrews, J. T., Larsen, B., Thors, K., Helgadottir, G., Olafsson, J., and Wittmaarck, A., 1991, Fjord-Shelf-Slope Sediment Continuum, East Greenland Margin: Cruise Report -- RS Bjarni Saemundsson B1191, p. 25.

Arbuszewski, J. A., Demenocal, P. B., Cleroux, C., Bradtmiller, L., and Mix, A., 2013, Meridional shifts of the Atlantic intertropical convergence zone since the Last Glacial Maximum: Nature Geoscience, v. 6, no. 11, p. 959-962.

Barber, D. C., Dyke, A., Hillaire-Marcel, C., Jennings, A. E., Andrews, J. T., Kerwin, M. W., Bilodeau, G., McNeely, R., Southon, J., Morehead, M. D., and Gagnon, J. M., 1999, Forcing of the cold event of 8,200 years ago by catastrophic drainage of Laurentide lakes: Nature, v. 400, no. 6742, p. 344-348.

Barker, S., Greaves, M., and Elderfield, H., 2003, A study of cleaning procedures used for foraminiferal Mg/Ca paleothermometry: Geochemistry Geophysics Geosystems, v. 4.

Bryan, S. P., and Marchitto, T. M., 2008, Mg/Ca-temperature proxy in benthic foraminifera: New calibrations from the Florida Straits and a hypothesis regarding Mg/Li: Paleoceanography, v. 23, no. 2.

Came, R. E., Oppo, D. W., and McManus, J. F., 2007, Amplitude and timing of temperature and salinity variability in the subpolar North Atlantic over the past 10 k.y: Geology, v. 35, no. 4, p. 315-318.

Clark, P. U., Marshall, S. J., Clarke, G. K. C., Hostetler, S. W., Licciardi, J. M., and Teller, J. T., 2001, Freshwater forcing of abrupt climate change during the last glaciation: Science, v. 293, no. 5528, p. 283-287.

Dekens, P. S., Lea, D. W., Pak, D. K., and Spero, H. J., 2002, Core top calibration of Mg/Ca in tropical foraminifera: Refining paleotemperature estimation: Geochemistry Geophysics Geosystems, v. 3.

Eiriksson, J., Knudsen, K. L., Haflidason, H., and Henriksen, P., 2000, Late-glacial and Holocene palaeoceanography of the North Icelandic shelf: Journal of Quaternary Science, v. 15, no. 1, p. 23-42.

Elderfield, H., Bertram, C. J., and Erez, J., 1996, Biomineralization model for the incorporation of trace elements into foraminiferal calcium carbonate: Earth and Planetary Science Letters, v. 142, no. 3-4, p. 409-423.

Elderfield, H., Yu, J., Anand, P., Kiefer, T., and Nyland, B., 2006, Calibrations for benthic foraminiferal Mg/Ca paleothermometry and the carbonate ion hypothesis: Earth and Planetary Science Letters, v. 250, no. 3-4, p. 633-649.

Ellison, C. R. W., Chapman, M. R., and Hall, I. R., 2006, Surface and deep ocean interactions during the cold climate event 8200 years ago: Science, v. 312, no. 5782, p. 1929-1932.

Engleman, E. E., Jackson, L. L., Norton, D. R., and Fisher, A. G., 1985, Determination of carbonate carbon in geological materials by coulometric titration: Chemical Geology, v. 53, p. 125-128.

Erez, J., 2003, The source of ions for biomineralization in foraminifera and their implications for paleoceanographic proxies: Reviews in Mineralogy and Geochemistry, v. 54, p. 115-149.

Farmer, E. J., Chapman, M. R., and Andrews, J. E., 2008, Centennial-scale Holocene North Atlantic surface temperatures from Mg/Ca ratios in Globigerina bulloides: Geochemistry Geophysics Geosystems, v. 9, p. 15.

Ferguson, J. E., Henderson, G. M., Kucera, M., and Rickaby, R. E. M., 2008, Systematic change of foraminiferal Mg/Ca ratios across a strong salinity gradient: Earth and Planetary Science Letters, v. 265, no. 1-2, p. 153-166.

Helgadottir, G., 1997, Paleoclimate (0 to >14ka) of W and NW Iceland: An Icelandic/USA contribution to PALE. Cruise Report B9-97 R/V Bjarni Saemundsson RE 30, 17-30 July 1997.

Hjelstuen, B. O., Kleiven, H. F., Haflidason, H., Kjennbakken, H., and Team, S., 2008, Marine Geological Cruise Report from Byfjorden, Salhusfjorden and Herdlefjorden. Report No. 100-01/08: Department of Earth Science, University of Bergen, Bergen, Norway, 16 pp.

Husum, K., 2010, CRUISE REPORT ForArc UiT 2010: Marine geological cruise to Kongsfjord and adjoining shelf, West Svalbard.

Jennings, A., Andrews, J., and Wilson, L., 2011, Holocene environmental evolution of the SE Greenland Shelf North and South of the Denmark Strait: Irminger and East Greenland current interactions: Quaternary Science Reviews, v. 30, no. 7-8, p. 980-998.

Jennings, A. E., Weiner, N. J., Helgadottir, G., and Andrews, J. T., 2004, Modern foraminferal faunas of the southwestern to northern Iceland shelf: oceanographic and environmental controls.: Journal of Foraminiferal Research, v. 34, no. 3, p. 180-207.

Johnsen, S. J., Clausen, H. B., Dansgaard, W., Fuhrer, K., Gundestrup, N., Hammer, C. U., Iversen, P., Jouzel, J., Stauffer, B., and Steffensen, J. P., 1992, IRREGULAR GLACIAL INTERSTADIALS RECORDED IN A NEW GREENLAND ICE CORE: Nature, v. 359, no. 6393, p. 311-313.

Johnsen, S. J., DahlJensen, D., Gundestrup, N., Steffensen, J. P., Clausen, H. B., Miller, H., Masson-Delmotte, V., Sveinbjornsdottir, A. E., and White, J., 2001, Oxygen isotope and palaeotemperature records from six Greenland ice-core stations: Camp Century, Dye-3, GRIP, GISP2, Renland and NorthGRIP: Journal of Quaternary Science, v. 16, no. 4, p. 299-307.

Justwan, A., Koc, N., and Jennings, A. E., 2008, Evolution of the Irminger and East Icelandic Current systems through the Holocene, revealed by diatom-based sea surface temperature reconstructions: Quaternary Science Reviews, v. 27, no. 15-16, p. 1571-1582.

Kaufman, D. S., Ager, T. A., Anderson, N. J., Anderson, P. M., Andrews, J. T., Bartlein, P. J., Brubaker, L. B., L.L., C., Cwynar, L. C., Duvall, M. L., Dyke, A. S., Edwards, M. E., Eisner, W. R., Gajewski, K., Geirsdottir, A., Hu, F. S., Jennings, A. E., Kaplan, M. R., Kerwin, M. W., Lozhkin, A. V., MacDonald, G. M., Miller, G. H., Mock, C. J., Oswald, W. W., Otto-Bliesner, B. L., Porinchu, D. F., Ruehland, K., Smol, J. P., Steig, E. J., and Wolfe, B. B., 2004, Holocene termal maximum in the western Arctic (0-180 deg W): Quaternary Science Reviews, v. 23, p. 529-560.

Kisakurek, B., Eisenhauer, A., Bohm, F., Garbe-Schonberg, D., and Erez, J., 2008, Controls on shell Mg/Ca and Sr/Ca in cultured planktonic foraminiferan, Globigerinoides ruber (white): Earth and Planetary Science Letters, v. 273, no. 3-4, p. 260-269.

Knudsen, K. L., Jiang, H., Jansen, E., Eiriksson, J., Heinemeier, J., and Seidenkrantz, M.-S., 2004, Environmental changes off North Iceland during the deglaciation and the Holocene: foraminifera, diatoms and stable isotopes: Marine Micropaleontology, v. 953, p. 1-3.

Kobashi, T., Severinghaus, J. P., Brook, E. J., Barnola, J. M., and Grachev, A. M., 2007, Precise timing and characterization of abrupt climate change 8200 years ago from air trapped in polar ice: Quaternary Science Reviews, v. 26, no. 9-10, p. 1212-1222.

Labeyrie, L., Jansen, E., and Cortijo, E., 2003, Les rapports des campagnes a la mer MD114/IMAGES V.

Lea, D. W., Mashiotta, T. A., and Spero, H. J., 1999, Controls on magnesium and strontium uptake in planktonic foraminifera determined by live culturing: Geochimica et Cosmochimica Acta, v. 63, no. 16, p. 2369-2379.

LeGrande, A. N., and Schmidt, G. A., 2008, Ensemble, water isotope-enabled, coupled general circulation modeling insights into the 8.2 ka event: Paleoceanography, v. 23, no. 3.

Lynch-Stieglitz, J., Curry, W. B., and Slowey, N. C., 1999, A geostrophic transport estimate for the Florida Current from the oxygen isotope composition of benthic foraminifera.: Paleoceanography, v. 14, no. 3, p. 360-373.

Marchitto, T. M., 2006, Nutrient proxies (d13C, Cd/Ca, Ba/Ca, Zn/Ca, d15N), *in* Elias, S., ed., Encyclopedia of Quaternary Science: Amsterdam, Elsevier.

Marchitto, T. M., Bryan, S. P., Curry, W. B., and McCorkle, D. C., 2007, Mg/Ca temperature calibration for the benthic foraminifer Cibicidoides pachyderma: Paleoceanography, v. 22, no. 1.

Mathien-Blard, E., and Bassinot, F., 2009, Salinity bias on the foraminifera Mg/Ca thermometry: Correction procedure and implications for past ocean hydrographic reconstructions: Geochemistry Geophysics Geosystems, v. 10.

Ólafsdóttir, S., jennings, A. J., Á., G., Andrews, J. T., and Miller, G. H., 2010, Holocene variability of the North Atlantic Irminger current on the south- and northwest shelf of Iceland Marine Micropaleontology, v. XXX.

Praetorius, S. K., McManus, J. F., Oppo, D. W., and Curry, W. B., 2008, Episodic reductions in bottom-water currents since the last ice age: Nature Geoscience, v. 1, no. 7, p. 449-452.

Quillmann, U., Jennings, A. J., and Andrews, J. T., 2010, Reconstructing Holocene palaeoclimate and palaeoceanography in ìsafjarðardjúp, northwest Iceland, from two fjord records overprinted by relative sea-level and local hydrographic changes.: Journal of Quaternary Science, v. 25, no. 7, p. 1144-1159.

Rohling, E. J., and Palike, H., 2005, Centennial-scale climate cooling with a sudden cold event around 8,200 years ago: Nature, v. 434, no. 7036, p. 975-979.

Rosenthal, Y., Boyle, E. A., and Slowey, N., 1997, Temperature control on the incorporation of magnesium, strontium, fluorine, and cadmium into benthic foraminiferal shells from Little Bahama Bank: Prospects for thermocline paleoceanography: Geochimica et Cosmochimica Acta, v. 61, no. 17, p. 3633-3643.

Rosenthal, Y., Lohmann, G. P., Lohmann, K. C., and Sherrell, R. M., 2000, Incorporation and preservation of Mg in Globigerinoides sacculifer: Implications for reconstructing the temperature and O-18/O-16 of seawater: Paleoceanography, v. 15, no. 1, p. 135-145.

Rosenthal, Y., Perron-Cashman, S., Lear, C. H., Bard, E., Barker, S., Billups, K., Bryan, M., Delaney, M. L., deMenocal, P. B., Dwyer, G. S., Elderfield, H., German, C. R., Greaves, M., Lea, D. W., Marchitto, T. M., Pak, D. K., Paradis, G. L., Russell, A. D., Schneider, R. R., Scheiderich, K., Stott, L., Tachikawa, K., Tappa, E., Thunell, R., Wara, M., Weldeab, S., and Wilson, P. A., 2004, Interlaboratory comparison study of Mg/Ca and Sr/Ca measurements in planktonic foraminifera for paleoceanographic research: Geochemistry Geophysics Geosystems, v. 5.

Scourse, J. D., Kennedy, H., Scott, G. A., and Austin, W. E. N., 2004, Stable isotopic analyses of modern benthic foraminifera from seasonally stratified shelf seas: disequilibria and the 'seasonal effect': Holocene, v. 14, no. 5, p. 747-758.

Stuiver, M., Reimer, P. J., and Braziunas, T. F., 1998, High-precision radiocarbon age calibration for terrestrial and marine samples: Radiocarbon, v. 40, no. 3, p. 1127-1151.

Thomas, E. R., Wolff, E. W., Mulvaney, R., Steffensen, J. P., Johnsen, S. J., Arrowsmith, C., White, J. W. C., Vaughn, B., and Popp, T., 2007, The 8.2 ka event from Greenland ice cores: Quaternary Science Reviews, v. 26, no. 1-2, p. 70-81.

Thornalley, D. J. R., Elderfield, H., and McCave, I. N., 2009, Holocene oscillations in temperature and salinity of the surface subpolar North Atlantic: Nature, v. 457, no. 7230, p. 711-714.

Chapter 3
The Roles of Winter Insolation and Ocean Dynamics on the Holocene History of the North Atlantic Subpolar Gyre

3.1 Abstract

The North Atlantic Oscillation (NAO) is a prominent weather maker, expected to have varied in the past as well as into the future. One of its major impacts on the ocean is its influence on the extent and temperature of the North Atlantic subpolar gyre. During the last 60 years, when the winter NAO was strong, the SPG expanded and cooled; when the winter NAO was weak, the SPG contracted and warmed. Little is known about the Holocene evolution of the SPG however. To understand the timescales of past variability we investigated six marine sediment cores from the northeastern and eastern reaches of the SPG. We reconstructed temperature and $\delta^{18}O_{sw}$ from paired measurement of $\delta^{18}O_{calcite}$ and Mg/Ca ratios of *Globigerina bulloides*. We observed that through the Holocene, the SPG region warmed and the ice-volume-corrected $\delta^{18}O_{sw}$ values became heavier (saltier). We attribute these trends to the weakening of NAO-like atmospheric circulation in response to increasing winter insolation through the Holocene. However, nearly half the variance in temperature is concentrated at sub-Milankovitch frequencies with variability above and below this trend identified on the basis of temperature and $\delta^{18}O_{sw}$. In the mid-Holocene the SPG went from being predominantly extended to being more contracted. Before the mid-Holocene shift we noted two distinct periods: 10,000 to 8,000 cal yr BP and 8,000 to 6,000 cal yr BP. The SPG was extended in both periods, but we suggest two different mechanisms to explain the extension. During the first interval, the SPG was likely extended because of very strong Westerlies winds and the presence of the freshwater coming from the decaying

Laurentide ice sheet, whereas during the latter interval the SPG was extended because of a combination of strong Westerlies and convection over the Labrador Sea. We identified two periods after the mid-Holocene shift: 6,000 to 4,000 cal yr BP and 4,000 to 800 cal yr BP. Between 6,000 and 4,000 cal yr BP, we suggest that the SPG started to contract due to decreased Westerlies. Between 4,000 and 800 cal yr BP, Westerlies continued to decrease, but increased freshwater from northern sources could have slowed down or shut down the convection of the Labrador Sea. These records add to the growing body of evidence revealing a rich spectrum of NAO variability.

3.2 Introduction

The North Atlantic subpolar gyre (SPG) plays a fundamental role on modern climate. The physical conditions set in the SPG are responsible for transferring heat meridionally via the thermohaline circulation (Hatun et al., 2005). In the SPG region of the North Atlantic, polar water masses from the north meet subtropical Atlantic waters from the south. The SPG regulates the partitioning of the Atlantic and polar water masses on interannual to decadal timescales by contracting and extending (Yashayaev and Clarke, 2008).

The SPG is composed of five surface currents and encompasses three ocean basins. The four surface currents are the North Atlantic Current (NAC), the Irminger Current (IC), the East Greenland Current (EGC), the West Greenland Current (WGC), and the Labrador Current (LC) (Figure 3.1). The NAC is an extension of the Gulf Stream and carries warm saline waters to the high latitudes. The IC branches off the NAC and turns counterclockwise along the SW Iceland shelf before crossing the Irminger Sea.

Here the denser waters of the IC subduct under the fresher, colder waters of the EGC. As the EGC and IC round the southern tip of Greenland, they join and part of the current continues north as the WGC and part of the current turns counterclockwise south and meets the LC. The LC is a cold fresh current coming from Baffin Bay and joining the SPG. The SPG can occupy three ocean basins: the Irminger Basin at the eastern boundary, the Irminger Sea at the northern boundary, and the Labrador Sea at the western boundary.

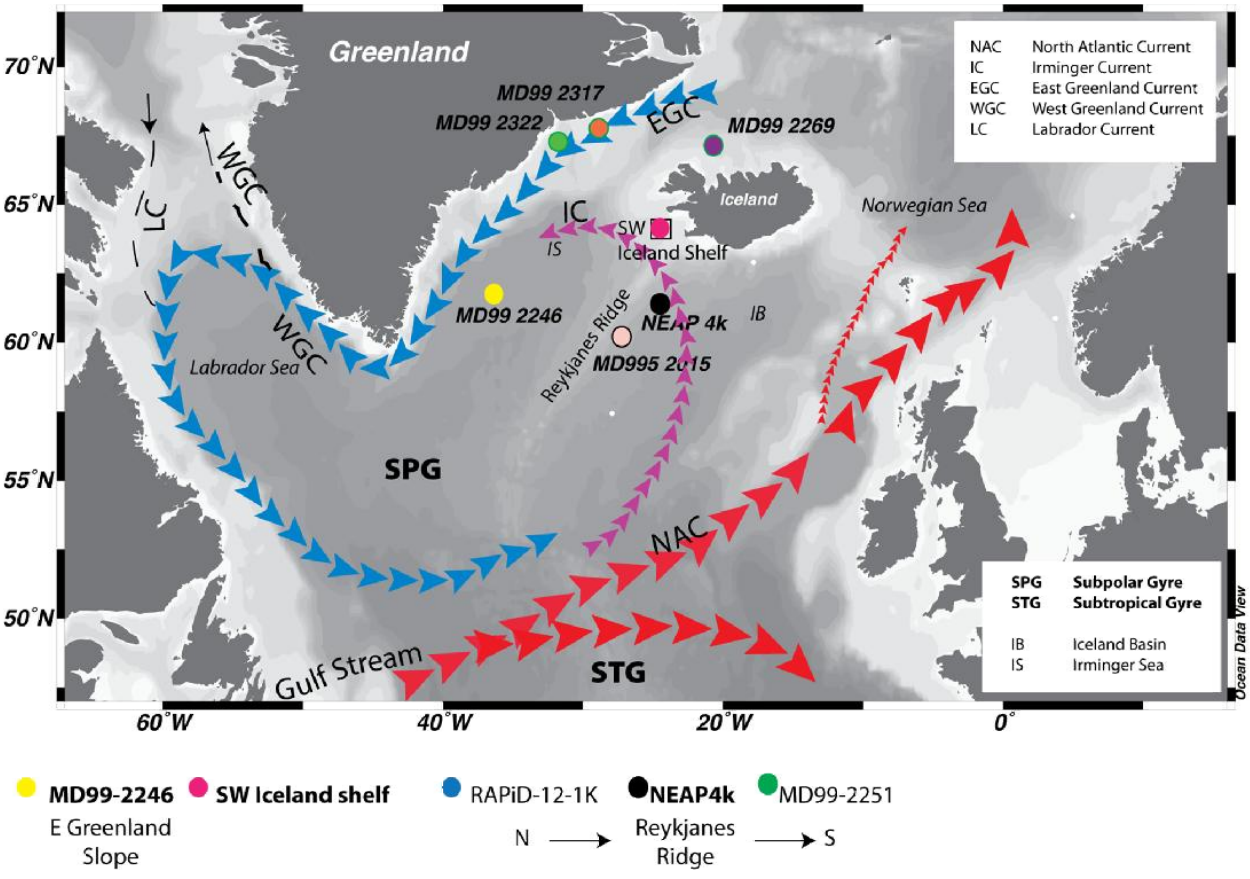

Figure 3.1 Study sites and schematic surface currents in the subpolar North Atlantic. The Gulf Stream, North Atlantic Current (NAC), and Irminger Current (IC) carry predominately warm, salty Atlantic water. The East Greenland Current (EGC), West Greenland Current (WGC), and Labrador Current (LC) carry colder, fresher Polar waters. The Subpolar Gyre (SPG) circulates counterclockwise and the Subtropical Gyre (STG) circulates clockwise in the North Atlanti

The subpolar gyre is located under a persistent atmospheric low-pressure system, the Iceland Low, which is half of the dipole defining the NAO. The NAO is the dominant and recurrent interannual wind variability in the North Atlantic. Its index describes the normalized sea surface atmospheric pressure between the Azores High and the Icelandic Low (Hurrell, 1995). The NAO pattern is most pronounced during the winter months. A positive NAO index describes a greater sea level pressure gradient with westerly surface winds stronger than normal. Interannually, SPG dynamics are driven by wind forcing, particularly during the wintertime, associated with the NAO (Reverdin, 2010). The NAO has been the principal force affecting the sea surface temperatures (SSTs) over the instrumental period (Sarafanov, 2009).

Over the past 50 years the SPG oscillated between two extreme states: an extended mode (high-gyre index) typically associated with positive NAO, and a contracted mode (low-gyre index) typically associated with negative NAO (Sarafanov, 2009). During the extended state, the subpolar front that delineates the southern and eastern boundary of the SPG extends into the Iceland Basin and the water in the eastern Atlantic becomes fresher and colder. With strong Westerlies the IC separates from the NAC after the NAC has crossed the Reykjanes Ridge, leading to a colder and fresher IC. During the contracted state, the subpolar front retreats into the western part of the subpolar Atlantic, and water masses from the subtropical gyre (STG) advance into the Iceland Basin and the water in the south of Iceland becomes more saline and warmer. With weak Westerlies the IC separates from the NAC earlier, leading to a warmer and saltier IC.

The impact of the NAO on the SPG can be overridden by surface freshening over the Labrador Sea, as was the case during the Great Salinity Anomaly (GSA) of 1968-1971 (Dickson et al., 1988). Hydrographic conditions in the Labrador Sea strongly affect SPG dynamics. When the convection over the Labrador Sea was shut down, as for example as a result of the GSA between 1969 and 1971, the SPG weakened and contracted. The shutdown occurred when winters were mild associated with a negative NAO-index. It took a severe winter that caused a large surface heat flux to restart the convection in 1972 and the intensity of the SPG circulation strengthened and the SPG zonally expanded. We would expect that during the early Holocene when freshwater from the Laurentide ice sheet would have inhibited the convection of the Labrador Sea and the SPG dynamics could have been largely decoupled from the NAO.

Given the sensitivity of the modern SPG to wind and freshwater forcing, and its relevance for heat transport and climate in the North Atlantic region, we are interested in its evolution through the Holocene as boundary conditions changed. We aim to reconstruct the SPG through the Holocene by investigating cores near its modern eastern boundary. We hypothesize that the planktonic foraminifer *Globigerina bulloides*, which calcifies in the upper 60m of the water column during the summer months (Schiebel et al., 1997), records SPG dynamics that persisted from the winter into the summer. We measured the oxygen isotopic composition ($\delta^{18}O_{calcite}$) of *G. bulloides*, which is a function of temperature and the oxygen isotopic composition of seawater ($\delta^{18}O_{sw}$). We also measured the Mg/Ca ratios of *G. bulloides*, which is primarily a function of temperature. Knowing the temperature, we then separated the $\delta^{18}O_{sw}$ contribution from the $\delta^{18}O_{calcite}$, lending some insight into the salinity history. Together

the temperature and $\delta^{18}O_{sw}$ records monitor the conservative properties of the seawater, thus the mixing of the water masses and air-sea exchanges over the past 10,000 to 12,000 years.

3.2.1 Marine Sediment Cores

We made measurements on four cores that lie along the northern and northeastern edges of the present-day SPG. The MD-cores (10-cm diameter Calypso cores) were raised during the 1999 IMAGES V cruise, Leg III, aboard the *R/V Marion Dusfresne* (Labeyrie et al., 2003).

MD99-2246 records conditions at the northern boundary of the SPG. MD99-2246 was collected at the East Greenland slope south of the Denmark Strait at 61°54.7'N and 36°21.5'W from a water depth of 2,750 m, and has a Holocene length of 140 cm. The surface currents at this site are precursors for the currents entering the Labrador Sea from the Irminger Basin.

Two cores were raised on the SW Iceland shelf in the SW-oriented Jökuldjup trough in the outer Faxafloi bay. MD99-2256 was raised at 64°18.19'N and 24°12.40'W from a water depth of 246 m, and has Holocene length of ~320 cm (Ólafsdóttir et al., 2010). MD99-2259 was raised at 63°57.79'N, 24°28.98'W from a water depth of ~385 m, and has a Holocene length of ~270 cm (Jennings et al., 2011). We combine these two cores into a composite record for the SW Iceland shelf (see Chapter 4). The SW Iceland shelf is a good site to monitor the water mass characteristics of the IC as it enters the Irminger Basin. Today the water mass characteristics of the IC are sensitive to SPG dynamics (Holland et al., 2008) and play a role in the stability of the Greenland

ice shelf (Jennings et al., 2011) and the hydrography of the West Greenland Current (Holland et al., 2008).

NEAP4k is located in the Bjorn Drift, located on the eastern flank of the Reykjanes Ridge. NEAP4k, a Kasten core, was raised at 61°05.43'N and 24°10.33'W (1627m water depth) during the 1988 R.R.S *Charles Darwin* Cruise for the North East Atlantic Paleoceanogrpahy and Climate Change (NEAP4KACC) program (McCave, 1994). The site is located in the Bjorn Drift, located on the eastern flank of the Reykjanes Ridge, and has Holocene length of ~182 cm (McCave, 1994)(Hall et al., 2004). The location is ideal to monitor the variability of the NAC and the north/northeastern boundary of the SPG.

We added two existing records to our study sites. Both cores have published Holocene Mg/Ca temperature records based on *G. bulloides*, and are from the eastern flank of the Reykjanes Ridge. RAPiD-12-1k was raised from the South Iceland Rise (62°05.439'N, 17°49.189'W; water depth of 1,938m) (Thornalley et al., 2009). This site is northeast of NEAP4k and a good site to monitor the northeastern boundary of the SPG. The site lies in the flow path of the NAC and during extreme extended modes of the SPG, RAPiD-12-1k should be close to the location where the IC separates from the NAC. The second record is from the Gardar Drift, MD99-2251 (57°26.87'N; 27°54.47'W; 2620m water depth) (Farmer et al., 2009). This site lies south of NEAP4k and records the southeastern boundary of the SPG.

3.2.2 Modern Relation of Each Site to SPG Dynamics

Modern surface temperature data at our sites between 1950 and 2012 showed that temperatures are closely tied to SPG dynamics (Figure 3.2). The state of the SPG

and its impact at our study sites was assessed using the monthly mean June-July-August SSTs from 1950 to 2012 from the Merged Hadley-OI.v2 SST and Sea Ice Concentration data set (Hurrell et al., 2008). The five sites we are investigating are situated along the east Greenland slope (MD99-2246), the SW Iceland shelf (MD99-2256 and MD99-2259 composite), and the eastern flank of the Reykjanes Ridge (RAPid-12-1k, NEAP4k, and MD99-2251 from north to south). All sites overall display the same trend: relatively warm temperatures from 1950 to the late 1960s, followed by colder temperatures lasting to the mid 1990s, and warmer temperatures after the mid-1990s, culminating at ~2008 with the highest temperatures in that time period. The temperature range was ~2°C from the coldest to the warmest temperatures, with the MD99-2246 displaying the largest range of ~2.5°C.

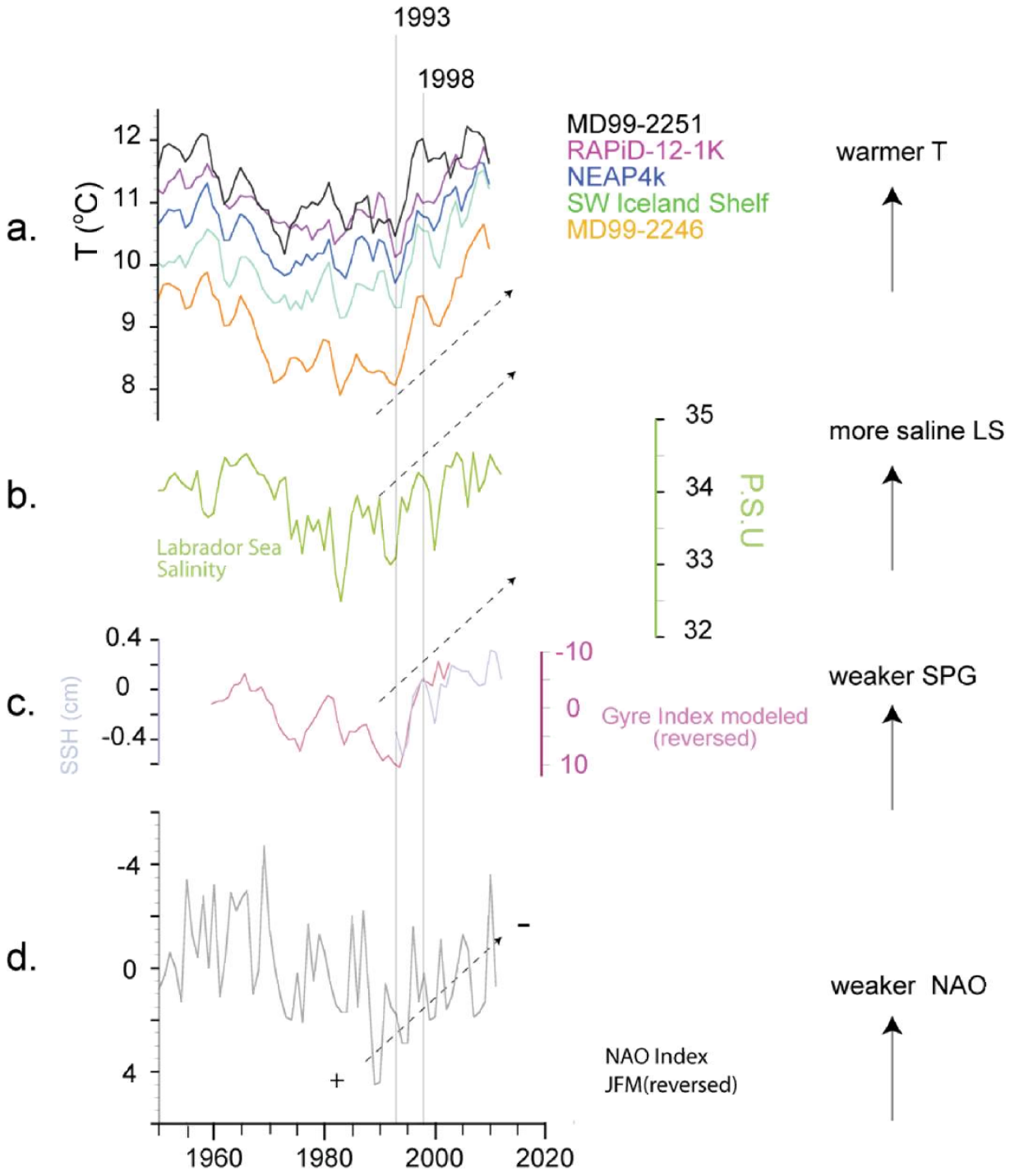
1993
1998
a.
T (°C)
12
11
10
9
8
MD99-2251
RAPiD-12-1K
NEAP4k
SW Iceland Shelf
MD99-2246
warmer T
b.
Labrador Sea
Salinity
35
34
33
32
P.S.U
more saline LS
c.
SSH (cm)
0.4
0
-0.4
-10
0
10
Gyre Index modeled
(reversed)
weaker SPG
d.
-4
0
4
+
-
NAO Index
JFM(reversed)
weaker NAO
1960
1980
2000
2020

Figure 3.2 Oceanic and atmospheric changes between 1950-2012. Comparison of SSTs at our sites to Labrador Sea salinity, SPG gyre index and winter NAO. Panel a: The SSTs for our sites were averaged for June, July, and August and the 3-year running means are displayed. Panel b: the annual summer salinity series (10-30 m) for the Labrador Sea is shown (courtesy of Igor Yashayaev). Panel c: annual gyre index (inverted axis) as modeled by Hatun et al. (2005) and the first EOF of the observed sea surface height from the eastern North Atlantic (Hatun et al. 2005) (Courtesy of Hjálmar Hátun). Panel d: annual January, February, March NAO index (inverted axis) (Hurrell, 1995). he vertical lines indicate a high-gyre index year (1993) and a low-gyre index year (1998), identified by Hatun et al. (2005). The January and August sea surface temperature patterns for these two years are shown in Figure 3.3.

The SPG changed on decadal to multidecadal timescales in this short instrumental record. Comparing sea surface height in the SPG region from altimetry data with direct current meters in the boundary current of the Labrador Sea revealed that the SPG circulation weakened since the early 1990s. Hatun et al. (2005) noted substantial changes in temperature and salinity in the Rockall Trough in the northeastern Atlantic related to the intensity and shape of the SPG. In the early 1990s, when the gyre index was high, the SPG had an overall east-west shape with “protrusions” into the northeastern North Atlantic basin. All of our sites recorded cold temperatures during this zonal extension of the SPG. By the late 1990s the gyre index was low and the SPG contracted towards the western North Atlantic, west of the Mid-Atlantic ridge, and had a less zonal shape. All of our sites recorded warmer temperatures during this interval. This warming is in accordance with a negative NAO index (Figure 3.2d).

The persistence of wintertime NAO forcing through the summer is illustrated in Figure 3.3, which shows the SPG in January and August 1993 (a high-gyre index year) and in January and August 1998 (a low-gyre index year). During the high-gyre index year that was associated with a positive NAO, the SPG was zonally expanded both in

the winter and in the summer and our study sites cooled. During the 1998 low-gyre index year, the gyre was contracted in the winter and more subtropical waters reached our study sites. We expect that the summer signal in our Holocene reconstructions were influenced by the wintertime conditions.

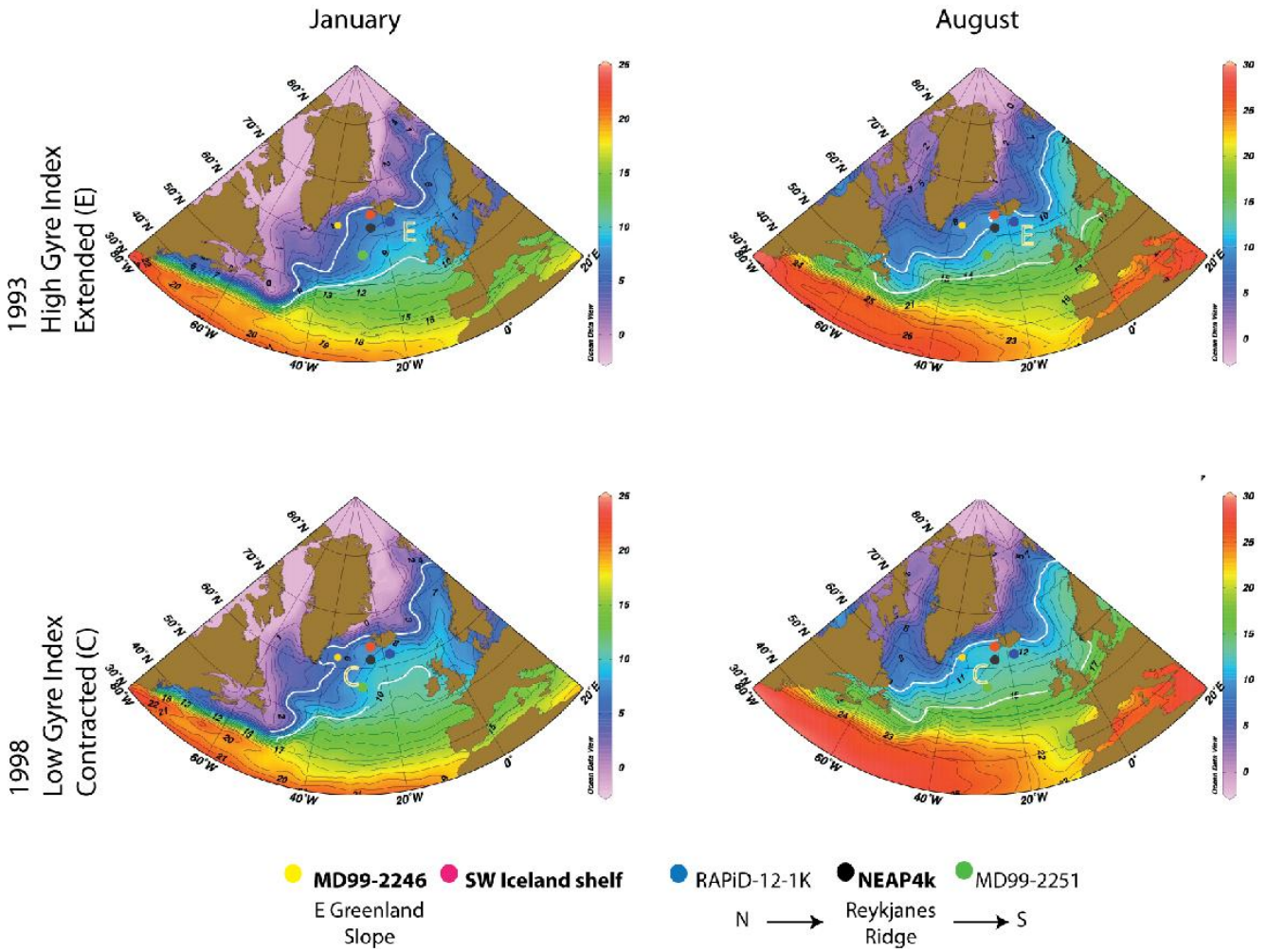

Figure 3.3 Subpolar gyre states. 1993 was a high gyre index year (Hatun et al., 2003) and the SPG was zonally extended. Our study sites are colder both in January and August compared to a low index year. 1998 was a low gyre index year and the SPG was contracted. Our study sites are relatively warm both in January and August compared to the high index years. For January, the 5° and 10°C and for August, the 10° and 15°C isolines are accentuated with white line

3.3 Paleoreconstructions: Methods

3.3.1 Chronology

The core chronologies are based upon accelerator mass spectrometry (AMS) radiocarbon dates on foraminifera and molluscs. The chronology for NEAP4k is based upon thirteen accelerator mass spectrometry (AMS) radiocarbon dates on *G. bulloides* (Hall et al., 2004). As described in Chapter 4, we combined cores MD99-2256 and MD99-2259 into a composite SW Iceland core. The combined age model is based upon 22 AMS radiocarbon dates on foraminifera and molluscs (Table in Ch 4). Radiocarbon dates were calibrated using the marine model curve of CALIB Version 6.0 (http://radiocarbon.-pa.qub.ac.uk/calib/) (Stuiver et al., 1998). We assumed $\Delta R=0$, corresponding to an average ocean reservoir age of ~400 years (Eiriksson et al., 2004; Kristjansdottir, 2005), with an uncertainty of ± 50 years in ΔR. The ages between the calibrated ^{14}C dates were calculated by applying a 0%-weighted fit though the median probability ages. The published ages for NEAP4k (Hall et al., 2004) were recalculated by applying the same method as for the SW Iceland composite core. Ian Hall provided the ages of the sample depths for MD99-2246.

3.3.2 Geochemical Analysis: Stable Oxygen Isotopic and Mg/Ca Ratios on *G. bulloides*

G. bulloides is a subpolar to transitional species that also has been associated with upwelling areas (e.g. (Be and Tolderlund, 1971). In the present day North Atlantic, *G. bulloides* thrives within the near-surface seasonal mixed layer (between 0 and 50 m water depth) (Ganssen and Kroon, 2000) with calcification depths within the upper 60 m

in the eastern N. Atlantic (Schiebel et al., 1997). The calcification season of *G. bulloides* is dependent on the timing of the phytoplankton bloom, which typically occurs May to June (Fennel et al., 2011; Ganssen and Kroon, 2000). *G. bulloides* abundance might not be a good temperature indicator but a rather a high nutrient indicator (Ganssen and Kroon, 2000).

We used *G. bulloides* from the 150-250 micron size fraction for both stable oxygen isotope and Mg/Ca ratio analyses. Between six and ten individuals of *G. bulloides* were submitted for each stable isotope analysis. The results are given in conventional delta notation in ‰ relative to the VPDB standard. The samples for MD99-2256 were run in the Curry lab at the Woods Hole Oceanographic Institution. Measurements were made on a Finnigan MAT 252 mass spectrometer with a Kiel Carbonate Device with precision better than 0.07‰. The samples for MD99-2259 were run at the Quinn lab at the Jackson School of Geosciences at the University of Texas at Austin. Measurements were made on a Thermo 253 with a Kiel IV carbonate device with a precision better 0.07‰. The results for isotopic analysis for NEAP4k were published in Hall et al., 2004.

Mg/Ca ratios were measured on a Thermo-Finnigan Element 2 magnetic-sector single-collector ICP-MS, following methods of (Marchitto, 2006; Rosenthal et al., 1999). Approximately 50 *G. bulloides* per sample were crushed between two class plates to open the chambers to the cleaning reagents. Mg/Ca samples were cleaned reductively and oxidatively, in a Class-1000 clean lab, according to the cleaning protocol from Boyle and Keigwin (1985) and modified by (Boyle and Rosenthal, 1996) and Boyle and

Rosenthal (1996). Long-term 1 sigma precision for Mg/Ca ratios is 0.5% (Marchitto, 2006).

G. bulloides have open chambered tests and therefore are prone to being packed with fine grained contaminants. Because of numerous active volcanoes on Iceland, tephra shards occur commonly in the surrounding marine sediments. The high Mg content of the tephra can lead to overestimation of paleotemperature if tephra contamination is not adequately removed from the foraminifera tests. Extra care was given to pick only clean tests of *G. bulloides* where possible. After crushing the tests, all visible tephra was removed with a fine brush. This method worked well in the NEAP4K4K core. However, many of the *G. bulloides* in MD99-2256, the core from the SW Iceland shelf and closest to land of all our study sites, were packed with tephra-rich sediments. The first step in the regular cleaning protocol is designed to remove clay-size contaminants and was not sufficient to get rid of the tephra fragments. As a result, initial Mg/Ca measurements in MD99-2256 were very elevated.

We experimented with various cleaning techniques in MD99-2256, but even with the most rigorous cleaning method, tephra contamination remained an issue. The most vigorous approach included transferring the crushed samples to leached microvials and filling the microvials with ultrapure water. The samples were heated in a water bath for 30 minutes and ultrasonicated for 30 minutes. The water then was siphoned out of the microvials and refilled with ultraclean water before repeating the heating and ultrasonification process. This process was repeated for a total of four times before each microvial was emptied onto 63micron sieve. All visible tephra fragments and test fragments with adhering tephra shards were discarded. The remaining test fragments

were transferred into new leached microvials and the regular cleaning protocol started. This method was not only time consuming but also caused a lot of material to be lost. A total of 73 samples were analyzed for MD99-2256.

MD99-2259, from the SW Iceland shelf, showed some visible tephra contamination, and therefore, we added one step prior to starting the regular cleaning protocol. We heated the crushed samples in a water bath for 60 minutes, ultrasonicating every 10 minutes for 2 minutes to loosen any foreign sediment grains from the tests (Yair Rosenthal, personal comm., 2011). For MD99-2259, 144 samples were run. The same method as for MD99-2259 was used for the MD99-2246 core. We ran 106 samples for MD99-2246. The NEAP4k core was run according to the regular cleaning protocol and no special measures were taken for potential tephra contamination. For NEAP4k, a total of 169 samples were run.

3.3.3 Influence of Tephra on Mg/Ca Ratios

Tephra shards and layers are commonly found in marine sediments around Iceland, which has a well-documented Holocene past of explosive volcanic activity (e.g.(Jennings et al., 2014)). Jennings et al. (2014) documented the covariance between Al, Fe, and Mg in Icelandic tephras. To ensure that the Mg in the *G. bulloides* samples is primary rather than detrital, Fe and Al, two elements commonly associated with post-depositional contamination, were also measured. Many of our samples were elevated in Fe and Al, which we attribute primarily to tephra contamination.

In three of our cores, *G. bulloides* Fe/Ca and Al/Ca are strongly correlated (Figure 3.4) suggesting a uniform dominant source (possibly multiple Icelandic volcanoes with similar chemistry) for the tephra contaminants in each core. The cores

MD99-2256 and MD99-2259 from the SW Iceland shelf, and NEAP4k from the Reykjanes Ridge, show similar Fe:Al slopes and intercepts, with MD99-2259 and NEAP4k being almost identical. The core from the SE Greenland slope, MD99-2246, has a different slope and intercept, and a weaker correlation, which suggests multiple source volcanoes with disparate chemistries.

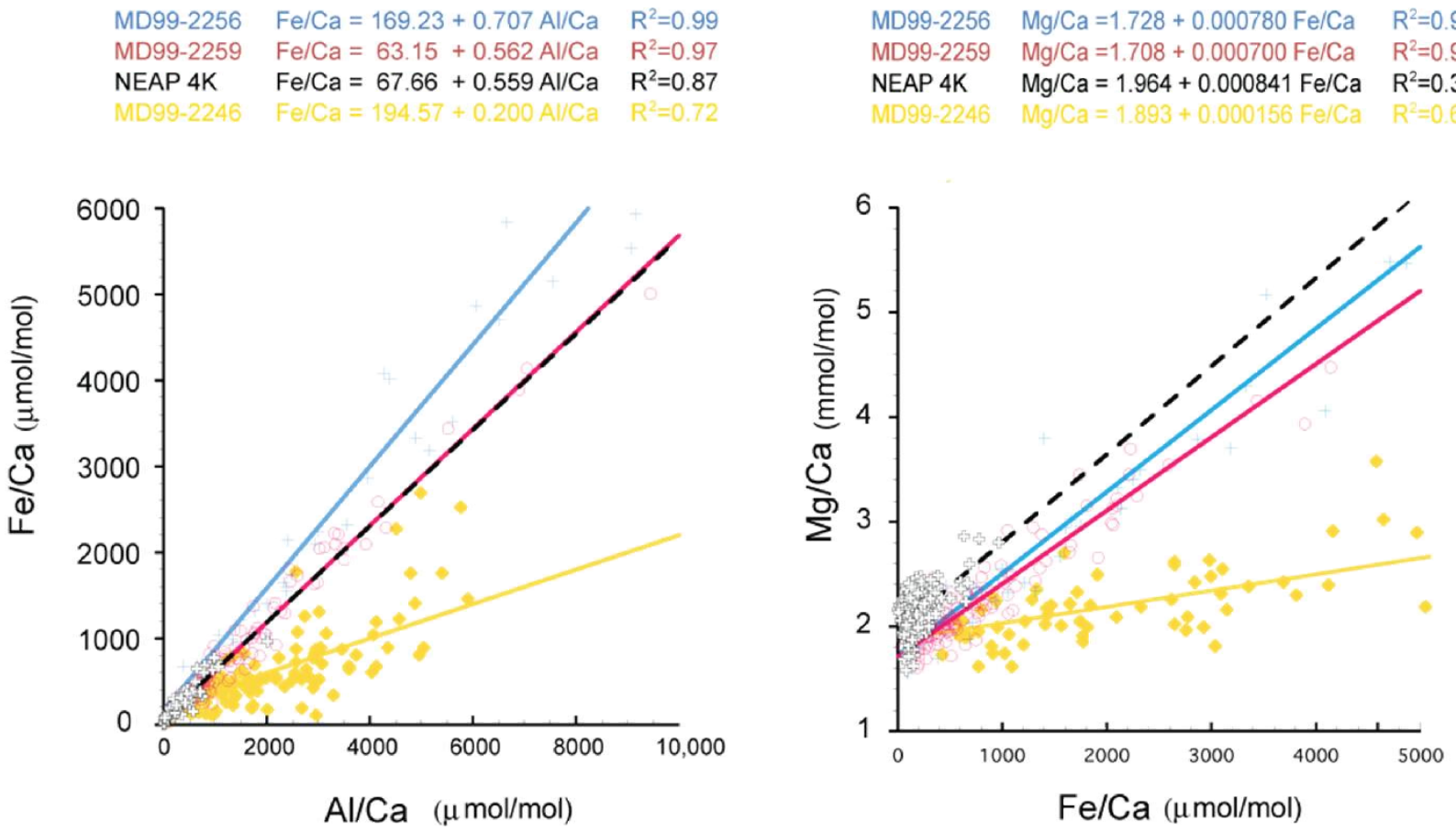

Figure 3.4 Tephra contamination. Correlations between measured Fe/Ca and Al/Ca, and Mg/Ca and Fe/Ca in individual analyses. Left graph: The strong correlation in MD99-2256, MD99-2259, and NEAP4k indicates that the tephras in each core were dominated by a single source. The samples with Fe in excess of the Fe:Al intercept suggests that tephra contamination is present. Right graph: The slope of the regression between Mg/Ca and Fe/Ca was used to correct samples with Fe/Ca ratios < 5000 mmol/mol

We adopted the strategy used by (Lea et al., 2005) to determine the primary Mg in tests before converting the Mg/Ca ratios into temperature. This process assumes that Fe in excess of the intercept of the Fe:Al regression is detrital (tephra) and that this material has a characteristic Mg/Fe ratio. The slope of the regression between Mg/Ca and Fe/Ca was used for the correction (Figure 3.4). All regressions were calculated after omitting 2-σ outliers. The Mg in samples with Fe/Ca smaller than the Fe:Al intercept is likely shell-bound Mg and therefore not corrected. Samples with Fe/Ca ratio greater than 5000 micromole/mole were excluded from the final data set. We only employed this method in the SW Iceland (MD99-2256 and MD99-2259) and Reykjanes Ridge (NEAP4k) cores; MD99-2246 could not be corrected because its Fe/Ca and Al/Ca was not very well explained by a linear regression (r^2 = 0.72).

3.3.4 Temperature and $\delta^{18}O_{sw}$ Reconstructions

The paired measurement of $\delta^{18}O_{calcite}$ and Mg/Ca ratios allows the Mg/Ca-based temperature to be used to isolate the $\delta^{18}O_{sw}$ contribution to the $\delta^{18}O$ signal in the calcite (e.g. (Elderfield and Ganssen, 2000; Lea, 2002; Mashiotta et al., 1999). This method has the advantage that the same phase (i.e. *G. bulloides*) is used for both measurements. In contrast, temporal and spatial distributions can become an issue when foraminiferal assemblages or alkenone-derived SSTs are combined with foraminiferal $\delta^{18}O_{calcite}$ measurements to reconstruct $\delta^{18}O_{sw}$, because the two proxies may carry two different environmental signals such as different seasons and different habitat depths.

The $\delta^{18}O$ of calcite reflects the $\delta^{18}O$ of seawater the foraminifera calcified in, in addition to the temperature-dependent fractionation during the calcification process. Mg ion incorporation into the calcite lattice is primarily a function of temperature at the time of calcification (Nurnberg et al., 1996; Rosenthal et al., 1997), but a salinity contribution to the Mg ion incorporation may play a role (Ferguson et al., 2008). The salinity contribution to the Mg signal is small, ~3-5% per salinity unit in laboratory-cultured planktonic foraminifera experiments (Honisch et al., 2013), compared to the ~10% per °C temperature. Honisch et al. (2013) argued that the salinity contributions to the Mg signal seen in recent field studies (Arbuszewski et al., 2010; Ferguson et al., 2008; Mathien-Blard and Bassinot, 2009) were overestimated and are likely caused by other environmental effects. Since it is not straightforward (Honisch et al., 2013) to correct Mg/Ca for the small salinity effect, we do not attempt to do so here. Partial dissolution in carbonate-undersaturated waters could potentially influence the Mg/Ca ratios of planktonic shells, but this effect is minimal in the shallow North Atlantic where bottom waters are supersaturated.

Our cleaning protocol includes a reductive cleaning step that yields slightly lower Mg/Ca ratios than in oxidative-only cleaning protocols. Therefore a correction is required if we want to compare data sets generated by these two different protocols. The analytical offset between the two different cleaning protocols can be corrected by either adding 0.2 mmol/mol (Elderfield et al., 2006) or 10-15% (Barker et al., 2003; Rosenthal et al., 2004) to the measured the Mg/Ca ratios in the reductively cleaned samples. We chose the 10% correction because it seems to be more realistic for cold temperatures where Mg/Ca is relatively low. This allows us to compare our data to the

oxidatively cleaned *G. bulloides* of Thornally et al. (2009) and Farmer et al. (2008), and to use temperature calibrations that were based on oxidatively cleaned samples.

Several Mg/Ca temperature calibrations for *G. bulloides* have been developed (Barker and Elderfield, 2002; Lea et al., 1999; Mashiotta et al., 1999). Applying these calibrations for temperature reconstructions showed temperature differences of several degrees depending on the calibration chosen. Mg/Ca temperature calibrations of planktonic foraminifera, including *G. bulloides*, show an exponential relationship written in the general form:

$$Mg/Ca = Ae^{0.1T} \qquad \text{Equation 3.1}$$

where T is the calcification temperature (°C) and A is a constant (Ganssen and Kroon, 2000). Previous studies using *G. bulloides* in the North Atlantic used the values 0.72 (Barker and Elderfield, 2002; Farmer et al., 2005) and 0.794 (Thornalley et al., 2009) for the pre-exponential coefficient A. We chose a mid-range value of 0.75 and applied it to all Mg/Ca data shown here, including the published data from Thornalley et al. (2009) and Farmer et al. (2008).

The $\delta^{18}O_{sw}$ was calculated using a species-specific equation for *G. bulloides* (Bemis et al., 1998).

$$T(°C) = 13.2 - 4.89(\delta^{18}O_{calcite} - \delta^{18}O_{sw}) \qquad \text{Equation 3.2}$$

Equation 3.2 was developed from cultured *G. bulloides* and the results compared well with core top data (Bemis et al., 1998). The changing global ice volume affected the $\delta^{18}O_{calcite}$ and the $\delta^{18}O_{sw}$ through the early to mid-Holocene, which we will discuss in section 3.4.2.

3.4 Results and Discussion of the Holocene Records

3.4.1 Mg/Ca Temperature Records

At all sites the Holocene temperature ranges inferred from Mg/Ca ratios of *G. bulloides* bracket and exceed modern (1950-2012) summer temperature ranges (Figure 3.2 and Figure 3.5). In the modern data set, the colder temperatures were associated with an extended SPG and the warmer temperatures with a contracted SPG, and our Holocene interpretations will follow that pattern. On the SW Iceland shelf, the modern temperatures ranged from 8.4 to 11.7°C, compared to 5.2 to 13.8°C between ~800 and 10,300 cal yr BP, with the majority of the data (~70%) falling within the modern range. Only two data points indicated warmer temperatures than the modern, but ~30% were lower than the modern range. The majority of the temperatures colder than present occurred between ~6000 and 9,500 cal yr BP.

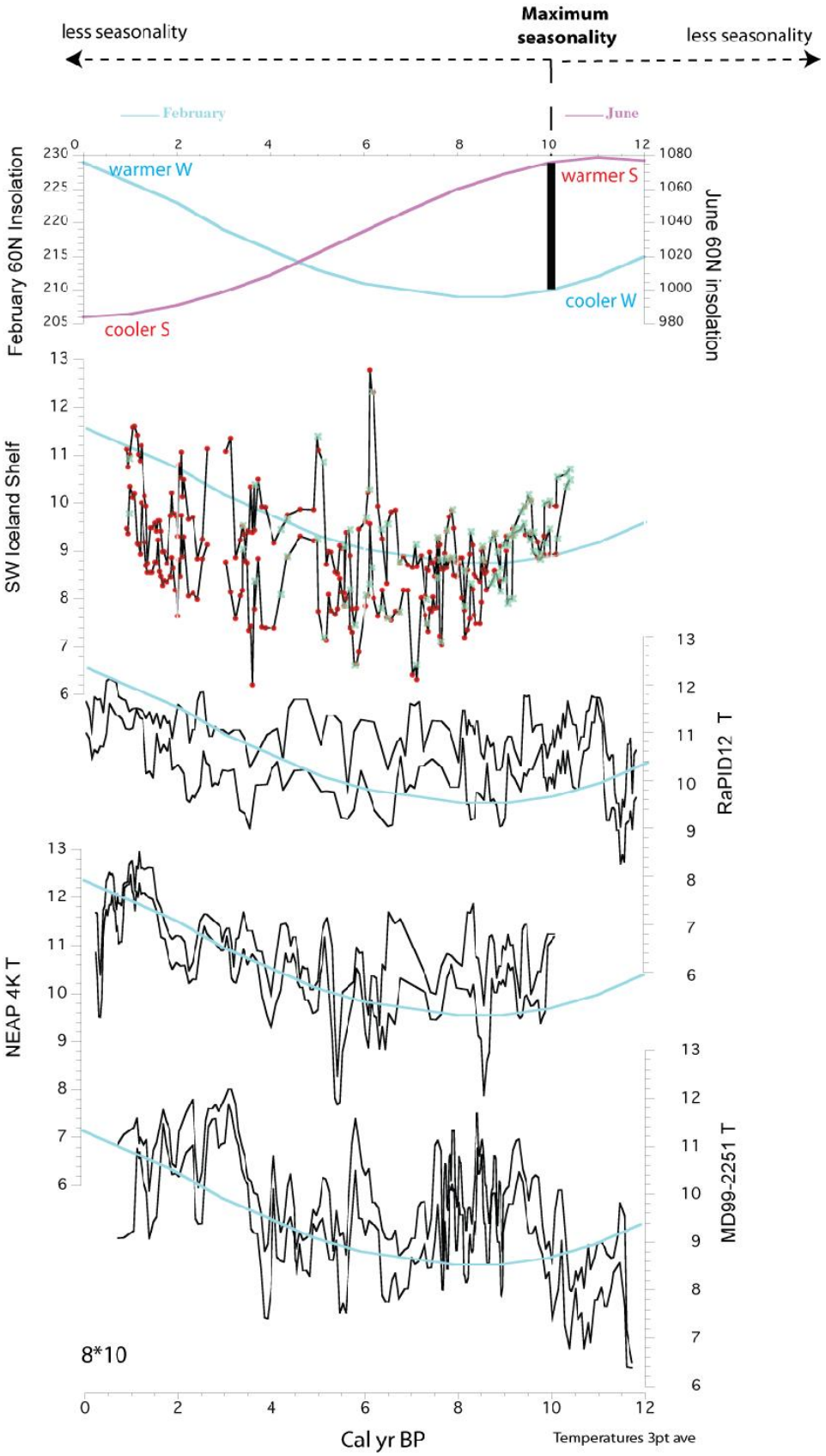
less seasonality
Maximum seasonality
less seasonality
February
June
February 60N Insolation
June 60N insolation
warmer W
warmer S
cooler W
cooler S
SW Iceland Shelf
RaPID12 T
NEAP 4K T
MD99-2251 T
8*10
Cal yr BP
Temperatures 3pt ave

Figure 3.5 The long-term trend in the temperature records appears to follow winter insolation rather than summer insolation. Winter insolation and summer insolation at 60N are shown in the top panel. The seasonality was largest in the early Holocene and decreased through the Holocene. The temperature envelopes shown here were calculated from the Standard Error of the Mg/Ca measurements. The SW Iceland core is a composite of the cores: MD99-2256 (green circles) and MD99-2259 (red circles).

At the RAPiD-12-1k site (Thornalley et al., 2009), the modern temperatures ranged from ~9.6 to 12.3°C (Figure 3.2). The temperatures between 12,000 and 0 cal yr BP ranged from ~8 to 12.5°C, with 81% of the data falling within the modern range. Only two data points exceeded modern temperatures and ~19% were lower than the modern range. The majority of the temperatures colder than present occurred in the early and mid Holocene. The coldest interval occurred between ~12,000 and 10,800 cal yr BP. Colder than present temperatures were recorded between ~10,000 and 3,500 cal yr BP.

At the NEAP4k site, the modern temperatures ranged from 9.2 to 11.8°C. The temperatures between 10,300 and 300 cal yr BP ranged from 7.4 to 13.3°C, with ~80% of the data falling within the modern range. Less than 1% of the data indicated cooler temperatures than today and ~20% were warmer than today. The most significant jump to warmer temperatures occurred at ~1,800 cal yr BP.

At the MD99-2251 site (Farmer et al., 2008), the modern temperatures ranged from 9.5 to 12.6°C. The temperatures between ~12,000 to 600 cal yr BP ranged from ~6.3 to 12.2°C, with ~54% falling within the modern range. None of the temperatures exceeded modern values, but 46% were colder than today. The coldest intervals occurred between ~12,000 to 9,800 cal yr BP and from ~8000 to 4000 cal yr BP.

In summary, the SW Iceland shelf, Rapid-12-1k, and MD99-2251 were rarely warmer than present but often cooler than present (~30%, ~19%, and ~46%,

respectively) and only the NEAP4k core was rarely cooler than today, but ~20% of the time warmer than today. During the 1950-2012 interval we analyzed, all our study sites cooled or warmed simultaneously, which was not always the case during the Holocene.

Most striking is the fact that all records generally show a cooler early to mid-Holocene and a warmer late Holocene, and the long trend is consistent with winter insolation forcing, with presumably colder winters in the early Holocene and warmer winters in the late Holocene (Figure 3.5). As noted above, wintertime forcing likely persisted into spring and summer when *G. bulloides* calcifies.

3.4.2 $\delta^{18}O$ of Calcite and of Seawater

The temperature from the Mg/Ca ratios in *G. bulloides* was used to separate the $\delta^{18}O_{sw}$ contribution in the $\delta^{18}O_{calcite}$, using equation 3.2. In this section, we are presenting the $\delta^{18}O_{calcite}$ (Figure 3.6) and the $\delta^{18}O_{sw}$ (Figure 3.7) both uncorrected and corrected for global ice volume. The discrepancy between the corrected and uncorrected values is largest in the early Holocene as the melt water of the decaying Laurentide ice sheet affected the $\delta^{18}O$ of the ocean water until ~6000 cal yr BP (Andersen et al., 2004a; Andersen et al., 2004b; Ellison et al., 2006; Jennings et al., 2011).

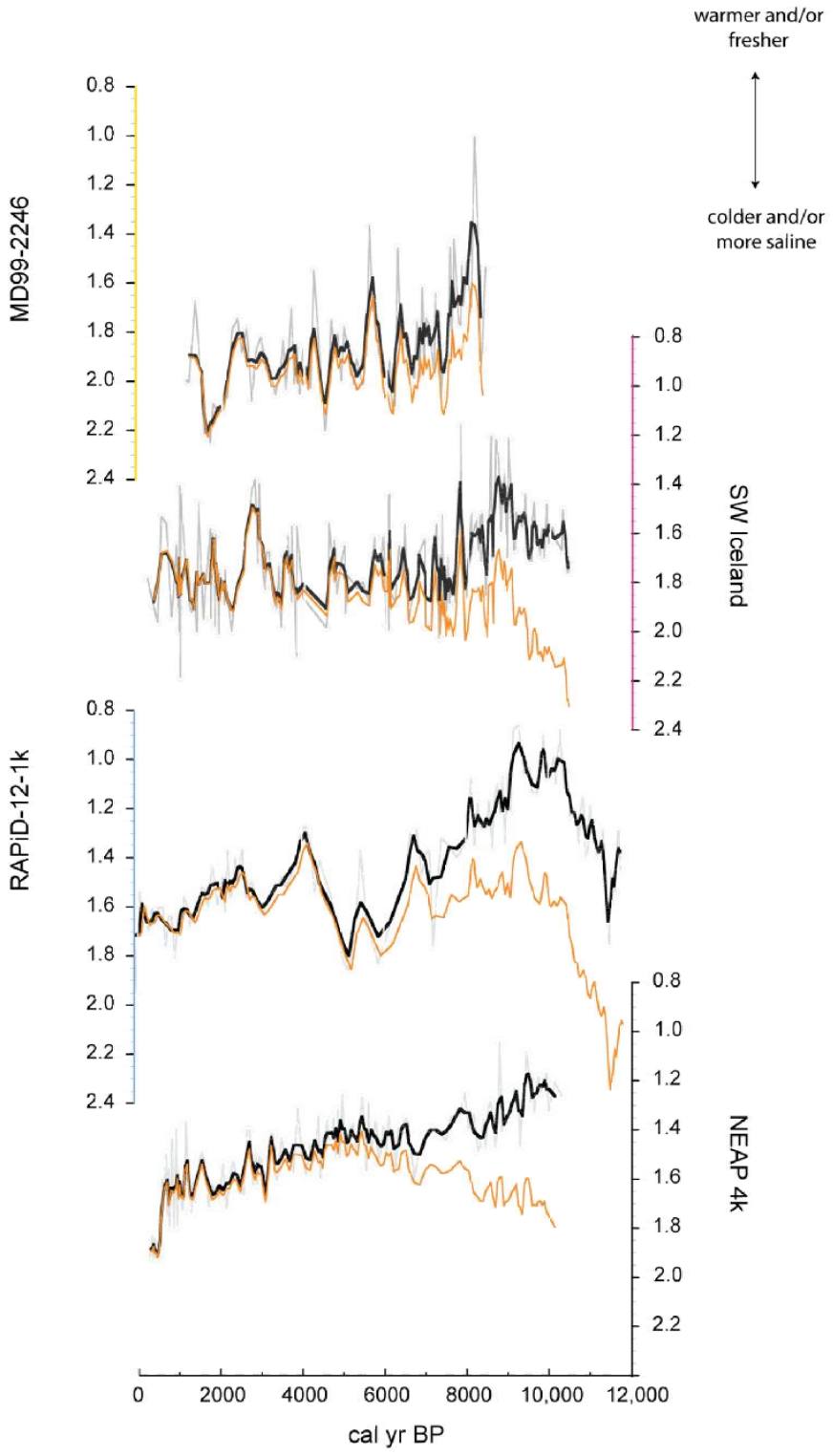

Figure 3.6 $\delta^{18}O_{calcite}$ for MD99-2246, the SW Iceland shelf, RAPiD-12-1k, and NEAP4k. The $\delta^{18}O_{calcite}$ is presented both corrected for global ice volume (individual measurements: gray lines with open circles; 3-point running mean: black line) and uncorrected (3-point running mean: orange line).

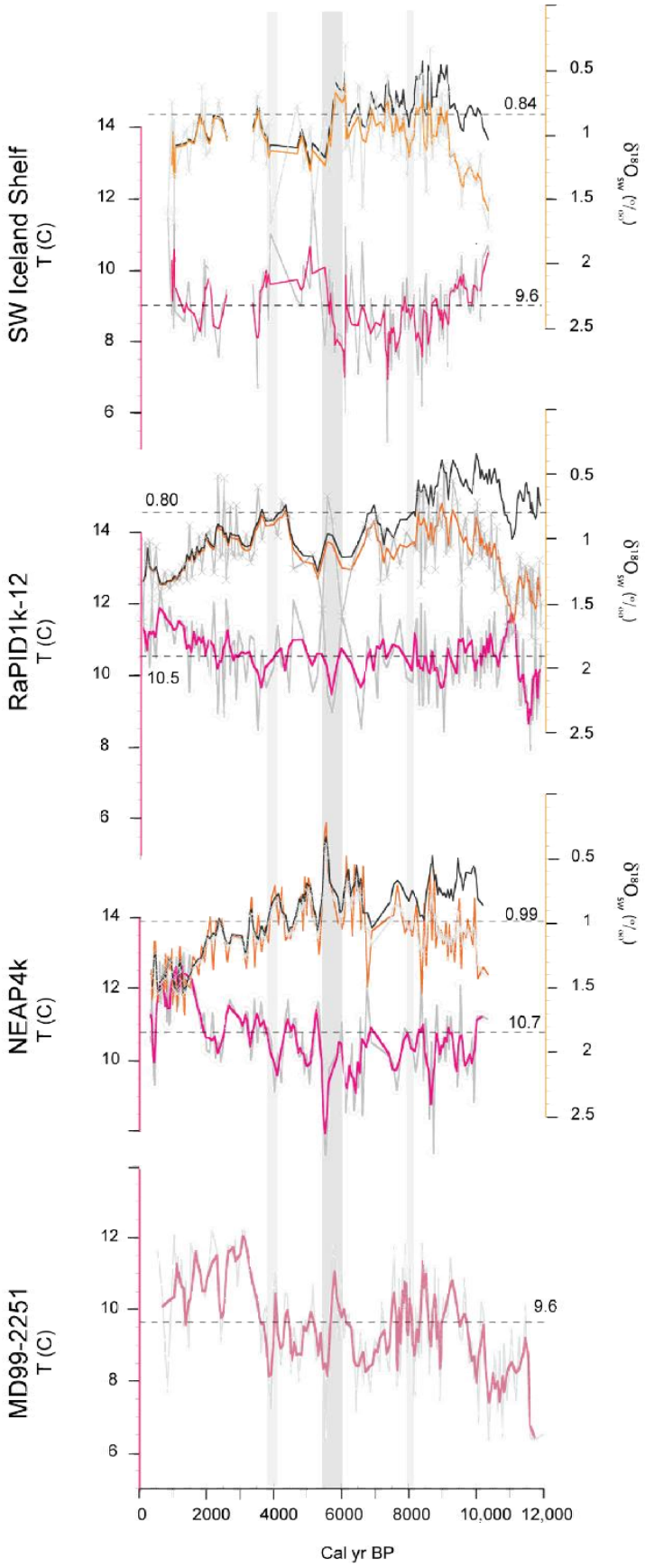
SW Iceland Shelf
T (C)
0.84
9.6
RaPID1k-12
T (C)
0.80
10.5
NEAP4k
T (C)
0.99
10.7
MD99-2251
T (C)
9.6
δ18Osw (‰)
0.5
1
1.5
2
2.5
14
12
10
8
6
0
2000
4000
6000
8000
10,000
12,000
Cal yr BP

Figure 3.7 Temperature and $\delta^{18}O_{sw}$ reconstructions. For each core, the Mg/Ca temperature (gray lines with open circles) and the 3-point running mean (red lines) are shown. The $\delta^{18}O_{sw}$ reconstructions are shown for the SW Iceland shelf, for RaPID1k-12 and NEAP4k. The $\delta^{18}O_{sw}$ is shown both uncorrected for sea level (gray lines with x-symbols) with the 3-point running mean (orange lines) and corrected for sea level (only 3-point running mean is shown, black line). Horizontal dashed lines indicate the mean of the mean temperature and $\delta^{18}O_{sw}$ calculated from the Rodinov regime shift. Gray vertical bars divide cores into time slices discussed in section 3.4.5.

During glacial times, ^{18}O-depleted water was evaporated from the ocean and stored on land, resulting in isotopically light water being stored in ice sheets and isotopically heavy water remaining in the ocean. In climate reconstructions, this ice volume effect is often removed by subtracting 0.11‰ per 10m sea level change from the measured $\delta^{18}O_{calcite}$ as suggested by Fairbanks (1989). Once the global signal has been removed, the residual should reflect a combination of temperature and local $\delta^{18}O_{sw}$ (if its history differed from that of the global mean) impacts on the $\delta^{18}O_{calcite}$. But in the North Atlantic we are interested in the impact of deglacial meltwater on the SPG, so there is an argument for not making any ice volume correction. Furthermore the correction method assumes an average isotopic composition of ~-42‰ of the melt water coming off the ice sheet (Fairbanks, 1989), and does not factor in that the isotopic composition of the ice sheet changed over time, from heavy values in the early stages of growth toward lighter values in later stages (Sima et al., 2006). In Figure 3.7 the uncorrected (orange) curve should be interpreted as the actual $\delta^{18}O_{sw}$ present at each site, while the corrected (black) curve is some measure of local $\delta^{18}O_{sw}$ change. The former includes the fact that the entire ocean was saltier and isotopically heavier during

the LGM, while the latter is meant to isolate changes relative to what the mean ocean experienced.

We expect large variations in $\delta^{18}O_{calcite}$ and $\delta^{18}O_{sw}$ in this dynamic region where water masses meet. In the MD99-2246 core, which is the coldest site in the modern data set, the $\delta^{18}O_{calcite}$ ranges from 1.26 to 2.27‰ (uncorrected) and from 1.00 to 2.25‰ (corrected). The lightest value occurred at ~8,300 cal yr BP. At ~7,700 cal yr BP, the overall light interval of $\delta^{18}O_{calcite}$ ends. There are, however, some light excursions centered around ~6,400, 5,700, and 4,300 cal yr BP. The heaviest $\delta^{18}O_{calcite}$ occurred at ~1,800 cal yr BP. This data point falls within an interval (2,200 to 1,600 cal yr BP) of relatively heavy $\delta^{18}O_{calcite.}$ The general trend after ~7,700 is towards heavier $\delta^{18}O_{calcite}$ in the corrected data set, whereas in the uncorrected data set the $\delta^{18}O_{calcite}$ shows no trend. No $\delta^{18}O_{sw}$ data is available because of the tephra contamination of Mg/Ca.

On the SW Iceland shelf, the $\delta^{18}O_{calcite}$ values range from 1.31 to 2.19‰ (uncorrected) and from 1.28 to 2.19‰ (corrected) and the $\delta^{18}O_{sw}$ range from 0.31 to 1.73‰ (uncorrected) and from 0.06 to 1.68‰ (corrected). A very light $\delta^{18}O_{calcite}$ occurred at ~2,700 cal yr BP but we don't have any $\delta^{18}O_{sw}$ available to represent this peak.

For the RAPiD-12-1k site, the $\delta^{18}O_{calcite}$ values range from 0.86 to 1.95‰ (uncorrected) and from 0.85 to 1.95‰ (corrected). This data set is characterized by a interval with heavy isotopic values centered around 6000 cal yr BP.

For the NEAP4k site, the $\delta^{18}O_{calcite}$ values range from 1.31 to 1.93‰ (uncorrected) and from 1.04 to 1.92‰ (corrected). The $\delta^{18}O_{sw}$ values range from 0.22 to 1.17‰ (uncorrected) and from 0.22 to 1.71‰ (corrected). The trend in the corrected data set can be best described by a trend from lighter isotopic values in the early

Holocene to heavy isotopes in the late Holocene. The trend in the uncorrected data set can be best described by a 2nd order polynomial with the lightest interval occurring in the mid-Holocene.

A linear $\delta^{18}O_{sw}$:salinity relationship for the present-day North Atlantic suggests a slope of 0.55 and an intercept of -18.98 (LeGrande and Schmidt, 2006). If we were to apply this linear relationship throughout the Holocene, the difference in P.S.U. at our sites from the early to late Holocene was ~0.5 (uncorrected for global ice volume; early Holocene S=35.4 P.S.U.) and ~0.9 (corrected for global ice volume, early Holocene S=35.8 P.S.U.). However the $\delta^{18}O_{sw}$:salinity relationship likely differed substantially from the early Holocene to the late Holocene, so we will not attempt to reconstruct the salinity from the $\delta^{18}O_{sw}$ values.

We do not have modern salinity measurements for our study sites, but from the salinity series of the Labrador Sea, we see that colder temperatures generally corresponded with fresher waters and warmer temperatures with more saline waters (Figure 3.2). Today our study sites are more influenced by warm, more saline Atlantic waters when the SPG is contracted and more influenced by cold, fresher polar waters when the SPG is extended (Hatun et al., 2005). We see the same relationship in the Holocene record: when the temperatures were warmer, the $\delta^{18}O_{sw}$ was heavier and when the temperatures were cooler, the $\delta^{18}O_{sw}$ was lighter (Figure 3.7)).

The averages of the corrected global ice volumes $\delta^{18}O_{sw}$ values were determined by the means from the (Rodionov, 2004) regime shifts , providing a way to describe Holocene trends. The means of the $\delta^{18}O_{sw}$ for the SW Iceland shelf and RAPiD-12-1k were similar (~0.84 and ~0.80‰, respectively), and the mean for the NEAP4k record

was heavier (~0.99‰) (no $\delta^{18}O_{sw}$ data available for MD99-2251). The heavier $\delta^{18}O_{sw}$ values for the NEAP4k core suggest that this site was influenced by more Atlantic waters than the two more northern cores were, which agrees with the temperature reconstructions. The coldest temperatures and the lightest $\delta^{18}O_{sw}$ values were recorded between 9,500 and 6,000 cal yr BP in the SW Iceland shelf. The lightest $\delta^{18}O_{sw}$ values in the RAPiD-12-1k core were recorded in the early Holocene, terminating at ~8,200 cal yr BP. This shift was not recorded in the temperature. The temperatures remained relatively cold until ~3,500 cal yr BP, when they started to warm and the $\delta^{18}O_{sw}$ values became heavier. The NEAP4k core remained fairly fresh until ~4,000 cal yr BP. At ~4,000 cal yr BP, the $\delta^{18}O_{sw}$ values became heavier with a sudden shift towards even heavier $\delta^{18}O_{sw}$ values occurring at ~1,800 cal yr BP, which is reflected in warming temperatures as well.

3.4.3 Potential Forcings on the Orbital-Scale Trends

In the modern data, these sites respond primarily to the winter NAO, via its influence on the zonal extent of the SPG. Applying these modern patterns to our temperature reconstruction, we suggest that during the early Holocene, atmospheric dynamics during the winter cooled the SPG region more than during the later Holocene. We suggest that these records reflect an orbital-scale trend in the NAO.

Model results from Rimbu et al. (2003) predicted a weakening of the NAO-like atmospheric circulation from the early to late Holocene, leading to a warming in the SPG region. They based their study on alkenone-derived SST records from the North Atlantic, which showed decreasing temperatures in the northeast Atlantic through the

Holocene, but a progressive warming in the subtropical Atlantic, the eastern Mediterranean, and the northern Red Sea, a spatial pattern that is consistent with a weakening NAO. Rimbu et al. (2003) compared these data to atmospheric general circulation model (GCM) simulations, which were solely forced by insolation and CO_2, to infer that NAO indeed weakened through the Holocene. Lower winter insolation in the Northern Hemisphere tropics during the early Holocene led to intensification of both the Azores High and the Icelandic Low. Their study predicted an orbital-scale warming the SPG region through the Holocene, but they lacked paleo data from the SPG. Our data agree with the prediction made by Rimbu et al., (2003). SPG dynamics have been linked to NAO dynamics (Sarafanov et al., 2009; Sarafanov et al., 2008), and with these four cores in the SPG region this linkage can be observed through the Holocene. Our two Mg/Ca temperature records and the two existing Mg/Ca temperature records, based on the planktonic foraminiferal species *G. bulloides*, follow winter insolation rather than summer insolation and are consistent with winter NAO forcing.

The Mg/Ca records differ from other limited paleo records from within the SPG. SSTs in the SPG regions of the North Atlantic have been reconstructed based on planktonic assemblages, including coccolithophores (e.g., (Giraudeau et al., 2000)) and diatoms (e.g., (Berner et al., 2008; Miller and Chapman, 2013). The coccolithophore assemblages at MD95-2015 from the Gardar Drift recorded a gradual warming of surface waters between ~10,000 to 6,000 cal yr BP (Giraudeau et al., 2000). The study linked the warming with the migration of the Subarctic Front northward. The Holocene Thermal Maximum (HTM) was recorded between ~7,000 and 6,000 cal yr BP, followed by a two-step cooling between 6,000 and 4,800 and 3,500 and 2,800 cal yr BP. The

diatom assemblage at LO09-14 at the Reykjanes Ridge recorded a cool and variable early Holocene from ~11,000 to 7,000 cal yr BP (Berner et al., 2008). The HTM took place between ~7,000 and 5,000 cal yr BP, followed by a cooler late Holocene. However, the SSTs were rising after ~1,500 cal yr BP. Another diatom assemblage study reconstructed SSTs at MD99-2251 (Miller and Chapman, 2013). The study pointed out unstable early Holocene conditions between ~11,500 and 9,000 cal yr BP. SSTs remained cold until the HTM between ~7,000 and 5,000 cal yr BP, followed by more stable SSTs but lightly cooler conditions between ~5,000 cal yr BP and the present.

Alkenone SSTs in the rest of the North Atlantic generally followed summer insolation (Leduc et al., 2010) with warmer temperatures in the early Holocene (~9,000 to 5,700 cal yr BP) followed by the onset of the Neoglacial with cooling temperatures from ~5,700 cal yr BP to the present, although it is worth noting that some assemblage records from the wider North Atlantic imply a warming or no trend (Marchal et al., 2002). Coccolithophores and diatoms live in the euphotic zone, which is more sensitive to summer heating, and coccolithophores in particular favor stratified conditions. Therefore, these species may be more sensitive to summer insolation forcing than *G. bulloides*.

3.4.4 Suborbital-Scale History of Each Site

3.4.4.1 SW Iceland Shelf

From 10,300 to 9,100 cal yr BP, the temperatures are relatively warm and $\delta^{18}O_{sw}$ values relatively heavy, indicating an Atlantic Water influence. The interval from 9,100 to

8,200 cal yr BP is the freshest interval with light $\delta^{18}O_{sw}$ values and cold temperatures. The temperature and $\delta^{18}O_{sw}$ reconstructions between 8,200 and 5,700 cal yr BP suggest that the heavier $^{18}O_{calcite}$ signal is a composite of colder temperature (heavier $^{18}O_{calcite}$) and lighter $\delta^{18}O_{sw}$ (lighter). Taking the modern SPG dynamics as an analog, the SPG would have been extended and incorporating fresher and colder water into the eastern subpolar North Atlantic.

The interval between 5,700 and 2,300 cal yr BP shows variable conditions. The $^{18}O_{calcite}$ is variable with the lightest spike centered at ~2,500 cal yr BP. We don't have Mg/Ca measurements for the light spike. The overall trend in this interval is for warming temperatures and heavier $\delta^{18}O_{sw}$. The IC carries a stronger AW signal, which is in concordance to a contracted SPG.

Between 2,300 and 800 cal yr BP we see a trend to warming and more saline conditions. The $^{18}O_{calcite}$ record is fairly flat in this interval, while the temperatures are warming and the $\delta^{18}O_{sw}$ becoming heavier. This trend suggests that the SPG is contracting and more subtropical water is advancing into the subpolar N Atlantic.

3.4.4.2 RAPiD-12-1k

By 10,800 cal yr BP, glacial conditions had ceased and warmer water was advancing over the study site. The 3-running mean of the temperature in RAPiD-12-1K oscillates around a mean of 10.5°C until ~3,500 cal yr BP. The lightest $\delta^{18}O_{sw}$ interval occurred between 10,800 and 8,200 cal yr BP.

The $\delta^{18}O_{sw}$ fluctuates until 3,500 cal yr BP. After 3,500 until 700 cal yr BP, the temperature is steadily rising accompanied by steadily heavier $\delta^{18}O_{sw}$ values,

suggesting that the SPG is contracting and more subtropical water is advancing over this site.

3.4.4.3 NEAP4k

The coldest, freshest interval takes place between 10,000 and 5,400 cal yr BP, with the coldest and lightest spikes centered around 8,600 and 5,500 cal yr BP. This interval suggests that the SPG was extended. The SPG started to contract at 5,400 until 570 cal yr BP, with a sudden jump in temperature at 1,800 cal yr BP, recording a strong Atlantic water signal. Between 570 and 300 cal yr BP, the gyre was extending again as the colder temperatures suggest.

3.4.4.4 MD99-2251

The temperature record in MD99-2251 suggests sudden shifts at the southeastern boundary of the SPG. The coldest temperature interval ended at ~9,800 cal yr BP, suggesting that the site was in the SPG prior to ~9,800 cal yr BP. Between ~9,800 and 7,800 the core was warming, indicating more subtropical water was reaching the core site, but with some colder intervals centered around ~8,600, 8,400, and 8,100 cal yr BP. A relatively cold interval occurred between 7,800 and 6,400 cal yr BP, suggesting an extended gyre. Between ~6,400 and 3,400 cal yr BP, the site was relatively cold and was located within the SPG. A sudden shift to warm temperatures occurred at ~3,400 cal yr BP, but then started to trend toward cooling until to ~560 cal yr BP, indicating a contraction in the SPG and more subtropical water overlying the core site. The site was no longer located in the SPG based on the warmer than average SSTs.

3.4.5 Synthesis of the SPG Through the Holocene

In this section, we compare each core to its mean of the temperature and $\delta^{18}O_{sw}$: SW Iceland shelf (9.6°C, 0.84‰) RAPiD-12-1k (10.5° C, 0.8‰) NEAP4k (10.7°C, 0.99‰), and MD99-2251 (9.6°C). Based on these departures from the mean, and our interpretation of how SST and $\delta^{18}O_{sw}$ reflect the zonal extent of the SPG, we are able to describe four circulation patterns during the Holocene.

3.4.5.1 Early Holocene: East-west Extended SPG with Colder and Fresher Water in the Northeastern Part of the North Atlantic (~10,000 - 8000 cal yr BP)

The interval between ~10,000 and 8,000 cal yr BP was generally cool with light $\delta^{18}O_{sw}$ values. The East Greenland slope, the SW Iceland shelf, and the northern area of the Reykjanes Ridge were cold and fresh. The southernmost Reykjanes Ridge core was relatively cold.

The winters were colder than today because winter insolation was lowest at ~10,000 cal yr BP. Cold winters today are associated with strong Westerlies. We assume that during this interval the Westerlies were stronger than today and could have zonally extended the SPG. At the same time, summer insolation was high and releasing freshwater from the melting LIS (Carlson et al., 2007; Carlson et al., 2008). Other studies point to the onset of Labrador Sea convection at ~8000 cal yr BP (Hillaire-Marcel et al., 2001). Based on the remarkably light $\delta^{18}O_{sw}$ observed in the three northern sites, we conclude that the SPG was zonally extended between ~10,000 and 8,000 cal yr BP because of the very strong Westerlies during the winter, despite the

absence of Labrador Sea convection. There is no modern analog for this oceanic circulation pattern.

3.4.5.2 Early Mid-Holocene: Ocean Dynamics Change (~8,000 - 6,000 cal yr BP)

The shift recorded in our data cannot be explained by changes in insolation forcing because they did not change dramatically enough but rather can be explained by changes in the oceanic circulation, possibly related to Labrador Sea convection. Melt water input had decreased as the catastrophic outburst of the proglacial lakes Agassiz and Ojibway were the final drainage of the LIS (Barber et al., 1999). The decrease of deglacial melt water to the Labrador Sea combined with strong winter winds, consistent with a positive NAO-like state during the Early Holocene, favored convection over the Labrador Sea, intensifying the SPG circulation. We saw in the modern data that it took a severe winter with strong winds to restart the convection in 1972 after the shutdown of the Labrador Sea convection due to the GSA. We speculate that a long period of severe winters finally cooled down the Labrador Sea enough to overcome or disperse the freshwater from the melting of the LIS. Also the LIS ended adding freshwater to the North Atlantic.

The timing of the heavier $\delta^{18}O_{sw}$ values seen in our data coincided with the start of the convection over the Labrador Sea, which set in at ~8000 cal yr BP (Hillaire-Marcel et al., 2001). In the easternmost core, RAPiD-12-1k, the $\delta^{18}O_{sw}$ suddenly became heavier than the Holocene mean. The $\delta^{18}O_{sw}$ values on the SW Iceland shelf and at NEAP4k became heavier as well but remained lighter than the mean, suggesting that the SPG was still zonally extended.

We posit that the shape of the SPG did not change much and still was zonally extended. But the mechanism behind the SPG shape differed in this interval from the previous interval. Our study sites showed no change in temperature and remained cool as seen today during times of intense SPG dynamics and zonally extended gyre. The SPG in this interval is zonally extended because of strong Westerlies and convection of the Labrador Sea. In the previous interval from ~10,000 to 8,000 cal yr BP, the SPG was extended because of the presence of freshwater from the LIS and the very strong intense Westerlies. We envision the SPG circulation to have been sluggish as the Labrador Sea was not yet convecting. In the modern realm, a convection Labrador Sea intensifies the SPG circulation.

3.4.5.3 Late Mid-Holocene: Minimal Freshwater Input (~6,000 - 3,800 cal yr BP)

Our sites record variable conditions associated with a changing SPG. On the SW Iceland shelf, the data show intervals of the warmest temperatures and heaviest $\delta^{18}O_{sw}$ between ~5,700 and 3,800 cal yr BP, which suggests a strong IC signal. The RAPiD-12-1k site shifted from heavier to lighter $\delta^{18}O_{sw}$ values but the temperature did not change. The NEAP4k core warmed and $\delta^{18}O_{sw}$ values became heavier. The temperature in the MD99-2251 core was relatively cool. We attribute these changes to a contracting gyre. Today when the gyre is contracted, the IC carries a stronger Atlantic signal to the SW Iceland shelf. The NEAP4k site showed a stronger Atlantic signal as well. The Atlantic water signal was only recorded in the $\delta^{18}O_{sw}$ signal at the RAPiD-12-1k site. This site remained cold as did the MD99-2251 site.

The SPG could have contracted due to major reorganization of global atmospheric circulation, which at our site was noted by a weakening of the Westerlies

and the negative NAO-like conditions. A mid-Holocene shift in the climate system has been noted in numerous other studies. (Mayewski et al., 2004). Oppo et al. (2003) saw evidence for reduced North Atlantic Deep Water production at ~5000 cal yr BP. Between ~5,000 and 6,100 cal yr BP, the sea salt accumulation, which is interpreted as a winter proxy, at Greenland ice cores (Summit was increased, indicating a more southerly position of the Polar Vortex (other times this happened: 0-610 and >11,300 cal yr BP). DeMenocal et al. (2000) noted the end of the African Humid Period at ~5,500 cal yr BP. Haug (2001) saw a shift of the Intertropical Convergence Zone in the Cariaco Basin at ~5,400 cal yr BP. Andrews et al. (1997) saw evidence for more ice rafted debris was seen in the last 6,000 years on the east Greenland Shelf (Andrews et al., 1997). Bauch et al. (2001) and Werner et al. (2013) saw the flooding of shallow Arctic shelves (Laptev Sea), and modern sea ice production was reached by ~5000 cal yr BP.

3.4.5.4 Neoglaciation (~3,800 - 800 cal yr BP)

The continued weakening of the Westerlies associated with more negative NAO-like conditions and increasing winter insolation are strongly expressed in our cores. The temperatures were rising on the SW Iceland shelf with heavier $\delta^{18}O_{sw}$ values, indicating the IC carried more Atlantic water. The RAPiD-12-1k core was also continuously warming and $\delta^{18}O_{sw}$ values became heavier. The same trend took place in the NEAP4k record. The temperature in the MD99-2251 core increased by ~4°C between ~4,000 and 3,400 cal yr BP. This interval is the warmest interval in this core, even though after ~3,400 cal yr BP the temperatures were starting to decrease slightly.

The SPG was contracting in this interval, leading to a warming at our sites. We posit that the SPG shape was similar to the shape that the SPG has today during negative NAO-like conditions. The contraction of the SPG also coincided with the onset of the Neoglacial, which was noted on the east Greenland shelf at ~3,500 cal yr BP (Jennings et al., 2011). During the Neoglaciation more fresh water from northern sources could have interfered with Labrador Sea convection.

At ~2000 cal yr BP, we observe a steep increase in temperature accompanied by heavier $\delta^{18}O_{sw}$. Warmer conditions and heavier $\delta^{18}O_{sw}$ can be seen in the NEAP4k core, and to a lesser extent in the RAPiD-12-1k, suggesting a contracting SPG. This sudden contraction at ~2,000 cal yr BP could also have been caused by increased freshwater coming from the Arctic Ocean and shutting down the Labrador Sea convection. Jennings et al. (2002) noted a pronounced freshening of the EGC at ~2,000 cal yr BP. The warming that started at ~2000 cal yr BP, was noted in other records as well. For example, the diatom assemblage at LO09-14 at the Reykjanes Ridge showed the SSTs were rising after ~1,500 cal yr BP (Berner et al., 2008). SST was rising after ~2000 cal yr BP on the East Greenland Shelf (Jennings et al. 2002).

Our synthesis shows an overall contracting SPG, which we attribute to a weakening of the NAO-like atmospheric circulation. The weakening of the atmospheric circulation has been shown in the Rimbu et al (2003) GCM to be linked to increasing winter precession through the Holocene.

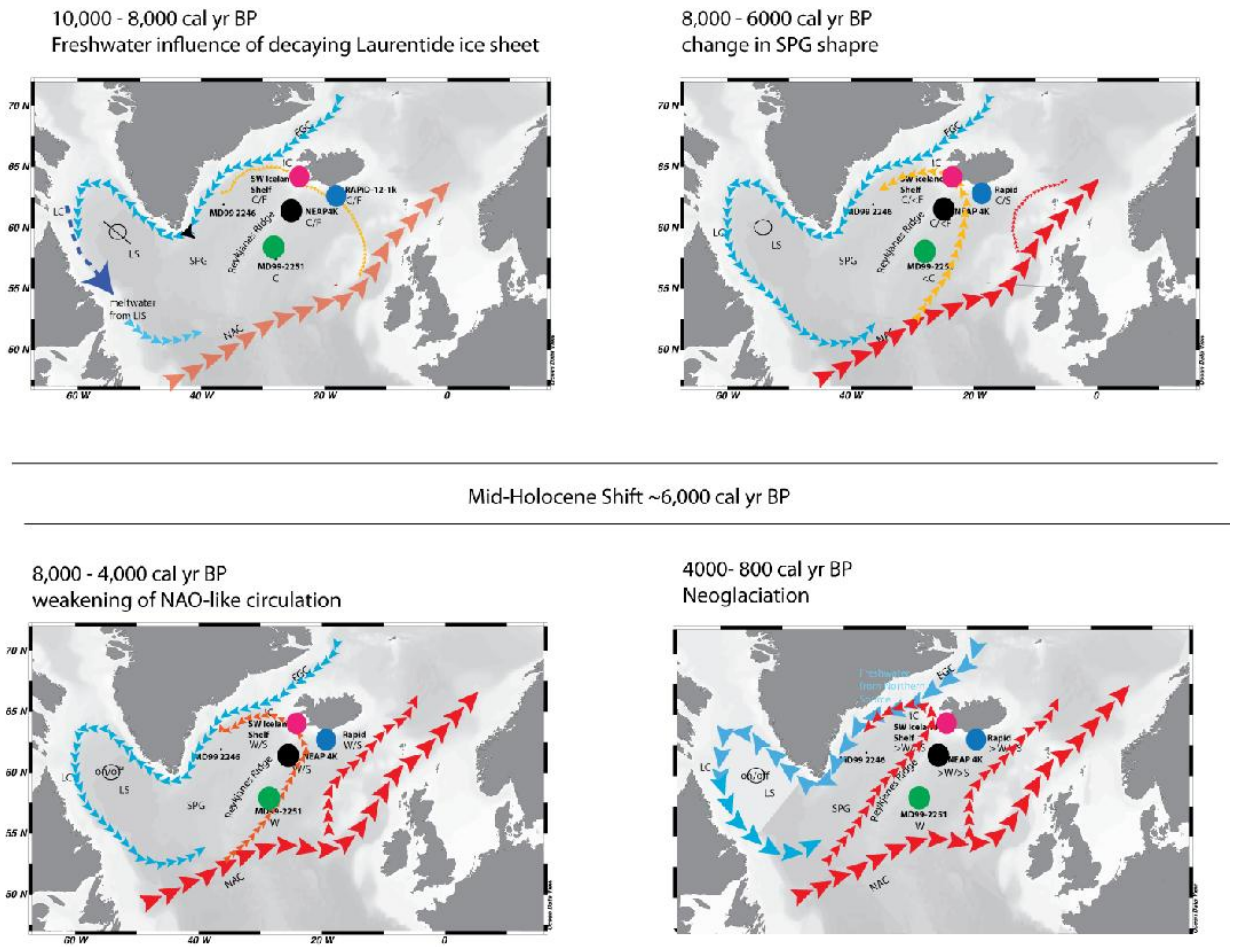

Figure 3.8 Schematic SPG surface currents in the four time intervals identified. Also shown is the Labrador Sea (LS) with a circle indicating that the LS is convecting, and a circle with slash indicating reduced or shutdown of LS convection. The recorded temperatures and $\delta^{18}O_{sw}$ are indicated by the core sites: W=Warm, C=Cold, F=Fresh (light $\delta^{18}O_{sw}$), S=Salty (heavy $\delta^{18}O_{sw}$).

3.5 Conclusions

We observed that through the Holocene, the SPG region warmed and the ice-volume-corrected $\delta^{18}O_{sw}$ values became heavier. We attribute these trends to the weakening of NAO-like atmospheric circulation in response to increasing winter insolation through the Holocene. The SPG did not respond to the winter insolation smoothly but rather in several abrupt shifts.

1. Between ~10,000 to 8,000 cal yr BP, freshwater from the decaying LIS was present yet the SPG. In the modern scenario, the SPG would have been contracted, even during NAO+ years. But in the early Holocene, the Westerlies were very strong Westerlies and the SPG was extended despite the absence of Labrador Sea convection.
2. Between 8,000 to 6,000 cal yr BP, the SPG was still extended but started to change in shape. Westerlies likely were still strong. The change in shape coincides with the onset of Labrador Sea convection. We posit that the gyre circulation strengthened.
3. Between 6,000 and 4,000 cal yr BP, the SPG started to contract, likely due to decreased Westerlies.
4. Between 4,000 and 800 cal yr BP, Westerlies may have continued to decrease, but increased freshwater from northern sources could also have inhibited convection of the Labrador Sea. Both effects would combine to contract and warm the SPG.

3.6 Acknowledgments

We would like to thank Ian Hall for providing the samples for MD99-2246 and NEAP4K. We would like to thank our undergraduate research assistants, Michelle Carlson and Vivian Underhill, for helping with sample preparation. We are grateful for the assistance Patrick Cappa provided in the ICP-MS laboratory. This project was funded by the National Science Foundation, Grant number 0823535, PIs: Anne E. Jennings, Tom M. Marchitto, and John T. Andrews.

3.7 Work Cited

Andersen, C., Koc, N., Jennings, A., and Andrews, J. T., 2004a, Nonuniform response of the major surface currents in the Nordic Seas to insolation forcing: Implications for the Holocene climate variability: Paleoceanography, v. 19, no. 2.

Andersen, C., Koc, N., and Moros, M., 2004b, A highly unstable Holocene climate in the subpolar North Atlantic: evidence from diatoms: Quaternary Science Reviews, v. 23, no. 20-22, p. 2155-2166.

Andrews, J. T., Smith, L. M., Preston, R., Cooper, T., and Jennings, A. E., 1997, Spatial and temporal patterns of iceberg rafting (IRD) along the East Greenland margin, ca 68 degrees N, over the last 14 cal ka: Journal of Quaternary Science, v. 12, no. 1, p. 1-13.

Arbuszewski, J., deMenocal, P., Kaplan, A., and Farmer, E. C., 2010, On the fidelity of shell-derived delta O-18(seawater) estimates: Earth and Planetary Science Letters, v. 300, no. 3-4, p. 185-196.

Barber, D. C., Dyke, A., Hillaire-Marcel, C., Jennings, A. E., Andrews, J. T., Kerwin, M. W., Bilodeau, G., McNeely, R., Southon, J., Morehead, M. D., and Gagnon, J. M., 1999, Forcing of the cold event of 8,200 years ago by catastrophic drainage of Laurentide lakes: Nature, v. 400, no. 6742, p. 344-348.

Barker, S., and Elderfield, H., 2002, Foraminiferal calcification response to glacial-interglacial changes in atmospheric CO2: Science, v. 297, no. 5582, p. 833-836.

Barker, S., Greaves, M., and Elderfield, H., 2003, A study of cleaning procedures used for foraminiferal Mg/Ca paleothermometry: Geochemistry Geophysics Geosystems, v. 4.

Be, A. W. H., and Tolderlund, D. S., 1971, Distribution and ecology of living planktonic foraminifera in the surface waters of the Atlantic and Indian Oceans: The Micropalaeontology of Oceans, p. 105-149.

Bemis, B. E., Spero, H. J., Bijma, J., and Lea, D. W., 1998, Reevaluation of the oxygen isotopic composition of planktonic foraminifera: Experimental results and revised paleotemperature equations: Paleoceanography, v. 13, no. 2, p. 150-160.

Berner, K. S., Koc, N., Divine, D., Godtliebsen, F., and Moros, M., 2008, A decadal-scale Holocene sea surface temperature record from the subpolar North Atlantic constructed using diatoms and statistics and its relation to other climate parameters: Paleoceanography, v. 23, no. 2.

Boyle, E., and Rosenthal, Y., 1996, Chemical hydrography of the South Atlantic during the last glacial maximum; Cd s d13C New York, Springer, The South Atlantic: Present and Past Circulation.

Dickson, R. R., Meincke, J., Malmberg, S. A., and Lee, A. J., 1988, THE GREAT SALINITY ANOMALY IN THE NORTHERN NORTH-ATLANTIC 1968-1982: Progress in Oceanography, v. 20, no. 2, p. 103-151.

Eiriksson, J., Larsen, G., Knudsen, K. L., Heinemeier, J., and Siminarson, L. A., 2004, Marine reservoir age variability and water mass distribution in the Iceland Sea.: Quaternary Science Review, v. 23, p. 2247-2268.

Elderfield, H., and Ganssen, G., 2000, Past temperture and d18O of surface ocean waters inferred from foraminiferal Mg/Ca ratios.: Nature, no. 405.

Elderfield, H., Yu, J., Anand, P., Kiefer, T., and Nyland, B., 2006, Calibrations for benthic foraminiferal Mg/Ca paleothermometry and the carbonate ion hypothesis: Earth and Planetary Science Letters, v. 250, no. 3-4, p. 633-649.

Ellison, C. R. W., Chapman, M. R., and Hall, I. R., 2006, Surface and deep ocean interactions during the cold climate event 8200 years ago: Science, v. 312, no. 5782, p. 1929-1932.

Fairbanks, R. G., 1989, A 17,000 year glacial-eustatic sea level record: influence of glacial melting rates on the Younger Dryas event and deep-ocean circulation: Nature, v. 342, p. 637-642.

Farmer, E. C., deMenocal, P. B., and Marchitto, T. M., 2005, Holocene and deglacial ocean temperature variability in the Benguela upwelling region: Implications for low-latitude atmospheric circulation: Paleoceanography, v. 20, no. 2.

Farmer, E. J., Chapman, M. R., and Andrew, J. E., Holocene temperature evolution of the subpolar North Atlantic recorded in the Mg/Ca ratios of surface and thermocline dwelling planktonic foraminifers2009, p. A355-A355.

Fennel, K., Cetinic, I., D'Asaro, E., Lee, C., and Perry, M. J., 2011, Autonomous data describe North Atlantic spring bloom: EOS, v. 92, p. 465-466.

Ferguson, J. E., Henderson, G. M., Kucera, M., and Rickaby, R. E. M., 2008, Systematic change of foraminiferal Mg/Ca ratios across a strong salinity gradient: Earth and Planetary Science Letters, v. 265, no. 1-2, p. 153-166.

Ganssen, G. M., and Kroon, D., 2000, The isotopic signature of planktonic foraminifera from NE Atlantic surface sediments: implications for the reconstruction of past oceanic conditions: Journal of the Geological Society, v. 157, p. 693-699.

Giraudeau, J., Cremer, M., Manthe, S., Labeyrie, L., and Bond, G., 2000, Coccoltith evidence for instabilities in the surface circulation south of Iceland during the Holocene times.: Earth and Planetary Science Letters, v. 179, p. 257-268.

Hall, I. R., Bianchi, G. G., and Evans, J. R., 2004, Centennial to millennial scale Holocene climate-deep water linkage in the North Atlantic: Quaternary Science Reviews, v. 23, no. 14-15, p. 1529-1536.

Hatun, H., Sando, A. B., Drange, H., Hansen, B., and Valdimarsson, H., 2005, Influence of the Atlantic subpolar gyre on the thermohaline circulation: Science, v. 309, no. 5742, p. 1841-1844.

Hillaire-Marcel, C., de Vernal, A., Bilodeau, G., and Weaver, A. J., 2001, Absence of deep-water formation in the Labrador Sea during the last interglacial period: Nature, v. 410, no. 6832, p. 1073-1077.

Holland, D. M., Thomas, R. H., De Young, B., Ribergaard, M. H., and Lyberth, B., 2008, Acceleration of Jakobshavn Isbrae triggered by warm subsurface ocean waters: Nature Geoscience, v. 1, no. 10, p. 659-664.

Honisch, B., Allen, K. A., Lea, D. W., Spero, H. J., Eggins, S. M., Arbuszewski, J., deMenocal, P., Rosenthal, Y., Russell, A. D., and Elderfield, H., 2013, The influence of salinity on Mg/Ca in planktic foraminifers - Evidence from cultures, core-top sediments and complementary delta O-18: Geochimica et Cosmochimica Acta, v. 121, p. 196-213.

Hurrell, J. W., 1995, DECADAL TRENDS IN THE NORTH-ATLANTIC OSCILLATION - REGIONAL TEMPERATURES AND PRECIPITATION: Science, v. 269, no. 5224, p. 676-679.

Jennings, A., Andrews, J., and Wilson, L., 2011, Holocene environmental evolution of the SE Greenland Shelf North and South of the Denmark Strait: Irminger and East Greenland current interactions: Quaternary Science Reviews, v. 30, no. 7-8, p. 980-998.

Jennings, A. E., Thordarson, T., Zalzal, K., Stoner, J. S., Geirsdottir, A., and Miller, G. H., 2014, Holocene tephra from Iceland and Alaska in SE Greenland shelf sediments: Geological Society London Special Publications, p. 398.

Kristjansdottir, G. B., 2005, Holocene changes in climate, environment, and ocean reservoir age on the Iceland shelf: Mg/Ca, del 18O, and tephrachronology of Core MD99-2269PhD]: University of Colorado, 423 p.

Labeyrie, L., Jansen, E., and Cortijo, E., 2003, Les rapports des campagnes a la mer MD114/IMAGES V.

Lea, D. W., 2002, New insights into glacial terminations from Mg-paleothermometry: Geochimica et Cosmochimica Acta, v. 66, no. 15A, p. A438-A438.

Lea, D. W., Mashiotta, T. A., and Spero, H. J., 1999, Controls on magnesium and strontium uptake in planktonic foraminifera determined by live culturing: Geochimica et Cosmochimica Acta, v. 63, no. 16, p. 2369-2379.

Lea, D. W., Pak, D. K., and Paradis, G., 2005, Influence of volcanic shards on foraminiferal Mg/Ca in a core from the Galapagos region: Geochemistry Geophysics Geosystems, v. 6.

Leduc, G., Schneider, R., Kim, J. H., and Lohmann, G., 2010, Holocene and Eemian sea surface temperature trends as revealed by alkenone and Mg/Ca paleothermometry: Quaternary Science Reviews, v. 29, no. 7-8, p. 989-1004.

LeGrande, A. N., and Schmidt, G. A., 2006, Global gridded data set of the oxygen isotopic composition in seawater: Geophysical Research Letters, v. 33, no. 12.

Marchal, O., Cacho, I., Stocker, T. F., Grimalt, J. O., Calvo, E., Martrat, B., Shackleton, N. J., Vautravers, M., Cortijo, E., van Kreveld, S., Andersson, C., Koc, N., Chapman, M., Sbaffi, L., Duplessy, J.-C., Sarntheim, M., Turon, J.-L., Duprat, J., and Jansen, E., 2002, Apparent long-term cooling in the sea surface in the northeast Atlantic and Mediterranean during the Holocene.: Quaternary Science Review, v. 21, p. 455-483.

Marchitto, T. M., 2006, Nutrient proxies (d13C, Cd/Ca, Ba/Ca, Zn/Ca, d15N), *in* Elias, S., ed., Encyclopedia of Quaternary Science: Amsterdam, Elsevier.

Mashiotta, T. A., Lea, D. W., and Spero, H. J., 1999, Glacial-interglacial changes in Subantarctic sea surface temperature and delta O-18-water using foraminiferal Mg: Earth and Planetary Science Letters, v. 170, no. 4, p. 417-432.

Mathien-Blard, E., and Bassinot, F., 2009, Salinity bias on the foraminifera Mg/Ca thermometry: Correction procedure and implications for past ocean hydrographic reconstructions: Geochemistry Geophysics Geosystems, v. 10.

Mayewski, P. A., Rohling, E. E., Stager, J. C., Karlen, W., Maasch, K. A., Meeker, L. D., Meyerson, E. A., Gasse, F., van Kreveld, S., JHolmgren, K., Lee-Thorp, J., Rosqvist, G., Rack, F., Staubwasser, M., Schneider, R. R., and Steig, E. J., 2004, Holocene climate variability: Science, v. 62, p. 243-255.

McCave, I. N., 1994, North East Atlantic Palaeoceanography and Climate Change: RRS Charles Darwin 88 (Cruise Report), Department of Earth Sciences, University of Cambridge, p. 44.

Miller, K. R., and Chapman, M. R., 2013, Holocene climate variability reflected in diatom-derived sea surface temperature records from the subpolar North Atlantic: Holocene, v. 23, no. 6, p. 882-887.

Nurnberg, D., Bijma, J., and Hemleben, C., 1996, Assessing the reliability of magnesium in foraminiferal calcite as a proxy for water mass temperatures (vol 60, pg 803, 1995): Geochimica et Cosmochimica Acta, v. 60, no. 13, p. 2483-2483.

Ólafsdóttir, S., jennings, A. J., Á., G., Andrews, J. T., and Miller, G. H., 2010, Holocene variability of the North Atlantic Irminger current on the south- and northwest shelf of Iceland Marine Micropaleontology, v. XXX.

Reverdin, G., 2010, North Atlantic Subpolar Gyre Surface Variability (1895-2009): Journal of Climate, v. 23, no. 17, p. 4571-4584.

Rodionov, S. N., 2004, A sequential algorithm for testing climate regime shifts: Geophysical Research Letters, v. 31, no. 9.

Rosenthal, Y., Boyle, E. A., and Slowey, N., 1997, Temperature control on the incorporation of magnesium, strontium, fluorine, and cadmium into benthic foraminiferal shells from Little Bahama Bank: Prospects for thermocline paleoceanography: Geochimica et Cosmochimica Acta, v. 61, no. 17, p. 3633-3643.

Rosenthal, Y., Field, M. P., and Sherrell, R. M., 1999, Precise determination of element/calcium ratios in calcereous samples using sector field inductively coupled plasma mass spectrometry: Analytical Chemistry, v. 71, p. 3248-3253.

Rosenthal, Y., Perron-Cashman, S., Lear, C. H., Bard, E., Barker, S., Billups, K., Bryan, M., Delaney, M. L., deMenocal, P. B., Dwyer, G. S., Elderfield, H., German, C. R., Greaves, M., Lea, D. W., Marchitto, T. M., Pak, D. K., Paradis, G. L., Russell, A. D., Schneider, R. R., Scheiderich, K., Stott, L., Tachikawa, K., Tappa, E., Thunell, R., Wara, M., Weldeab, S., and Wilson, P. A., 2004, Interlaboratory comparison study of Mg/Ca and Sr/Ca measurements in planktonic foraminifera for paleoceanographic research: Geochemistry Geophysics Geosystems, v. 5.

Sarafanov, A., 2009, On the effect of the North Atlantic Oscillation on temperature and salinity of the subpolar North Atlantic intermediate and deep waters.: ICES Journal of Marine Science, v. 66, p. 1448-1454.

Sarafanov, A., Falina, A., Mercier, H., Lherminier, P., and Sokov, A., 2009, Recent changes in the Greenland-Scotland overflow-derived water transport inferred from hydrographic observations in the southern Irminger Sea: Geophysical Research Letters, v. 36.

Sarafanov, A., Falina, A., Sokov, A., and Demidov, A., 2008, Intense warming and salinification of intermediate waters of southern origin in the eastern subpolar North Atlantic in the 1990s to mid-2000s: Journal of Geophysical Research-Oceans, v. 113, no. C12.

Schiebel, R., Bijma, J., and Hemleben, C., 1997, Population dynamics of the planktic foraminifer Globigerina bulloides from the eastern North Atlantic: Deep-Sea Research Part I-Oceanographic Research Papers, v. 44, no. 9-10, p. 1701-1713.

Stuiver, M., Reimer, P. J., and Braziunas, T. F., 1998, High-precision radiocarbon age calibration for terrestrial and marine samples: Radiocarbon, v. 40, no. 3, p. 1127-1151.

Thornalley, D. J. R., Elderfield, H., and McCave, I. N., 2009, Holocene oscillations in temperature and salinity of the surface subpolar North Atlantic: Nature, v. 457, no. 7230, p. 711-714.

Yashayaev, I., and Clarke, A., 2008, EVOLUTION OF NORTH ATLANTIC WATER MASSES INFERRED FROM LABRADOR SEA SALINITY SERIES: Oceanography, v. 21, no. 1, p. 30-45.

Chapter 4
The Implications of Freshwater Forcing on the Hydrography of the Irminger Current Through the Holocene

4.1 Abstract

Subtropical, saline Atlantic water is transported by the Irminger Current (IC) to regions that are important to deep water formation. In recent years, the IC has contributed to the acceleration of the Greenland ice sheet mass balance loss by submarine melting of outlet glaciers. To gain insight to the recent changes in the climate system we need to place them into the context of past climate changes. We analyzed two sediment cores from the SW Iceland shelf that lie in the flow path of the IC as it enters the Irminger Sea. An extensive suite of proxies allowed us to document changes in the hydrography of the IC, including paired measurements of Mg/Ca and $\delta^{18}O_{calcite}$ of the planktonic foraminifer *Globigerina bulloides* to reconstruct water temperature and $\delta^{18}O$ of seawater. Between ~10,000 to 8,000 cal yr BP, the glacial melt water from the Laurentide ice sheet cooled and freshened the Atlantic waters in the IC. Between ~8,000 and 6,000 cal yr BP, Mg/Ca reconstructs continued cool and relatively fresh IC, while the planktonic and benthic foraminifera recorded a warming. The warmest temperatures and heaviest $\delta^{18}O_{sw}$ were recorded between ~6,000 and 3,800 cal yr BP by all proxies. Neoglacial cooling began at ~3,800 cal yr BP, documented by the foraminiferal sea surface and bottom water temperature records and in the quartz feldspar record, which indicates drift ice transport from spreading of the East Greenland Current toward the SW Iceland shelf.

4.2 Introduction

Climate models predict that the largest future temperature changes will occur in the high latitude North Atlantic region; in the twenty-first century, the ocean near the vicinity of the Greenland ice sheet is expected to warm by ~1.7 to 2.0°C, which is about twice the global mean (Yin et al., 2011). Large changes in the wind-driven ocean circulation have been observed in the high latitude North Atlantic Ocean (Hakkinen and Rhines, 2009). At the same time as more fresh water is added to this region via melting of the Greenland ice sheet (Rignot and Kanagaratnam, 2006) and via sea ice and fresh water export from the Arctic Ocean (Serreze et al., 2007), more subtropical water is advecting northward (Hakkinen and Rhines, 2009). The high-latitude North Atlantic shows a multidecadal trend toward longer seasonal stratification in surface water, which affects biological activity; prolonged stratification is associated with rapid nutrient depletion and less productivity (Taboada and Anadon, 2012).

The observational record to assess the wide breadth of imminent climate change and its consequences for societies is rather short. Placing present day climate change into a paleoclimatic context can provide insights for understanding natural processes and rates of natural climate change under a broader spectrum of Holocene boundary conditions.

Sediment cores from the SW Iceland shelf lend themselves to paleoclimatic reconstructions because the SW Iceland shelf is located in a climatically dynamic region. Today, the Icelandic Low, a low atmospheric pressure system that varies in strength, influences storm tracks across the North Atlantic affecting the climate on the SW Iceland shelf. The SW Iceland shelf is also located at the intersection of two contrasting ocean currents. The Irminger Current (IC) transports relatively warm and

saline waters northward and the East Greenland Current (EGC) transports relatively cold and fresh waters southward in the Denmark Strait (Figure 4.1).

The IC has received increased attention in recent years because of its impact on the moving margins of the Greenland ice sheet; if the subtropical water carried in the IC is present in the SW and W Greenland fjords, the relatively warm water contributes to the submarine melting of the marine glacier termini (Holland et al., 2008; Straneo et al., 2011; Straneo et al., 2013; Sutherland and Straneo, 2012). The melting of the Greenland ice sheet can be anticipated to be key factors in climate change over the next few centuries (Blaschek and Renssen, 2013a).

The IC is a crucial component in the formation of Labrador Sea water. By the time, the relative saline IC water reach the Labrador Sea, it has cooled sufficiently in their transit that it it takes only a severe winter for the waters to convect and for Labrador Sea Water (LSW) to form (Yashayaev and Clarke, 2008). Over the past five decades, the Labrador Sea has had periods of unusually active formation of Labrador Sea water and periods when the formation nearly ceased (Yashayaev and Clarke, 2008). Labrador Sea water contributes to the meridional overturning of the North Atlantic. The Holocene reconstruction of the density of the Atlantic waters in the IC will add to our understanding of the formation of deep water.

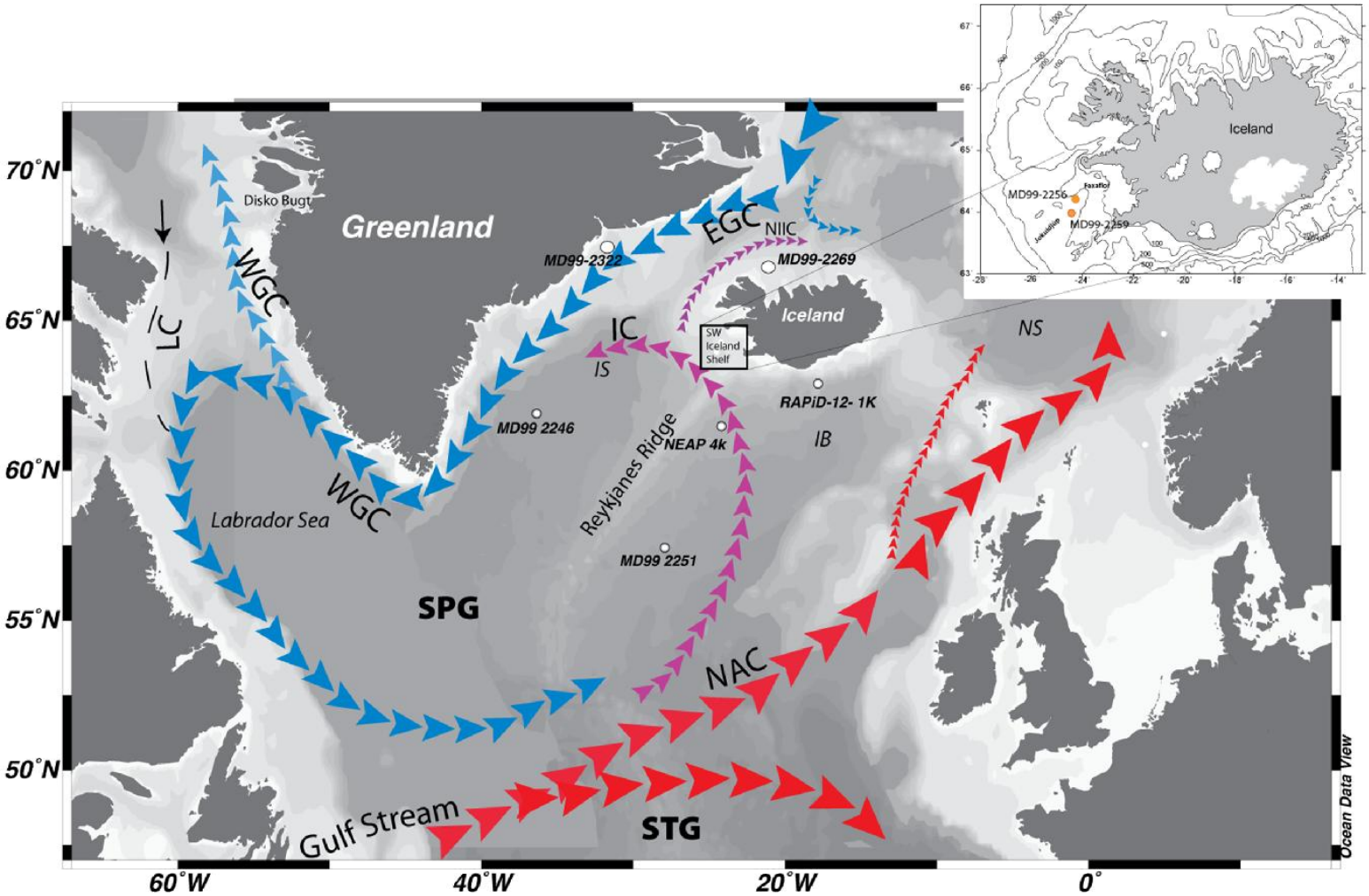

Figure 4.1 Location map with schematic surface currents. Surface currents: NAC-North Atlantic Current; IC-Irminger Current; EGC-East Greenland Current; WGC-West Greenland Current; LC-Labrador Current. Ocean basins: NS-Norwegian Sea, IB-Iceland Basin; IS-Irminger Sea, and Labrador Sea. SPG-Subpolar Gyre; STG-Subtropical Gyre. Insert shows a bathymetric map of the SW Iceland Shelf with study sites.

This paper documents the history of Irminger Atlantic Water and freshwater interactions through the Holocene. We are testing the hypothesis that 1.) in the early Holocene, the Atlantic water inflow was cooled and freshened from the final decay of the Laurentide ice sheet, 2.) in the mid Holocene the Irminger Water temperature and salinity influence were strongest with minor freshwater forcing, and 3.) in the late Holocene, the influence of IC decreased due to increasing freshwater in the East Greenland Current. By monitoring the IC on the SW Iceland shelf, we also gain insights into climate forcings on the subpolar North Atlantic.

We reconstructed the climatic history on the SW Icelandic shelf using a comprehensive suite of proxies on a composite Holocene sediment record. We combined two cores from the SW Iceland shelf, MD99-2256 and MD99-2259, to obtain a high-resolution SW Iceland record and to improve the age model. Some of the results have been previously published (Jennings et al., submitted; Ólafsdóttir et al., 2010) and are being used in this study to understand the full range of climate variability at our study site. We reconstructed sea surface temperature (SST) and $\delta^{18}O$ of seawater by paired measurement of $\delta^{18}O_{calcite}$ of the planktonic foraminifera *Globigerina bulloides* (Quillmann et al, in prep). *G. bulloides* calcifies in the upper 60m of the water column (Schiebel et al., 2001) and we have tuned the Mg/Ca temperature calibration to modern day SST in the subpolar North Atlantic (Quillmann et al, in prep). We also reconstructed summer SST using planktonic foraminiferal transfer functions; SSTs between ~12,000 and 7,000 cal yr BP have been published in Jennings et al. (subm.). Bottom water temperatures were reconstructed using benthic foraminiferal assemblages (Olafsdottir

et al., 2010). Environmental changes, such as water column stratification and nutrient content, will be interpreted using benthic and planktonic foraminiferal assemblage variations. Carbonate content in the sediments allows us to assess marine productivity because carbonate of the Icelandic shelf is generally biogenic (Andrews and Helgadottir, 2002; Giraudeau et al., 2000). Quartz and potassium feldspar are two minerals not native to Icelandic bedrock, and the presence of these two minerals implies that ice rafting took place (Andrews, 2009; Moros et al., 2006a). Lithofacies were described based on x-radiographs of the archive halves of the cores, and augmented by the core description, magnetic susceptibility (MS) that were made on board the research vessel, the carbonate content, and quartz and potassium feldspar. Our proxies are suitable for detecting changes in the Atlantic waters, potential influences of advected polar waters from the North or polar water mixed into the subpolar gyre, stratification of the water column, and variations in productivity, which reflect detecting environmental changes.

4.3 Currents of the Subpolar Gyre

In the SPG region of the North Atlantic, polar water masses from the north meet subtropical Atlantic waters from the south. The SPG regulates the partitioning of the Atlantic and polar water masses on an interannual to decadal timescale by contracting and extending (Yashayaev and Clarke, 2008). The IC forms the northern boundary current of the SPG (Figure 4.1). The SPG consists of four surface currents. The southern boundary of the SPG is the North Atlantic Current (NAC), which is an extension of the Gulf Stream carrying warm, subtropical waters northward. As the NAC

crosses the North Atlantic, it separates into several branches. One of these branches, the IC, turns northwestward and follows the flank of the Reykjanes Ridge to the southwest and west Iceland shelf. South of the Denmark Strait, the IC splits into two branches. The smaller branch continues northward around Iceland and becomes the North Icelandic Irminger Current (NIIC), while the larger branch, carrying the major portion of the Atlantic water, turns southward. The southward flowing branch of the IC flows along the East Greenland shelf and slope and meets the East Greenland Current (EGC), which carries cold, fresh water southward. As the EGC and the IC round the southern tip of Greenland, they continue north as the West Greenland Current (WGC); eddies from the WGC turn counterclockwise south and meet the LC. The LC is a cold fresh current coming from the north and joining the SPG.

The location and intensity of the storm tracks associated with the NAO influence the surface currents in the subpolar gyre (SPG) region in the North Atlantic. The NAO index describes variations in atmospheric pressure differences between the Azores High and the Icelandic Low. It is the dominant mode of winter climate variability in the North Atlantic region (Hurrell et al., 2003). If the pressure gradient is higher than normal (NAO+), the increased pressure system creates more frequent and more intense winter storms crossing the North Atlantic on a more northerly track. The SPG gyre extends eastward and the flow of the IC is reduced (Holland et al., 2008). If the pressure gradient is low (NAO-), the storms diminish in strength and frequency and cross the North Atlantic zonally. During NAO- states, the SPG contracts and the flow of the IC is increased (Holland et al., 2008). In the past 50 years, the SPG gyre oscillated between these two states (Sarafanov et al., 2008).

The IC carries saline waters necessary for the formation of Labrador Sea Water (LSW) formation. A second location of LSW formation has been discovered in recent years to take place in the Irminger Basin during severe winters (e.g.(Vage et al., 2011)). Vage et al. (2011) showed that during the early 1990s, when the winter NAO index was particularly high and the SPG was extended, deep convection occurred locally in the Irminger Basin. The sea surface temperatures (SSTs) on the SW Iceland shelf, where the IC enters the Irminger Basin, were cool. The NAO shifted to a negative state in the mid-1990s and the SPG contracted. SSTs on the SW Iceland shelf were warm and LSW formation was significantly reduced (Yashayaev, 2007).

The IC also has been shown to affect the stability of Greenland outlet glaciers (Straneo et al., 2010; Straneo et al., 2012; Sutherland and Straneo, 2012). Outlet glaciers in SE Greenland retreated in response to warmer SSTs in the 1930s (Bjork et al., 2012); temperature reconstruction based on alkenones suggested warming of the IC waters (8-12°C compared to 0-4° during colder intervals) (Andresen et al., 2013). When the retroflected IC flows southward along the East Greenland shelf, a sharp temperature and salinity front separates the polar waters in the EGC from the Atlantic waters in the IC along the shelf break and continental slope (Sutherland et al., 2009). The cold, fresh Arctic surface waters in the EGC and WGC flowing along the Greenland shelf keep the warmer Atlantic waters in the IC offshore (Yin et al., 2011). But deep cross shelf troughs allow for the Atlantic water carried in the IC to enter fjords, as was observed along the shelves and in E and SE Greenland fjords (Azetsu-Scott and Syvitski, 1999; Jennings et al., 2011; Sutherland et al., 2013). Submarine melting and subsequent retreat of

Greenland outlet glaciers have have been triggered by the incursion of warm IC water in W Greenland fjords (Holland et al., 2008; Motyka et al., 2011).

4.4 Previous Work on the Holocene History of the Irminger Current

Postglacial marine conditions were reached on the SW Iceland shelf, and the shelf was under the influence of Atlantic water transported by the IC by ~10,300 cal yr BP (~9,600 ^{14}C cal yr BP) (Jennings et al., 2000). Based on benthic foraminiferal transfer functions, the warmest bottom water temperatures (BWT) (~1.5°C warmer than today) were recorded between 7,800 and 4,000 cal yr BP (Ólafsdóttir et al., 2010). According to the same study, the Neoglaciation began at ~4,000 cal yr BP, marked by a drop of ~1°C in temperature in BWTs.

The Holocene thermal maximum on the N and NW Iceland shelf has been attributed to the influence of the Atlantic waters moving north in the NIIC (Andrews and Giraudeau, 2003; Andrews et al., 2003a; Castaneda et al., 2004; Geirsdottir et al., 2009). The NIIC is the northward flowing branch of the IC that flows along the western and northern Icelandic shelf. Stronger influence of the IC results in an increase of Atlantic water in the NIIC on the N. Icelandic shelf (Kristjansdottir, 2005). The warmest BTWs were recorded between ~10,000 and 9,300 cal yr BP (Kristjansdottir, 2005). On the north Iceland shelf the strongest influence of NIIC was also recorded in the surface waters and peaked between ~8,000 and 7,000 cal yr BP based on diatoms (Ran et al., 2008) and between ~8,000 and 7,300 cal yr BP based on benthic and planktonic foraminiferal assemblages (Knudsen et al., 2008).

The IC transports Atlantic water southward along the SE Greenland shelf. Stronger IC advection into the Denmark Strait with the farthest northward transport was

recorded between ~6,800 and 3,500 cal yr BP based on “Atlantic” foraminiferal species and stable isotopes (Jennings et al., 2011). Far-reaching effects of the IC have been recorded from the W Greenland shelf through greater flux of the IC component of the WGC. Relative stable conditions have been attributed to the IC at the seafloor between ~6600 and 1,600 cal yr BP on the W Greenland shelf south of Disko Bugt (Erbs-Hansen et al., 2013). In Disko Bugt warm temperatures between ~5,500 to 3,500 cal yr BP (“thermal optimum-like conditions”) have been attributed to the enhanced contribution from the Atlantic waters carried in the IC to the WGC (Perner et al., 2013). During this interval, the influence of fresh water either from the Greenland ice sheet and/or from the EGC was minimal (Perner et al., 2013).

4.5 Materials, Methods, and Proxies

4.5.1 Core Information

The two calypso cores, MD99-2256 (64°18.19’N and 24°12.40’W, 246 m water depth) and MD99-2259 (63°57.79’N, 24° 28.98′W, 385 m water depth), were collected during Leg IV of the *Images V cruise* of the French research vessel, *Marion Dufresne* (Labeyrie et al., 2003). Both cores were raised on the SW Iceland shelf in the SW-oriented Jökuldjup trough in the outer Faxafloi Bay (Jennings et al., 2000) (Figure 4.1).

4.5.2 Chronology

4.5.2.1 Calibration

Accelerator mass spectrometer (AMS) radiocarbon (^{14}C) dates of mollusks and foraminifera provide the age control for both cores (Table 4.1) The samples were dated

at the Accelerator Mass Spectrometry Laboratory at the University of Arizona; or prepared at the Laboratory for AMS Radiocarbon Preparation and Research (NSRL) at the Institute of Arctic and Alpine Research (INSTAAR), University of Colorado at Boulder and analyzed at the W.M. Keck Carbon Cycle Accelerator Mass Spectrometry Laboratory at the University of California at Irvine. All radiocarbon dates were calibrated using the marine model calibration curve of CALIB ^{14}C Calibration Program, Version 6.0 (http://radiocarbon.-pa.qub.ac.uk/calib/) (Stuiver et al., 1998). We obtained 15 radiocarbon dates for MD99-2259. We recalibrated the published thirteen ages in Olafsdottir et al., 2010, between 6.5 cm and 343.5 cm in MD99-2256, which comprise the Holocene portion of the core, using Calib 6.0. We assumed $\Delta R=0$, corresponding to an ocean reservoir age of 400 years (Eiriksson et al., 2004; Kristjansdottir, 2005), and an uncertainty of $\pm$50 years in ΔR for the time interval between 500 and 10,000 cal yr BP, investigated in this paper. Even though assuming a constant reservoir age of 400 years may be incorrect (Eiriksson et al, 2004), the SW shelf had reached fully postglacial conditions between ~9,900 and 9,700 ^{14}C yr BP (10,300 cal yr BP), with a strong influence of warm AW carried in the IC (Jennings et al., 2000). Significant shifts in reservoir age are linked to shifts in ocean currents (e.g. AW vs. polar waters) (Eiriksson et al., 2004; Jennings et al., 2011), which likely did not occur at our site. The North Icelandic shelf has been shown to have shifts in marine reservoir age that have been attributed to the transport of polar waters to their site (Eiriksson et al, 2004). The ages between the calibrated ^{14}C dates were calculated by applying a 0%-weighted fit though the median probability ages.

Table 4.1 Holocene dating control for the combined age model. Dates were combined from cores MD99-2256 and MD99-2259. The MD99-2259 depths were adjusted to the MD99-2256 depth scale.

Core	Central Depths (cm)	Adjusted Depths (cm)	14C lab #	Material	Reported age		relative probability	median probability age BP	1σ age range lower	1σ age range upper	rel. prob.	1σ age range lower	1σ age range upper	Previously published age BP*
MD99-2256	6.5	6.5	AA-58402	*Dentaliidae*	652 ±	36	1	302	248	393				295
MD99-2256	11	11.0	C-5729	*Scaphopod*	775 ±	40	0.95	408	355	476	0.05	335	343	423
MD99-2259	3	27.4	CURL-16660	*Uvigerina* sp	1370 ±	30	1	915	838	978				
MD99-2256	37.5	37.5	AA-58403	*Dentaliidae*	1466 ±	38	1	1017	933	1077				1005
MD99-2259 S	22.5	41.3	AA-81065	*Scaphapod*	766 ±	43	1	362	307	409				
MD99-2256	47.5	47.5	AA-58404	*Dentaliidae*	2154 ±	38	1	1745	1671	1832				1750
MD99-2259	32.5	53.9	CURL-12677	*Uvigerina* sp	2295 ±	15	1	1851	1818	1877				
MD99-2259	44.5	71.4	AA-81066	*Asarte undulatum*	2535 ±	45	0.956	2148	2075	2220	0.044	2148	2202	
MD99-2256	81	81.0	AA-70939	*Uvigerina* sp	2910 ±	40	1	2679	2595	2760				2701
MD99-2256 X**	113.5	113.5	AA-65331	*Hyalinea baltica, Uvigerina*	3840 ±	39	1	3794	3699	3875				3787
MD99-2256 A	123.5	123.5	AA-58405	Dentaliidae	3624 ±	41	1	3524	3441	3604				3516
MD99-2259 A	56.5	126.0	CURL-12678	*Uvigerina* sp	3525 ±	15	1	3359	3330	3384				
averaged		124.7						3441.5						
MD99-2259	70.5	139.0	CURL-12681	*Uvigerina* sp	3970 ±	20	1	3899	3858	3941				
MD99-2256 A	141.5	141.5	AA-70940	*Uvigerina* and *Globobulimina auriculata arctica*	4568 ±	44	1	4769	4676	4853				4746
MD99-2259 A	74.5	142.8	CURL 15596	*Uvigerina sp*	4235 ±	20	1	4276	4228	4330				
averaged		142.1						4522.5						
MD99-2259	84.5	152.1	AA-81067	*Asarte undulatum*	4950 ±	57	1	5214	5122	5301				
MD99-2256	163.5	163.5		*G, bulloides, N. incompta*	5636 ±	57	1	6042	5938	6126				6032
MD99-2259	104.5	171.2	CURL-12675	*G. bulloides, N. incompta*	5760 ±	20	1	6132	6097	6178				
MD99-2256	181.5	181.5	AA-70941	*Uvigerina* and *Globobulimina auriculata arctica*	6200 ±	56	1	6642	6546	6733				6634
MD99-2259	117.5	189.6	CURL-15501	*Uvigerina* sp	6845 ±	20	1	7323	7286	7360				
MD99-2259	130.5	195.0	AA-85200	*G. bulloides, N. incompta*	7361 ±	47	1	7774	7712	7831				
MD99-2259 S	130.5	195.0	AA-81068	*scaphapod*	1287 ±	44	1	829	762	902				
MD99-2256 R	197.5	197.5	CURL-7757	*Melonis barleeanus, Uvigerina* sp	7095 ±	25	1	7574	7516	7624				7577
MD99-2259	140.5	199.2	AA-85201	*G. bulloides, N. incompta*	7915 ±	49	1	8334	8289	8385				
MD99-2256	241	241	AA-70942	*Melonis barleeanus*	8379 ±	51	1	8969	8856	9084				8979
MD99-2256 A	281	281	AA-70943	*Bulimina marginata, Uvigerina* sp, *Melonis barleanus*	8978 ±	53	1	9659	9532	9742				9623
MD99-2259 A	178.5	285.6	CURL-1219	unid molusc	8990 ±	50	1	9599	9526	9654				
averaged		283.3						9629						
MD99-2256	315.5	315.5	AA-58406	*Dentaliidae*	9393 ±	66	1	10248	10159	10348				10,242
MD99-2256	343.5	343.5	AA-58407	*Axinopsis*	9424 ±	48	1	10281	10196	10357				10,266
MD99-2259 S	461.5	660.95	AA-81069	*scaphapod*	2869 ±	54	1	2615	2525	2725				

X** rejected in the original age model by Olafsdottir et al. (2010)

* previously published ages (Olafsdotir et al., 2010)

4.5.2.2 Composite Record for the Southwest Iceland Shelf

The motivation behind combining MD99-2256 and MD99-2259 into one composite record was to gain a high resolution record for the SW Iceland shelf and to compensate for the hiatus in MD99-2259 between ~3,600 and 2,700 cal yr BP (Figure 4.2).

We used AnalySeries 2.0 to correlate the magnetic susceptibility (MS) records from MD99-2256 and MD99-2259 measured during the MD99 cruise. The existing ages provided additional constraints on the correlation. Nine correlation pointers resulted in a correlation factor of 0.82. We used MD99-2256 as the reference core because it has the higher sedimentation rates (~320 cm of sediments in MD99-2256 is equivalent to ~205 cm in MD99-2259), and obtained the depths of MD99-2259 on the MD99-2256 depth scale, which allowed us to combine our records for a high resolution SW Iceland shelf record. (Figure 4.2)

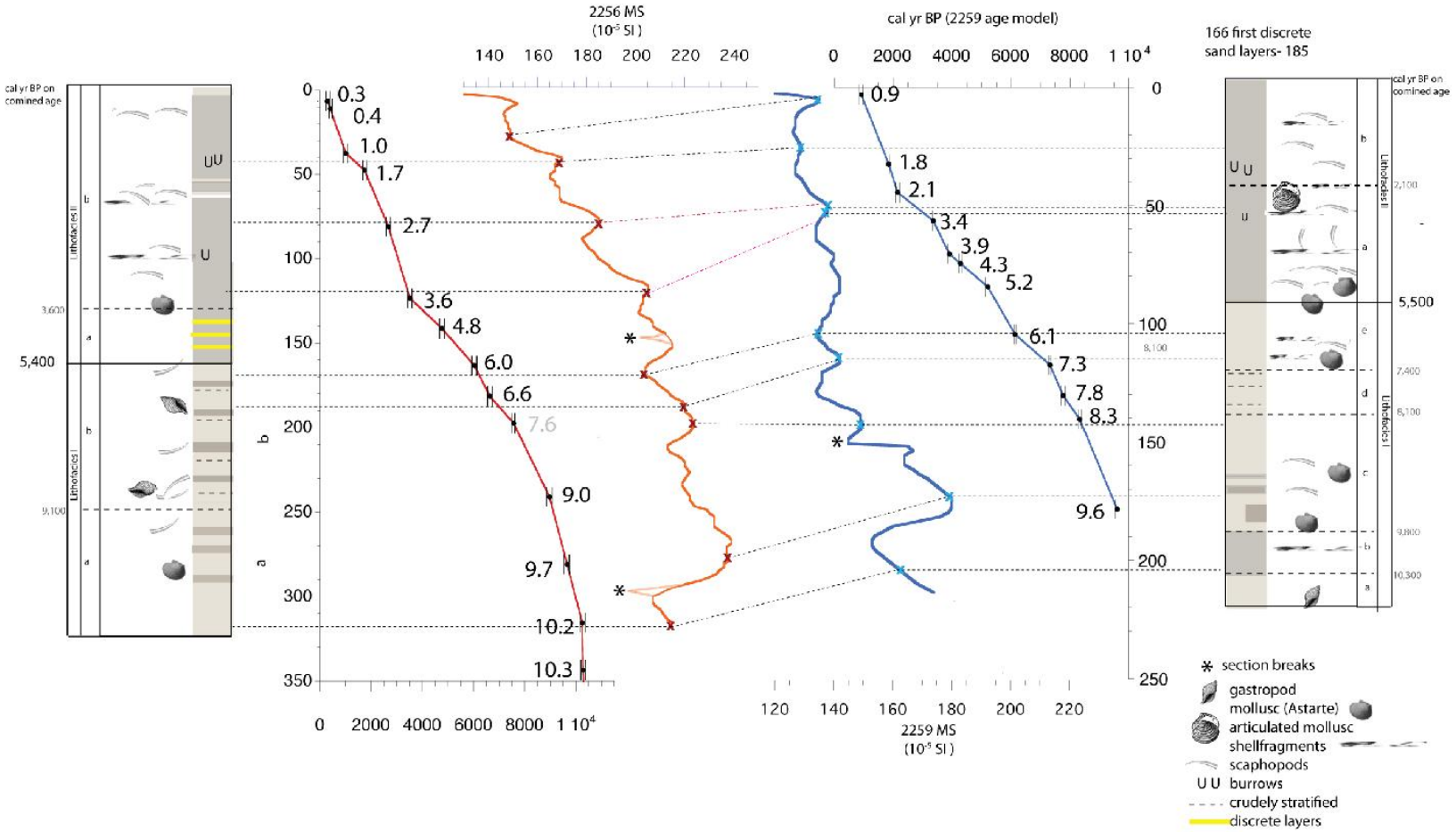

Figure 4.2 Composite core for the Southwest Iceland shelf

Based on the results of AnalySeries we comingled the ages for MD99-2256 and MD99-2259 onto the newly combined depth scale, expressed as MD99-2256 depths. Table 4.1 shows the dates that were used in the combined age model.

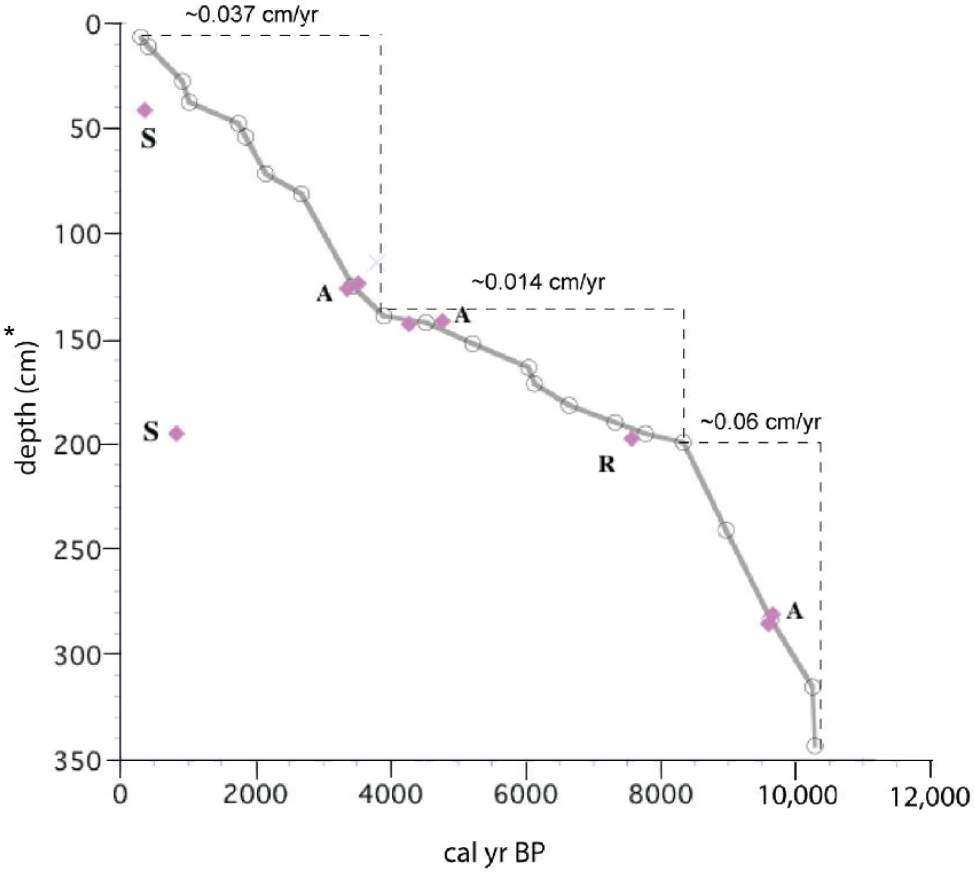

Figure 4.3 Combined chronologies with sedimentation rates for the SW Iceland shelf. The open circles indicate dates incorporated into the age model. A 0%-weighted line was fitted through the median probability age. Excluded dates are: S - scaphopods dates, dated too young; A - averaged dates; R – rejected dates for age reversals; X – date excluded in the 2256 original age model (see text for details). *- depth is expressed on the MD99-2256 depth scale

4.5.3 Sedimentological Proxies

4.5.3.1 Core description

The core descriptions are based on the visual inspection of the cores on board the ship (Labeyrie et al., 2003) supplemented by structures, such as lamination, changes in density, burrows, and shells, recognized in x-radiographs of the split cores.

4.5.3.2 Magnetic Susceptibility

Magnetic susceptibility (MS) was measured onboard the ship using a Geotek MultiSensor Track (MST), to which a Bartington loop sensor was mounted to minimize potential effect of the magnetic or metallic components of the MST (Labeyrie et al., 2003). The measurements were taken at 2-cm spacing. We used the MS of cores MD99-2256 and MD-2259 to find tie points to combine the two records into a composite SW Iceland Shelf record. Iceland is a volcanic island, and high MS indicates erosion of the Icelandic basalts that have a high concentration of the mineral magnetite (Andrews et al., 2003b). Variation in MS can indicate changes in source material or dilution by diamagnetic components, such as biologically derived carbonates.

4.5.3.3 Mineralogy

Calcium carbonate ($CaCO_3$%) content was determined at the INSTAAR Sedimentology Laboratory, using two different methods. In MD99-2256 the $CaCO_3$% was measured by coulometer on the <2mm sediment fraction, after the samples were ground to <74 μm. A 1-cm wide sediment slice was analyzed every 2cm. Weight% of $CaCO_3$ was evaluated on the >2mm sediment fraction in MD99-2256 and MD99-2259 using quantitative x-ray diffraction (q-XRD), following the protocol developed by Eberl

(2004). A 1-cm wide sediment slice was analyzed every 10cm. To distinguish the two methods we will refer to the $CaCO_3$ measured by coulometer as $CaCO_3$% and to the $CaCO_3$ measured by q-XRD as Calcite%. The $CaCO_3$ measurements are at a much higher resolution than the Calcite% but are only available for MD99-2256. To compare the biological production at the two sites we use the Calcite% data.

Quartz and potassium feldspar (Q-kspar) content were determined by q-XRD. Erosion of the late-Tertiary basalts that contain some intercalated sedimentary units and erosion yield calcic feldspars (Andrews et al., 2009). Therefore, Q-kspar can be used as a proxy for enhanced drift ice. Drift ice includes sea ice transport sediments from the Arctic Ocean through the Fram Strait (Andrews, 2009; Moros et al., 2006b), and can be either carried from the northwest to the SW Iceland shelf or carried around Iceland in the East Icelandic Current to the SW Iceland shelf (Jennings et al., 2001). Drift ice also includes suspended sediments carried in the EGC from icebergs that calved off the Greenland ice sheet (Andrews, 2009; Moros et al., 2006b).

4.5.4 Biological Proxies

The planktonic foraminiferal assemblages were established for MD99-2256. The sample resolution is ~100 yr. The thickness of the slices was 1cm, which represents 4 to 40 years. Sediment samples were freeze-dried and weighed, before they were wet-sieved in a stacked sieve set-up, separating them into three size fractions: 63-106 μm, a 106-1000 μm, and >1000 μm. Each sieved fraction was air dried and weighed, providing grain size information for each subsample depth. The 106-1000 μm was dry-sieved at 150 μm, and the planktonic foraminiferal analysis was performed at the >150-1000 μm

fraction. Samples were split to contain between ~200 and 300 planktonic foraminifera, which were then identified to species and expressed in percentages.

Summer sea surface temperatures (SSTs) were determined from the Pflaumann et al. (1996; 2003) planktonic foraminifera transfer functions.

The planktonic and benthic assememblages in MD99-2256 were analyzed using the statistical program Multivariate Statistical Package (MVSP) (Kovach, 1998). Only species that occurred at ≥2% in at least one sample were included. Foraminiferal assemblage zones were determined using constrained cluster analysis to leave the samples in their original stratigraphic order. Cluster analysis was run using squared Euclidean distances and minimum variance to find the centroid of each cluster. For each pair of clusters, the centroid is calculated and the variance of the new cluster is calculated. The pairs of the lowest variances are joined together. To determine which were the important foraminiferal species Principal Components Analysis (PCA) was performed. For the PCA, the data were standardized to reduce the effect of dominant species, giving rarer species a greater role (Davis, 1973); the data were centered and log-ratio transformed to avoid closed arrays, where data add up to 100% (Aitchison, 1986; Andrews et al., 2001a). The principal component (PC) axes were extracted applying the Kaiser Rule, which states that the minimum eigenvalue should be the average of all eigenvalues (Legendre and Legendre, 1983). Diversity patterns of foraminiferal assemblages were determined using the Shannon Diversity Index. This index is sensitive to changes in the number of species and their abundances and has been suggested to reflect variations in the physical structure of the ocean (Rutherford et al., 1999).

4.6 Results and Interpretation

4.6.1 Lithofacies

MD99-2256 and MD99-2259 are divided in two lithofacies. We used the combined age model to determine the ages of lithofacies. Table 4.2 shows the lithofacies ages on the MD99-2256 and MD99-2259 age models and the combined age model. Based on the MD99-2256 chronology alone, the entire core between ~350cm (~10,300 cal yr BP) and ~6.5cm (~300 cal yr BP) has a linear sedimentation rate of ~0.03cm/yr. By comingling the ages, we were able to get a more detailed age model. The sedimentation rates are derived from the combined age model.

Table 4.2 Lithofacies ages. The lithofaces ages presented in this chapter are based on the combined age model. Lithofacies ages based on the MD99-2256 and the MD99-2259 age model are shown in this table for comparison.

Core	Lithofacies	Subfacies	MD99-2256 age model (cal yr BP)	Combined age model (cal yr BP)
MD99-2256	I		~10,000-5,400	~!0,000-5,600
		Ia	~10,000-9,100	~10,000-9,100
		Ib	~9,100-5,400	~9,100-5,600
	II		~5,400-300	~5,600-300
		IIa	~5,400-3,600	~5,600-3,900
		IIb	~3,600-300	~3,900-300

Core	Lithofacies	Subfacies	MD99-2259 age model (cal yr BP)	Combined age model (cal yr BP)
MD99-2259	I		~10,300-5,500	~10,300-5,600
		Ia	~10300-10,300	~10,300-10,200
		Ib	~10,300-9,800	~10,300-9,800
		Ic	~9,800-8,100	~9,800-8,100
		Id	~8,100-7,400	~8,100-7,400
		Ie	~7,400-5,500	~7,400-5,400
	II		~5,500-700	~5,600-700
		IIa	~5,500-2,100	~5,600-2,100
		IIb	~2,100-700	~2,100-700

4.6.1.1 Lithofacies: MD99-2256

MD99-2256 consists of two lithofacies: Lithofacies I: ~300-155cm (~10,000-5,600 cal yr BP) and Lithofacies II: ~155 – core top (~5,400 cal yr BP to 300 cal yr BP).

The interpretation of the environmental changes preserved in the lithfacies of MD99-2256 is augmented by the results of the >1mm size fraction, Q-kspar%, and $CaCO_3$%. The weight percent of >1mm size fraction ranges from 0 to 2.2%, the Q-kspar% from 0 to 2.6%, and the $CaCO_3$% from ~2.6 to 8.2%.

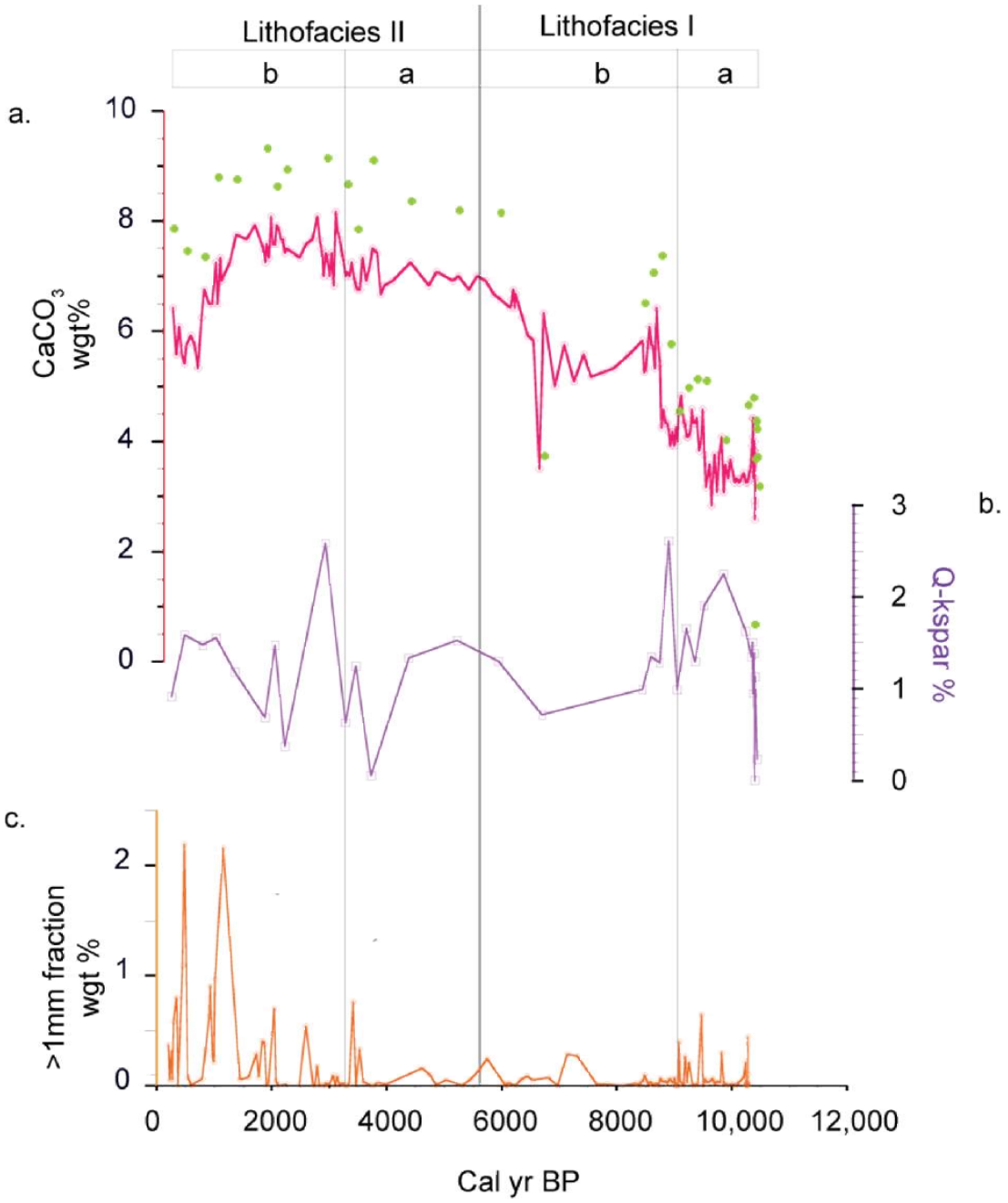

Figure 4.4 MD99-2256 Lithofacies and Sedimentology. In panel a., the $CaCO_3$ weight% is shown in red. Green symbols indicate measurements for Calcite weight%. The Calcite% tracks the measurements of $CaCO_3$%. In panel b. the combined weight percentages of quartz and potassium feldspar (q-kspar%) are presented. Panel c shows the >1mm sieve-fraction weight percent.

Lithofacies I is subdivided into two subfacies (a, b) based on the amount of macrofossils and the MS values. Subfacies “a” (~10,300-9,100 cal yr BP) consists of sandy mud, interspersed with mud intervals. It contains few macrofossils. The sedimentation rates are high (0.06cm/yr) in this interval. The weight% of the >1mm size fraction and Q-kspar are elevated, accompanied by low $CaCO_3$%. Sediments in this interval show a strong terrestrial signal based on the elevated MS values (compared to the entire record), with some ice rafted debris present as the Q-kspar% suggest with a peak of ~2.8% at ~9,800 cal yr BP. The biological productivity was low between ~10,300 and 9,100 as recorded in the $CaCO_3$%, and some of the $CaCO_3$ was detritral carbonate from the Laurentide ice sheet {Jennings, submitted #1110}.

Subfacies “b” (~9,100 to 5,600 cal yr BP) is bioturbated, crudely stratified and consists of sandy mud. It differs from subfacies “a” because it contains frequent and well-defined mud layers. There are also more macrofossils and MS values are higher in subfacies “b” than in subfacies “a”. Subfacies “b” has the highest MS values, beginning at ~9,000 cal yr BP and ending ~ 8,300 cal yr. The highest ice rafting event in the entire Holocene occurred at ~8,700 cal yr BP, as recorded in the percent of Q-kspar (~2.6%). The $CaCO_3$% increases stepwise at ~9,400 cal yr BP, from <4% to >4%. Between ~8,700 cal yr BP and 8,600 cal yr BP the largest increase occurred in the $CaCO_3$ content, increasing from ~4.5 to 6.4%. The end of the highest MS intervals at ~8,600 cal yr BP coincides with the termination of rapid postglacial isostatic rebound in south Iceland. Postglacial isostatic rebound was rapid in Iceland and uplift had ended between ~8,700 and 8,400 cal yr BP (IntCal13) (7,800$\pm$60 ^{14}C yr BP; (Norddahl and Petursson, 2005). The age for the end of postglacial rebound is based on the extensive flow of the

fijórsárhraun lava, which flowed into the sea at ~15 m below modern sea level at ~8,600 cal yr BP (Norddahl and Petursson, 2005).

Sedimentation rates are highest (0.06 cm/yr) until ~8,300 cal yr BP. The period of high sedimentation rates coincides with the maximum input of terrestrial material as interpreted from the high MS values. We interpret that the eustatic sea level was still rising in the interval and terrestrial erosion was high. At ~8,300 cal yr BP the interval with the lowest sedimentation rates (0.014cm/yr) starts. Sedimentation rates remained low until ~3,900 cal yr BP. MS was lowest between ~6,100 and 5,500 cal yr BP falling within the low sedimentation rate interval (0.014 cm/yr). A brief excursion with an ~3% drop in $CaCO_3$% was centered around ~6,500 cal yr BP.

Lithofacies II (~5,600 cal yr BP to 300 cal yr BP) is divided into two subfacies based on macrofossils. Subfacies “a” (~5,600-3,900 cal yr BP) consists of stratified muddy sand with discrete layers of sand, containing no macrofossils. This is in an interval of slow sedimentation rates (0.014 cm/yr). Subfacies “b” (~3,600 to 300 cal yr BP) consists of bioturbated muddy sand with layers of scaphopods (not in life position). This subfacies contains more macrofossils than any of the previous facies. The sedimentation rates (~0.037 cm/yr) increased starting at ~3,900 cal yr BP and stayed fairly linear to the core top. The very top (0-7cm) is coarser again with fragmented scaphopods.

4.6.1.2 Lithofacies: MD99-2259

MD99-2259 consists of two lithofacies: Lithofacies I (~220-90cm) (~10,300-5,600 cal yr BP) and Lithofacies II (~90cm-core top) (~5,600 cal yr BP to core top). MS values for the entire core range from ~124 to 180 with a mean of ~145. Between ~10,300 and

8,000 cal yr BP, the MS values are above the mean and after 8,000 they drop below the mean. The interpretation of the lithofacies in MD99-2259 is augmented by the results of the >1mm size fraction, Q-kspar%, and $CaCO_3$%. The weight percent of >1mm size fraction ranges from 0 to ~4%, the Q-kspar% from 0 to ~6.7% and the Calcite% from ~7 to 16%.

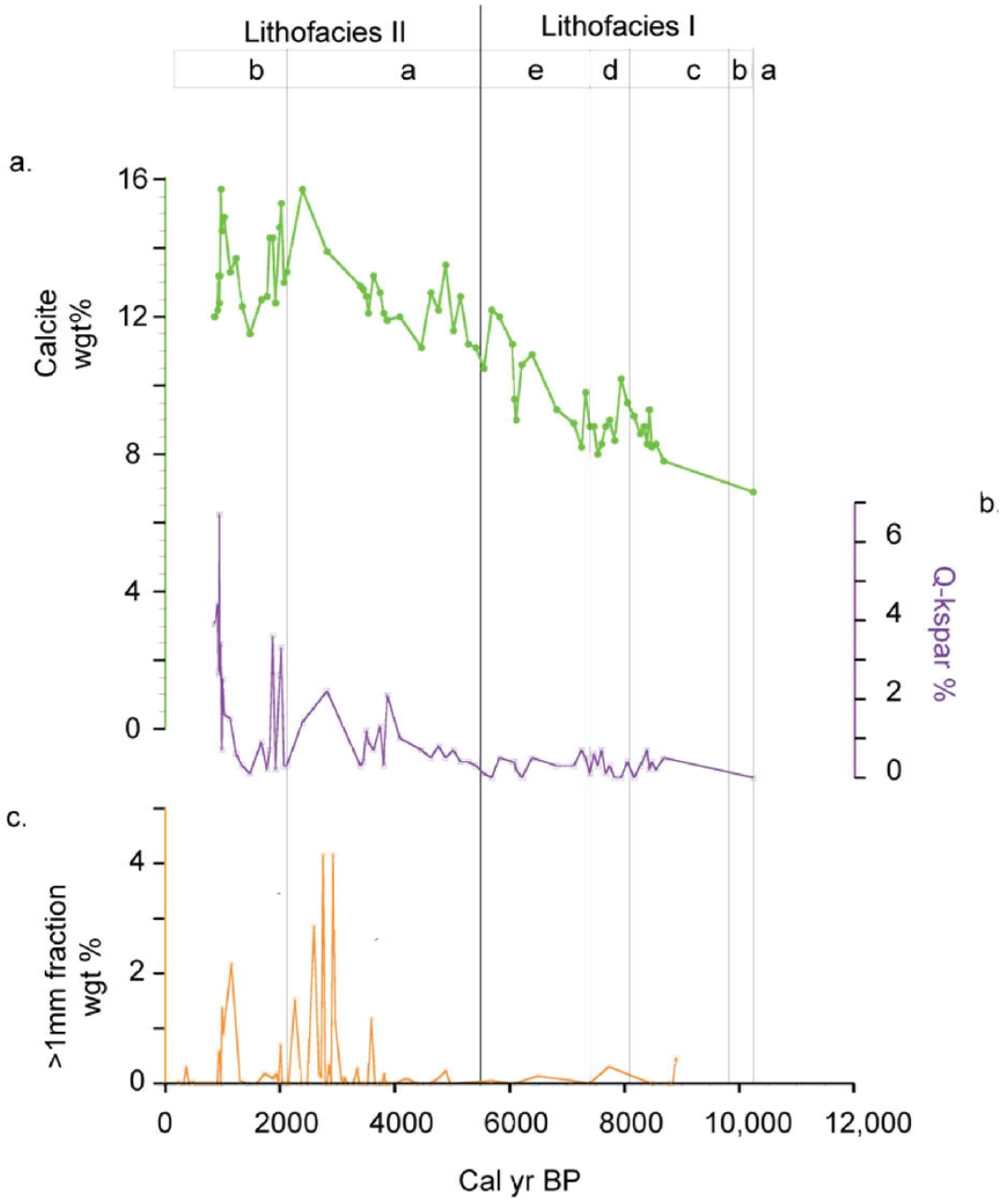

Figure 4.5 MD99-2259 Lithofacies and Sedimentology. In panel a., the Calcite weight% is shown in green. In panel b the combined weight percentages of quartz and potassium feldspar (q-kspar%) are presented. Panel c shows the >1mm sieve-fraction weight percent.

Lithofacies I can be divided into five subfacies based on structure and macrofossil content. Subfacies “a” consists of sandy mud, ending at *~10,200 cal yr BP*. The high MS values between 168 to 157cm suggest an increase in terrestrial erosion. Calcite% is at its lowest value (~6.9%). Subfacies “b” ~10,300-9,800 cal yr BP is an interval of muddy sand that contains a layer of current reworked scaphopods. Sedimentation rates are high (~0.06 cm/yr).

Subfacies “c” (~9,800-8,100 cal yr BP) consists of sandy mud with some intervals of muddy sand. It contains better-preserved macrofossils than in the earlier subfacies. Sedimentation rates were high (0.06 cm/yr) and MS values peaked in this interval, suggesting that terrestrial material was deposited to the site, likely due to rising sea level. Subfacies “d” (~8,100-7,400 cal yr BP) is crudely stratified, consisting of muddy sand. The sedimentation rates in this interval dropped to ~0.014 cm/yr. MS rates were declining linearly all the way to the core top. These characteristics suggest that the site had experienced less terrestrial input than in the early Holocene. Subfacies “e” (~7,400-5,600 cal yr BP) consists of muddy sand with more macrofossils than the previous subfacies. The Calcite% is steadily increasing from ~6% to 8% but interrupted by a drop centered around ~6,100 cal yr BP. Sedimentation rates are the same as in the previous facies (~0.014 cm/yr).

Lithofacies II consists of sandy mud. It can be divided into two subfacies based on macrofossils. Subfacies “a” (~5,600-2,100 cal yr BP) contained the most macrofossils in the core. The interval is bioturbated. Sedimentation rates increase at ~3900 cal yr BP from 0.014cm/yr to 0.059 cm/yr. This change coincides roughly with one of the layers of scaphopod fragments. Calcite% peaks at ~2,400 cal yr BP at ~16%.

The highest >1mm fraction weight % occur between ~3,000 and 2,500 cal yr BP. Subfacies “b” (~2,100 to core top) (~2,100 to core top) is more bioturbated than the subfacies below. Even though MS is fairly linear after ~8,100 cal yr BP the MS is slightly lower in this interval. There are scaphopods and several burrows visible. Sedimentation rate in this interval was 0.059 cm/yr.

4.6.2 Foraminifers

4.6.2.1 Planktonic Foraminifers

Ten species of planktonic foraminifera were identified in 92 samples between 10,300 and 200 cal yr BP (Table 4.3), of which nine were statistically significant. Cluster analysis divided the fauna into three planktonic foraminiferal zones (PFZ) (Figure 4.5).

Table 4.3 Planktonic and benthic foraminifera species list. All planktonic species identified are listed; statistically insignificant species in gray font. Only statistically significant benthic foraminifera are listed; complete species list in Olafsdottir et al., (2010).

Planktonic Foraminiferal Species
Globigerina bulloides (d'Orbigny, 1826)
Globigerinita quinqueloba (Natland, 1938)
Globigerinita glutinata (Egger, 1893)
Globigerinita uvula (Ehrenberg, 1861)
Globorotalia inflata (d'Orbigny, 1839)
Neogloboquadrina dutertrei (d'Orbigny, 1839)
Neogloboquadrina incompta (Cifelli, 1961; *N. pachyderma* (dextral) (Ehrenberg, 1861)
Neogloboquadrina pachyderma (sinistral) (Ehrenberg, 1861)
Orbulina universa (d'Orbigny, 1839)
Pachyderma-Dutertrei Integrade (Kipp, 1976)

Benthic Foraminiferal Species
Astrononion gallowayi (Loeblich and Tappan, 1953)
Bulimina marginata (d'Orbigny, 1826)
Cassidulina laevigata (d'Orbigny, 1826)
Cassidulina neoteretis (Seidenkrantz, 1995)
Cassidulina obtusa (Willianson, 1858)
Cassidulina reniforme (*Cassidulina crassa* var. *reniforme*; Norvang, 1945)
Cassidulinoides bradyi (Norman, 1880)
Cibicides lobatulus (Walker and Jacob, 1798)
Hyalinea balthica (Schroeter, 1783)
Melonis barleeanus (Williamson, 1858)
Nonionella auricula (Heron-Allen and Earland, 1930)
Nonionella iridea (Heron-Allen and Earland, 1932)
Nonionella turgida (Williamson, 1858)
Pullenia bulloides (d'Orbigny, 1839) (*Nonionina bulloides*, d'Orbigny 1846)
Pullenia osloensis (Feylind-Hanssen, 1954)
Pullenia subcarinata (d'Orbigny, 1839)
Stainforthia fusiformis (Williamson, 1858)
Trifarina angulosa, also *Angulogerina angulosa* (Williamson, 1858)
Uvigerina mediterranea (Hofker, 1932)

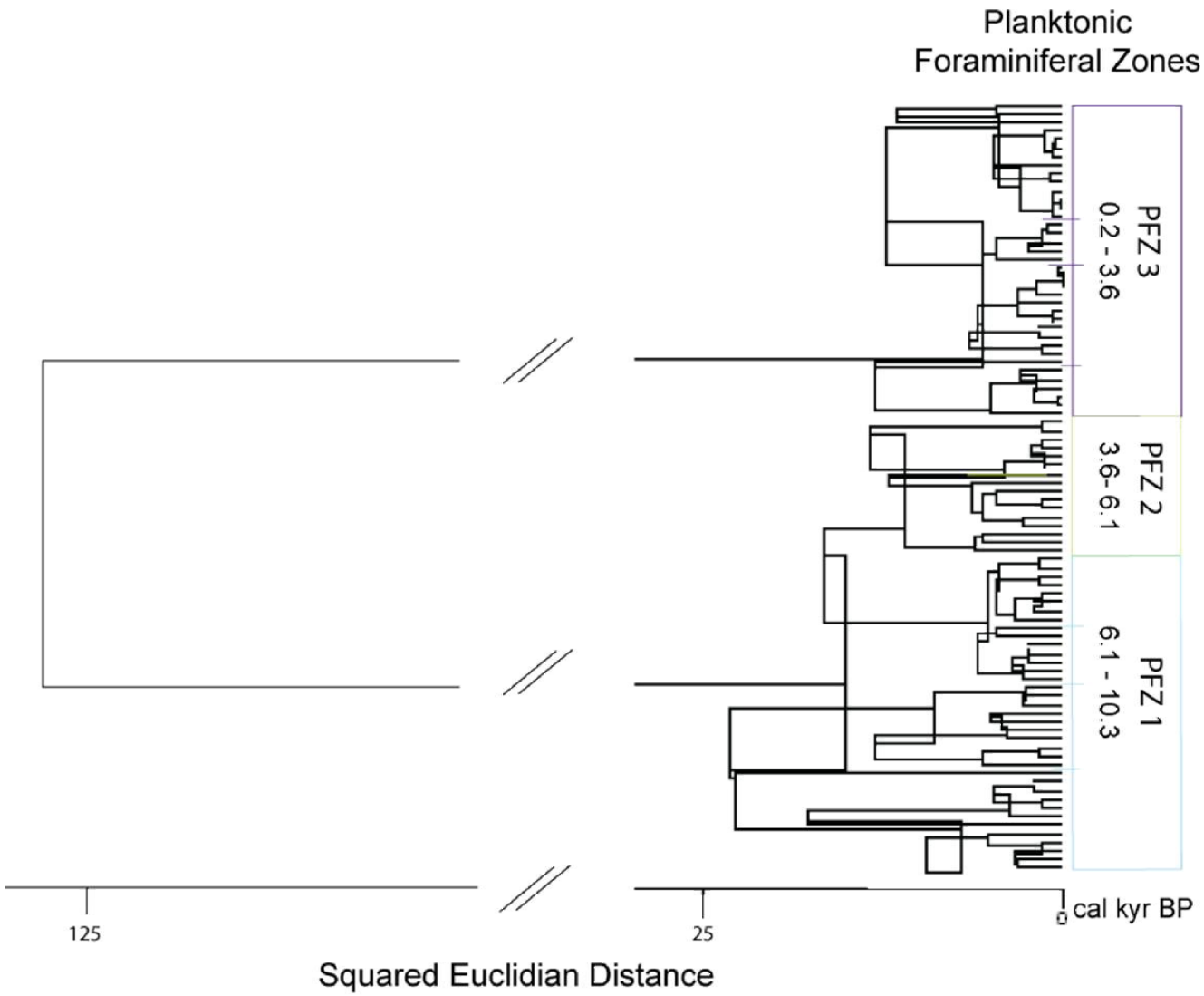

Figure 4.6 Dendrogram: planktonic foraminiferal assemblages. Three planktonic foraminiferal zones (PFZs) were identified.

PFZ 1 extends from 10,300 to 6,100 cal yr BP (Figure 4.4). This zone is dominated by *G. bulloides,* ranging from ~37% to 85%. The distribution of *G. bulloides* has been linked to nutrient availability (Schiebel and Hemleben, 2000). G. bulloides thives in a well-mixed water column, usually ~40-60m deep in the eastern North Atlantic, but can deepen with intense storms (Schiebel and Hemleben, 2000) rather than to temperature. (Schiebel et al., 2001). The percentages of *G. bulloides* drop to ~40% at 8,700 cal yr BP and ~37% at ~7,800 cal yr BP. These drops in the percentages of *G. bulloides* coincide with increases in the percentages of *Neogloboquadrina pachyderma* (sinistral) (NPS) and T. *quinqueloba*. NPS is an arctic species and suggests cooling. *T. quinqueloba* varies between 0 to 33% between 10,300 and 7,800 cal yr BP, peaking at 7,800 cal yr BP. After ~7,800 cal yr BP, the percentages of *T. quinqueloba* drop and remain relatively low until ~3,000 cal yr BP. This species is associated with oceanic fronts where available nutrients are increased (Pflaumann et al., 1996). The *T. quinqueloba* spike at ~7,800 cal yr BP may suggest an advance of Polar water.

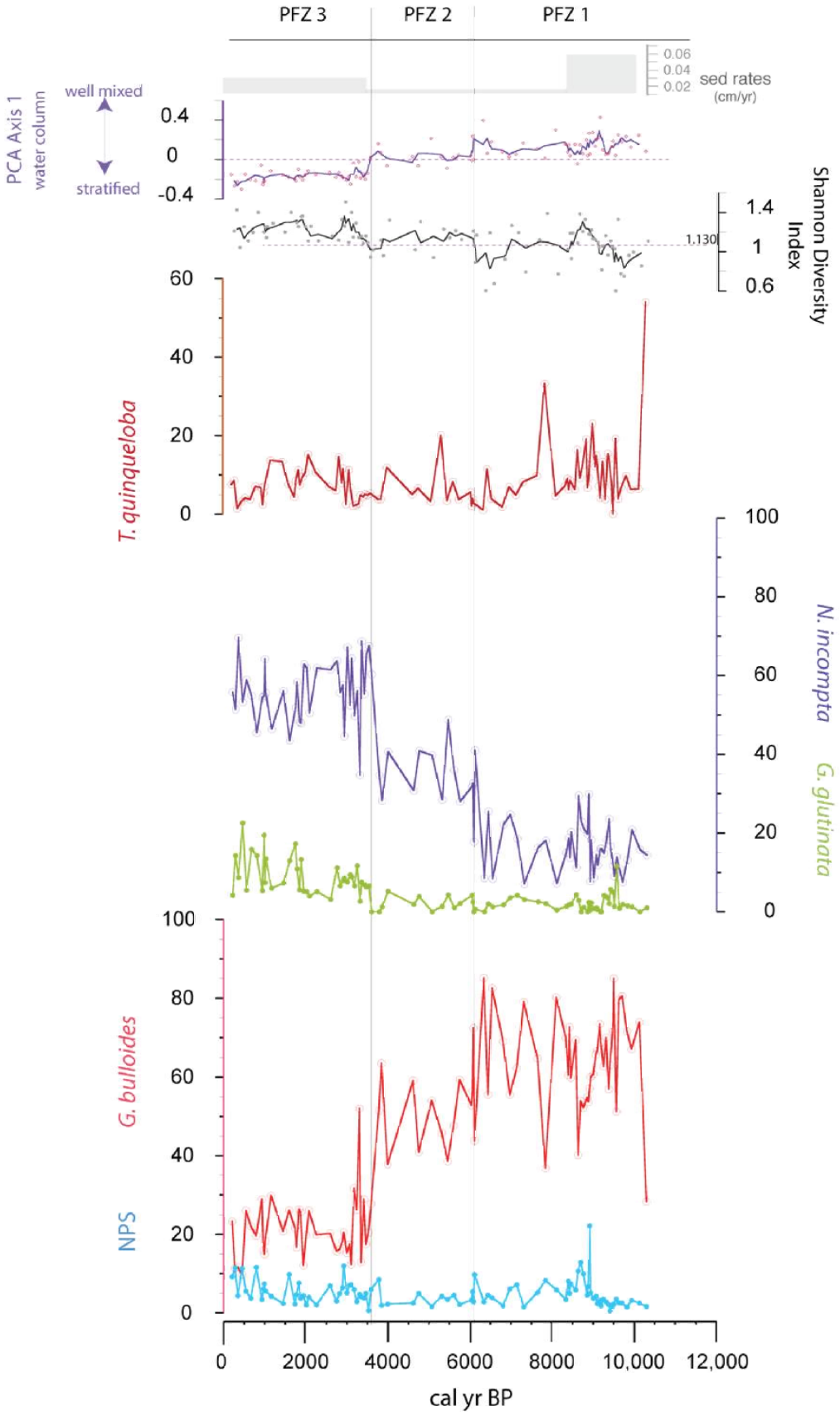
PFZ 3
PFZ 2
PFZ 1
0.06
0.04
0.02
sed rates
(cm/yr)
PCA Axis 1
water column
well mixed
stratified
0.4
0
-0.4
1.4
1
0.6
1.130
Shannon Diversity
Index
60
40
20
0
T. quinqueloba
100
80
60
40
20
0
N. incompta
G. glutinata
100
80
60
40
20
0
G. bulloides
NPS
0
2000
4000
6000
8000
10,000
12,000
cal yr BP

Figure 4.7 Planktonic foraminiferal zones (PFZs). Three PFZs were identified: PFZ 1 from ~10,300 to 6,100 cal yr BP, PFZ 2 from ~6,100 to 3,600 cal yr BP, and PFZ 3 from ~3,600 to 200 cal yr BP. Shown (top to bottom): sedimentation rates, PC Axis 1, Shannon Diversity Index, and percentages of selected planktonic foraminiferal species.

PFZ 2 extends from ~6,100 to 3,600 cal yr BP. This zone is characterized by lower percentages of *G. bulloides*, ranging from 38 to 72%, averaging ~50%, and by higher percentages of *N. incompta,* ranging from 22 to 41%. *N. incompta* has been associated with decreased nutrient supply in shallow mixed layer depths (stratified water column) (Schiebel et al., 2001).The percentages of *T.quinqueloba* range from 2 to 12%, except for one spike of ~20% at 5,300 cal yr BP.

PFZ 3 extends from ~3,600 to 200 cal yr BP. In this zone, *N. incompta* is the dominant species, ranging from 46% to 64%; percentages of *G. bulloides* fall to 10 to 32%, except for an interval of higher percentages between ~3,200 and 3,400 cal yr BP, that reaches ~52% at ~3,300 cal yr BP. The percentages of NPS are slightly increased, suggesting cooling after ~3,800 cal yr BP. The percentages of *T. quinqueloba* increase overall and range between 1 and 15% and may signal the proximity of the marine Polar front (Johannessen et al., 1994). The assemblages in this zone resemble modern assemblages. The percentages of *G. glutinata* increase. This species blooms in early spring (Schiebel and Hemleben, 2000) and occur adjacent to upwelling areas {Hilbrecht, 1996 #1022}. The recent planktonic assemblages on the SW Icelandic shelf discussed in Jennings et al. (2004) consist of ~45% *N. incompta*, <10% of *G. bulloides*, and ~20% of *T. quinqueloba* (Jennings et al., 2004). Today, *N. incompta* occurs in the warmer water masses associated with the NAC and the IC, while NPS dominates the very cold Polar water masses of the EGC. *G. bulloides* has a “scattered distribution” in the North Atlantic along the flow paths of the NAC and the IC (Pflaumann et al., 1996), which is

consistent with the faunal distribution in PFZ3. But it occurs at high abundances, similar to PFZ1, at gyre boundaries in the North Atlantic.

Principle component analysis (PCA) (Davis, 1973) of the first four axes (>1 eigenvalue) explains 71% of the variance (Table 4.4). PC Axis 1 explains ~29% of the variance (Table 4.4). PC Axes 2, 3, and 4 explain ~16, 14, and 12% of the variance, respectively, which make interpreting the possible environmental controls on the variances difficult. We will limit our discussion to the first PC axis. Strongly positively loaded on PC Axis 1 are species that thrive in nutrient-rich waters, such as *G. bulloides* (0.552) and *Neogloboquadrina dutertrei* (0.331). *G. bulloides* is abundant in well-mixed upper water columns with high nutrient content (Schiebel et al., 2001) and *N. dutertrei* in upwelling regions, which are also associated with high nutrient content (Be and Tolderlund, 1971). Negatively loaded on Axis 1 are *Globigerinta glutinata* (-0.512) and *Neogloboquadrina incompta* (-0.492). *G. glutinata* is found at the margins of upwelling regions with elevated nutrients (Hilbrecht, 1996) and *N. incompta* is found in regions in the northeast North Atlantic in areas of low nutrients (Schiebel et al., 2001). PCA Axis 1 is interpreted to reflect water column stratification, with the end members being well mixed and stratified. Well-mixed waters are nutrient rich (Schiebel et al., 2001), because mixing renews the nutrients. The surface layer in stratified waters is usually nutrient poor (Taboada and Anadon, 2012) because nutrients in the surface water are quickly consumed and not renewed.

Table 4.4 Planktonic foraminiferal PCA loadings. Data were centered-logratio transformed. Data were standardized.

Planktonic foraminifera				
	Axis 1	Axis 2	Axis 3	Axis 4
Eigenvalue	2.613	1.458	1.259	1.068
Percentage	29.031	16.2	13.987	11.866
Cumulative Percentage	29.031	45.231	59.218	71.084
PCA variable loadings				
NPS	-0.096	**-0.200**	**-0.207**	**-0.756**
N. incompta	**-0.492**	0.062	-0.083	**0.179**
G. bulloides	**0.552**	0.024	0.024	0.070
G. glutinata	**-0.512**	-0.085	-0.037	**0.162**
T. quinqueloba	0.059	**-0.582**	**0.152**	**0.269**
G. inflata	0.045	**0.650**	**-0.202**	**-0.183**
Orbulina sp.	**0.223**	**0.187**	**-0.433**	**0.485**
G. dutertrei	**0.331**	**-0.331**	**-0.298**	**-0.144**
P-D intergrade	**0.132**	**0.208**	**0.780**	-0.061

4.6.2.2 Benthic Foraminifers

Olafsdottir et al. (2010) identified 61 calcareous benthic species in the interval ~10,300 and 200 cal yr BP. Nineteen of the 61 species identified were statistically significant. The entire species list has been published in Olafsdottir et al., 2010. Olafsdottir et al., 2010 used the benthic assemblages primarily to reconstruct bottom water temperatures, whereas our goal is to assess the influence of the SPG on the marine environment on the SW Iceland shelf. We expect to find different benthic assemblages when the SPG is extended compared to the benthic assemblages when the SPG contracted. In the extended state, the IC entrains more polar water in its transit in the SPG and the IC is fresher and colder. We expect the water column to be more mixed because of stronger winds in the NAO+ mode. In the contracted state, the IC

carries warmer and more saline Atlantic waters. We expect the water column to be less mixed because of weaker winds in the NAO- mode. If polar waters from the EGC spread onto the SW Iceland shelf, we expect to see a stratified water column. Warm Atlantic waters overlain by a lens of the polar freshwater favor increased cocolithosphore production on the North Icelandic shelf (Giraudeau et al., 2004) and more organic matter accumulates on the sea floor.

Cluster analysis between ~10,300 and 200 cal yr BP divided the benthic assemblages into three benthic foraminiferal zones (BFZ) (Figure 4.8).

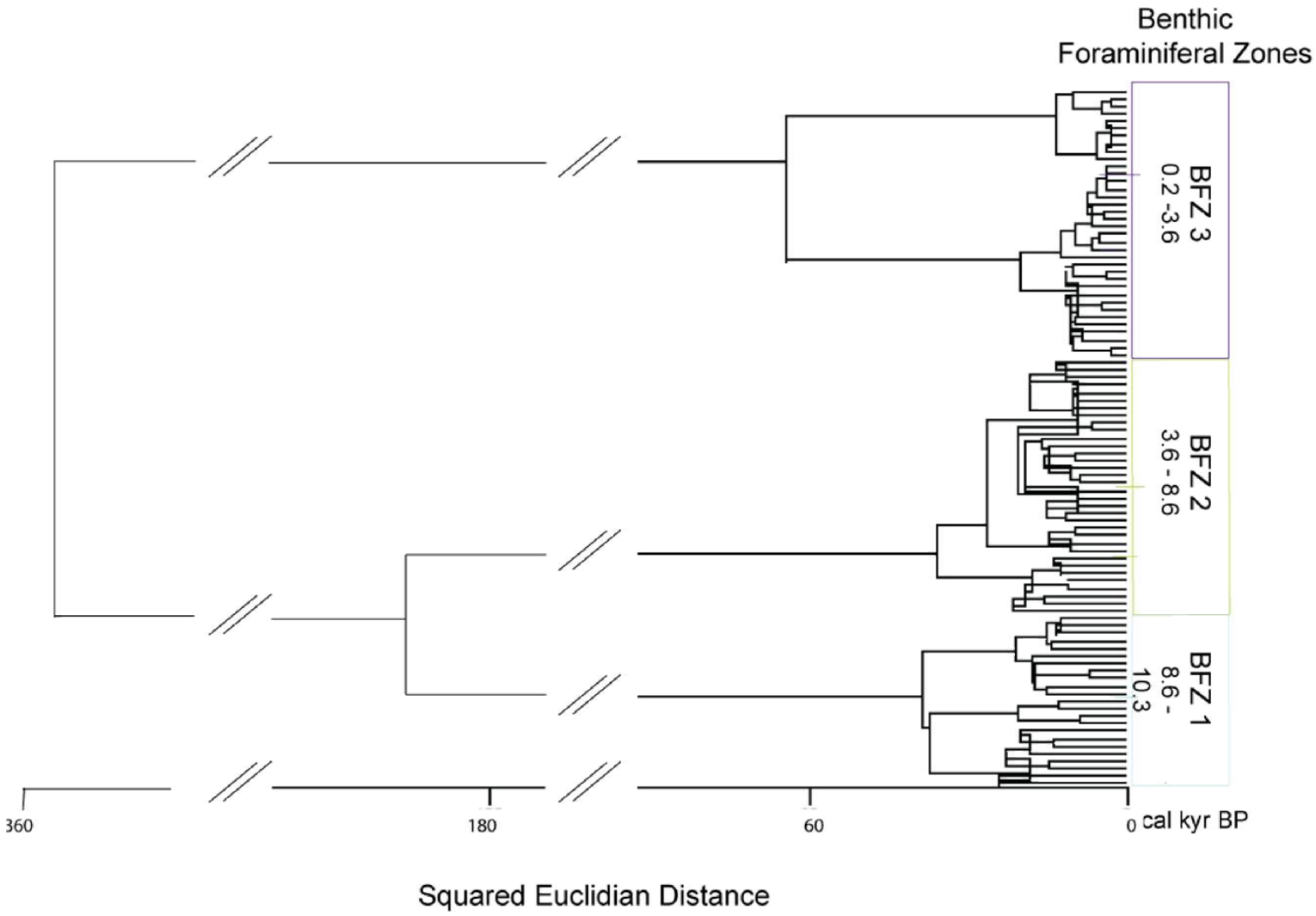

Figure 4.8 Dendrogram: benthic foraminiferal assemblages. Three Benthic foraminiferal zones (BFZs) were identified.

BFZ 1 extends from ~10,300 to 8,600 cal yr BP. This interval is characterized by high percentages of *Bulimina marginata*, ranging from ~22 to 37% and relatively high percentages of *Cassidulina neoteretis*, ranging from 7 to 20%. *B. marginata* is an opportunistic infaunal species and has been associated with high amounts of labile nutrients (Murray, 2006). *C. neoteretis* is limited to arctic and “cold boreal” regions (Jennings et al., 2004; Seidenkrantz, 1995) and is found on the Greenland shelf in chilled Atlantic water, associated with chilled IC water and a stratified water column (Jennings et al., 2011). It may be related to the high nutrient content of Atlantic water and with phytoplankton blooms (Jennings et al., 2004). *Cassidulina laevigata*, a shallow infaunal (Alve and Bernhard, 1995) boreal species (Jennings et al., 2004), is present throughout the record but is less dominant in this zone and only comprises ~38% of the assemblage because of the high percentages of *B. marginata*. This zone falls within the interval with the highest sedimentation rates

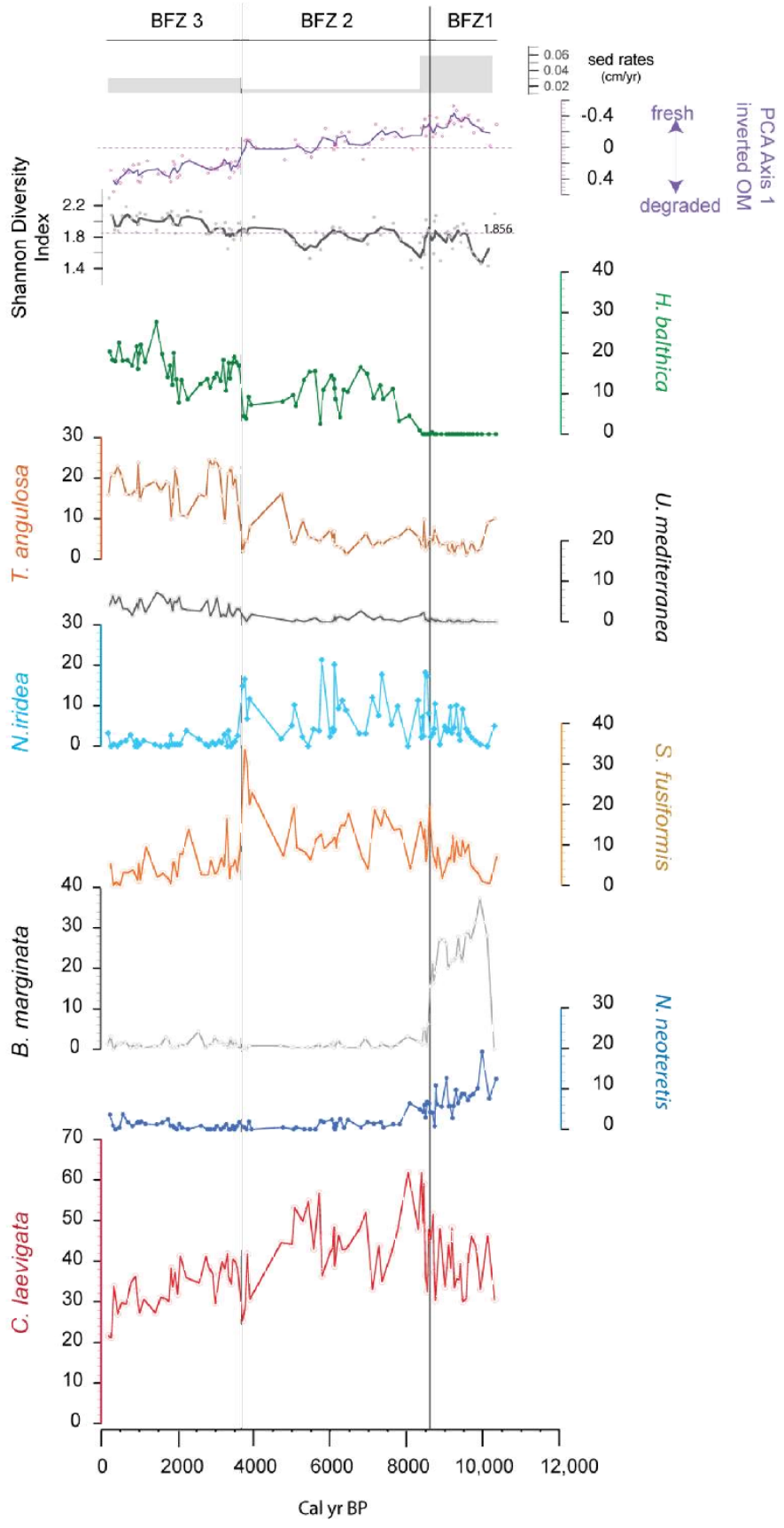
BFZ 3
BFZ 2
BFZ1
sed rates (cm/yr)
0.06
0.04
0.02
-0.4
0
0.4
fresh
degraded
PCA Axis 1 inverted OM
Shannon Diversity Index
2.2
1.8
1.4
1.856
H. balthica
40
30
20
10
0
T. angulosa
30
20
10
0
U. mediterranea
20
10
0
N.iridea
30
20
10
0
S. fusiformis
40
30
20
10
0
B. marginata
40
30
20
10
0
N. neoteretis
30
20
10
0
C. laevigata
70
60
50
40
30
20
10
0
0
2000
4000
6000
8000
10,000
12,000
Cal yr BP

Figure 4.9 Benthic foraminiferal zones (BFZs). Three BFZs were identified: BFZ 1 from ~10,300 to 8,600 cal yr BP, BFZ 2 ~8,600 to 3,600 cal yr BP, and BFZ 3 from ~3,600 and 200 cal yr BP. The sedimentation rates are shown in the upper most panel. Highest sedimentation rates fall within BFZ 1 and lowest sedimentation rates in BFZ 2. Shown are PC Axis 1 (inverted) (OM=organic matter), Shannon Diversity Index, and percentages of selected benthic foraminiferal species.

BFZ 2 extends from 8,600 to 3,600 cal yr BP. Two opportunistic infaunal species characterize this interval, are *Nonionella iridea*, a shallow infaunal species (Gooday and Hughes, 2002), which is most common after the spring bloom and feeds on fresh detritus (Alve, 2010) and thrives as soon as food becomes available (Gooday and Hughes, 2002) and *Stainforthia fusiformis,* an infaunal opportunistic species (Alve, 1995; Alve and Bernhard, 1995) that responds rapidly to input of food (Alve and Murray, 1999). *C. laevigata* has its highest abundances in this interval, ranging from ~25 to 62%. It is an infaunal boreal species, found in regions with ample food supply (Murray, 2006). *Hyalinea balthica*, ranging from 0 to 16%, and *Angulogerina angulosa*, ranging from ~1 to 16%, appear in this interval but occur at higher percentages in the BFZ3 interval between ~3,600 and 200 cal yr BP. *H. balthica* is a shallow infaunal species (Hess and Jorissen, 2009) and is found in muddy substrates in seasonally stratified waters (Murray, 2006). A*. angulosa* is an epifaunal (Murray, 2006) and shallow infauna speciesl (Duros et al., 2011) common in areas with high productivity in the surface waters (Gupta, 1997).

BFZ 3 extends from ~3,600 to 200 cal yr BP. *H. balthica*, ranging ~8 to 28%, and *A. angulosa*, ranging from 9 to 24%, have their highest distributions in this interval. These species indicate that the water column is stratified and productivity in the surface

waters is high (Gupta, 1997; Murray, 2006). *Uvigerina mediterranea* has the highest percentages in this interval, ranging from ~1 to 7%. This shallow infaunal species is found in regions with high content of labile organic matter that has been decomposed by bacteria (den Dulk et al., 2000). *C. neoteretis*, never exceeding 4%, and *B. marginata*, never exceeding 5%, return to the assemblages but never reach the high percentages that they had in the BFZ1. Other arctic species (not shown) appear in very low percentages in this interval, such *Cassidulina reniforme* (<0.5%), the deep-infaunal *Nonionella auricula* (<1%), and *Elphidium excavatum* forma *clavata* (<2%) that can tolerate fluctuating environments (Hald and Korsun, 1997).

Principle component analysis (PCA) (Davis, 1973) of the first five axes (>1 eigenvalue) explained 70% of the variance (Table 4.4). We will limit our discussion to PC Axis 1, which explains ~36% of the variance. PC Axes 2,3,4, and 5 explain ~14%, 8%, 6%, and 5%, respectively, which make interpreting the possible environmental controls on the variances difficult. We limit our discussion to the first PC axis.

Table 4.5 Benthic foraminiferal PCA loadings. Data were centered-logratio transformed. Data were standardized.

Benthic foraminifera					
	Axis 1	Axis 2	Axis 3	Axis 4	Axis 5
Eigenvalues	6.758	2.727	1.489	1.227	1.019
Percentage	35.57	14.352	7.835	6.457	5.361
Cumulative Percentage	35.57	49.922	57.757	64.214	69.575
PCA variable loadings					
C. laevigata	**-0.163**	0.083	**-0.460**	**-0.294**	**0.119**
T. angulosa	**0.325**	0.089	**-0.164**	-0.042	0.031
H. balthica	**0.307**	**-0.286**	-0.032	-0.005	0.040
M. barleeanus	**0.176**	**0.175**	**-0.455**	0.037	**-0.381**
U. mediterranea	**0.314**	-0.004	0.052	0.078	**0.226**
B. marginata	**-0.193**	**0.436**	-0.023	**-0.237**	0.022
P. bulloides	**0.243**	**0.216**	0.016	**0.256**	**-0.171**
P. osloensis	**-0.26**	**-0.129**	**0.208**	**0.274**	-0.034
P. subcarinata	**0.122**	0.039	**0.325**	**-0.659**	0.057
C. obtusa	**0.192**	-0.012	**0.251**	**0.116**	**0.152**
C.neoteretis	**-0.227**	**0.362**	**0.142**	-0.037	0.030
C.reniforme	**-0.154**	0.094	**-0.291**	**0.316**	**0.352**
C. bradyi	**0.314**	**-0.247**	-0.080	-0.066	0.092
C. lobatalus	0.053	**0.286**	**0.250**	**0.284**	**-0.442**
N. iridea	**-0.296**	**-0.267**	**0.170**	0.076	-0.089
N.turgida	**-0.132**	**-0.325**	**-0.342**	-0.042	**-0.336**
N.auricula	**-0.139**	**0.138**	**-0.126**	**0.181**	**0.489**
S.fusiformis	**-0.251**	**-0.373**	0.046	0.005	0.018
A.gallowayi	**-0.253**	-0.005	-0.031	**-0.183**	-0.201

Species loaded positively on PC Axis 1 are associated with buried organic matter, including *A. angulosa* (0.325) (Duros et al., 2011; Gooday and Hughes, 2002), *U. mediterranea* (0.314) (den Dulk et al., 2000), *H. balthica* (0.243) (Murray, 2006), *Pullenia bulloides* (0.243), and *M. barleaanus* (0.176) (Jennings et al., 2004) (Figure 4.9). Negatively loaded species on PC Axis 1 are associated with increased nutrient supply /fresh organic matter and include *N. iridea* (-0.296), (Alve, 2010), *Stainforthia*

fusiformis (-0.251) (Alve and Murray, 1999), *C. neoteretis* (-0.227) (Jennings et al., 2004), *B. marginata* (-0.193) (Murray, 2006), *C. laevigata* (-0.163) (Murray, 2006), *C. reniforme* (-0.154) (Murray, 2006) p103), and *Nonionella turgida* (-0.132) (Sengupta and Machaincastillo, 1993).

We interpret PC Axis 1 to separate species that prefer to feed on fresh organic matter (negatively loaded) from species that prefer buried organic matter (positively loaded) (Figure 4.9). The most negatively loaded species correspond to highest sedimentation rates that fall within BFZ1. The most positively loaded species fall within BFZ3, a zone associated with an increase in sedimentation rate compared to BFZ2. The species in this zone prefer organic matter related to stratified waters, where the surface productivity is high until the nutrients are depleted. And, the species in this zone are associated with increased sedimentation rates,

4.6.3 Temperature Reconstructions

SSTs were reconstructed using two different methods. One reconstruction is based on Mg/Ca analysis of the planktonic foraminifer *G. bulloides* in the composite core MD99-2256 and MD99-2259 (Quillmann et al., in prep), and the other reconstruction is based on planktonic foraminiferal assemblages in core MD99-2256 (Figure 4.8). Jennings et al. (submitted) have published the planktonic assemblages and the SST reconstructions based on the planktonic assemblages and $\delta^{18}O_{calcite}$ of *G. bulloides* between 11,500 and 7,000 cal yr BP on the MD99-2256 age model of Olafsdottir et al. (2010). The BWTs were reconstructed using benthic assemblages. The BWTs have been published in Olafsdottir et al. (2010).

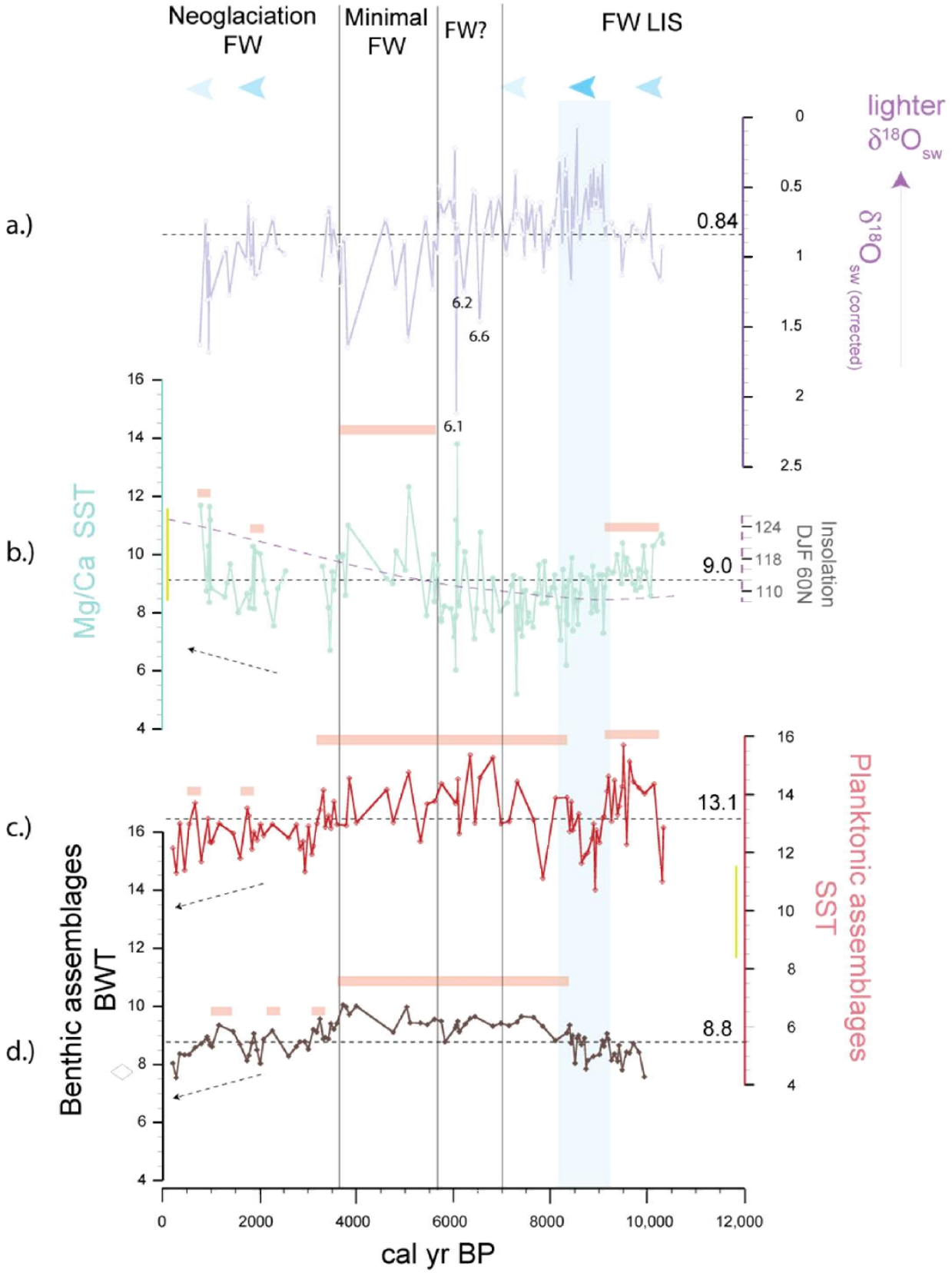
Neoglaciation
FW
Minimal
FW
FW?
FW LIS
a.)
b.)
c.)
d.)
lighter
$\delta^{18}O_{sw}$
$\delta^{18}O_{sw}$ (corrected)
0.84
6.2
6.6
6.1
Mg/Ca SST
9.0
Insolation
DJF 60N
124
118
110
Benthic assemblages
BWT
13.1
Planktonic assemblages
SST
8.8
cal yr BP

Figure 4.10 Temperature and $\delta^{18}O_{sw}$ reconstructions. Panel a.) and b.) show the $\delta^{18}O_{sw}$ and SST reconstructions based on paired measurements of Mg/Ca ratios and $\delta^{18}O_{calcite}$ of *G. bulloides*. The $\delta^{18}O_{sw}$ values have been corrected for global ice volume (Fairbanks, 1989). Panel c.) shows the SST reconstruction based planktonic assemblages. Modern summer SSTs range from 8.4 to 13.8°C (vertical light green bar) between 1950 and 2012 on the SW Iceland. Panel d.) shows the BWT reconstruction based on benthic foraminiferal assemblages; the mean BTW between 1983 and 2008 was 7.8°C (diamond symbol) (Ólafsdóttir et al., 2010). The dashed horizontal lines mark the average temperatures and $\delta^{18}O_{sw}$ between ~10,300 and 200 cal yr BP. The boundaries (vertical gray lines) show shifts in freshwater forcing. The blue vertical shaded area is the interval with lightest $\delta^{18}O_{sw}$ values. Warm periods are indicated in horizontal pink bars. The December, January, February (DJF) insolation is plotted on the Mg/Ca temperature reconstruction.

The Mg/Ca reconstructed mean SST ($SST_{Mg/Ca}$) was ~9.0°C, ranging from 5.2 to 13.8°C between ~800 and 10,300 cal yr BP, with the majority of the data (~66%) falling within the modern range. Between 1950 and 2012, summer SSTs ranged from 8.4 to 11.7°C on the SW Iceland shelf (Figure 4.8). The $SSTs_{Mg/Ca}$ are based on a single species *G. bulloides,* which calcifies in the summer in the upper 60m of the water column. The equation used to convert the Mg/Ca ratios into temperatures was tuned to modern summer temperatures in the SPG region.

Only four data points in the $SSTs_{Mg/Ca}$ fall above and ~33% below the modern temperature range. The majority of the colder than present temperatures occurred between ~9,200 and 5,700 cal yr BP. The mean $SST_{Mg/Ca}$ was higher between ~10,300 and 9,100 cal yr BP than the overall mean, then dropped below the mean between ~9,100 to 5,700 cal yr BP. In the interval between ~5,700 and ~3,800 cal yr BP temperatures were generally the warmest with the caveat that this interval is the interval with the sparse Mg/Ca data. The sparse data can be in part contributed to the low

percentages of *G. bulloides* and sample size was too small for a reliable temperature reconstruction.

The reconstructed $SSTs_{Mg/Ca}$ show some large temperature swings over short time intervals, with the largest swing having occurred between ~6,100 to 6,000 cal yr BP when the $SSTs_{Mg/Ca}$ dropped by ~7.8°, exceeding the ~3.3°C range seen in the record between 1959 and 2012. Large swings expressed by only a couple of data points within a short time interval could be due to Mg-contamination by tephra and not necessarily an indication for changes in the environment. Explosive volcanic activity through the Holocene has resulted in hundreds of tephra layers found in Icelandic paleorecords (Jennings et al., 2014). The elements Al, Fe, and Mg covary in the Icelandic tephras (Jennings et al., 2014). To ensure that the Mg measured in *G. bulloides* is foraminiferal Mg, we measured Fe and Al, which are two elements associated with post-depositional contamination. Many samples showed elevated values for these two elements, which we interpret as tephra contamination. In Chapter 3.3.3, we discuss the cleaning protocol and the post analytical steps taken to correct for tephra contamination. If the SSTs based on Mg/Ca temperature reconstructions show large swings that are not recorded in any of our other proxies, the temperature swings likely are caused by elevated Mg occurring the in tephra, despite our efforts to get rid of any contamination effects.

The SSTs reconstructed from planktonic foraminiferal assemblages (SST_{PF}) have a mean of 13.1°C, ranging from 15.7 to 10.7°C between 10,500 and 200 cal yr BP. Only ~8% of the reconstructed SST_{PF} fall within the modern SST range and the rest is warmer than today. The mean SST_{PF} between ~10,300 and 9,100 cal yr BP was warmer than the mean. A colder than mean SST_{PF} was recorded between ~ 9,000 and 8,200 cal

yr BP. The interval between ~8,200 and 3,800 cal yr BP is warmer than the mean. Between ~3,800 and 200 cal yr BP, the temperatures were lower than the mean.

The differences in the SST reconstructions may be explained in that one reconstruction provides us with a snapshot in time when G. bulloides calcified and the other with an annually integrated signal. Planktonic foraminifera species, on the other hand, inhabit a wide range of depths and may calcify at different times throughout the year, thus the SST_{PF} provides an integration of different depth habitats and different seasons. The transfer function that was used for the temperature reconstruction best reflects the temperature at 10m depth in the North Atlantic (Plaumann et al., (2003).

The overall trends in the $SSTs_{pf}$ and the BWTs reconstructed on foraminiferal assemblages are similar. The BWTs reconstructed from benthic foraminifera have a mean of 8.8°C, ranging from 7.3 to 10.1°C between 10,000 and 200 cal yr BP. The yearly mean BWT in the interval from 1983 to 2008 was from 6.6°C (Ólafsdóttir et al., 2010). Both the $SSTs_{pf}$ and BWTs reconstructions show the warmest interval between ~8,600 and 3,600 cal yr BP. After ~3,600 cal yr BP, both $SSTs_{pf}$ and BWTs fall below the mean but are punctuated by two intervals warmer than the mean (Figure 4.8). The BWT reconstructions are based on transfer functions including 61 calcareous benthic species. (Ólafsdóttir et al., 2010). Olafsdottir et al. (2010) pointed out that the late Holocene assemblage consists mostly of boreal species, but the return of low abundances of arctic species suggests a cooling or a return to unstable conditions. The return of low abundances of arctic species is also seen in the planktonic foraminiferal assemblages.

A striking difference between the temperature reconstructions based on the geochemical method ($SSTs_{Mg/Ca}$) and on the foraminiferal assemblages ($SSTs_{pf}$ and BWTs) is the general trend over the past ~3,800 cal yr BP. The temperature reconstructions based on the assemblages show a cooling associated with an increase in colder fauna. The Mg/Ca temperature reconstruction shows that the coldest peaks are getting warmner.

4.7 Discussion

4.7.1 Hydrographic History of the Irminger Current

4.7.1.1 Relative Sea Level Changes in the Early Holocene

Both the $SSTs_{pf}$ and the $SSTs_{Mg/Ca}$ show a relatively warm interval between 10,300 and 9,100 cal yr BP. The relatively heavy $\delta^{18}O_{sw}$ during this interval suggests a strong influence of AW in the IC (Figure 4.8). The warm signal of the IC was also recorded on the North Icelandic shelf, when the warmest bottom water temperatures were recorded between ~10,000 and 9,300 cal yr BP on the North Icelandic shelf, which was attributed to warm Atlantic water in the North Iceland Irminger Current (Kristjansdottir, 2005).

The highest sedimentation rates of 0.06cm/yr occurred between ~10,300 and 8,300 cal yr BP on the SW Iceland shelf. The high MS values that lasted until ~8,600 cal yr BP suggests that the source for these sediments came from transport of the Icelandic basalts, which are high in magnetic minerals. Isostatic rebound on Iceland was rapid

after glacial unloading because of the low viscosity of the asthenosphere overlying hot mantle material (Ingolfsson et al., 1995). Glacio-isostatic uplift rates exceeded the rate of eustatic sea level rise until ~8,600 cal yr BP on the SW Icelandic shelf (Norodahl et al., 2008). Isostatic uplift ended between ~8,700 and 8,400 cal yr BP (IntCal13) (7,800 $\pm$60^{14}C yr BP; (Norddahl and Petursson, 2005) and the shelf was flooded due to eustatic sea level rise (Quillmann et al., 2010a). This age was based on the extensive flow of the fijórsárhraun lava, which had met the sea at ~15m below modern sea level (Norddahl and Petursson, 2005). The end of the isostatic uplift coincides with a shift in the benthic foraminiferal fauna. The percentage of *B. marginata* dropped to nearly 0% after 8,600 cal yr BP and never rose to more than 5% during the entire record. Eustatic sea level rose until ~7,000 cal yr BP (Lambeck and Chappell, 2001).

4.7.1.2 Fresh Water Forcing (~10,300 to 5,700 cal yr BP)

The effects of the final decay of the LIS were recorded in the cool $SSTs_{Mg/Ca}$ and light $\delta^{18}O_{sw}$ values recorded on the SW Icelandic shelf with the lightest interval between ~9,100 and 8,200 cal yr BP. The $SSTs_{Mg/Ca}$, $SSTs_{pf}$ and BWT record a cooling during the interval. Whereas the $SSTs_{pf}$ and BWT are warming at the end of this interval, the $SSTs_{Mg/Ca}$ remain cool until ~5,700 cal yr BP. In the planktonic assemblages the interval between ~9,100 and 8,200 cal yr BP is marked with an increase of the arctic species NPS and a decrease of *G. bulloides*. The percentages of T. *quinqueloba* are high between ~9,700 and 7,200 cal yr BP (Figure 4.7). The most pronounced and consistent freshwater forcing from the Hudson Strait outlet of the LIS has been constrained to the interval from 9,700 and 7,800 cal yr BP (Jennings et al., submitted), which is consistent

with our results. Carlson et al., (2007) suggested that the melt water influence of the LIS had ceased by 7,000 cal yr BP.

The $\delta^{18}O_{sw}$ values remained light until ~5,700 cal yr BP, however. The freshwater interval between ~7,000 and 5,700 cal yr BP is too late to be coming from the LIS but can be assumed to be Polar Water coming from the North. Jennings et al. (2011) shows support for the southward advance of Polar Water on the E. Greenland shelf south of Denmark Strait; they record a strong SST cooling with fresher surface waters as recorded in the lighter $\delta^{18}O_{calcite}$ of NPS and the return of *Nonionellina labradorica.* Carbonate records from the N Icelandic shelf, E. Greenland shelf, and SW Iceland shelf show a sharp decline between ~7,000 and 6,300 cal yr BP, which suggests less bioproductivity.

A diatom record from south of Iceland shows the highest percentages of "N. Atlantic" diatom species in their Holocene record between ~7,000 and 5,000 cal yr BP, but still have relatively high percentages of "Greenland Current" species in this interval (Berner et al., 2008). We posit that the fresh water recorded on the SW Iceland shelf between ~7,000 and 5,700 cal yr BP might have come from the Arctic Ocean by sea ice export. This interval corresponds to a period of strong IC influence on the E. Greenland shelf, recorded in a shift to Atlantic benthic foraminiferal fauna north of the Denmark Strait on the E. Greenland shelf, starting at ~6,800 cal yr BP (Jennings et al., 2011). Increased sea export from the Arctic by ~5,000 cal yr BP has been suggested by Bauch et al. (2001) and Werner et al. (2013), who documented the flooding of shallow Arctic shelves (Laptev Sea) and inferred that modern sea ice production was reached by ~5000 cal yr BP.

4.7.1.3 Minimal Fresh Water Forcing (~5,700 to 3,800 cal yr BP)

The interval with the heaviest values in the $\delta^{18}O_{sw}$ occurred between ~5,700 and 3,800 cal yr BP but with some fresher intervals, suggesting that the Atlantic waters in the IC were diluted minimally by fresh water. It is also the warmest interval according to the $SSTs_{Mg/Ca}$, which corresponds with IC advection to the SE Greenland shelf between ~6,800 and 3,500 cal yr BP. Peak SSTs in response to the increased dominance of the IC on the SW Greenland shelf were recorded between ~5,200 to 4,200 cal yr BP (Andresen et al., 2013).

The SPG had contracted and more Atlantic water was advancing into the eastern region of the SPG at ~5,700 cal yr BP (Quillmann et al., in prep). The NAO-like atmospheric circulation had weakened compared to the NAO-like circulation intensity in the early Holocene (Rimbu et al., 2003). Advection of IC waters into the Denmark Strait on the E. Greenland shelf was recorded between 6,800 and 4,800 cal yr BP; south of the Denmark Strait the strongest advection of IC waters continued until ~3,500 cal yr BP (Andresen et al., 2013; Jennings et al., 2011). In Disko Bugt, the strongest signal of the IC was noted between 5,500 and 3,500 cal yr BP (Perner et al., 2013), while the Greenland ice sheet had retreated onto land (Briner et al., 2010) and minimal melt water reached Disko Bugt (Perner et al., 2013). Timing of these observations of minimal melt water and strong IC influence agree with our findings. The IC showed minimal freshwater forcing as it entered the SW Iceland shelf.

4.7.1.4 Fresh Water Forcing in the Neoglaciation

The Mg/Ca record has sparse data but suggests that the onset of Neoglaciation occurred at ~3,800 cal yr BP (Figure 4.4). A warming trend is more obvious in the temperature record (RAPiD-12-1k; (Thornalley et al., 2009)) from the eastern flank on the Reykjanes Ridge. The $SSTs_{pf}$ and BWT show the onset of Neoglacial cooling. The fauna indicates that the water column was stratified and nutrient-depleted. As suggested earlier, wind strength decreased through the Holocene and that could have contributed to the less mixed water column. But the delivery of quartz/kspar suggests that drift ice was being transported to the SW Iceland shelf and indicates a spreading of the EGC. The reoccurrence of cold foraminiferal fauna species, such as NPS and *G. glutinata*, support the notion Polar Water. On historical time scales it has been observed that sea ice can be carried in the NIIC around Iceland and can arrive at the SW Iceland shelf from the south in the coastal current or it can be carried directly from the northwest to the SW Iceland shelf (Jennings et al., 2001). Our data suggest that during the Neoglaciation the likely pathway was from the northwest because the increase in Q-kspar occurs in the outer core and not in the inner core.

The Neoglacial cooling has been noted along from the SW to the N Icelandshelf. The timing of the onset varies but all studies agree that the climate was unstable. Neoglacial cooling on the SW Iceland shelf started in bottom water temperatures ~4,000 cal yr BP (Ólafsdóttir et al., 2010) but no marked cooling of the surface water was noted on the SW Iceland shelf (Smith et al., 2005); on the NW Icelandic shelf at ~6,000 cal yr BP (Ólafsdóttir et al., 2010) and at ~3,000 cal yr BP (Andrews et al., 2009); on the N. Icelandic shelf at ~6,000 (Giraudeau et al., 2004). On the east Greenland shelf the

onset of the Neoglaciation has been linked to an increase of polar waters from the Arctic Ocean, the advance of the Greenland ice sheet, and a southward shift of the polar front at ~3,500 cal yr BP with some erratic cooling episodes having started at ~5,000 cal yr BP (Jennings et al., 2011). The onset of Neoglaciation on the SW Greenland shelf was dated to ~3,200 cal yr BP (Seidenkrantz et al., 2007) and in Disko Bugt to ~3,500 cal yr BP (Perner et al., 2013). The onset of Neoglaciation has been associated with a reorganization of oceanic and atmospheric conditions (Perner et al., 2013; Seidenkrantz et al., 2007).

4.7.2 Holocene Trend of the NAO/SPG and the Irminger Current

The seasonal contrast was greater in the early Holocene than today (Blaschek and Renssen, 2013b). In the early Holocene winters were colder. In a modern-day cold winters are associated with stronger surface winds during NAO+ years (Bader et al., 2011; Deser et al., 2000). NAO+ winter are associated with increased precipitation on Iceland (Hurrell, 1995). In the early Holocene, we can deduce that the water column was well mixed and nutrient-rich, as recorded in the first PCA axes, and shifted toward a more stratified and nutrient poor water column the late Holocene (Figure 4.9). Environmental shifts recorded in all of our proxies were not gradual but rather happened abruptly, which cannot be explained by the changes in insolation.

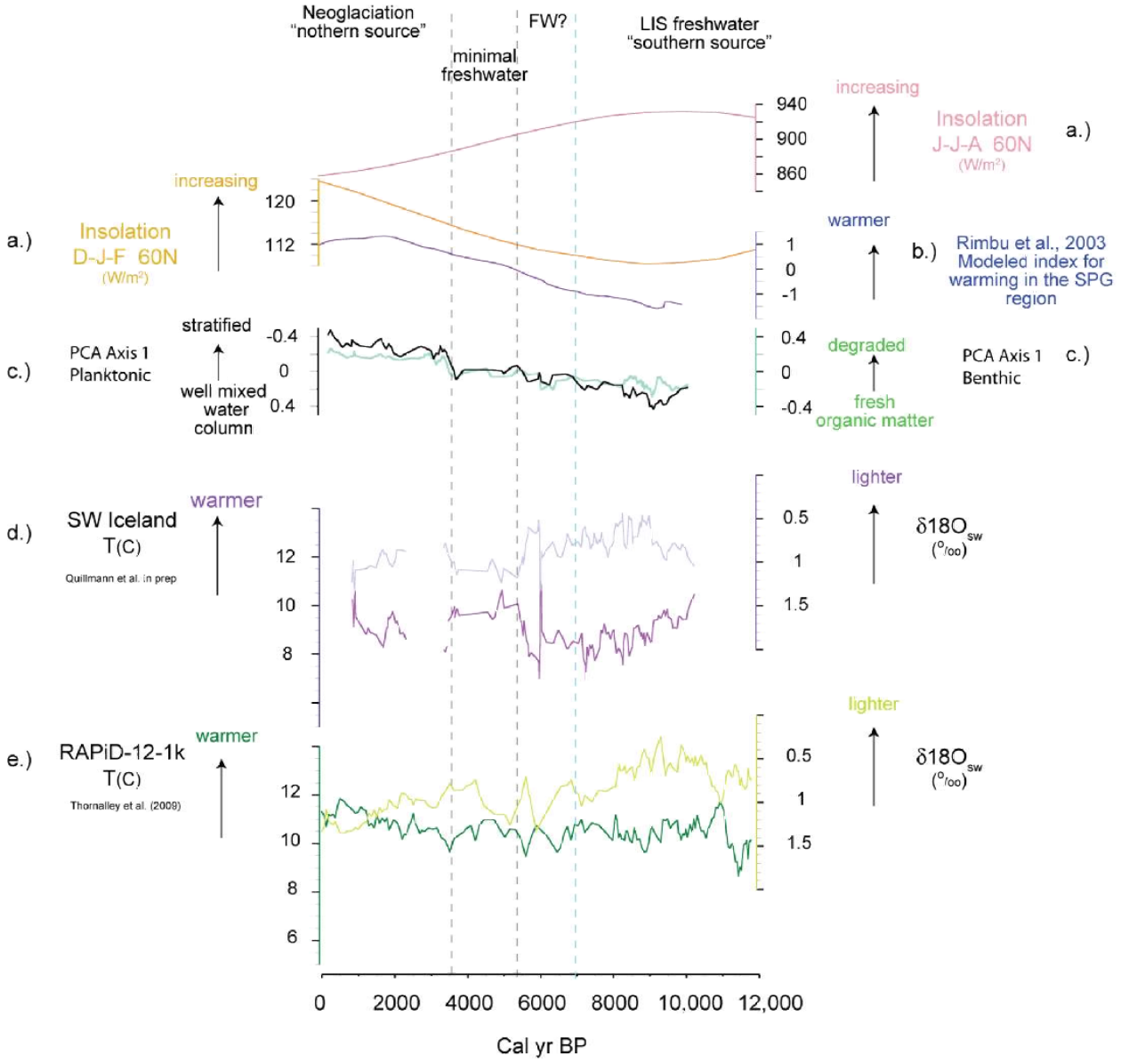

Figure 4.11 General trends through the Holocene. Panel a.) show summer (June-July-August (JJA)) 60N insolation and winter (December-January-February (DJF)) insolation. Panel b.) shows Rimbu et al's (2003) model prediction for the Holocene temperature trend in the SPG region. Panel c.) shows the first PC axes for planktonic (black) and benthic (green). Panel d.) shows the temperature and $\delta^{18}O_{sw}$ reconstruction on the SW Iceland shelf and Panel e.) shows the temperature and $\delta^{18}O_{sw}$ reconstruction for the RAPid-12-1k site on the eastern flank on the Reykjanes Ridge (Thornalley et al., 2009).

We suggest that the NAO-like atmospheric circulation weakened and the SPG contracted through the Holocene. It is important to point out that the overall trend is the weakening of the NAO-like atmospheric circulation and the contraction of the SPG but with millennial-scale variations around this trend. Within each of these time slices, there was still significant variation in the strength of the SPG circulation and in the SPG shape, similar to what has been happening over the last decades in the SPG region (Hakkinen and Rhines, 2004; Hatun et al., 2009; Hatun et al., 2005; Sarafanov, 2009; Yashayaev, 2007).

Rimbu et al. (2003) suggested that the NAO-like atmospheric circulation weakened through the Holocene in response to strengthening winter (December, January, and February) insolation. Their atmospheric general circulation model showed SST warming for the SPG region through the Holocene (Rimbu et al., 2003). This model showed that the long-term Holocene trend is related to wintertime oceanic circulation changes. The wintertime ocean circulation has a long memory and persists through the summer (Rimbu et al., 2003) when the alkenone-producing coccolithosphores are blooming (Iglesias-Rodriguez et al., 2002). The long-term warming trends are manifested in the RAPiD-12-1k (Thornalley et al., 2009) (Figure 4.9). These Mg/Ca derived temperature reconstructions, which are based on *G. bulloides*, a species calcifying in the summer, follow winter insolation. Warming is consistent with weakening of the NAO-like circulation pattern through the Holocene, agreeing with Rimbu et al.'s (2003) model predictions. Other records that show a warming over the past ~2,000 cal yr BP include a summer SST record based on planktonic foraminifera on the SE Greenland shelf south of Denmark Strait {Jennings, 2011 #882}. Marine and terrestrial

records from southern Greenland do not show a homogenous cooling during the Neoglacial but some records show a warming (Briner 2014, personal communication). We posit that some records, such as our Mg/Ca temperature reconstruction record conditions set by the SPG dynamics during the winter/spring. Other data, such as the $SSTs_{pf}$ and BWTs record the annual signal, which captured the decreasing summer insolation and the spreading of Polar Water. The water column on the SW Iceland shelf became more stratified because of the Arctic sea ice increase.

4.7.3 The Potential Role of the IC in the Carbonate Productivity

Calcium carbonate records have been used on the Iceland shelf, in the Denmark Strait, and on the Greenland shelf as a proxy for productivity (e.g. (Andrews et al., 2001b; Andrews and Jennings, 2014; Andrews et al., 2001c; Stoner et al., 2007)), with the productivity depending on the nutrients (Stefansson, 1968; Stefansson and Olafsson, 1991). On the Iceland shelf, calcium carbonate is biogenic after ~7,000 cal yr BP and is used to interpret biological production. Some carbonate peaks prior to ~7,000 cal yr BP are detrital carbonate peaks from the Hudson Strait outlet of the LIS (Jennings et al., submitted). Between ~12,000 and 10,300 cal yr BP, the percentage of calcium carbonate ($CaCO_3$%) increased from ~1% to ~3%. Between ~10,300 and 8,600 cal yr BP, the $CaCO_3$% increased gradually from ~3% to 4.6%. During this interval, the relative sea level was lower than today because Iceland was still isostatically rebounding.

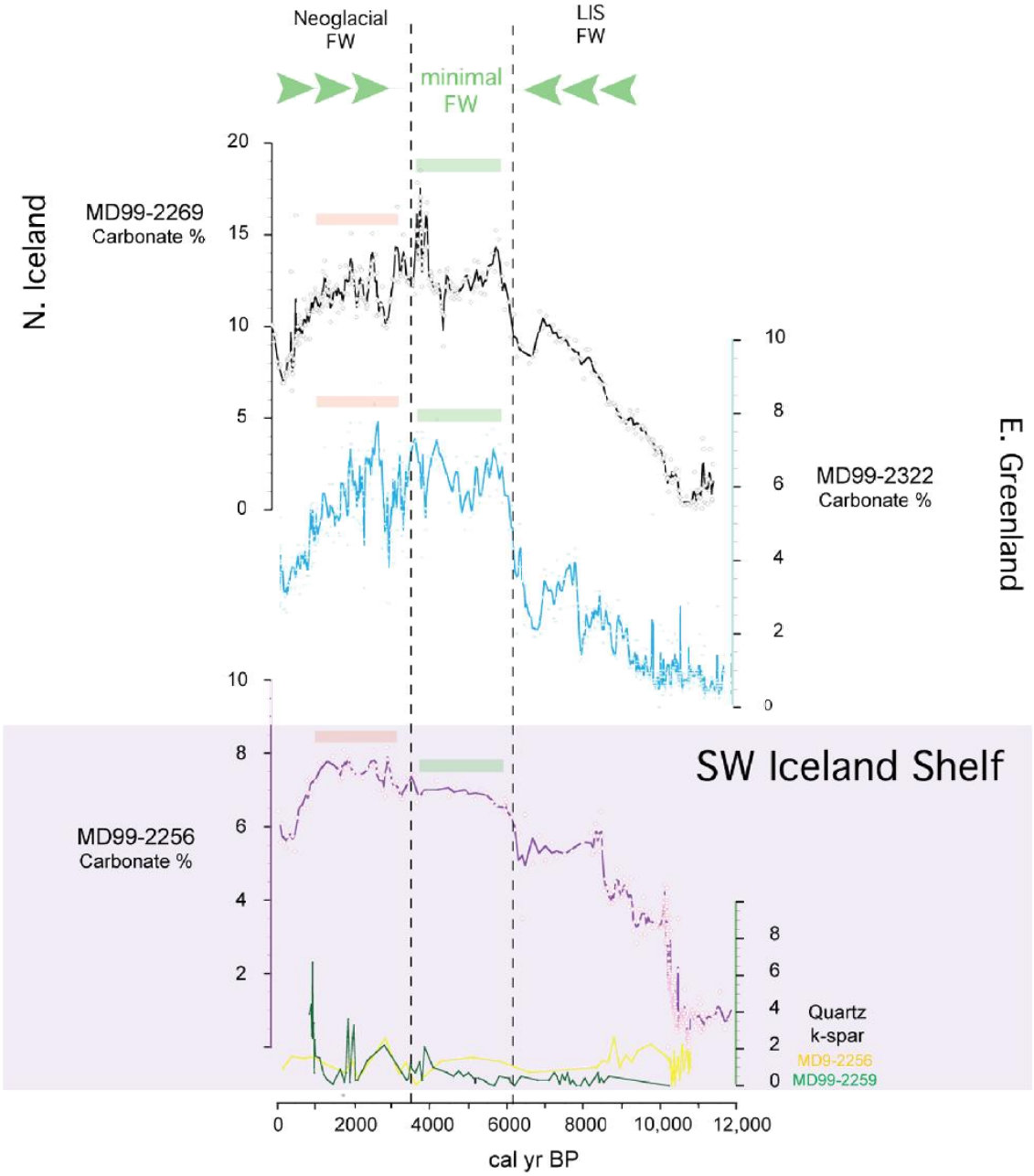

Figure 4.12 Carbonate records. Carbonate records from the N Icelandic shelf and the E. Greenland shelf are compared to the SW Iceland record. The peak Atlantic Water influence on the SW Iceland shelf is marked by a horizontal green bar. The peak carbonate % on the SW Iceland shelf is marked by a horizontal pink bar. Note the different scales on the y-axis. Quartz and k-spar percentages are shown for the SW Iceland shelf.

The interval between ~5,700 to 3,800 cal yr BP, when $SSTs_{Mg/Ca}$ were warmest and the values of $\delta^{18}O_{sw}$ were the heaviest, precedes the interval of the highest $CaCO_3$%. Increased $CaCO_3$ production has been attributed to enhanced production of *Coccolithus pelagicus*, which is a heavily calcified cold end member among coccolithosphores, and *Emiliania huxleyi*, an ubiquitous species in transitional/subarctic waters (Andrews and Giraudeau, 2003; Giraudeau et al., 2004; Thordardottir, 1986).

Satellite data between 1997 and 1999 showed huge blooms of Coccolithosphores south of Iceland, following the flow path of the IC (Iglesias-Rodriguez et al., 2002). The onset of the blooms coincided with a sharp decrease in the depth of the seasonal upper mixed layer in the N. Atlantic between 48°N to 75°N; the most productive blooms were found where the temperatures ranged from 5°C to 15°C (Iglesias-Rodriguez et al., 2002). Large-scale seasonal blooms detected in the Sea-viewing Wide Field-of-view Sensor (SeaWiFS) satellite imagery were limited to nutrient-depleted and seasonally stratified waters (Iglesias-Rodriguez et al., 2002).

Several proxies support the notion for a stratified water column, which are usually associated with nutrient depletion (Stefansson and Olafsson, 1991; Taboada and Anadon, 2012). A shift in the faunal assemblages at ~3,600 cal yr BP signaled the onset of a stratified water column with nutrient depleted surface waters. The percentages of *G. bulloides*, an indicator species for high nutrients, diminished while the percentages of *N. incompta* increased. *N. incompta* is found in regions in the North Atlantic where the nutrient supply is low (Schiebel et al., 2001). However, intense coccolithosphore blooms occur in limited to nutrient-depleted and seasonally stratified waters (Iglesias-Rodriguez

et al., 2002). Organic matter produced by these coccolithosphore blooms could explain the increase in sedimentation rates during the Neoglaciation.

The organic matter from the enhanced bloom in the surface layer would have settled to the ocean floor, creating new niches for benthic foraminifera thriving in degraded organic matter, which is reflected in the higher diversity index. The percentage of Quartz and k-spar increases in this interval, suggesting that freshwater from the melting of drift ice would have contributed to the stratified water column. A freshwater lens overlying warmer nutrient-rich Atlantic water favors coccolithosphores production (Giraudeau et al., 2000).

The highest percentages of $CaCO_3$ in MD99-2269 on the N. Iceland shelf between ~6,500 and 3,500 cal yr BP (with the highest peak between ~4,000 and 3,500 cal yr BP), coincide with the interval of minimal freshwater forcing and warmest IC on the SW Iceland shelf. The high $CaCO_3$ production on the N. Iceland shelf was contributed to strong advection of warm, nutrient-rich IC water, which was capped by polar/arctic surface water, resulting in excess carbonate production. The N. Iceland shelf received northern source water before the SW Iceland shelf.

A longer interval of highest $CaCO_3$ production was recorded on the E. Greenland shelf (MD99-2322) between ~6,000 and 1,900 cal yr BP, with the peak production centered around ~2,700 cal yr BP. The timing of the high $CaCO_3$ production coincides with strong advection of the IC on the E. Greenland shelf and could have triggered the $CaCO_3$ production.

4.8 Conclusions

In this paper we analyzed the implications of freshwater forcing on the hydrography of the Irminger Current through the Holocene. We identified three time intervals based on shifts in $\delta^{18}O_{sw}$ values:

1. Light $\delta^{18}O_{sw}$ values from ~10,300 to 5,700 cal yr BP. The glacial melt water from the decaying LIS explains the cool $SSTs_{Mg/Ca}$ and the light $\delta^{18}O_{sw}$ values until ~7,000 cal yr BP. However the $SSTs_{Mg/Ca}$ and $\delta^{18}O_{sw}$ values remained cool and light until ~5,700 cal yr BP. The freshwater interval between ~7,000 and 5,700 cal yr BP is too late to be coming from the LIS and we posit that the freshwater came from the Arctic Ocean via the EGC and itno the East Iceland Current.
2. Minimal freshwater forcing from ~5,700 to 3,800 cal yr BP. During this interval the IC was diluted minimally by fresh water. It is also the warmest interval according to the $SSTs_{Mg/Ca}$ and BWT. This interval falls within or coincides with the strongest advection of IC waters into the Denmark Strait and to the Greenland shelf.
3. Neoglaciation started at ~3,800 cal yr BP. The Mg/Ca record has sparse data, but together with other Mg/Ca temperature records from the SPG region (Quillmann et al., in prep) suggests that the onset of Neoglaciation occurred at ~3,800 cal yr BP. The delivery of quartz/kspar suggests that drift ice was being transported to the SW Iceland shelf and indicates a southward

movement of the subpolar front. Peak carbonate production occurred during this time.

The SST reconstruction by planktonic foraminiferal assemblages and BWT reconstruction based on the benthic foraminiferal assemblages differ from the SSTs reconstructed by Mg/Ca ratios. The SST and BWT based on assemblages show a Holocene Thermal Maximum from ~~8,600 and 3,800 cal yr BP. The onset of Neoglacition at ~3,800 cal yr BP is recorded in both SSTs and BWT reconstruction.

Based on the planktonic foraminiferal assemblages we infer that the water column was well mixed in the early Holocene and transitioned to a stratified water column in the late Holocene. A similar trend can be seen in the benthic assemblages. In the early Holocene, species that prefer fresh organic matter, which is associated with well-mixed water columns, dominated. In the late Holocene, species that feed on degraded organic matter, indicating a stratified water column, dominated.

The peak carbonate production occurred during the Neoglaciation when the water column was stratified. The SPG was contracted and more Atlantic Water reached the SW Iceland shelf capped by freshwater from the spreading of Polar Water.

4.9 Acknowledgments

This project was funded by NSF grant 0823535, PIs Anne E. Jennings, Thomas Marchitto, and John T. Andrews. We would like to thank Michelle Carlson and Wendy Freeman for their help with sample preparations. We appreciate Patrick Cappa's assistance in the ICP-MS laboratory. We would like to thank Lindsay Wilson for

providing the planktonic SSTs, and Timothy Jull at the NSF laboratory provided five radiocarbon dates for MD99-2259.

4.10 Work Cited

Aitchison, J., 1986, The statistical analysis of compositional data, London, Chapman and Hall, 146 p.:

Alley, R. B., Mayewski, P. A., Sowers, T., Stuiver, M., Taylor, K. C., and Clark, P. U., 1997, Holocene climatic instability: a prominent, widespread event 8200 yr ago.: Geology, v. 25, no. 6, p. 483-486.

Alve, E., 1995, Benthic foraminiferal distribution and recolonization of formerly anoxic enrionments in Drammensfjord, Southern Norway.: Marine Micropaleontology, v. 25, no. 2-3, p. 169-186.

Alve, E., 2010, Benthic foraminiferal responses to absence of fresh phytodetritus: A two-year experiment: Marine Micropaleontology, v. 76, no. 3-4, p. 67-75.

Alve, E., and Bernhard, J. M., 1995, VERTICAL MIGRATORY RESPONSE OF BENTHIC FORAMINIFERA TO CONTROLLED OXYGEN CONCENTRATIONS IN AN EXPERIMENTAL MESOCOSM: Marine Ecology Progress Series, v. 116, no. 1-3, p. 137-151.

Alve, E., and Murray, J. W., 1999, Marginal marine environments of the Skagerrak and Kattegat: a baseline study of living (stained) benthic foraminiferal ecology: Palaeogeography Palaeoclimatology Palaeoecology, v. 146, no. 1-4, p. 171-193.

Andersen, C., Koc, N., Jennings, A., and Andrews, J. T., 2004a, Nonuniform response of the major surface currents in the Nordic Seas to insolation forcing: Implications for the Holocene climate variability: Paleoceanography, v. 19, no. 2.

Andersen, C., Koc, N., and Moros, M., 2004b, A highly unstable Holocene climate in the subpolar North Atlantic: evidence from diatoms: Quaternary Science Reviews, v. 23, no. 20-22, p. 2155-2166.

Andresen, C. S., Hansen, M. J., Seidenkrantz, M. S., Jennings, A. E., Knudsen, M. F., Norgaard-Pedersen, N., Larsen, N. K., Kuijpers, A., and Pearce, C., 2013, Mid- to late-Holocene oceanographic variability on the Southeast Greenland shelf: Holocene, v. 23, no. 2, p. 167-178.

Andrews, J. T., 2009, Seeking a Holocene drift ice proxy: non-clay mineral variations from the SW to N-central Iceland shelf: trends, regime shifts, and periodicities: Journal of Quaternary Science, v. 24, no. 7, p. 664-676.

Andrews, J. T., Belt, S. T., Olafsdottir, S., Masse, G., and Vare, L. L., 2009, Sea ice and marine climate variability for NW Iceland/Denmark Strait over the last 2000 cal. yr BP: Holocene, v. 19, no. 5, p. 775-784.

Andrews, J. T., Caseldine, C., Weiner, N. J., and Hatton, J., 2001a, Late Holocene (ca. 4 ka) marine and terrestrial environmental change in Reykjarfjordur, north Iceland: climate and/or settlement?: Journal of Quaternary Science, v. 16, no. 2, p. 133-143.

Andrews, J. T., and Giraudeau, J., 2003, Multi-proxy records showing significant Holocene environmental variability: the inner N. Iceland shelf (Hunafloi): Quaternary Science Reviews, v. 22, no. 2-4, p. 175-193.

Andrews, J. T., Hardadottir, J., Stoner, J. S., Mann, M. E., Kristjansdottir, G. B., and Koc, N., 2003a, Decadal to millennial-scale periodicities in North Iceland shelf sediments over the last 12000 cal yr: long-term North Atlantic oceanographic variability and solar forcing: Earth and Planetary Science Letters, v. 210, no. 3-4, p. 453-465.

Andrews, J. T., Hardardottir, J., Stoner, J. S., Mann, M. E., Kristjansdottir, G. B., and Koc, N., 2003b, Decadal to millennial-scale periodicities in North Iceland shelf sediments over the last 12000 cal yr: long-term North Atlantic oceanographic variability and solar forcing.: Earth and Planetary Science Letters, v. 210, p. 453-465.

Andrews, J. T., and Helgadottir, G., 2002, Late Quaternary ice cap extent and deglaciation, Hunafloaall, northwest Iceland: evidence from marine cores: Arctic, Antarctic and Alpine Research, v. 35, no. 2, p. 218-232.

Andrews, J. T., Helgadottir, G., Geirsdottir, A., and Jennings, A. E., 2001b, Multicentury-scale records of carbonate (hydrographic ?) variability on the northern Iceland margin over the last 5000 years: Quaternary Research, v. 56, no. 2, p. 199-206.

Andrews, J. T., and Jennings, A. E., 2014, Multidecadal to millennial marine climate oscillations across the Denmark Strait (similar to 66 degrees N) over the last 2000 cal yr BP: Climate of the Past, v. 10, no. 1, p. 325-343.

Andrews, J. T., Kristjansdottir, G. B., Geirsdottir, A., Hardardottir, J., Helgadottir, G., Sveinbjornsdottir, A. E., Jennings, A. E., and Smith, L. M., 2001c, Late Holocene (~5 cal ka) trends and century-scale variability of the N. Iceland marine records: measures of surface hydrology, productivity, and land/ocean interactions.: The Oceans and Rapid Climate Change: Past, Present, and Future. Geophysical Monograph, v. 126, p. 69-80.

Andrews, J. T., Larsen, B., Thors, K., Helgadottir, G., Olafsson, J., and Wittmaarck, A., 1991, Fjord-Shelf-Slope Sediment Continuum, East Greenland Margin: Cruise Report -- RS Bjarni Saemundsson B1191, p. 25.

Andrews, J. T., Smith, L. M., Preston, R., Cooper, T., and Jennings, A. E., 1997, Spatial and temporal patterns of iceberg rafting (IRD) along the East Greenland margin, ca 68 degrees N, over the last 14 cal ka: Journal of Quaternary Science, v. 12, no. 1, p. 1-13.

Arbuszewski, J., deMenocal, P., Kaplan, A., and Farmer, E. C., 2010, On the fidelity of shell-derived delta O-18(seawater) estimates: Earth and Planetary Science Letters, v. 300, no. 3-4, p. 185-196.

Arbuszewski, J. A., Demenocal, P. B., Cleroux, C., Bradtmiller, L., and Mix, A., 2013, Meridional shifts of the Atlantic intertropical convergence zone since the Last Glacial Maximum: Nature Geoscience, v. 6, no. 11, p. 959-962.

Azetsu-Scott, K., and Syvitski, J. P. M., 1999, Influence of melting icebergs on distribution, characteristics and transport of marine particles in an East Greenland fjord: Journal of Geophysical Research-Oceans, v. 104, no. C3, p. 5321-5328.

Bader, J., Mesquita, M. D. S., Hodges, K. I., Keenlyside, N., Osterhus, S., and Miles, M., 2011, A review on Northern Hemisphere sea-ice, storminess and the North Atlantic Oscillation: Observations and projected changes: Atmospheric Research, v. 101, no. 4, p. 809-834.

Barber, D. C., Dyke, A., Hillaire-Marcel, C., Jennings, A. E., Andrews, J. T., Kerwin, M. W., Bilodeau, G., McNeely, R., Southon, J., Morehead, M. D., and Gagnon, J. M., 1999, Forcing of the cold event of 8,200 years ago by catastrophic drainage of Laurentide lakes: Nature, v. 400, no. 6742, p. 344-348.

Barker, S., and Elderfield, H., 2002, Foraminiferal calcification response to glacial-interglacial changes in atmospheric CO2: Science, v. 297, no. 5582, p. 833-836.

Barker, S., Greaves, M., and Elderfield, H., 2003, A study of cleaning procedures used for foraminiferal Mg/Ca paleothermometry: Geochemistry Geophysics Geosystems, v. 4.

Be, A. W. H., and Tolderlund, D. S., 1971, Distribution and ecology of living planktonic foraminifera in the surface waters of the Atlantic and Indian Oceans: The Micropalaeontology of Oceans, p. 105-149.

Bemis, B. E., Spero, H. J., Bijma, J., and Lea, D. W., 1998, Reevaluation of the oxygen isotopic composition of planktonic foraminifera: Experimental results and revised paleotemperature equations: Paleoceanography, v. 13, no. 2, p. 150-160.

Berner, K. S., Koc, N., Divine, D., Godtliebsen, F., and Moros, M., 2008, A decadal-scale Holocene sea surface temperature record from the subpolar North Atlantic constructed

using diatoms and statistics and its relation to other climate parameters: Paleoceanography, v. 23, no. 2.
Blaschek, M., and Renssen, H., 2013a, The Holocene thermal maximum in the Nordic Seas: the impact of Greenland Ice Sheet melt and other forcings in a coupled atmosphere-sea-ice-ocean model: Climate of the Past, v. 9, no. 4, p. 1629-1643.
-, 2013b, The impact of early Holocene Arctic shelf flooding on climate in an atmosphere-ocean-sea-ice model: Climate of the Past, v. 9, no. 6, p. 2651-2667.
Boyle, E., and Rosenthal, Y., 1996, Chemical hydrography of the South Atlantic during the last glacial maximum; Cd s d13C New York, Springer, The South Atlantic: Present and Past Circulation.
Briner, J. P., Stewart, H. A. M., Young, N. E., Philipps, W., and Losee, S., 2010, Using proglacial-threshold lakes to constrain fluctuations of the Jakobshavn Isbrae ice margin, western Greenland, during the Holocene: Quaternary Science Reviews, v. 29, no. 27-28, p. 3861-3874.
Bryan, S. P., and Marchitto, T. M., 2008, Mg/Ca-temperature proxy in benthic foraminifera: New calibrations from the Florida Straits and a hypothesis regarding Mg/Li: Paleoceanography, v. 23, no. 2.
Came, R. E., Oppo, D. W., and McManus, J. F., 2007, Amplitude and timing of temperature and salinity variability in the subpolar North Atlantic over the past 10 k.y: Geology, v. 35, no. 4, p. 315-318.
Carlson, A. E., Clark, P. U., Raisbeck, G. M., and Brook, E. J., 2007, Rapid Holocene deglaciation of the Labrador sector of the Laurentide Ice Sheet: Journal of Climate, v. 20, no. 20, p. 5126-5133.
Carlson, A. E., Legrande, A. N., Oppo, D. W., Came, R. E., Schmidt, G. A., Anslow, F. S., Licciardi, J. M., and Obbink, E. A., 2008, Rapid early Holocene deglaciation of the Laurentide ice sheet: Nature Geoscience, v. 1, p. 620-624.
Castaneda, I. S., Smith, L. M., Kristjansdottir, G. B., and Andrews, J. T., 2004, Temporal changes in Holocene del18O records from the northwest and central North Iceland Shelf: Journal of Quaternary Science, v. 19, no. 4, p. 321-334.
Clark, P. U., Marshall, S. J., Clarke, G. K. C., Hostetler, S. W., Licciardi, J. M., and Teller, J. T., 2001, Freshwater forcing of abrupt climate change during the last glaciation: Science, v. 293, no. 5528, p. 283-287.
Corliss, B. H., 1991, Morpholgy and microhabitat preferences of benthic foraminifera from the northwest Atlantic Ocean: Marine Micropaleontology, v. 17, p. 195-236.
Davis, J. C., 1973, Statistics and data analysis in geology, New York, John Wiley and Sons, 646 p.:
Dekens, P. S., Lea, D. W., Pak, D. K., and Spero, H. J., 2002, Core top calibration of Mg/Ca in tropical foraminifera: Refining paleotemperature estimation: Geochemistry Geophysics Geosystems, v. 3.
den Dulk, M., Reichart, G. J., van Heyst, S., Zachariasse, W. J., and Van der Zwaan, G. J., 2000, Benthic foraminifera as proxies of organic matter flux and bottom water oxygenation? A case history from the northern Arabian Sea: Palaeogeography Palaeoclimatology Palaeoecology, v. 161, no. 3-4, p. 337-359.
Deser, C., Walsh, J. E., and Timlin, M. S., 2000, Arctic sea ice variability in the context of recent atmospheric circulation trends.: Journal of Climate, v. 13, no. 3, p. 617-633.
Dickson, R. R., Meincke, J., Malmberg, S. A., and Lee, A. J., 1988, THE GREAT SALINITY ANOMALY IN THE NORTHERN NORTH-ATLANTIC 1968-1982: Progress in Oceanography, v. 20, no. 2, p. 103-151.

Duros, P., Fontanier, C., Metzger, E., Pusceddu, A., Cesbron, F., de Stigter, H. C., Bianchelli, S., Danovaro, R., and Jorissen, F. J., 2011, Live (stained) benthic foraminifera in the Whittard Canyon, Celtic margin (NE Atlantic): Deep-Sea Research Part I-Oceanographic Research Papers, v. 58, no. 2, p. 128-146.

Eiriksson, J., Knudsen, K. L., Haflidason, H., and Henriksen, P., 2000, Late-glacial and Holocene palaeoceanography of the North Icelandic shelf: Journal of Quaternary Science, v. 15, no. 1, p. 23-42.

Eiriksson, J., Larsen, G., Knudsen, K. L., Heinemeier, J., and Siminarson, L. A., 2004, Marine reservoir age variability and water mass distribution in the Iceland Sea.: Quaternary Science Review, v. 23, p. 2247-2268.

Elderfield, H., Bertram, C. J., and Erez, J., 1996, Biomineralization model for the incorporation of trace elements into foraminiferal calcium carbonate: Earth and Planetary Science Letters, v. 142, no. 3-4, p. 409-423.

Elderfield, H., and Ganssen, G., 2000, Past temperture and d18O of surface ocean waters inferred from foraminiferal Mg/Ca ratios.: Nature, no. 405.

Elderfield, H., Yu, J., Anand, P., Kiefer, T., and Nyland, B., 2006, Calibrations for benthic foraminiferal Mg/Ca paleothermometry and the carbonate ion hypothesis: Earth and Planetary Science Letters, v. 250, no. 3-4, p. 633-649.

Ellison, C. R. W., Chapman, M. R., and Hall, I. R., 2006, Surface and deep ocean interactions during the cold climate event 8200 years ago: Science, v. 312, no. 5782, p. 1929-1932.

Emilliani, C., 1955, Pleistocene temperatures: Journal of Geology, v. 63, p. 538-578.

Engleman, E. E., Jackson, L. L., Norton, D. R., and Fisher, A. G., 1985, Determination of carbonate carbon in geological materials by coulometric titration: Chemical Geology, v. 53, p. 125-128.

Erbs-Hansen, D. R., Knudsen, K. L., Olsen, J., Lykke-Andersen, H., Underbjerg, J. A., and Sha, L., 2013, Paleoceanographical development off Sisimiut, West Greenland, during the mid- and late Holocene: A multiproxy study: Marine Micropaleontology, v. 102, p. 79-97.

Erez, J., 2003, The source of ions for biomineralization in foraminifera and their implications for paleoceanographic proxies: Reviews in Mineralogy and Geochemistry, v. 54, p. 115-149.

Fairbanks, R. G., 1989, A 17,000 year glacial-eustatic sea level record: influence of glacial melting rates on the Younger Dryas event and deep-ocean circulation: Nature, v. 342, p. 637-642.

Farmer, E. C., deMenocal, P. B., and Marchitto, T. M., 2005, Holocene and deglacial ocean temperature variability in the Benguela upwelling region: Implications for low-latitude atmospheric circulation: Paleoceanography, v. 20, no. 2.

Farmer, E. J., Chapman, M. R., and Andrew, J. E., Holocene temperature evolution of the subpolar North Atlantic recorded in the Mg/Ca ratios of surface and thermocline dwelling planktonic foraminifers2009, p. A355-A355.

Farmer, E. J., Chapman, M. R., and Andrews, J. E., 2008, Centennial-scale Holocene North Atlantic surface temperatures from Mg/Ca ratios in Globigerina bulloides: Geochemistry Geophysics Geosystems, v. 9, p. 15.

Fennel, K., Cetinic, I., D'Asaro, E., Lee, C., and Perry, M. J., 2011, Autonomous data describe North Atlantic spring bloom: EOS, v. 92, p. 465-466.

Ferguson, J. E., Henderson, G. M., Kucera, M., and Rickaby, R. E. M., 2008, Systematic change of foraminiferal Mg/Ca ratios across a strong salinity gradient: Earth and Planetary Science Letters, v. 265, no. 1-2, p. 153-166.

Ganssen, G. M., and Kroon, D., 2000, The isotopic signature of planktonic foraminifera from NE Atlantic surface sediments: implications for the reconstruction of past oceanic conditions: Journal of the Geological Society, v. 157, p. 693-699.

Geirsdottir, A., Miller, G. H., Axford, Y., and Olafsdottir, S., 2009, Holocene and latest Pleistocene climate and glacier fluctuations in Iceland: Quaternary Science Reviews, v. 28, no. 21-22, p. 2107-2118.

Giraudeau, J., Cremer, M., Manthe, S., Labeyrie, L., and Bond, G., 2000, Coccoltith evidence for instabilities in the surface circulation south of Iceland during the Holocene times.: Earth and Planetary Science Letters, v. 179, p. 257-268.

Giraudeau, J., Jennings, A. E., and Andrews, J. T., 2004, Timing and mechanisms of surface and intermediate water circulation changes in the Nordic seas over the last 10,000 cal years: a view from the North Iceland shelf.: Quaternary Science Review, v. 23, p. 2127-2139.

Gooday, A. J., and Hughes, J. A., 2002, Foraminifera associated with phytodetritus deposits at a bathyal site in the northern Rockall Trough (NE Atlantic) seasonal contrasts and a comparison of stained and dead assemblages: Marine Micropaleontology, v. 46, p. 83-110.

Gupta, A. K., 1997, Paleoceanographic and paleoclimatic history of the Somali Basin during the Pliocene-Pleistocene: Multivariate analyses of benthic foraminifera from DSDP Site 241 (Leg 25): Journal of Foraminiferal Research, v. 27, no. 3, p. 196-208.

Hakkinen, S., and Rhines, P. B., 2004, Decline of subpolar North Atlantic circulation during the 1990s: Science, v. 304, no. 5670, p. 555-559.

-, 2009, Shifting surface currents in the northern North Atlantic Ocean: Journal of Geophysical Research-Oceans, v. 114.

Hald, M., and Korsun, S., 1997, Distribution of modern benthic foraminifera from fjords of Svalbard, European Arctic: Journal of Foraminiferal Research, v. 27, p. 101-122.

Hall, I. R., Bianchi, G. G., and Evans, J. R., 2004, Centennial to millennial scale Holocene climate-deep water linkage in the North Atlantic: Quaternary Science Reviews, v. 23, no. 14-15, p. 1529-1536.

Hartmann, D. L., A.M.G., K. T., Rusticucci, M., Alexander, L. V., Broennimann, S., Charabi, Y., Dentener, F. J., Dlugokencky, E. J., Easterling, D. R., Kaplan, A., Soden, B. J., Thorne, P. W., Wild, M., and Zhai, P. M., 2013, Observations: Atmosphere and Surface; Climate Change 2013: The Physical Basis. Contribution of Working Group I to the Fifth Assessment Report of the Intergovernmental Panel on Climate Change.

Hatun, H., Payne, M. R., Beaugrand, G., Reid, P. C., Sando, A. B., Drange, H., Hansen, B., Jacobsen, J. A., and Bloch, D., 2009, Large bio-geographical shifts in the north-eastern Atlantic Ocean: From the subpolar gyre, via plankton, to blue whiting and pilot whales: Progress in Oceanography, v. 80, no. 3-4, p. 149-162.

Hatun, H., Sando, A. B., Drange, H., Hansen, B., and Valdimarsson, H., 2005, Influence of the Atlantic subpolar gyre on the thermohaline circulation: Science, v. 309, no. 5742, p. 1841-1844.

Helgadottir, G., 1997, Paleoclimate (0 to >14ka) of W and NW Iceland: An Icelandic/USA contribution to PALE. Cruise Report B9-97 R/V Bjarni Saemundsson RE 30, 17-30 July 1997.

Hess, S., and Jorissen, F. J., 2009, Distribution patterns of living benthic foraminifera from Cap Breton canyon, Bay of Biscay: Faunal response to sediment instability: Deep-Sea Research Part I-Oceanographic Research Papers, v. 56, no. 9, p. 1555-1578.

Hilbrecht, H., 1996, Extanct planktic foraminifera and the physical environment in the Atlantic and Indian Oceans; An atlas based on CLIMAP and Levitus (1982) data: Mitteilungen aus dem Geologischen Institut der Eidg. Technischen Hochschule und der Universitaet Zuerich, v. Neue Folge Nr. 200, p. 93.

Hillaire-Marcel, C., de Vernal, A., Bilodeau, G., and Weaver, A. J., 2001, Absence of deep-water formation in the Labrador Sea during the last interglacial period: Nature, v. 410, no. 6832, p. 1073-1077.

Hjelstuen, B. O., Kleiven, H. F., Haflidason, H., Kjennbakken, H., and Team, S., 2008, Marine Geological Cruise Report from Byfjorden, Salhusfjorden and Herdlefjorden. Report No. 100-01/08: Department of Earth Science, University of Bergen, Bergen, Norway, 16 pp.

Holland, D. M., Thomas, R. H., De Young, B., Ribergaard, M. H., and Lyberth, B., 2008, Acceleration of Jakobshavn Isbrae triggered by warm subsurface ocean waters: Nature Geoscience, v. 1, no. 10, p. 659-664.

Honisch, B., Allen, K. A., Lea, D. W., Spero, H. J., Eggins, S. M., Arbuszewski, J., deMenocal, P., Rosenthal, Y., Russell, A. D., and Elderfield, H., 2013, The influence of salinity on Mg/Ca in planktic foraminifers - Evidence from cultures, core-top sediments and complementary delta O-18: Geochimica et Cosmochimica Acta, v. 121, p. 196-213.

Hurrell, J. W., 1995, DECADAL TRENDS IN THE NORTH-ATLANTIC OSCILLATION - REGIONAL TEMPERATURES AND PRECIPITATION: Science, v. 269, no. 5224, p. 676-679.

Hurrell, J. W., Kushnir, Y., Ottersen, G., and Visbeck, M., 2003, An Overview of the North Atlantic Oscillation, *in* Union, A. G., ed., The North Atlantic Oscillation: Climatic Significance and Environmental Impact; Geophysical Monograph 134.

Husum, K., 2010, CRUISE REPORT ForArc UiT 2010: Marine geological cruise to Kongsfjord and adjoining shelf, West Svalbard.

Husum, K., and Hald, M., 2012, Arctic planktic foraminiferal assemblages: Implications for subsurface temperature reconstructions: Marine Micropaleontology, v. 96-97, p. 38-47.

Iglesias-Rodriguez, M. D., Brown, C. W., Doney, S. C., Kleypas, J., Kolber, D., Kolber, Z., Hayes, P. K., and Falkowski, P. G., 2002, Representing key phytoplankton functional groups in ocean carbon cycle models: Coccolithophorids: Global Biogeochemical Cycles, v. 16, no. 4.

Ingolfsson, O., Norddahl, H., and Haflidason, H., 1995, RAPID ISOSTATIC REBOUND IN SOUTHWESTERN ICELAND AT THE END OF THE LAST GLACIATION: Boreas, v. 24, no. 3, p. 245-259.

Jennings, A., Andrews, J., and Wilson, L., 2011, Holocene environmental evolution of the SE Greenland Shelf North and South of the Denmark Strait: Irminger and East Greenland current interactions: Quaternary Science Reviews, v. 30, no. 7-8, p. 980-998.

Jennings, A. E., Andrews, J. T., Pearce, C., Wilson, L., and Olafsdottir, S., submitted, Detrital Carbonate Peaks on the Labrador Shelf, a 13 to 7 cal yr BP Template for Freshwater Forcing from the Hudson Strait Outlet of the Laurentide Ice Sheet into the Subpolar Gyre: Quaternary Science Reviews.

Jennings, A. E., Hagen, S., Hardardottir, J., Stein, R., Ogilvie, A. E. J., and Jonsdottir, I., 2001, Oceanographic change and terrestrial human impacts in a post A.D. 1400 sediment record from the southwest of Iceland.: Climate Change, v. 48, p. 83-100.

Jennings, A. E., Syvitski, J. P. M., Gerson, L., Groenvold, K., Geirsdottir, A., Hardardottir, J., Andrews, J. T., and Hagen, S., 2000, Chronology and paleoenvironments during the last Weichselian deglaciation of the southwest Iceland shelf.: Boreas, v. 29, p. 167-183.

Jennings, A. E., Thordarson, T., Zalzal, K., Stoner, J. S., Geirsdottir, A., and Miller, G. H., 2014, Holocene tephra from Iceland and Alaska in SE Greenland shelf sediments: Geological Society London Special Publications, p. 398.

Jennings, A. E., Weiner, N. J., Helgadottir, G., and Andrews, J. T., 2004, Modern foraminferal faunas of the southwestern to northern Iceland shelf: oceanographic and environmental controls.: Journal of Foraminiferal Research, v. 34, no. 3, p. 180-207.

Johannessen, T., Jansen, E., Flatoy, A., and Ravelo, A. C., 1994, The relationship between surface water masses, oceanographic fronts and paleoclimatic proxies in surface sediments of the Greenland, Iceland, Norwegian Seas, *in* Zahn, R., Pedersen, T. F., Kaminski, M. A., and Labeyrie, L., eds., Carbon Cycling in the Glacial Ocean: Constraints on the Ocean's Role in Global Change, Volume 17: Berlin Heidelberg, Springer p. pp 61-85.

Johnsen, S. J., Clausen, H. B., Dansgaard, W., Fuhrer, K., Gundestrup, N., Hammer, C. U., Iversen, P., Jouzel, J., Stauffer, B., and Steffensen, J. P., 1992, IRREGULAR GLACIAL INTERSTADIALS RECORDED IN A NEW GREENLAND ICE CORE: Nature, v. 359, no. 6393, p. 311-313.

Johnsen, S. J., DahlJensen, D., Gundestrup, N., Steffensen, J. P., Clausen, H. B., Miller, H., Masson-Delmotte, V., Sveinbjornsdottir, A. E., and White, J., 2001, Oxygen isotope and palaeotemperature records from six Greenland ice-core stations: Camp Century, Dye-3, GRIP, GISP2, Renland and NorthGRIP: Journal of Quaternary Science, v. 16, no. 4, p. 299-307.

Justwan, A., Koc, N., and Jennings, A. E., 2008, Evolution of the Irminger and East Icelandic Current systems through the Holocene, revealed by diatom-based sea surface temperature reconstructions: Quaternary Science Reviews, v. 27, no. 15-16, p. 1571-1582.

Kaufman, D. S., Ager, T. A., Anderson, N. J., Anderson, P. M., Andrews, J. T., Bartlein, P. J., Brubaker, L. B., L.L., C., Cwynar, L. C., Duvall, M. L., Dyke, A. S., Edwards, M. E., Eisner, W. R., Gajewski, K., Geirsdottir, A., Hu, F. S., Jennings, A. E., Kaplan, M. R., Kerwin, M. W., Lozhkin, A. V., MacDonald, G. M., Miller, G. H., Mock, C. J., Oswald, W. W., Otto-Bliesner, B. L., Porinchu, D. F., Ruehland, K., Smol, J. P., Steig, E. J., and Wolfe, B. B., 2004, Holocene termal maximum in the western Arctic (0-180 deg W): Quaternary Science Reviews, v. 23, p. 529-560.

Kisakurek, B., Eisenhauer, A., Bohm, F., Garbe-Schonberg, D., and Erez, J., 2008, Controls on shell Mg/Ca and Sr/Ca in cultured planktonic foraminiferan, Globigerinoides ruber (white): Earth and Planetary Science Letters, v. 273, no. 3-4, p. 260-269.

Knudsen, K. L., Jiang, H., Jansen, E., Eiriksson, J., Heinemeier, J., and Seidenkrantz, M.-S., 2004, Environmental changes off North Iceland during the deglaciation and the Holocene: foraminifera, diatoms and stable isotopes: Marine Micropaleontology, v. 953, p. 1-3.

Knudsen, K. L., Sondergaard, M. K. B., Eiriksson, J., and Jiang, H., 2008, Holocene thermal maximum off North Iceland: Evidence from benthic and planktonic foraminifera in the 8600-5200 cal year BP time slice: Marine Micropaleontology, v. 67, no. 1-2, p. 120-142.

Kobashi, T., Severinghaus, J. P., Brook, E. J., Barnola, J. M., and Grachev, A. M., 2007, Precise timing and characterization of abrupt climate change 8200 years ago from air trapped in polar ice: Quaternary Science Reviews, v. 26, no. 9-10, p. 1212-1222.

Kovach, 1998, Multi-Variate Statistical Package, Pentraeth, Wales, Kovach Computing Services, 127 p.:

Kristjansdottir, G. B., 2005, Holocene changes in climate, environment, and ocean reservoir age on the Iceland shelf: Mg/Ca, del 18O, and tephrachronology of Core MD99-2269PhD]: University of Colorado, 423 p.

Labeyrie, L., Jansen, E., and Cortijo, E., 2003, Les rapports des campagnes a la mer MD114/IMAGES V.

Lambeck, K., and Chappell, J., 2001, Sea level change through the last glacial cycle: Science, v. 292, no. 5517, p. 679-686.

Lea, D. W., 2002, New insights into glacial terminations from Mg-paleothermometry: Geochimica et Cosmochimica Acta, v. 66, no. 15A, p. A438-A438.
Lea, D. W., Mashiotta, T. A., and Spero, H. J., 1999, Controls on magnesium and strontium uptake in planktonic foraminifera determined by live culturing: Geochimica et Cosmochimica Acta, v. 63, no. 16, p. 2369-2379.
Lea, D. W., Pak, D. K., and Paradis, G., 2005, Influence of volcanic shards on foraminiferal Mg/Ca in a core from the Galapagos region: Geochemistry Geophysics Geosystems, v. 6.
Leduc, G., Schneider, R., Kim, J. H., and Lohmann, G., 2010, Holocene and Eemian sea surface temperature trends as revealed by alkenone and Mg/Ca paleothermometry: Quaternary Science Reviews, v. 29, no. 7-8, p. 989-1004.
Legendre, L., and Legendre, P., 1983, Numerical Ecology, New York, Elsevier Scientific Publishing Company.
LeGrande, A. N., and Schmidt, G. A., 2006, Global gridded data set of the oxygen isotopic composition in seawater: Geophysical Research Letters, v. 33, no. 12.
-, 2008, Ensemble, water isotope-enabled, coupled general circulation modeling insights into the 8.2 ka event: Paleoceanography, v. 23, no. 3.
Lynch-Stieglitz, J., Curry, W. B., and Slowey, N. C., 1999, A geostrophic transport estimate for the Florida Current from the oxygen isotope composition of benthic foraminifera.: Paleoceanography, v. 14, no. 3, p. 360-373.
Lynch-Stieglitz, J., Liu, Z., Koutavas, A., Marchitto, T., and Brady, E., 2002, Sea surface temperature patterns in the Early Holocene: Global Ocean response to insolation forcing: Geochimica et Cosmochimica Acta, v. 66, no. 15A, p. A467-A467.
Marchal, O., Cacho, I., Stocker, T. F., Grimalt, J. O., Calvo, E., Martrat, B., Shackleton, N. J., Vautravers, M., Cortijo, E., van Kreveld, S., Andersson, C., Koc, N., Chapman, M., Sbaffi, L., Duplessy, J.-C., Sarntheim, M., Turon, J.-L., Duprat, J., and Jansen, E., 2002, Apparent long-term cooling in the sea surface in the northeast Atlantic and Mediterranean during the Holocene.: Quaternary Science Review, v. 21, p. 455-483.
Marchitto, T. M., 2006, Nutrient proxies (d13C, Cd/Ca, Ba/Ca, Zn/Ca, d15N), *in* Elias, S., ed., Encyclopedia of Quaternary Science: Amsterdam, Elsevier.
Marchitto, T. M., Bryan, S. P., Curry, W. B., and McCorkle, D. C., 2007, Mg/Ca temperature calibration for the benthic foraminifer Cibicidoides pachyderma: Paleoceanography, v. 22, no. 1.
Mashiotta, T. A., Lea, D. W., and Spero, H. J., 1999, Glacial-interglacial changes in Subantarctic sea surface temperature and delta O-18-water using foraminiferal Mg: Earth and Planetary Science Letters, v. 170, no. 4, p. 417-432.
Mathien-Blard, E., and Bassinot, F., 2009, Salinity bias on the foraminifera Mg/Ca thermometry: Correction procedure and implications for past ocean hydrographic reconstructions: Geochemistry Geophysics Geosystems, v. 10.
Mayewski, P. A., Rohling, E. E., Stager, J. C., Karlen, W., Maasch, K. A., Meeker, L. D., Meyerson, E. A., Gasse, F., van Kreveld, S., JHolmgren, K., Lee-Thorp, J., Rosqvist, G., Rack, F., Staubwasser, M., Schneider, R. R., and Steig, E. J., 2004, Holocene climate variability: Science, v. 62, p. 243-255.
McCave, I. N., 1994, North East Atlantic Palaeoceanography and Climate Change: RRS Charles Darwin 88 (Cruise Report), Department of Earth Sciences, University of Cambridge, p. 44.
Miller, K. R., and Chapman, M. R., 2013, Holocene climate variability reflected in diatom-derived sea surface temperature records from the subpolar North Atlantic: Holocene, v. 23, no. 6, p. 882-887.

Moros, M., Andrews, J. T., Eberl, D. D., and Jansen, E., 2006a, Holocene history of drift ice in the northern North Atlantic: Evidence for different spatial and temporal modes: Paleoceanography, v. 21, no. 2.

Moros, M., Jensen, K. G., and Kuijpers, A., 2006b, Mid- to late-Holocene hydrological and climatic variability in Disko Bugt, central West Greenland: Holocene, v. 16, no. 3, p. 357-367.

Motyka, R. J., Truffer, M., Fahnestock, M., Mortensen, J., Rysgaard, S., and Howat, I., 2011, Submarine melting of the 1985 Jakobshavn Isbrae floating tongue and the triggering of the current retreat: Journal of Geophysical Research-Earth Surface, v. 116.

Murray, J. W., 2006, Ecology and Applications of Benthic Foraminifera, Cambridge, Cambridge University Press, 426 p.:

Norddahl, H., and Petursson, H., 2005, Relative sea level change in Iceland: new aspects of the Weichselian deglaciation of Iceland, *in* Caseldine, C., Russel, A., Hardardottir, J., and Knudsen, O., eds., Iceland - modern processes and past environments, Volume 5: Amsterdam, Elsevier, p. 407.

Norodahl, H., Ingolfsson, O., Petursson, H. G., and Hallsdottir, M., 2008, Late Weichselian and Holocene environmental history of Iceland: Jokull, v. 58, p. 343-364.

Nurnberg, D., Bijma, J., and Hemleben, C., 1996, Assessing the reliability of magnesium in foraminiferal calcite as a proxy for water mass temperatures (vol 60, pg 803, 1995): Geochimica et Cosmochimica Acta, v. 60, no. 13, p. 2483-2483.

Ólafsdóttir, S., jennings, A. J., Á., G., Andrews, J. T., and Miller, G. H., 2010, Holocene variability of the North Atlantic Irminger current on the south- and northwest shelf of Iceland Marine Micropaleontology, v. XXX.

Perner, K., Moros, M., Jennings, A., Lloyd, J. M., and Knudsen, K. L., 2013, Holocene palaeoceanographic evolution off West Greenland: Holocene, v. 23, no. 3, p. 374-387.

Pflaumann, U., Duprat, J., Pujol, C., and Labeyrie, L. D., 1996, SIMMAX: A modern analog technique to deduce Atlantic sea surface temperatures from planktonic foraminifera in deep-sea sediments: Paleoceanography, v. 11, no. 1, p. 15-35.

Pflaumann, U., Sarnthein, M., Chapman, M., d'Abreu, L., Funnell, B., Huels, M., Kiefer, T., Maslin, M., Schulz, H., Swallow, J., van Kreveld, S., Vautravers, M., Vogelsang, E., and Weinelt, M., 2003, Glacial North Atlantic: Sea-surface conditions reconstructed by GLAMAP 2000: Paleoceanography, v. 18, no. 3.

Praetorius, S. K., McManus, J. F., Oppo, D. W., and Curry, W. B., 2008, Episodic reductions in bottom-water currents since the last ice age: Nature Geoscience, v. 1, no. 7, p. 449-452.

Quillmann, U., Jennings, A., and Andrews, J., 2010a, Reconstructing Holocene palaeoclimate and palaeoceanography in Isafjaroardjup, northwest Iceland, from two fjord records overprinted by relative sea-level and local hydrographic changes: Journal of Quaternary Science, v. 25, no. 7, p. 1144-1159.

Quillmann, U., Jennings, A. J., and Andrews, J. T., 2010b, Reconstructing Holocene palaeoclimate and palaeoceanography in ìsafjarðardjúp, northwest Iceland, from two fjord records overprinted by relative sea-level and local hydrographic changes.: Journal of Quaternary Science, v. 25, no. 7, p. 1144-1159.

Ran, L. H., Jiang, H., Knudsen, K. L., and Eiriksson, J., 2008, A high-resolution Holocene diatom record on the North Icelandic shelf: Boreas, v. 37, no. 3, p. 399-413.

Reverdin, G., 2010, North Atlantic Subpolar Gyre Surface Variability (1895-2009): Journal of Climate, v. 23, no. 17, p. 4571-4584.

Rhein, M., Rintoul, S. R., Aoki, S., Campos, E., Chanmbers, D., Freely, R. A., Gulev, S., Johnson, G. C., Josey, S. A., Kostianoy, A., Mauritzen, C., Roemich, D., Talley, L. D., and Wang, F., 2013, Observation Ocean, Cambridge University Press, "Climate Change

2013: The Physical Science Basis. Contribution of Working Group I to the Fifth Assessment Report of the Intergovernmental panel on Climaet Change.
Rignot, E., and Kanagaratnam, P., 2006, Changes in the velocity structure of the Greenland ice sheet: Science, v. 311, no. 5763, p. 986-990.
Rimbu, N., Lohmann, G., Kim, J. H., Arz, H. W., and Schneider, R., 2003, Arctic/North Atlantic Oscillation signature in Holocene sea surface temperature trends as obtained from alkenone data: Geophysical Research Letters, v. 30, no. 6.
Rodionov, S. N., 2004, A sequential algorithm for testing climate regime shifts: Geophysical Research Letters, v. 31, no. 9.
Rohling, E. J., and Palike, H., 2005, Centennial-scale climate cooling with a sudden cold event around 8,200 years ago: Nature, v. 434, no. 7036, p. 975-979.
Rosenthal, Y., Boyle, E. A., and Slowey, N., 1997, Temperature control on the incorporation of magnesium, strontium, fluorine, and cadmium into benthic foraminiferal shells from Little Bahama Bank: Prospects for thermocline paleoceanography: Geochimica et Cosmochimica Acta, v. 61, no. 17, p. 3633-3643.
Rosenthal, Y., Field, M. P., and Sherrell, R. M., 1999, Precise determination of element/calcium ratios in calcereous samples using sector field inductively coupled plasma mass spectrometry: Analytical Chemistry, v. 71, p. 3248-3253.
Rosenthal, Y., Lohmann, G. P., Lohmann, K. C., and Sherrell, R. M., 2000, Incorporation and preservation of Mg in Globigerinoides sacculifer: Implications for reconstructing the temperature and O-18/O-16 of seawater: Paleoceanography, v. 15, no. 1, p. 135-145.
Rosenthal, Y., Perron-Cashman, S., Lear, C. H., Bard, E., Barker, S., Billups, K., Bryan, M., Delaney, M. L., deMenocal, P. B., Dwyer, G. S., Elderfield, H., German, C. R., Greaves, M., Lea, D. W., Marchitto, T. M., Pak, D. K., Paradis, G. L., Russell, A. D., Schneider, R. R., Scheiderich, K., Stott, L., Tachikawa, K., Tappa, E., Thunell, R., Wara, M., Weldeab, S., and Wilson, P. A., 2004, Interlaboratory comparison study of Mg/Ca and Sr/Ca measurements in planktonic foraminifera for paleoceanographic research: Geochemistry Geophysics Geosystems, v. 5.
Rutherford, S., D'Hondt, S., and Prell, W., 1999, Environmental controls on the geographic distribution of zooplankton diversity: Nature, v. 400, no. 6746, p. 749-753.
Rytter, F., Knudsen, K. L., Seidenkrantz, M.-S., and Eiriksson, J., 2002, Modern distribution of benthic foraminifera on the North Icelandic shelf and slope: Journal of Foraminiferal Research, v. 32, p. 217-244.
Sarafanov, A., 2009, On the effect of the North Atlantic Oscillation on temperature and salinity of the subpolar North Atlantic intermediate and deep waters.: ICES Journal of Marine Science, v. 66, p. 1448-1454.
Sarafanov, A., Falina, A., Mercier, H., Lherminier, P., and Sokov, A., 2009, Recent changes in the Greenland-Scotland overflow-derived water transport inferred from hydrographic observations in the southern Irminger Sea: Geophysical Research Letters, v. 36.
Sarafanov, A., Falina, A., Sokov, A., and Demidov, A., 2008, Intense warming and salinification of intermediate waters of southern origin in the eastern subpolar North Atlantic in the 1990s to mid-2000s: Journal of Geophysical Research-Oceans, v. 113, no. C12.
Schiebel, R., Bijma, J., and Hemleben, C., 1997, Population dynamics of the planktic foraminifer Globigerina bulloides from the eastern North Atlantic: Deep-Sea Research Part I-Oceanographic Research Papers, v. 44, no. 9-10, p. 1701-1713.
Schiebel, R., and Hemleben, C., 2000, Interannual variability of planktic foraminiferal populations and test flux in the eastern North Atlantic Ocean (JGOFS): Deep-Sea Research Part Ii-Topical Studies in Oceanography, v. 47, no. 9-11, p. 1809-1852.

Schiebel, R., Waniek, J., Bork, M., and Hemleben, C., 2001, Planktic foraminiferal production stimulated by chlorophyll redistribution and entrainment of nutrients: Deep-Sea Research Part I-Oceanographic Research Papers, v. 48, no. 3, p. 721-740.

Scourse, J. D., Kennedy, H., Scott, G. A., and Austin, W. E. N., 2004, Stable isotopic analyses of modern benthic foraminifera from seasonally stratified shelf seas: disequilibria and the 'seasonal effect': Holocene, v. 14, no. 5, p. 747-758.

Seidenkrantz, M.-S., 1995, Cassidulina teretis Tappan and Casidulina neoteretis new species (foraminifera): strategraphic markers for deep sea and outer shelf areas: Journal of Microopalaeontology, v. 14, p. 145-157.

Seidenkrantz, M. S., Aagaard-Sorensen, S., Sulsbruck, H., Kuijpers, A., Jensen, K. G., and Kunzendorf, H., 2007, Hydrography and climate of the last 4400 years in a SW Greenland fjord: implications for Labrador Sea palaeoceanography: Holocene, v. 17, no. 3, p. 387-401.

Sengupta, B. K., and Machaincastillo, M. L., 1993, BENTHIC FORAMINIFERA IN OXYGEN-POOR HABITATS: Marine Micropaleontology, v. 20, no. 3-4, p. 183-201.

Serreze, M. C., Holland, M. M., and Stroeve, J., 2007, Perspectives on the Arctic's shrinking sea-ice cover: Science, v. 315, no. 5818, p. 1533-1536.

Shackelton, N. J., 1967, Oxygen isotope analyses and Pleistocene temperature re-assessed.: Nature, v. 215, p. 15-17.

Smith, L. M., Andrews, J. T., Castaneda, I. S., Kristjansdottir, G. B., Jennings, A. E., and Sveinbjornsdottir, A. E., 2005, Temperature reconstructions for SW and N Iceland waters over the last 10cal ka based on delta O-18 records from planktic and benthic Foraminifera: Quaternary Science Reviews, v. 24, no. 14-15, p. 1723-1740.

Stefansson, U., 1968, DISSOLVED NUTRIENTS OXYGEN AND WATER MASSES INNORTHERN IRMINGER SEA: Deep-Sea Research, v. 15, no. 5, p. 541-&.

Stefansson, U., and Olafsson, J., 1991, Nutrients and fertility of the Icelandic waters: Rit Fiskideildar, v. 19, p. 18-28.

Stoner, J. S., Jennings, A., Kristjansdottir, G. B., Dunhill, G., Andrews, J. T., and Hardardottir, J., 2007, A paleomagnetic approach toward refining Holocene radiocarbon-based chronologies: Paleoceanographic records from the north Iceland (MD99-2269) and east Greenland (MD99-2322) margins: Paleoceanography, v. 22, no. 1.

Straneo, F., Curry, R. G., Sutherland, D. A., Hamilton, G. S., Cenedese, C., Vage, K., and Stearns, L. A., 2011, Impact of fjord dynamics and glacial runoff on the circulation near Helheim Glacier: Nature Geoscience, v. 4, no. 5, p. 322-327.

Straneo, F., Hamilton, G. S., Sutherland, D. A., Stearns, L. A., Davidson, F., Hammill, M. O., Stenson, G. B., and Rosing-Asvid, A., 2010, Rapid circulation of warm subtropical waters in a major glacial fjord in East Greenland: Nature Geoscience, v. 3, no. 3, p. 182-186.

Straneo, F., Heimbach, P., Sergienko, O., Hamilton, G., Catania, G., Griffies, S., Hallberg, R., Jenkins, A., Joughin, I., Motyka, R., Pfeffer, W. T., Price, S. F., Rignot, E., Scambos, T., Truffer, M., and Vieli, A., 2013, Challenges to Understanding the Dynamic Response of Greenland's Marine Terminating Glaciers to Oceanic and Atmospheric Forcing: Bulletin of the American Meteorological Society, v. 94, no. 8, p. 1131-1144.

Straneo, F., Sutherland, D. A., Holland, D., Gladish, C., Hamilton, G. S., Johnson, H. L., Rignot, E., Xu, Y., and Koppes, M., 2012, Characteristics of ocean waters reaching Greenland's glaciers: Annals of Glaciology, v. 53, no. 60, p. 202-210.

Stuiver, M., Reimer, P. J., and Braziunas, T. F., 1998, High-precision radiocarbon age calibration for terrestrial and marine samples: Radiocarbon, v. 40, no. 3, p. 1127-1151.

Sutherland, D. A., Pickart, R. S., Jones, E. P., Azetsu-Scott, K., Eert, A. J., and Olafsson, J., 2009, Freshwater composition of the waters off southeast Greenland and their link to the Arctic Ocean: Journal of Geophysical Research-Oceans, v. 114.

Sutherland, D. A., and Straneo, F., 2012, Estimating ocean heat transports and submarine melt rates in Sermilik Fjord, Greenland, using lowered acoustic Doppler current profiler (LADCP) velocity profiles: Annals of Glaciology, v. 53, no. 60, p. 50-58.

Sutherland, D. A., Straneo, F., Stenson, G. B., Davidson, F. J. M., Hammill, M. O., and Rosing-Asvid, A., 2013, Atlantic water variability on the SE Greenland continental shelf and its relationship to SST and bathymetry: Journal of Geophysical Research-Oceans, v. 118, no. 2, p. 847-855.

Taboada, F. G., and Anadon, R., 2012, Patterns of change in sea surface temperature in the North Atlantic during the last three decades: beyond mean trends: Climatic Change, v. 115, no. 2, p. 419-431.

Thomas, E. R., Wolff, E. W., Mulvaney, R., Steffensen, J. P., Johnsen, S. J., Arrowsmith, C., White, J. W. C., Vaughn, B., and Popp, T., 2007, The 8.2 ka event from Greenland ice cores: Quaternary Science Reviews, v. 26, no. 1-2, p. 70-81.

Thordardottir, T., 1986, TIming and duration of spring blooming south and southwest of Iceland, *in* Skreslet, S., ed., The role of freshwater outflow in coastal marine ecosystems, Springer-Verlag, Berlin, p. 345-360.

Thornalley, D. J. R., Elderfield, H., and McCave, I. N., 2009, Holocene oscillations in temperature and salinity of the surface subpolar North Atlantic: Nature, v. 457, no. 7230, p. 711-714.

Vage, K., Pickart, R. S., Sarafanov, A., Knutsen, O., Mercier, H., Lherminier, P., van Aken, H. M., Meincke, J., Quadfasel, D., and Bacon, S., 2011, The Irminger Gyre: Circulation, convection, and interannual variability: Deep-Sea Research Part I-Oceanographic Research Papers, v. 58, no. 5, p. 590-614.

Yashayaev, I., 2007, Changing freshwater content: Insights from the subpolar North Atlantic and new oceanographic challenges: Progress in Oceanography, v. 73, no. 3-4, p. 203-209.

Yashayaev, I., and Clarke, A., 2008, EVOLUTION OF NORTH ATLANTIC WATER MASSES INFERRED FROM LABRADOR SEA SALINITY SERIES: Oceanography, v. 21, no. 1, p. 30-45.

Yashayaev, I., van Aken, H. M., Holliday, N. P., and Bersch, M., 2007, Transformation of the Labrador sea water in the subpolar North Atlantic: Geophysical Research Letters, v. 34, no. 22.

Yin, J. J., Overpeck, J. T., Griffies, S. M., Hu, A. X., Russell, J. L., and Stouffer, R. J., 2011, Different magnitudes of projected subsurface ocean warming around Greenland and Antarctica: Nature Geoscience, v. 4, no. 8, p. 524-528.

Zhang, X. B., and Church, J. A., 2012, Sea level trends, interannual and decadal variability in the Pacific Ocean: Geophysical Research Letters, v. 39.

Zweng, M. M., and Munchow, A., 2006, Warming and freshening of Baffin Bay, 1916-2003: Journal of Geophysical Research-Oceans, v. 111, no. C7.

Chapter 5
Thesis Summary and Further Research

In Chapter 2 “Cooling and freshening at 8.2 ka on the NW Iceland Shelf recorded in paired $\delta^{18}O$ and Mg/Ca measurements of the benthic foraminifera *Cibicides lobatulus*”, we took advantage of the high sedimentation rates at a shallow site (water depth ~100m) at the mouth of Ìsafjarðardjúp in NW Iceland, which allowed for an ~18-yr sampling resolution between 8,400 and 7,600 cal yr BP. The high sedimentation rate allowed us to assess the history of the 8.2 ka event. We reconstructed near surface temperature and $\delta^{18}O_{sw}$ by paired measurements of $\delta^{18}O_{calcite}$ of a benthic foraminifer *C. lobatulus*. We found evidence for a near-surface cooling between ~8,300 and 8,100 cal yr BP that was recorded in several proxies. The Mg/Ca temperature dropped by ~3 to 5°C accompanied by heavier $\delta^{18}O_{sw}$ values, the percentages of two Arctic benthic foraminifers, *C. reniforme* and *E. excavatum* f. *clavata,* rose, and calcium carbonate percent fell. The freshwater outburst could have spread far from the source, into the high latitude North Atlantic. This freshwater input could have directly caused substantial high latitude cooling, with reduced North Atlantic Deep Water formation amplifying the climatic impact. We also developed a new Mg/Ca temperature calibration for *C. lobatulus* based on 27 surface sediment and core top samples from the North Atlantic. The timing of the cooling is similar to the timing and 160 year duration recorded in the Greenland ice cores and is consistent with the hypothesis that the catastrophic outburst flood of the proglacial lakes Oijbway and Agassiz caused the 8.2 ka event.

In Chapter 3, “The Roles of Winter Insolation and Ocean Dynamics on the Holocene History of the North Atlantic Subpolar Gyre”, we found evidence that through the Holocene, the SPG region warmed and the $\delta^{18}O_{sw}$ values became heavier. We attribute this trend to the weakening of NAO-like atmospheric circulation in response to increasing winter insolation through the Holocene. The SPG did not respond to the winter insolation smoothly but rather in several abrupt shifts. Between ~10,000 to 8,000 cal yr BP, freshwater from the decaying LIS was present yet the SPG was extended because of very strong Westerlies. Between 8,000 to 6,000 cal yr BP, the SPG was still extended but started to change in shape. Westerlies likely were still strong and the SPG circulation intensified, coinciding with the onset of Labrador Sea convection. The biggest shift occurred in the mid Holocene ~6,000 cal yr BP. This shift coincided with a major reorganization in atmospheric and oceanic circulation recorded in many records. Between 6,000 and 4,000 cal yr BP, the SPG started to contract, likely due to decreased Westerlies. Between 4,000 and 800 cal yr BP, Westerlies may have continued to decrease, but increased freshwater from northern sources could also have inhibited convection of the Labrador Sea. Both effects would combine to contract and warm the SPG.

In Chapter 4, “*The Influence of the Subpolar Gyre on the Hydrographic Properties of the Irminger Current on Southwest Icelandic Shelf and its Implication on Adjacent*”, we documented the history of Irminger Atlantic Water and freshwater interactions through the Holocene on the SW Iceland shelf. In the early Holocene, the Atlantic water inflow was dampened by freshwater from the final decay of the Laurentide ice sheet. Isostatic rebound ended at ~8,600 cal yr BP. Benthic and planktonic

foraminiferal assemblages suggest that the water column was well mixed. in the mid Holocene the Irminger Water influence was strongest with minor freshwater forcing. In the late Holocene, the influence of IC decreased due to increasing freshwater forcing from the Greenland ice sheet advance and southward advancing polar front. By monitoring the IC on the SW Iceland shelf, we also gain insights into climate forcings on the subpolar North Atlantic. By the time the Atlantic water masses carried in the IC reach the SW Iceland shelf, these water masses have been transformed by their interaction with the atmosphere during their transit in the subpolar gyre (SPG).

The commonly accepted hypothesis is that Atlantic water carries nutrients to the Icelandic shelf. This hypothesis can be refined with the understanding we have gained about SPG dynamics. Today, most of the nutrients come from the melt water of the Greenland ice sheet and the upwelling in the SPG region. The working hypothesis to be tested is: when the SPG is contracted, the IC carries more volume to the Icelandic shelf and entrains more nutrients from the SPG gyre. The pathway is shorter and therefore nutrients are less likely to be depleted. But as an added caveat is to consider the stratification of the water column. A stratified water column as we have observed the Neoglaciation is more nutrient depleted. The nutrient history of the SPG and the IC in particular, can be resolved by analyzing the Cd/Ca records.

There are several questions that we could not answer. One of question is the discrepancy between the reconstructions of sea surface temperature based on planktonic assemblages and on Mg/Ca ratios. Husum and Hald (2012) developed a new transfer functions, using planktonic foraminifera >100μm . The SSTs in this thesis were reconstructed on the size > 150μm. According to the Husum and Hald (2012) study,

using the smaller size fraction yields cooler temperatures. They found that the species *T. quinqueloba* becomes the very frequent (Figure 5.1). We can test the hypothesis, using the Husum and Hald (2012) method the temperature reconstructions based on assemblages would be similar to the temperature reconstruction by Mg/Ca method.

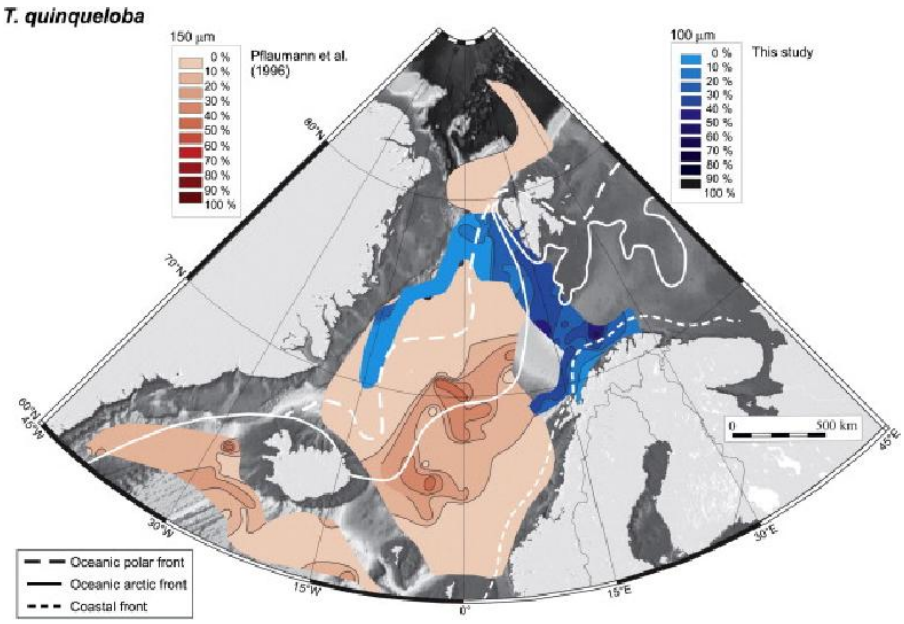

Figure 5.1 Comparison of percentages of *T. quinqueloba* in the >150µm fraction (Pflaumann et al., 1996) and in the >100µm fraction *(Husum and Hald, 2012)* . (Figure from Husum and Hald (2012); their Figure 4)

Another pressing research objective is to document the connection between the strength of the SPG with the Labrador Sea convection through the Holocene. In modern observations, these two are tightly linked but we have no certain indication if the Labrador Sea convection operated like it does today. Analyzing sediment cores from the Labrador Sea using the paired measurement of Mg/Ca and $\delta^{18}O_{calcite}$ would yield important answers.

This thesis did not document the temperature and salinity of the of the Atlantic water masses from the Gulf Stream as it separates from the North American continental shelf entering the SPG. The understanding of SPG dynamics would benefit from such a study.

Work Cited for Chapter 1 and Chapter 5

Blaschek, M., and Renssen, H., 2013, The Holocene thermal maximum in the Nordic Seas: the impact of Greenland Ice Sheet melt and other forcings in a coupled atmosphere-sea-ice-ocean model: Climate of the Past, v. 9, no. 4, p. 1629-1643.

Dickson, R. R., Meincke, J., Malmberg, S. A., and Lee, A. J., 1988, THE GREAT SALINITY ANOMALY IN THE NORTHERN NORTH-ATLANTIC 1968-1982: Progress in Oceanography, v. 20, no. 2, p. 103-151.

Emilliani, C., 1955, Pleistocene temperatures: Journal of Geology, v. 63, p. 538-578.

Hakkinen, S., and Rhines, P. B., 2009, Shifting surface currents in the northern North Atlantic Ocean: Journal of Geophysical Research-Oceans, v. 114.

Hartmann, D. L., A.M.G., K. T., Rusticucci, M., Alexander, L. V., Broennimann, S., Charabi, Y., Dentener, F. J., Dlugokencky, E. J., Easterling, D. R., Kaplan, A., Soden, B. J., Thorne, P. W., Wild, M., and Zhai, P. M., 2013, Observations: Atmosphere and Surface; Climate Change 2013: The Physical Basis. Contribution of Working Group I to the Fifth Assessment Report of the Intergovernmental Panel on Climate Change.

Holland, D. M., Thomas, R. H., De Young, B., Ribergaard, M. H., and Lyberth, B., 2008, Acceleration of Jakobshavn Isbrae triggered by warm subsurface ocean waters: Nature Geoscience, v. 1, no. 10, p. 659-664.

Husum, K., and Hald, M., 2012, Arctic planktic foraminiferal assemblages: Implications for subsurface temperature reconstructions: Marine Micropaleontology, v. 96-97, p. 38-47.

Hurrell, J. W., 1995, DECADAL TRENDS IN THE NORTH-ATLANTIC OSCILLATION - REGIONAL TEMPERATURES AND PRECIPITATION: Science, v. 269, no. 5224, p. 676-679.

Hurrell, J. W., Kushnir, Y., Ottersen, G., and Visbeck, M., 2003, An Overview of the North Atlantic Oscillation, *in* Union, A. G., ed., The North Atlantic Oscillation: Climatic Significance and Environmental Impact; Geophysical Monograph 134.

Jennings, A., Andrews, J., and Wilson, L., 2011, Holocene environmental evolution of the SE Greenland Shelf North and South of the Denmark Strait: Irminger and East Greenland current interactions: Quaternary Science Reviews, v. 30, no. 7-8, p. 980-998.

Kaufman, D. S., Ager, T. A., Anderson, N. J., Anderson, P. M., Andrews, J. T., Bartlein, P. J., Brubaker, L. B., L.L., C., Cwynar, L. C., Duvall, M. L., Dyke, A. S., Edwards, M. E., Eisner, W. R., Gajewski, K., Geirsdottir, A., Hu, F. S., Jennings, A. E., Kaplan, M. R., Kerwin, M. W., Lozhkin, A. V., MacDonald, G. M., Miller, G. H., Mock, C. J., Oswald, W. W., Otto-Bliesner, B. L., Porinchu, D. F., Ruehland, K., Smol, J. P., Steig, E. J., and Wolfe, B. B., 2004, Holocene termal maximum in the western Arctic (0-180 deg W): Quaternary Science Reviews, v. 23, p. 529-560.

LeGrande, A. N., and Schmidt, G. A., 2008, Ensemble, water isotope-enabled, coupled general circulation modeling insights into the 8.2 ka event: Paleoceanography, v. 23, no. 3.

Lynch-Stieglitz, J., Liu, Z., Koutavas, A., Marchitto, T., and Brady, E., 2002, Sea surface temperature patterns in the Early Holocene: Global Ocean response to insolation forcing: Geochimica et Cosmochimica Acta, v. 66, no. 15A, p. A467-A467.

Marchal, O., Cacho, I., Stocker, T. F., Grimalt, J. O., Calvo, E., Martrat, B., Shackleton, N. J., Vautravers, M., Cortijo, E., van Kreveld, S., Andersson, C., Koc, N., Chapman, M., Sbaffi, L., Duplessy, J.-C., Sarntheim, M., Turon, J.-L., Duprat, J., and Jansen, E., 2002, Apparent long-term cooling in the sea surface in the northeast Atlantic and Mediterranean during the Holocene.: Quaternary Science Review, v. 21, p. 455-483.

Nurnberg, D., Bijma, J., and Hemleben, C., 1996, Assessing the reliability of magnesium in foraminiferal calcite as a proxy for water mass temperatures (vol 60, pg 803, 1995): Geochimica et Cosmochimica Acta, v. 60, no. 13, p. 2483-2483.

Pflaumann, U., Duprat, J., Pujol, C., and Labeyrie, L. D., 1996, SIMMAX: A modern analog technique to deduce Atlantic sea surface temperatures from planktonic foraminifera in deep-sea sediments: Paleoceanography, v. 11, no. 1, p. 15-35.

Rhein, M., Rintoul, S. R., Aoki, S., Campos, E., Chanmbers, D., Freely, R. A., Gulev, S., Johnson, G. C., Josey, S. A., Kostianoy, A., Mauritzen, C., Roemich, D., Talley, L. D., and Wang, F., 2013, Observation Ocean, Cambridge University Press, "Climate Change 2013: The Physical Science Basis. Contribution of Working Group I to the Fifth Assessment Report of the Intergovernmental panel on Climaet Change.

Rignot, E., and Kanagaratnam, P., 2006, Changes in the velocity structure of the Greenland ice sheet: Science, v. 311, no. 5763, p. 986-990.

Rimbu, N., Lohmann, G., Kim, J. H., Arz, H. W., and Schneider, R., 2003, Arctic/North Atlantic Oscillation signature in Holocene sea surface temperature trends as obtained from alkenone data: Geophysical Research Letters, v. 30, no. 6.

Rosenthal, Y., Boyle, E. A., and Slowey, N., 1997, Temperature control on the incorporation of magnesium, strontium, fluorine, and cadmium into benthic foraminiferal shells from Little Bahama Bank: Prospects for thermocline paleoceanography: Geochimica et Cosmochimica Acta, v. 61, no. 17, p. 3633-3643.

Sarafanov, A., 2009, On the effect of the North Atlantic Oscillation on temperature and salinity of the subpolar North Atlantic intermediate and deep waters.: ICES Journal of Marine Science, v. 66, p. 1448-1454.

Serreze, M. C., Holland, M. M., and Stroeve, J., 2007, Perspectives on the Arctic's shrinking sea-ice cover: Science, v. 315, no. 5818, p. 1533-1536.

Shackelton, N. J., 1967, Oxygen isotope analyses and Pleistocene temperature re-assessed.: Nature, v. 215, p. 15-17.

Straneo, F., Curry, R. G., Sutherland, D. A., Hamilton, G. S., Cenedese, C., Vage, K., and Stearns, L. A., 2011, Impact of fjord dynamics and glacial runoff on the circulation near Helheim Glacier: Nature Geoscience, v. 4, no. 5, p. 322-327.

Straneo, F., Heimbach, P., Sergienko, O., Hamilton, G., Catania, G., Griffies, S., Hallberg, R., Jenkins, A., Joughin, I., Motyka, R., Pfeffer, W. T., Price, S. F., Rignot, E., Scambos, T., Truffer, M., and Vieli, A., 2013, Challenges to

Understanding the Dynamic Response of Greenland's Marine Terminating Glaciers to Oceanic and Atmospheric Forcing: Bulletin of the American Meteorological Society, v. 94, no. 8, p. 1131-1144.

Sutherland, D. A., and Straneo, F., 2012, Estimating ocean heat transports and submarine melt rates in Sermilik Fjord, Greenland, using lowered acoustic Doppler current profiler (LADCP) velocity profiles: Annals of Glaciology, v. 53, no. 60, p. 50-58.

Taboada, F. G., and Anadon, R., 2012, Patterns of change in sea surface temperature in the North Atlantic during the last three decades: beyond mean trends: Climatic Change, v. 115, no. 2, p. 419-431.

Thornalley, D. J. R., Elderfield, H., and McCave, I. N., 2009, Holocene oscillations in temperature and salinity of the surface subpolar North Atlantic: Nature, v. 457, no. 7230, p. 711-714.

Vage, K., Pickart, R. S., Sarafanov, A., Knutsen, O., Mercier, H., Lherminier, P., van Aken, H. M., Meincke, J., Quadfasel, D., and Bacon, S., 2011, The Irminger Gyre: Circulation, convection, and interannual variability: Deep-Sea Research Part I-Oceanographic Research Papers, v. 58, no. 5, p. 590-614.

Yashayaev, I., and Clarke, A., 2008, EVOLUTION OF NORTH ATLANTIC WATER MASSES INFERRED FROM LABRADOR SEA SALINITY SERIES: Oceanography, v. 21, no. 1, p. 30-45.

Yashayaev, I., van Aken, H. M., Holliday, N. P., and Bersch, M., 2007, Transformation of the Labrador sea water in the subpolar North Atlantic: Geophysical Research Letters, v. 34, no. 22.

Yin, J. J., Overpeck, J. T., Griffies, S. M., Hu, A. X., Russell, J. L., and Stouffer, R. J., 2011, Different magnitudes of projected subsurface ocean warming around Greenland and Antarctica: Nature Geoscience, v. 4, no. 8, p. 524-528.

Zhang, X. B., and Church, J. A., 2012, Sea level trends, interannual and decadal variability in the Pacific Ocean: Geophysical Research Letters, v. 39.

Zweng, M. M., and Munchow, A., 2006, Warming and freshening of Baffin Bay, 1916-2003: Journal of Geophysical Research-Oceans, v. 111, no. C7.

Appendix 1: MD99-2256 Data

run name	mid depth	# bugs	[Ca]	Li/Ca	B/Ca	Mg/Ca	Mn/Ca	Zn/Ca	Sr/Ca	Cd/Ca	U/Ca	Al/Ca	Fe/Ca
Patrick_40_041509	23.5	69	1.777	15.132	27.738	2.390	37.311	1.012	1.376	0.030	0.018	695.568	468.392
Patrick_40_041509	23.5	70	1.767	15.244	34.323	2.327	34.846	0.988	1.386	0.035	0.020	455.375	373.359
Patrick_40_041509	35.5	70	2.388	16.159	30.726	2.011	30.988	0.476	1.404	0.029	0.013	221.171	142.578
Patrick_40_041509	35.5	101	1.522	16.283	29.949	2.109	31.921	2.416	1.405	0.029	0.012	236.915	193.443
Ursula_19_111209	105.5	18	0.298	15.792	87.524	3.795	43.318	115.955	1.415	0.243	0.010	1998.023	1400.622
Ursula_19_111209	117.5	25	0.454	17.798	21.445	2.540	29.310	20.717	1.440	0.044	0.009	1068.867	1044.846
Ursula_20_111909	123.5	14	0.166	8.962	5.910	6.827	113.980	8.672	1.445	0.018	0.008	11826.903	6441.882
Ursula_17_201009	125.5	17	0.215	10.303	69.261	4.513	77.316	17.023	1.421	0.034	0.007	4394.671	4017.616
Ursula_17_201009	133.5	14	0.487	16.976	16.884	2.062	24.362	4.305	1.426	0.019	0.009	407.628	375.457
Ursula_19_111209	135.5	20	0.492	13.482	31.527	2.958	39.140	12.191	1.420	0.027	0.007	2485.042	1743.229
Ursula_17_201009	137.5	15	0.107	9.067	-6.861	18.699	298.512	9.242	1.464	0.013	0.008	27847.369	20837.004
Ursula_7_022709	143.5	46	0.349	6.462	6.952	61.806	1080.646	13.532	1.431	0.010	0.005	96636.423	67153.851
Ursula_19_111209	145.5	22	0.605	12.729	18.270	3.403	56.755	11.308	1.430	0.025	0.007	3000.530	2246.260
Patrick_38_031809	147.75	87	0.424	7.544	19.287	5.789	96.306	9.857	1.431	0.011	0.009	6646.704	5838.948
Patrick_38_031809	147.75	88	0.137	10.809	7.753	20.095	325.176	11.495	1.514	0.011	0.010	42105.318	22428.061
Patrick_38_031809	147.75	65	0.129	18.791	44.940	1.881	52.451	128.004	1.167	0.182	0.007	380.210	680.210
Ursula_7_022709	150	61	0.509	9.096	6.949	38.417	625.820	7.740	1.465	0.014	0.010	54580.731	47812.385
Ursula_17_201009	150	18	0.470	10.163	7.725	7.166	120.295	5.653	1.414	0.011	0.010	8643.198	7242.904
Ursula_7_022709	153.5	55	0.373	7.323	6.957	37.384	607.967	11.427	1.437	0.014	0.008	59307.328	49618.380
Ursula_7_022709	155.5	66	0.644	9.828	9.522	18.605	311.333	25.262	1.428	0.014	0.011	26527.858	22227.763
Ursula_20_111909	155.5	20	0.340	14.415	16.088	2.327	35.210	2.562	1.454	0.015	0.009	1986.202	1054.999
Ursula_19_111209	157.5	28	0.138	18.902	14.803	2.366	24.646	101.204	1.413	0.132	0.012	1583.918	752.295
Ursula_19_111209	159.5	42	1.378	16.208	24.041	2.420	41.417	7.636	1.414	0.030	0.012	1492.502	1208.040
Ursula_17_201009	163.5	18	1.324	15.745	22.199	2.043	34.444	7.107	1.411	0.032	0.010	746.334	712.806
Ursula_20_111909	165.5	21	0.300	15.777	22.822	2.295	25.718	91.180	1.416	0.051	0.009	544.967	445.537
Ursula_7_022709	167.5	65	0.941	9.339	9.311	12.041	200.429	6.214	1.425	0.013	0.010	15747.104	13262.929
Ursula_20_111909	167.5	17	0.678	12.331	14.871	5.173	68.815	8.296	1.417	0.022	0.010	5605.438	3520.752
Ursula_20_111909	169.5	20	0.622	13.964	13.916	4.056	72.194	5.557	1.396	0.016	0.011	4264.921	4083.967

Ursula_17_201009	173.5	21	0.952	12.616	12.393	5.483	95.970	8.263	1.411	0.019	0.011	6503.361	4703.007
run name	mid depth	# bugs	[Ca]	Li/Ca	B/Ca	Mg/Ca	Mn/Ca	Zn/Ca	Sr/Ca	Cd/Ca	U/Ca	Al/Ca	Fe/Ca
Ursula_7_022709	175.5	84	5.312	9.466	11.274	12.421	204.461	8.443	1.416	0.017	0.014	18874.450	13286.224
Ursula_20_111909	175.5	15	0.225	12.743	8.850	9.796	138.990	18.619	1.452	0.029	0.019	19009.613	8409.202
Ursula_19_111209	177.5	35	0.939	16.757	20.619	1.697	24.744	8.787	1.420	0.034	0.011	409.165	377.647
Ursula_7_022709	179.5	69	2.021	19.819	21.335	6.379	110.791	12.187	1.435	0.027	0.027	9065.860	5529.789
Ursula_19_111209	183.5	48	0.772	15.576	9.701	3.123	50.645	3.541	1.433	0.014	0.010	2408.380	2138.589
Ursula_19_111209	185.5	30	0.107	9.238	5.837	30.322	488.450	24.486	1.424	0.051	0.010	53194.923	37635.103
Ursula_7_022709	187.5	66	1.843	15.934	18.030	6.361	116.135	8.364	1.456	0.022	0.016	9157.119	5929.057
Ursula_7_022709	189.5	56	1.725	13.584	13.120	11.338	194.488	8.911	1.428	0.017	0.013	15660.976	11671.109
Ursula_20_111909	189.5	17	1.257	17.441	23.993	3.700	76.560	11.442	1.421	0.033	0.018	5159.559	3185.821
Ursula_7_022709	193.5	48	1.820	7.070	7.839	13.128	223.875	5.683	1.428	0.009	0.007	17150.067	13763.441
Ursula_20_111909	193.5	20	0.636	14.202	24.729	2.668	44.029	6.597	1.426	0.027	0.011	2390.194	1551.109
Ursula_7_022709	195.5	52	1.677	11.615	11.792	11.663	198.217	10.244	1.426	0.019	0.011	17720.572	12482.650
Ursula_7_022709	197.5	101	1.661	10.403	9.457	12.350	215.683	6.824	1.427	0.014	0.012	17590.757	12778.077
Ursula_20_111909	197.5	22	0.537	15.906	16.810	3.326	55.084	4.463	1.415	0.018	0.016	2952.433	2098.558
Ursula_7_022709	199.5	60	2.072	13.157	15.126	8.103	141.855	8.940	1.439	0.014	0.013	10589.118	7506.075
Ursula_20_111909	199.5	21	0.754	15.716	18.876	2.337	44.086	4.210	1.412	0.022	0.013	1766.604	1322.534
Ursula_7_022709	203.5	57	1.898	14.456	22.400	5.473	90.722	14.278	1.436	0.018	0.012	6067.886	4862.979
Ursula_7_022709	205.5	65	1.545	13.388	14.136	7.552	132.862	75.583	1.420	0.018	0.014	9510.796	8107.650
Ursula_19_111209	207.5	15	1.696	15.506	25.784	2.307	33.186	3.083	1.413	0.018	0.011	650.041	692.559
Ursula_7_022709	215.5	40	1.420	12.298	14.793	5.507	108.079	7.789	1.436	0.018	0.013	7546.121	5148.358
Ursula_7_022709	219.5	98	2.720	13.187	18.127	4.296	95.616	4.964	1.417	0.023	0.015	4893.302	3332.698
Ursula_7_022709	223.5	59	1.616	10.073	12.916	7.452	121.236	7.838	1.425	0.013	0.007	10182.306	6931.475
Ursula_19_111209	227.5	20	1.013	16.038	23.888	1.832	30.599	1.200	1.409	0.017	0.009	190.338	214.455
Ursula_7_022709	233.5	72	2.481	15.508	25.181	2.243	41.634	3.413	1.429	0.025	0.011	1343.346	932.517
Ursula_7_022709	235.5	78	1.836	15.300	23.494	3.015	51.080	8.781	1.442	0.022	0.012	2328.207	1653.224
Ursula_7_022709	237.5	61	1.737	11.616	17.666	3.791	67.790	5.897	1.447	0.014	0.009	3958.129	2865.447
Ursula_19_111209	239.5	32	1.190	15.675	17.556	1.972	36.994	1.463	1.419	0.017	0.009	531.981	455.248

Ursula_17_201009	243.5	20	2.213	12.649	20.231	3.498	64.424	6.766	1.417	0.021	0.009	3558.591	2318.553
Ursula_19_111209	247.5	37	1.774	16.000	20.200	1.898	40.064	3.746	1.423	0.021	0.011	321.980	278.694
run name	mid depth	# bugs	[Ca]	Li/Ca	B/Ca	Mg/Ca	Mn/Ca	Zn/Ca	Sr/Ca	Cd/Ca	U/Ca	Al/Ca	Fe/Ca
Ursula_20_111909	253.5	16	1.022	16.100	22.142	1.804	29.594	2.199	1.419	0.019	0.009	162.983	156.854
Ursula_19_111209	255.5	25	2.924	15.998	21.176	2.281	46.201	1.528	1.423	0.019	0.010	883.741	732.792
Ursula_17_201009	263.5	22	1.214	13.868	17.488	2.945	58.009	3.415	1.414	0.016	0.009	2393.718	1599.651
Ursula_17_201009	267.5	20	4.472	13.738	21.757	2.552	46.691	2.471	1.414	0.018	0.009	1326.043	995.942
Ursula_20_111909	273.5	12	0.425	16.164	24.059	1.794	25.489	12.061	1.424	0.025	0.009	140.504	196.125
Patrick_38_031809	275.5	70	3.435	16.575	26.699	1.960	39.860	0.581	1.425	0.018	0.013	83.072	125.536
Patrick_38_031809	279.5	80	3.187	16.546	25.037	1.813	31.780	3.403	1.411	0.016	0.011	84.138	157.758
Ursula_19_111209	287.5	20	6.828	15.329	35.416	1.764	31.925	1.596	1.407	0.020	0.010	35.674	93.879
Ursula_19_111209	293.5	37	1.852	16.686	20.521	1.845	27.928	2.475	1.425	0.020	0.009	193.377	181.064
Ursula_20_111909	299.5	16	0.966	15.380	26.497	1.993	37.170	2.347	1.425	0.028	0.011	295.549	222.649
Ursula_19_111209	309.5	20	1.882	17.196	24.686	1.996	41.190	1.383	1.431	0.022	0.010	209.486	227.849
Ursula_20_111909	363.5	10	0.205	13.269	15.365	2.406	27.801	5.082	1.423	0.015	0.006	1075.526	667.868
Ursula_20_111909	387.5	25	1.076	14.748	18.093	2.361	32.605	3.909	1.432	0.015	0.009	727.691	681.804
Ursula_19_111209	395.5	18	2.303	16.380	23.391	2.159	36.431	2.398	1.417	0.016	0.009	380.234	367.899

Appendix 2: MD99-2259 Data

run name	mid depth	# bugs:	[Ca]	Li/Ca	B/Ca	Mg/Ca	Mn/Ca	Zn/Ca	Sr/Ca	Cd/Ca	U/Ca	Al/Ca	Fe/Ca
Ursula_37_071812	3.5	17	0.514	15.041	19.566	1.946	24.517	1.934	1.419	0.020	0.010	460.240	360.350
Ursula_37_071812	4.5	20	0.516	13.879	21.085	2.068	23.091	1.537	1.388	0.016	0.014	780.869	505.795
Ursula_36_071712	5.5	24	1.144	16.211	24.947	2.318	35.472	3.242	1.408	0.029	0.015	779.462	652.087
Ursula_36_071712	7.5	16	0.380	16.570	10.129	2.120	29.268	7.754	1.402	0.027	0.012	393.971	305.421
Ursula_36_071712	8.5	27	0.193	11.574	1.195	3.450	38.663	12.173	1.441	0.023	0.013	2599.950	1736.638
Ursula_37_071812	9.5	8	0.124	15.174	9.186	2.688	20.338	2.850	1.426	0.012	0.009	655.153	338.949
Ursula_36_071712	10.5	38	0.517	13.410	15.244	3.452	60.132	5.919	1.414	0.025	0.012	3385.524	2209.913
Ursula_37_071812	11.5	22	0.828	15.972	26.422	2.033	27.223	2.839	1.421	0.021	0.015	691.283	550.698
Ursula_36_071712	12.5	44	0.923	11.640	13.105	3.699	42.321	5.263	1.403	0.025	0.013	3308.506	2223.658
Ursula_36_071712	13.5	21	0.489	15.521	17.792	2.134	28.978	3.788	1.392	0.033	0.013	857.175	460.962
Ursula_35_071212	14.5	51	1.644	15.295	26.155	3.114	38.755	6.260	1.410	0.046	0.015	1708.500	1007.064
Ursula_33_071012	15.5	27	0.562	14.582	26.269	2.095	14.864	2.049	1.411	0.026	0.008	338.240	225.144
Ursula_36_071712	16.5	54	0.555	12.682	13.383	4.158	58.831	5.698	1.393	0.025	0.012	5515.250	3439.320
Ursula_34_071112	17.5	39	1.114	15.174	25.609	1.836	15.740	1.108	1.404	0.017	0.008	356.072	239.748
Ursula_33_071012	19.5	27	0.912	15.801	26.809	2.176	33.042	3.260	1.409	0.026	0.010	1106.232	718.401
Ursula_36_071712	20.5	59	0.936	15.639	16.082	2.366	35.462	203.418	1.413	0.022	0.012	1647.636	722.226
Ursula_33_071012	21.5	22	0.132	18.428	24.372	3.572	28.447	7.930	1.473	0.021	0.007	3619.011	697.948
Ursula_35_071212	22.5	28	0.906	12.950	22.817	3.130	44.637	3.303	1.409	0.014	0.014	3489.494	2053.488
Ursula_36_071712	23.5	20	0.285	15.559	-0.048	2.069	20.269	13.944	1.396	0.064	0.009	688.088	480.448
Ursula_33_071012	24.5	66	3.915	14.958	23.161	2.293	36.183	1.870	1.399	0.024	0.018	1305.176	671.016
Ursula_34_071112	25.5	18	0.963	15.338	23.087	1.997	18.154	1.550	1.409	0.024	0.009	414.614	273.740
Ursula_36_071712	26.5	44	0.413	13.423	15.010	2.776	44.337	6.942	1.424	0.025	0.013	2984.169	1653.551
Ursula_34_071112	27.5	32	0.668	14.582	18.600	1.934	17.185	2.955	1.401	0.027	0.008	542.730	256.848
Ursula_35_071212	28.5	64	3.427	15.252	25.497	2.229	42.878	1.924	1.415	0.026	0.016	1116.686	772.065
Ursula_34_071112	30.5	28	0.737	13.503	27.322	2.627	44.867	2.788	1.394	0.019	0.013	2159.565	1415.870
Ursula_35_071212	31.5	33	1.309	15.413	25.996	3.043	19.558	2.377	1.413	0.024	0.010	775.316	416.004

run name	mid depth	# bugs:	[Ca]	Li/Ca	B/Ca	Mg/Ca	Mn/Ca	Zn/Ca	Sr/Ca	Cd/Ca	U/Ca	Al/Ca	Fe/Ca
Ursula_37_071812	32.5	59	3.505	17.074	27.414	2.031	39.759	1.014	1.398	0.033	0.015	789.449	465.779
Ursula_36_071712	33.5	46	0.561	15.004	36.038	2.472	29.069	23.469	1.402	0.099	0.015	1177.413	800.254
Ursula_34_071112	34.5	54	1.829	14.814	24.019	2.003	30.516	2.572	1.394	0.026	0.010	836.493	547.386
Ursula_35_071212	35.5	34	2.022	13.257	20.214	2.583	27.777	3.025	1.414	0.022	0.010	1610.072	987.853
Ursula_35_071212	37.5	14	0.294	14.990	37.307	2.120	21.216	11.255	1.385	0.033	0.007	972.114	493.610
Ursula_33_071012	38.5	38	0.336	16.349	33.836	4.477	80.678	32.539	1.431	0.047	0.027	7045.783	4139.066
Ursula_37_071812	39.5	24	0.204	13.195	16.028	3.155	37.276	8.367	1.422	0.019	0.012	2439.528	1805.836
Ursula_35_071212	40.5	52	1.971	14.631	21.698	2.387	40.747	49.369	1.408	0.025	0.015	1821.682	1125.043
Ursula_33_071012	41.5	28	1.237	15.888	26.032	2.358	100.069	2.705	1.389	0.026	0.010	477.401	410.261
Ursula_33_071012	42.5	53	2.280	15.261	25.992	2.306	43.134	2.812	1.418	0.024	0.015	1861.412	797.041
Ursula_34_071112	43.5	31	1.254	15.589	29.214	2.323	25.773	94.570	1.416	0.024	0.014	722.795	506.851
Ursula_33_071012	44.5	48	1.997	16.282	23.469	2.206	37.159	2.314	1.423	0.024	0.013	1279.007	735.661
Ursula_34_071112	45.5	32	0.542	13.418	21.954	2.265	19.738	2.528	1.443	0.018	0.009	888.923	511.356
Ursula_33_071012	46.5	39	0.877	14.849	20.956	2.710	46.848	4.588	1.400	0.021	0.018	2919.885	1639.185
Ursula_33_071012	47.5	53	2.399	15.243	23.807	2.224	37.305	1.786	1.406	0.019	0.015	1415.264	810.498
Ursula_33_071012	47.5	28	1.608	15.897	22.728	1.987	26.484	1.746	1.403	0.021	0.013	882.359	401.800
Ursula_33_071012	48.5	42	1.438	16.343	22.280	2.424	36.241	2.261	1.393	0.021	0.016	1863.787	1012.400
Ursula_35_071212	49.5	54	2.741	16.542	24.659	2.327	43.783	6.556	1.395	0.035	0.020	1455.605	762.876
Ursula_33_071012	53.5	23	0.483	18.244	23.982	2.918	43.991	4.215	1.412	0.025	0.016	1961.917	1047.519
Ursula_36_071712	54.5	32	0.519	13.854	9.572	3.249	57.663	4.693	1.402	0.020	0.018	4313.167	2286.967
Ursula_33_071012	55.5	22	0.736	15.164	19.788	2.112	25.705	1.976	1.382	0.014	0.010	1297.603	539.899
Ursula_34_071112	56.5	73	2.686	13.233	20.888	2.990	52.638	3.567	1.405	0.020	0.013	3022.806	2045.365
Ursula_37_071812	57.5	36	2.036	15.734	24.783	1.996	26.274	1.262	1.437	0.018	0.009	496.611	307.043
Ursula_35_071212	58.5	20	0.467	12.544	19.650	3.937	73.316	5.326	1.424	0.014	0.019	6895.247	3891.794
Ursula_34_071112	58.5	17	0.164	20.123	31.157	3.543	58.751	9.748	1.388	0.024	0.016	4156.387	2589.072
Ursula_33_071012	59.5	37	1.403	15.165	31.492	1.902	30.920	3.145	1.436	0.020	0.008	721.432	289.586
Ursula_35_071212	60.5	20	1.266	12.980	19.012	2.123	38.324	4.211	1.417	0.024	0.009	1772.593	1055.993

run name	mid depth	# bugs:	[Ca]	Li/Ca	B/Ca	Mg/Ca	Mn/Ca	Zn/Ca	Sr/Ca	Cd/Ca	U/Ca	Al/Ca	Fe/Ca
Ursula_34_071112	60.5	26	0.389	15.530	17.262	2.949	38.507	6.009	1.463	0.023	0.011	2356.405	1294.119
Ursula_34_071112	61.5	29	0.347	16.593	49.266	2.032	19.878	1.305	1.429	0.019	0.008	786.412	256.026
Ursula_32_070912	62.5	30	1.632	15.409	29.237	1.875	38.876	4.401	1.413	0.029	0.014	1181.058	747.954
Ursula_36_071712	63.5	27	0.119	17.311	-25.900	2.160	21.254	18.651	1.429	0.045	0.009	474.274	275.757
Ursula_32_070912	64.5	22	1.185	15.940	31.658	1.976	34.370	2.040	1.400	0.022	0.012	851.619	562.735
Ursula_34_071112	64.5	35	0.113	15.421	30.573	5.594	95.908	12.778	1.423	0.019	0.017	9441.219	5006.766
Ursula_33_071012	65.5	30	0.102	14.880	49.072	2.980	37.984	3.940	1.444	0.022	0.010	2182.505	922.779
Ursula_32_070912	66.5	33	1.278	15.306	23.048	2.304	58.838	4.282	1.404	0.053	0.018	1977.505	1050.628
Ursula_32_070912	68.5	19	0.234	14.948	38.221	4.066	58.815	9.416	1.443	0.027	0.017	7128.342	2880.478
Ursula_34_071112	70.5	48	2.672	12.386	19.202	2.435	48.048	3.852	1.397	0.036	0.013	2267.938	1315.781
Ursula_32_070912	72.5	32	2.160	14.077	26.875	2.104	37.144	3.122	1.390	0.023	0.014	1404.171	776.565
Ursula_32_070912	74.5	20	0.960	11.961	20.010	2.354	51.402	4.151	1.397	0.014	0.010	2460.355	1664.479
Ursula_33_071012	75.5	32	1.796	16.050	24.721	1.979	25.739	1.540	1.434	0.045	0.010	346.218	327.053
Ursula_34_071112	77.5	29	0.490	16.403	161.003	2.668	27.244	4.269	1.431	0.024	0.007	483.586	338.707
Ursula_35_071212	78.5	29	0.254	16.112	38.208	2.055	16.558	4.602	1.440	0.025	0.007	945.304	247.631
Ursula_33_071012	81.5	37	2.660	15.340	23.361	2.015	24.032	1.114	1.390	0.025	0.012	448.874	319.916
Ursula_32_070912	82.5	16	0.738	17.787	43.610	2.466	34.541	2.154	1.457	0.034	0.016	630.972	338.299
Ursula_31_110410	84.5	18	0.512	17.225	21.313	2.218	34.011	6.014	1.387	0.017	0.011	979.017	913.284
Ursula_33_071012	85.5	40	2.500	15.020	19.229	2.172	31.241	1.469	1.415	0.022	0.014	835.441	568.833
Ursula_31_110410	86.5	25	0.823	14.542	21.742	3.154	62.072	50.689	1.415	0.020	0.014	3331.629	2094.293
Ursula_31_110410	88.5	20	0.456	12.934	16.256	2.970	72.942	10.750	1.414	0.031	0.024	3116.595	2058.360
Ursula_33_071012	89.5	36	0.335	17.204	36.838	1.980	29.280	1.851	1.425	0.023	0.012	627.371	433.635
Ursula_31_110410	90.5	34	2.929	11.522	19.772	2.880	73.489	1.858	1.409	0.015	0.010	1734.973	1375.327
Ursula_31_110410	90.5	23	0.738	14.908	28.770	1.826	30.215	7.106	1.403	0.018	0.016	1581.950	645.563
Ursula_33_071012	91.5	32	0.885	16.557	31.858	2.090	35.335	2.130	1.401	0.020	0.014	644.195	391.431
Ursula_29_102710	92.5	38	0.643	15.272	13.879	2.159	35.968	2.816	1.415	0.021	0.013	893.601	824.260
Ursula_34_071112	93.5	51	3.305	15.124	24.038	2.062	35.595	1.722	1.404	0.020	0.015	922.137	613.163

run name	mid depth	# bugs:	[Ca]	Li/Ca	B/Ca	Mg/Ca	Mn/Ca	Zn/Ca	Sr/Ca	Cd/Ca	U/Ca	Al/Ca	Fe/Ca
Ursula_31_110410	94.5	22	0.969	13.298	23.452	2.683	44.629	5.425	1.403	0.021	0.013	2537.947	2176.093
Ursula_33_071012	95.5	49	0.983	8.785	80.371	1.709	99.902	2.821	0.686	0.110	0.007	280.364	135.346
Ursula_35_071212	96.5	40	1.269	14.472	19.386	2.657	48.570	5.940	1.420	0.046	0.017	3506.534	1915.653
Ursula_31_110410	96.5	33	1.028	14.658	16.429	2.557	38.120	3.609	1.400	0.016	0.020	2135.118	1360.516
Ursula_31_110410	98.5	28	1.083	13.600	20.256	2.156	36.365	3.913	1.386	0.016	0.014	1376.360	1100.782
Ursula_31_110410	99.5	35	2.691	14.363	26.178	2.130	36.172	2.990	1.389	0.017	0.014	1188.605	764.144
Ursula_31_110410	102.5	28	0.908	12.145	18.756	4.397	74.733	5.637	1.424	0.016	0.013	5336.316	3471.704
Ursula_35_071212	103.5	61	4.409	16.291	28.634	2.023	42.025	3.188	1.406	0.024	0.016	1047.600	538.191
Ursula_29_102710	104.5	40	1.813	15.645	22.310	1.971	35.635	2.094	1.394	0.032	0.015	685.121	483.336
Ursula_35_071212	105.5	30	1.613	12.346	19.201	3.225	61.809	4.549	1.390	0.014	0.009	3916.959	2096.675
Ursula_29_102710	106.5	38	1.043	16.768	4.808	1.647	47.739	3.769	1.400	0.041	0.018	303.067	200.848
Ursula_34_071112	107.5	64	4.517	15.695	23.507	1.975	37.339	2.170	1.399	0.025	0.010	650.729	449.246
Ursula_34_071112	108.5	55	3.995	16.125	25.957	1.722	36.648	0.628	1.386	0.019	0.014	265.216	202.902
Ursula_29_102710	108.5	35	0.894	15.460	19.539	1.947	35.078	2.546	1.410	0.024	0.011	729.009	479.336
Ursula_34_071112	109.5	60	2.822	15.655	25.140	2.567	38.035	2.537	1.427	0.026	0.016	1717.630	831.567
Ursula_29_102710	110.5	45	1.626	15.105	24.304	1.783	34.076	1.185	1.424	0.026	0.015	391.776	255.220
Ursula_34_071112	111.5	41	2.430	16.404	25.601	1.956	32.561	0.891	1.419	0.021	0.014	540.921	288.962
Ursula_29_102710	112.5	46	0.739	15.374	181.334	1.981	40.947	5.642	1.434	0.026	0.012	761.135	532.217
Ursula_34_071112	113.5	37	2.121	16.612	26.589	1.907	35.543	2.281	1.416	0.025	0.015	805.332	378.896
Ursula_29_102710	114.5	35	0.342	14.096	-0.858	2.493	42.305	8.489	1.446	0.029	0.011	1497.323	1090.577
Ursula_35_071212	115.5	60	6.571	16.344	28.517	1.989	37.985	0.961	1.428	0.028	0.020	620.478	319.261
Ursula_29_102710	116.5	41	0.910	14.678	14.921	1.832	36.730	3.137	1.404	0.027	0.013	451.625	357.762
Ursula_35_071212	117.5	51	3.111	15.589	25.051	1.883	38.914	1.535	1.423	0.023	0.013	490.890	365.587
Ursula_29_102710	118.5	32	0.583	15.992	40.963	1.858	35.064	2.359	1.405	0.025	0.009	602.423	461.607
Ursula_36_071712	119.5	39	1.940	14.124	18.879	2.347	48.860	3.135	1.426	0.029	0.013	1170.768	842.483
Ursula_29_102710	120.5	40	0.580	15.894	14.235	1.692	37.652	2.464	1.400	0.023	0.011	276.504	270.135
Ursula_36_071712	121.5	52	1.558	14.459	18.892	2.332	45.966	1.748	1.413	0.033	0.012	1556.690	899.734

run name	mid depth	# bugs:	[Ca]	Li/Ca	B/Ca	Mg/Ca	Mn/Ca	Zn/Ca	Sr/Ca	Cd/Ca	U/Ca	Al/Ca	Fe/Ca
Ursula_29_102710	122.5	35	0.401	15.200	0.734	2.071	45.710	7.009	1.419	0.032	0.011	661.498	530.807
Ursula_35_071212	123.5	39	3.563	15.626	24.328	1.826	37.540	1.137	1.413	0.023	0.012	911.619	382.238
Ursula_29_102710	124.5	41	1.224	15.864	12.621	1.812	49.762	2.331	1.427	0.037	0.013	268.156	306.322
Ursula_35_071212	125.5	68	3.539	15.898	24.430	1.975	46.618	1.081	1.433	0.035	0.015	436.587	308.332
Ursula_29_102710	126.5	50	1.481	17.402	27.024	1.769	34.766	0.421	1.427	0.029	0.008	23.904	38.574
Ursula_35_071212	127.5	56	5.430	16.131	25.863	1.733	40.364	0.560	1.414	0.027	0.008	75.881	89.242
Ursula_29_102710	128.5	35	1.009	15.796	43.324	1.901	40.594	1.126	1.410	0.034	0.011	322.279	314.246
Ursula_34_071112	129.5	65	5.239	15.149	24.315	2.021	44.332	1.160	1.398	0.025	0.014	709.302	483.433
Ursula_29_102710	130.5	42	0.454	15.683	19.567	1.954	32.474	3.265	1.423	0.043	0.012	180.649	200.310
Ursula_36_071712	131.5	80	1.676	15.833	28.782	1.830	46.961	1.769	1.412	0.034	0.021	395.739	270.539
Ursula_29_102710	132.5	60	1.299	15.257	19.433	2.082	44.804	1.988	1.428	0.045	0.014	320.827	357.155
Ursula_34_071112	133.5	98	5.168	15.861	26.630	1.776	46.734	0.462	1.408	0.029	0.017	106.602	194.213
Ursula_29_102710	134.5	55	2.319	15.366	22.010	1.811	54.353	1.543	1.409	0.035	0.015	158.087	186.887
Ursula_35_071212	135.5	62	5.761	15.571	28.442	2.051	42.316	1.702	1.413	0.017	0.014	763.154	483.952
Ursula_29_102710	136.5	58	2.424	15.391	26.915	1.901	51.557	3.724	1.413	0.035	0.015	349.492	279.995
Ursula_36_071712	137.5	63	1.304	14.761	20.319	1.954	46.762	18.410	1.419	0.026	0.018	641.795	469.979
Ursula_29_102710	138.5	50	1.754	15.181	19.824	1.609	52.339	2.624	1.414	0.042	0.015	183.828	184.694
Ursula_29_102710	138.5	50	0.467	14.911	65.103	1.719	41.530	34.972	1.416	0.053	0.010	1243.865	509.598
Ursula_36_071712	139.5	57	2.107	14.866	22.232	2.322	58.103	2.245	1.426	0.034	0.017	1259.867	747.550
Ursula_29_102710	140.5	40	0.747	13.338	37.462	1.921	29.846	2.189	1.447	0.025	0.008	729.397	501.408
Ursula_35_071212	141.5	46	2.889	13.641	22.761	2.473	59.926	1.925	1.434	0.019	0.011	1755.111	1067.761
Ursula_31_110410	142.5	22	1.165	14.629	19.764	2.186	44.352	1.835	1.399	0.011	0.010	1392.272	897.991
Ursula_36_071712	145.5	59	1.710	13.920	19.276	2.046	58.080	2.789	1.403	0.030	0.014	987.985	734.226
Ursula_31_110410	146.5	50	3.501	11.403	21.426	2.872	64.081	1.839	1.399	0.011	0.009	2035.608	1651.325
Ursula_36_071712	147.5	60	2.743	14.712	21.859	2.023	39.962	2.120	1.429	0.028	0.011	657.878	449.222
Ursula_35_071212	148.5	58	4.083	15.401	29.349	1.801	36.698	1.308	1.428	0.026	0.010	218.791	212.785
Ursula_31_110410	149.5	34	3.726	15.633	27.130	1.926	40.951	1.111	1.397	0.014	0.011	446.891	345.663

run name	mid depth	# bugs:	[Ca]	Li/Ca	B/Ca	Mg/Ca	Mn/Ca	Zn/Ca	Sr/Ca	Cd/Ca	U/Ca	Al/Ca	Fe/Ca
Ursula_29_102710	154.5	45	1.084	15.050	26.767	2.209	59.049	3.188	1.427	0.034	0.022	808.725	668.314
Ursula_31_110410	158.5	40	3.065	13.487	23.642	2.206	51.537	2.395	1.406	0.014	0.017	1461.180	844.318
Ursula_31_110410	162.5	10	0.905	12.093	19.373	2.961	64.169	7.759	1.412	0.016	0.009	2175.873	1761.251
Ursula_31_110410	166.5	30	1.929	15.367	22.925	2.178	51.553	1.943	1.406	0.016	0.012	751.126	568.177
Ursula_31_110410	174.5	44	2.832	15.566	23.816	2.150	52.375	1.426	1.411	0.018	0.017	604.092	428.148
Ursula_31_110410	178.5	44	4.036	15.329	25.351	1.878	79.778	1.247	1.399	0.028	0.019	166.302	138.014
Ursula_31_110410	182.5	33	1.770	15.699	23.956	1.904	48.312	1.000	1.400	0.017	0.010	324.043	295.433
Ursula_31_110410	186.5	25	2.351	15.437	25.539	1.879	95.237	1.141	1.408	0.019	0.018	1451.643	240.509
Ursula_31_110410	190.5	33	3.252	15.391	24.800	1.822	78.566	0.907	1.403	0.020	0.013	66.380	35.694
Ursula_31_110410	194.5	40	3.148	14.941	26.625	1.773	70.106	1.279	1.413	0.017	0.014	186.331	148.051

core	species	mid depth	d13C PDB	d13C PDB std dev	d18O PDB	d18O PDB std dev
MD99-2259	*G. bulloides*	3.5	-0.3880	0.0100	1.6613	0.0351
MD99-2259	*G. bulloides*	7.5	-0.5585	0.0161	1.9151	0.0321
MD99-2259	*G. bulloides*	11.5	-0.2154	0.0140	1.8808	0.0331
MD99-2259	*G. bulloides*	12.5	-0.3829	0.0120	2.0112	0.0161
MD99-2259	*G. bulloides*	14.5	-0.5134	0.0171	1.9273	0.0271
MD99-2259	*G. bulloides*	16.5	-0.2706	0.0090	2.1993	0.0341
MD99-2259	*G. bulloides*	21.5	-0.3308	0.0120	1.9131	0.0361
MD99-2259	*G. bulloides*	22.5	-0.2244	0.0080	1.9374	0.0241
MD99-2259	*G. bulloides*	23.5	-0.4813	0.0090	1.8160	0.0171
MD99-2259	*G. bulloides*	24.5	-0.0990	0.0171	2.0152	0.0351
MD99-2259	*G. bulloides*	26.5	-0.3035	0.0150	1.9668	0.0181
MD99-2259	*G. bulloides*	28.5	-0.2474	0.0110	1.9658	0.0261
MD99-2259	*G. bulloides*	30.5	-0.2173	0.0211	1.6594	0.0391
MD99-2259	*G. bulloides*	31.5	-0.4391	0.0211	1.6362	0.0281
MD99-2259	*G. bulloides*	32.5	-0.3207	0.0140	1.9976	0.0181
MD99-2259	*G. bulloides*	33.5	-0.2725	0.0130	1.6225	0.0351
MD99-2259	*G. bulloides*	34.5	-0.0899	0.0060	1.7802	0.0411
MD99-2259	*G. bulloides*	35.5	-0.3809	0.0161	1.7964	0.0241
MD99-2259	*G. bulloides*	36.5	-0.3528	0.0100	1.7832	0.0381
MD99-2259	*G. bulloides*	39.5	-0.4842	0.0161	1.7760	0.0221
MD99-2259	*G. bulloides*	42.5	-0.2986	0.0100	1.7710	0.0401
MD99-2259	*G. bulloides*	44.5	-0.1922	0.0130	1.8812	0.0221
MD99-2259	*G. bulloides*	45.5	-0.6367	0.0171	1.3069	0.0381
MD99-2259	*G. bulloides*	46.5	-0.2414	0.0181	1.8994	0.0401
MD99-2259	*G. bulloides*	47.5	-0.1120	0.0140	1.8468	0.0261
MD99-2259	*G. bulloides*	49.5	-0.0297	0.0181	1.7811	0.0552
MD99-2259	*G. bulloides*	54.5	0.0004	0.0140	1.9500	0.0130

core	species	mid depth	d13C PDB	d13C PDB std dev	d18O PDB	d18O PDB std dev
MD99-2259	*G. bulloides*	57.5	-0.4942	0.0231	1.8044	0.0381
MD99-2259	*G. bulloides*	58.5	-0.6538	0.0130	1.7245	0.0191
MD99-2259	*G. bulloides*	61.5	-0.6257	0.0211	1.6476	0.0361
MD99-2259	*G. bulloides*	64.5	-0.1372	0.0120	1.9164	0.0451
MD99-2259	*G. bulloides*	68.5	-0.0599	0.0130	2.1398	0.0211
MD99-2259	*G. bulloides*	74.5	0.0755	0.0171	2.0317	0.0181
MD99-2259	*G. bulloides*	75.5	-0.2294	0.0161	1.6062	0.0441
MD99-2259	*G. bulloides*	77.5	0.0496	0.0130	1.6790	0.0391
MD99-2259	*G. bulloides*	78.5	0.1909	0.0171	1.8968	0.0201
MD99-2259	*G. bulloides*	80.5	-0.3338	0.0201	1.7431	0.0231
MD99-2259	*G. bulloides*	81.5	-0.0147	0.0140	1.7043	0.0472
MD99-2259	*G. bulloides*	82.5	-0.3920	0.0201	1.8271	0.0331
MD99-2259	*G. bulloides*	90.5	-0.4944	0.0090	1.9211	0.0411
MD99-2259	*G. bulloides*	91.5	-0.9788	0.0171	1.7619	0.0110
MD99-2259	*G. bulloides*	92.5	-0.1964	0.0251	1.7735	0.0301
MD99-2259	*G. bulloides*	93.5	-0.2243	0.0070	1.7932	0.0301
MD99-2259	*G. bulloides*	94.5	-0.0078	0.0040	1.7977	0.0281
MD99-2259	*G. bulloides*	95.5	-0.0588	0.0161	1.6982	0.0502
MD99-2259	*G. bulloides*	96.5	0.1076	0.0110	2.0606	0.0271
MD99-2259	*G. bulloides*	97.5	-0.5114	0.0120	1.8795	0.0612
MD99-2259	*G. bulloides*	98.5	-0.3710	0.0161	1.7755	0.0191
MD99-2259	*G. bulloides*	99.5	-0.3589	0.0140	2.0010	0.0130
MD99-2259	*G. bulloides*	102.5	-0.1713	0.0090	1.6592	0.0532
MD99-2259	*G. bulloides*	103.5	-0.2837	0.0110	1.8553	0.0331
MD99-2259	*G. bulloides*	104.5	-0.3539	0.0110	1.9272	0.0221
MD99-2259	*G. bulloides*	108.5	-0.0218	0.0120	1.6703	0.0271
MD99-2259	*G. bulloides*	109.5	-0.5255	0.0140	2.0646	0.0271

core	species	mid depth	d13C PDB	d13C PDB std dev	d18O PDB	d18O PDB std dev
MD99-2259	*G. bulloides*	110.5	-0.4944	0.0110	1.9767	0.0341
MD99-2259	*G. bulloides*	111.5	-0.4422	0.0181	1.8047	0.0191
MD99-2259	*G. bulloides*	112.5	0.1849	0.0100	1.7512	0.0261
MD99-2259	*G. bulloides*	113.5	-0.4352	0.0120	2.1151	0.0301
MD99-2259	*G. bulloides*	114.5	-0.2535	0.0130	1.7657	0.0281
MD99-2259	*G. bulloides*	115.5	-0.2225	0.0120	1.7118	0.0301
MD99-2259	*G. bulloides*	117.5	-0.4282	0.0130	1.8432	0.0331
MD99-2259	*G. bulloides*	118.5	0.0625	0.0110	2.0529	0.0331
MD99-2259	*G. bulloides*	119.5	-0.5033	0.0181	1.6850	0.0110
MD99-2259	*G. bulloides*	120.5	-0.0248	0.0100	2.1014	0.0261
MD99-2259	*G. bulloides*	121.5	-0.3799	0.0191	1.9085	0.0401
MD99-2259	*G. bulloides*	122.5	-0.1030	0.0201	2.0852	0.0211
MD99-2259	*G. bulloides*	123.5	-0.6899	0.0231	1.8721	0.0532
MD99-2259	*G. bulloides*	124.5	-0.3348	0.0110	2.0610	0.0271
MD99-2259	*G. bulloides*	128.5	-0.2014	0.0211	2.0788	0.0231
MD99-2259	*G. bulloides*	129.5	-0.2073	0.0150	1.7973	0.0361
MD99-2259	*G. bulloides*	130.5	-0.8445	0.0140	1.6248	0.0451
MD99-2259	*G. bulloides*	131.5	-0.3088	0.0150	1.8138	0.0150
MD99-2259	*G. bulloides*	132.5	-0.3940	0.0130	2.0232	0.0211
MD99-2259	*G. bulloides*	133.5	-0.1402	0.0090	2.0342	0.0221
MD99-2259	*G. bulloides*	134.5	-0.3549	0.0130	2.0960	0.0251
MD99-2259	*G. bulloides*	135.5	-0.4190	0.0130	1.8944	0.0181
MD99-2259	*G. bulloides*	136.5	-0.1111	0.0161	1.9302	0.0291
MD99-2259	*G. bulloides*	137.5	-0.5153	0.0070	1.8327	0.0221
MD99-2259	*G. bulloides*	138.5	-0.3449	0.0120	1.7998	0.0181
MD99-2259	*G. bulloides*	139.5	-0.5524	0.0050	1.9247	0.0381
MD99-2259	*G. bulloides*	140.5	-0.4221	0.0161	1.7846	0.0431

core	species	mid depth	d13C PDB	d13C PDB std dev	d18O PDB	d18O PDB std dev
MD99-2259	*G. bulloides*	141.5	-0.5053	0.0100	1.8013	0.0441
MD99-2259	*G. bulloides*	142.5	-0.3930	0.0110	1.7805	0.0301
MD99-2259	*G. bulloides*	143.5	-0.8765	0.0150	1.9045	0.0391
MD99-2259	*G. bulloides*	145.5	-0.6217	0.0181	2.0096	0.0311
MD99-2259	*G. bulloides*	146.5	-0.5174	0.0181	1.9838	0.0150
MD99-2259	*G. bulloides*	148.5	-0.5725	0.0140	1.9823	0.0421
MD99-2259	*G. bulloides*	149.5	-0.5666	0.0191	1.9706	0.0251
MD99-2259	*G. bulloides*	154.5	-0.6047	0.0130	1.9100	0.0261
MD99-2259	*G. bulloides*	158.5	-0.6499	0.0130	2.0394	0.0181
MD99-2259	*G. bulloides*	162.5	-0.4994	0.0080	2.0333	0.0191
MD99-2259	*G. bulloides*	166.5	-0.7552	0.0100	1.9181	0.0171
MD99-2259	*G. bulloides*	170.5	-0.7843	0.0110	2.0869	0.0251
MD99-2259	*G. bulloides*	174.5	-0.8445	0.0130	1.9868	0.0130
MD99-2259	*G. bulloides*	178.5	-0.4392	0.0100	2.0991	0.0311
MD99-2259	*G. bulloides*	182.5	-0.8024	0.0080	2.1597	0.0231
MD99-2259	*G. bulloides*	186.5	-0.8556	0.0140	2.1890	0.0231
MD99-2259	*G. bulloides*	190.5	-0.7994	0.0161	2.1486	0.0231
MD99-2259	*G. bulloides*	194.5	-0.8807	0.0040	2.0991	0.0261

Appendix 3: NEAP4K Data

run	mid depth	[Ca]	Li/Ca	B/Ca	Mg/Ca	Mn/Ca	Zn/Ca	Sr/Ca	Cd/Ca	U/Ca	Al/Ca	Fe/Ca
Ursula_9_051409-TM	0.5	0.228	4.965	14.159	3.299	28.544	66.096	1.432	0.019	0.005	3994.598	2756.028
Ursula_11_092809	1.5	1.032	16.221	27.501	2.021	22.303	10.255	1.375	0.036	0.013	109.939	120.560
Ursula_14_061509_TM	2.5	1.048	15.403	32.204	2.413	32.009	7.235	1.381	0.028	0.016	487.095	341.963
Ursula_14_061509_TM	3.5	3.008	15.650	31.745	2.144	42.890	2.133	1.372	0.031	0.021	125.634	126.629
Ursula_11_092809	4.5	1.718	15.309	33.752	1.893	39.665	3.004	1.350	0.031	0.020	64.484	105.740
Ursula_14_061509_TM	5.5	3.589	15.363	31.914	1.848	39.665	4.417	1.356	0.027	0.019	59.181	115.424
Ursula_14_061509_TM	6.5	0.909	15.686	23.120	2.114	43.962	10.696	1.362	0.025	0.017	197.131	196.158
Ursula_15_062909_TM	7.5	0.427	14.362	24.220	2.321	29.145	5.430	1.378	0.024	0.017	447.004	356.324
Ursula_10_052609_TM	8.5	1.410	14.305	29.032	2.860	45.041	10.025	1.382	0.028	0.014	952.650	634.054
Ursula_21_030310_TM	8.5	0.775	14.898	54.757	2.116	56.230	2.285	1.334	0.040	0.017	189.876	179.545
Ursula_8_042209_TM	9.5	2.769	16.222	30.826	2.158	21.311	12.806	1.388	0.027	0.015	7.299	2.950
Ursula_11_092809	10.5	1.496	16.515	41.365	2.358	29.024	5.757	1.408	0.031	0.016	67.256	86.405
Ursula_8_042209_TM	11.5	2.714	16.409	31.825	2.148	24.456	1.640	1.391	0.041	0.014	10.759	39.981
Ursula_11_092809	12.5	1.788	15.874	31.348	2.288	19.850	9.975	1.389	0.035	0.015	136.709	125.770
Ursula_21_030310_TM	13.5	0.567	15.856	48.208	2.378	47.186	1.642	1.325	0.039	0.017	222.440	132.820
Ursula_9_051409-TM	14.5	3.125	16.269	31.190	2.206	25.297	1.666	1.378	0.025	0.013	6.541	10.253
Ursula_9_051409-TM	15.5	1.644	16.316	26.854	2.222	31.286	4.137	1.373	0.026	0.016	228.428	168.850
Ursula_10_052609_TM	16.5	2.385	16.411	33.966	2.201	37.744	2.173	1.392	0.027	0.014	92.525	76.984
Ursula_9_051409-TM	17.5	2.856	15.487	29.924	2.261	35.404	3.579	1.381	0.028	0.018	750.404	327.986
Ursula_11_092809	18.5	2.427	16.408	30.267	2.257	33.500	2.030	1.383	0.038	0.018	8.284	47.297
Ursula_8_042209_TM	19.5	1.646	16.668	33.816	2.053	22.444	3.237	1.390	0.032	0.014	12.433	21.961
Ursula_9_051409-TM	20.5	1.859	16.010	59.881	2.153	27.615	2.377	1.353	0.035	0.020	209.684	164.558
Ursula_11_092809	21.5	2.146	16.670	31.241	2.247	28.603	3.657	1.378	0.034	0.022	45.923	72.122
Ursula_14_061509_TM	22.5	3.012	15.893	30.755	2.272	33.457	4.399	1.397	0.035	0.026	74.142	60.004
Ursula_9_051409-TM	24.5	2.642	16.475	28.800	2.352	42.784	1.738	1.395	0.041	0.033	220.044	199.571
Ursula_11_092809	25.5	0.432	15.706	23.634	2.447	37.379	12.756	1.400	0.045	0.024	455.218	314.461
Ursula_8_042209_TM	26.5	2.989	16.180	28.951	2.389	63.173	3.523	1.403	0.108	0.053	38.361	96.615

run	mid depth	[Ca]	Li/Ca	B/Ca	Mg/Ca	Mn/Ca	Zn/Ca	Sr/Ca	Cd/Ca	U/Ca	Al/Ca	Fe/Ca
Ursula_11_092809	27.5	0.635	12.583	19.472	2.836	42.571	12.399	1.406	0.029	0.019	981.814	778.466
Ursula_9_051409-TM	28.5	1.365	14.857	30.003	2.596	34.479	27.329	1.395	0.031	0.023	790.715	686.118
Ursula_21_030310_TM	28.5	0.716	13.221	49.978	3.112	63.673	2.564	1.344	0.046	0.023	1034.134	731.108
Ursula_14_061509_TM	29.5	1.722	15.786	26.793	2.441	35.001	5.787	1.395	0.036	0.025	317.024	320.341
Ursula_10_052609_TM	30.5	2.121	16.730	30.675	2.318	36.317	4.911	1.387	0.035	0.028	243.759	200.771
Ursula_9_051409-TM	31.5	1.183	15.463	32.504	2.478	37.492	1.358	1.418	0.040	0.028	312.927	215.900
Ursula_8_042209_TM	32.5	2.690	16.222	33.529	2.215	32.460	4.098	1.399	0.033	0.020	39.764	77.455
Ursula_8_042209_TM	33.5	1.462	16.280	36.558	2.466	43.452	3.089	1.399	0.049	0.028	126.201	175.758
Ursula_8_042209_TM	34.5	1.422	15.394	29.973	2.190	27.886	2.593	1.394	0.034	0.015	177.372	179.095
Ursula_8_042209_TM	34.5	0.621	15.053	32.167	2.487	34.122	21.800	1.413	0.030	0.014	551.568	382.476
Ursula_9_051409-TM	36.5	2.793	16.221	27.420	2.374	41.768	3.879	1.419	0.030	0.017	339.673	277.066
Ursula_8_042209_TM	37.5	2.484	16.749	32.601	2.382	35.322	1.949	1.407	0.039	0.016	28.278	73.373
Ursula_14_061509_TM	38.5	0.861	15.604	18.165	2.331	37.886	23.524	1.418	0.026	0.017	446.865	231.144
Ursula_14_061509_TM	39.5	1.662	16.429	27.044	2.302	54.597	2.677	1.415	0.029	0.021	131.799	198.417
Ursula_14_061509_TM	40.5	2.249	16.227	25.126	2.328	56.797	27.053	1.402	0.024	0.018	320.774	315.444
Ursula_9_051409-TM	41.5	1.777	14.959	26.766	2.267	63.642	2.082	1.384	0.031	0.025	719.146	373.789
Ursula_11_092809	42.5	0.492	13.469	34.832	2.416	61.913	27.099	1.286	0.044	0.018	1063.203	669.265
Ursula_21_030310_TM	42.5	0.434	15.052	72.540	2.433	78.712	1.922	1.324	0.042	0.024	249.348	223.927
Ursula_10_052609_TM	43.5	1.735	16.443	37.387	2.003	52.167	5.797	1.412	0.040	0.022	198.170	139.901
Ursula_10_052609_TM	44.5	4.754	16.048	39.321	1.991	59.521	7.056	1.389	0.047	0.026	214.993	136.416
Ursula_21_030310_TM	45.5	2.484	15.316	48.365	2.213	81.870	1.315	1.322	0.050	0.032	62.074	104.407
Ursula_8_042209_TM	45.5	2.386	16.733	31.428	1.947	47.542	2.909	1.391	0.035	0.026	105.919	120.239
Ursula_21_030310_TM	45.5	0.893	15.395	46.660	2.256	76.056	1.314	1.335	0.046	0.030	56.926	100.538
Ursula_8_042209_TM	46.5	1.900	16.824	29.743	1.942	58.512	2.900	1.389	0.038	0.029	64.141	102.044
Ursula_21_030310_TM	47.5	2.151	15.162	50.843	2.014	75.743	1.297	1.322	0.042	0.029	56.432	97.292
Ursula_8_042209_TM	47.5	1.803	16.545	30.319	1.950	52.447	6.216	1.402	0.035	0.026	103.521	126.252
Ursula_21_030310_TM	47.5	1.570	15.174	49.755	2.117	76.954	1.812	1.329	0.045	0.031	141.047	147.342

run	mid depth	[Ca]	Li/Ca	B/Ca	Mg/Ca	Mn/Ca	Zn/Ca	Sr/Ca	Cd/Ca	U/Ca	Al/Ca	Fe/Ca
Ursula_8_042209_TM	48.5	1.624	16.531	31.877	1.945	49.421	1.407	1.395	0.033	0.026	77.799	125.620
Ursula_10_052609_TM	49.5	1.953	17.256	34.195	2.028	49.011	5.011	1.394	0.035	0.028	76.197	84.623
Ursula_14_061509_TM	50.5	1.922	16.129	21.705	2.270	77.257	3.675	1.394	0.038	0.034	475.824	302.240
Ursula_11_092809	51.5	0.868	16.738	26.463	2.225	62.185	15.401	1.405	0.047	0.027	135.901	148.676
Ursula_9_051409-TM	52.5	1.494	15.865	26.809	2.383	79.549	2.604	1.395	0.041	0.037	393.070	384.876
Ursula_14_061509_TM	58.5	1.234	15.463	25.509	2.234	64.309	2.855	1.398	0.029	0.028	428.646	301.245
Ursula_8_042209_TM	59.5	1.120	16.666	33.997	2.087	50.556	1.692	1.405	0.031	0.020	131.406	155.229
Ursula_9_051409-TM	60.5	2.117	16.599	25.918	2.177	63.620	2.153	1.380	0.035	0.027	168.494	209.820
Ursula_14_061509_TM	61.5	1.449	16.574	21.817	2.295	64.616	8.268	1.394	0.027	0.024	361.169	311.844
Ursula_9_051409-TM	62.5	2.817	16.715	29.223	2.229	70.229	5.452	1.394	0.031	0.025	219.922	233.307
Ursula_11_092809	63.5	2.170	16.808	31.381	2.020	65.506	1.692	1.390	0.032	0.024	45.266	87.784
Ursula_11_092809	64.5	1.521	16.248	29.427	2.118	61.821	11.566	1.396	0.045	0.021	432.068	346.463
Ursula_14_061509_TM	65.5	1.758	14.921	25.645	2.431	83.124	6.497	1.393	0.029	0.023	761.919	599.114
Ursula_21_030310_TM	65.5	0.247	16.187	50.854	2.359	89.014	2.158	1.337	0.035	0.023	774.844	604.645
Ursula_10_052609_TM	66.5	1.227	16.108	29.157	2.359	72.344	5.503	1.410	0.035	0.021	353.969	318.057
Ursula_9_051409-TM	67.5	1.829	16.572	27.258	2.147	78.150	3.135	1.397	0.039	0.025	326.496	291.119
Ursula_11_092809	68.5	1.530	16.095	30.288	2.240	65.870	20.689	1.302	0.049	0.021	226.770	182.542
Ursula_14_061509_TM	69.5	1.258	16.341	21.549	2.143	67.079	11.178	1.388	0.028	0.022	222.612	247.545
Ursula_21_030310_TM	70.5	3.693	15.112	50.390	2.198	86.824	1.347	1.332	0.049	0.023	86.299	117.325
Ursula_11_092809	70.5	1.002	16.583	25.647	2.059	69.136	6.807	1.392	0.034	0.022	156.738	189.021
Ursula_14_061509_TM	71.5	2.076	16.402	23.461	2.075	63.508	3.910	1.391	0.032	0.021	176.464	192.390
Ursula_11_092809	72.5	1.309	16.120	29.165	1.939	61.517	9.097	1.379	0.032	0.019	347.940	272.298
Ursula_8_042209_TM	73.5	3.610	17.752	31.831	2.029	60.266	1.348	1.397	0.035	0.019	187.246	189.542
Ursula_11_092809	74.5	0.985	16.478	19.262	1.990	64.642	5.464	1.395	0.029	0.018	279.277	294.177
Ursula_10_052609_TM	75.5	3.053	17.531	29.911	2.147	64.284	2.110	1.399	0.034	0.023	217.503	180.480
Ursula_9_051409-TM	76.5	2.454	17.629	27.686	2.168	74.562	4.078	1.382	0.036	0.020	25.433	20.256
Ursula_9_051409-TM	77.5	3.395	16.917	32.995	2.067	64.183	5.020	1.395	0.034	0.021	574.308	153.988

run	mid depth	[Ca]	Li/Ca	B/Ca	Mg/Ca	Mn/Ca	Zn/Ca	Sr/Ca	Cd/Ca	U/Ca	Al/Ca	Fe/Ca
Ursula_10_052609_TM	78.5	0.604	16.667	32.313	2.021	75.768	2.922	1.392	0.036	0.030	80.424	96.174
Ursula_11_092809	79.5	2.090	17.048	35.271	2.142	81.904	4.937	1.404	0.035	0.029	116.540	151.876
Ursula_11_092809	80.5	0.378	16.769	25.725	2.263	73.310	16.492	1.394	0.037	0.023	337.358	309.983
Ursula_11_092809	81.5	1.550	15.940	35.587	2.088	82.361	9.830	1.406	0.040	0.026	329.042	242.209
Ursula_11_092809	82.5	1.614	16.464	29.319	1.986	89.243	4.579	1.394	0.035	0.032	112.640	152.529
Ursula_9_051409-TM	83.5	2.290	16.062	28.631	2.077	93.199	1.827	1.378	0.040	0.033	365.312	270.439
Ursula_9_051409-TM	84.5	1.574	15.824	30.202	2.275	133.129	6.239	1.387	0.076	0.069	458.983	411.676
Ursula_9_051409-TM	85.5	1.617	16.318	29.067	1.945	83.792	3.070	1.392	0.035	0.031	128.268	191.843
Ursula_8_042209_TM	86.5	2.103	16.740	30.756	1.957	98.115	2.976	1.391	0.038	0.032	119.809	100.498
Ursula_9_051409-TM	87.5	1.452	15.659	31.348	2.117	100.634	1.671	1.385	0.037	0.033	455.766	361.268
Ursula_8_042209_TM	88.5	1.328	11.649	21.944	1.933	61.871	4.100	1.396	0.018	0.021	219.673	224.272
Ursula_9_051409-TM	89.5	1.637	16.016	24.271	2.272	92.719	1.960	1.392	0.030	0.028	615.551	497.380
Ursula_9_051409-TM	90.5	1.624	16.179	28.747	2.168	91.873	9.461	1.400	0.033	0.027	598.904	390.880
Ursula_21_030310_TM	91.5	1.617	15.866	52.319	2.213	107.729	1.637	1.313	0.040	0.032	255.384	200.722
Ursula_21_030310_TM	91.5	0.847	14.457	57.733	2.228	101.194	2.060	1.336	0.038	0.034	169.133	165.657
Ursula_8_042209_TM	91.5	0.684	15.650	32.775	4.734	80.529	24.478	1.405	0.047	0.019	711.168	383.541
Ursula_11_092809	92.5	2.072	17.243	30.207	2.132	86.699	5.520	1.388	0.036	0.027	22.496	6.370
Ursula_11_092809	93.5	0.887	15.458	30.628	2.308	87.736	10.878	1.393	0.063	0.028	366.308	270.225
Ursula_17_201009	95.5	0.615	15.969	16.028	1.991	74.748	1.393	1.383	0.033	0.026	122.264	192.189
.Ursula_18_110509	96.5	0.511	15.594	19.766	1.714	81.779	5.982	1.393	0.030	0.019	75.730	105.624
.Ursula_18_110509	97.5	0.749	16.033	24.708	1.626	80.270	5.953	1.396	0.038	0.022	172.567	149.626
.Ursula_18_110509	98.5	1.493	13.729	26.865	1.728	87.923	0.763	1.404	0.023	0.027	118.212	158.080
Ursula_15_062909_TM	99.5	0.608	15.892	25.098	2.039	91.562	3.049	1.397	0.029	0.029	524.462	287.754
Ursula_14_061509_TM	103.5	2.032	16.440	27.397	2.056	91.832	8.235	1.394	0.027	0.027	253.198	224.139
.Ursula_18_110509	104.5	0.852	17.077	31.988	2.060	78.885	32.538	1.397	0.024	0.020	498.478	230.589
Ursula_21_030310_TM	105.5	1.647	15.802	54.953	2.112	109.348	1.523	1.315	0.039	0.024	54.263	102.292
Ursula_21_030310_TM	105.5	1.098	15.810	48.632	2.176	106.598	1.394	1.328	0.040	0.024	74.311	117.443

run	mid depth	[Ca]	Li/Ca	B/Ca	Mg/Ca	Mn/Ca	Zn/Ca	Sr/Ca	Cd/Ca	U/Ca	Al/Ca	Fe/Ca
Ursula_16_101309_TM	105.5	0.114	16.644	-70.587	1.987	102.177	32.207	1.406	0.050	0.024	1166.974	83.811
Ursula_21_030310_TM	106.5	1.884	16.779	47.449	2.100	110.126	2.358	1.323	0.038	0.023	78.715	100.370
.Ursula_18_110509	106.5	0.189	16.697	20.436	2.669	104.393	14.877	1.371	0.022	0.018	1182.498	1358.682
.Ursula_18_110509	107.5	1.420	17.665	29.997	1.727	103.830	1.651	1.372	0.028	0.021	65.148	91.153
Ursula_16_101309_TM	108.5	1.527	17.199	24.921	1.898	118.225	4.661	1.405	0.037	0.027	225.071	166.086
Ursula_15_062909_TM	109.5	1.719	16.841	25.686	2.030	133.757	5.459	1.388	0.036	0.036	428.593	301.731
Ursula_21_030310_TM	110.5	1.733	15.312	48.805	2.011	146.125	1.325	1.330	0.047	0.040	352.734	115.710
Ursula_16_101309_TM	110.5	0.877	14.557	12.339	2.802	131.097	6.720	1.413	0.028	0.028	2014.314	966.444
Ursula_21_030310_TM	110.5	0.762	15.623	57.694	1.846	126.916	6.762	1.316	0.039	0.027	66.399	106.587
Ursula_14_061509_TM	111.5	1.377	16.603	24.384	1.778	97.979	3.081	1.397	0.025	0.025	96.236	149.779
Ursula_16_101309_TM	112.5	0.490	16.823	-0.014	1.871	117.984	0.606	1.407	0.025	0.022	218.737	135.581
Ursula_15_062909_TM	113.5	1.397	16.294	26.921	1.878	95.536	2.835	1.390	0.026	0.020	227.941	170.755
Ursula_16_101309_TM	114.5	0.981	16.427	26.293	2.199	119.027	0.798	1.397	0.028	0.023	179.299	220.469
.Ursula_18_110509	115.5	2.748	16.711	33.303	1.728	94.374	1.261	1.385	0.022	0.018	70.472	104.495
Ursula_16_101309_TM	116.5	0.687	17.221	29.784	2.323	118.397	1.550	1.411	0.024	0.019	123.001	189.362
.Ursula_18_110509	117.5	1.895	16.250	29.023	2.007	104.789	0.555	1.404	0.025	0.018	52.239	101.151
Ursula_14_061509_TM	121.5	2.482	16.437	27.266	1.943	110.611	4.565	1.400	0.025	0.017	87.855	92.083
Ursula_16_101309_TM	122.5	0.540	16.531	28.536	1.915	109.550	1.897	1.418	0.027	0.015	61.709	97.136
Ursula_16_101309_TM	123.5	0.693	16.201	40.387	1.818	111.220	1.913	1.391	0.021	0.014	198.098	100.856
Ursula_17_201009	124.5	0.545	16.968	15.493	2.085	112.405	0.922	1.393	0.016	0.010	190.013	297.851
.Ursula_18_110509	125.5	0.796	16.855	27.054	2.057	125.925	2.624	1.390	0.026	0.014	41.585	89.078
Ursula_16_101309_TM	126.5	0.551	15.880	12.350	2.052	110.989	0.711	1.394	0.023	0.016	120.869	119.797
.Ursula_18_110509	127.5	0.990	16.705	27.600	2.003	109.941	0.997	1.406	0.021	0.014	5455.711	214.049
Ursula_21_030310_TM	127.5	0.782	15.596	50.124	2.078	130.487	11.272	1.335	0.044	0.018	72.431	94.186
.Ursula_18_110509	128.5	1.356	17.249	32.460	1.865	123.895	1.184	1.383	0.033	0.020	26.832	72.089
Ursula_14_061509_TM	129.5	2.149	16.522	26.590	2.035	136.550	6.826	1.376	0.065	0.017	129.748	140.519
Ursula_17_201009	130.5	2.034	17.271	24.995	2.284	140.697	0.665	1.410	0.023	0.015	34.838	76.315

run	mid depth	[Ca]	Li/Ca	B/Ca	Mg/Ca	Mn/Ca	Zn/Ca	Sr/Ca	Cd/Ca	U/Ca	Al/Ca	Fe/Ca
Ursula_18_110509	131.5	0.565	15.816	21.691	2.000	104.776	12.459	1.418	0.053	0.010	218.682	298.752
.Ursula_18_110509	132.5	0.754	16.162	28.291	2.105	133.376	1.407	1.400	0.022	0.011	62.529	98.271
.Ursula_18_110509	133.5	0.450	16.214	9.714	1.922	117.784	4.786	1.406	0.028	0.010	12.467	61.976
.Ursula_18_110509	134.5	1.270	16.123	22.297	1.688	89.668	2.779	1.399	0.027	0.010	12.071	58.892
Ursula_17_201009	135.5	1.619	17.544	21.372	2.020	117.380	1.252	1.415	0.025	0.011	62.987	118.039
.Ursula_18_110509	136.5	0.455	15.842	19.435	1.582	69.058	8.527	1.411	0.023	0.008	65.973	81.590
.Ursula_18_110509	137.5	0.417	16.060	20.716	2.022	109.053	26.272	1.388	0.037	0.009	3.304	75.044
Ursula_15_062909_TM	138.5	0.884	16.150	24.319	2.194	114.677	5.392	1.400	0.029	0.011	149.921	139.893
.Ursula_18_110509	139.5	1.396	16.928	28.706	1.900	107.744	0.862	1.399	0.020	0.009	11.761	58.359
Ursula_16_101309_TM	140.5	2.223	17.587	31.745	1.919	124.088	0.731	1.386	0.026	0.010	18.155	50.433
Ursula_14_061509_TM	141.5	2.547	15.879	24.715	2.198	116.485	4.155	1.398	0.029	0.013	406.016	371.156
Ursula_16_101309_TM	142.5	1.493	17.549	35.008	2.022	117.058	2.157	1.386	0.033	0.014	20.983	92.959
.Ursula_18_110509	143.5	1.350	16.651	27.712	1.968	117.588	0.925	1.376	0.027	0.013	118.056	154.006
Ursula_16_101309_TM	144.5	1.519	17.214	26.674	2.109	133.550	1.480	1.406	0.031	0.013	72.892	89.796
Ursula_16_101309_TM	145.5	1.590	17.331	26.123	1.973	154.731	0.465	1.390	0.024	0.014	76.396	95.849
.Ursula_18_110509	146.5	2.186	16.681	29.040	2.124	128.358	1.152	1.391	0.021	0.012	91.440	115.288
Ursula_16_101309_TM	147.5	1.275	16.913	17.415	2.020	184.456	0.648	1.402	0.024	0.015	27.817	86.358
Ursula_15_062909_TM	148.5	1.398	16.624	24.806	2.019	158.362	2.685	1.401	0.027	0.014	157.822	135.424
Ursula_16_101309_TM	149.5	1.389	16.904	21.778	1.929	169.456	2.398	1.377	0.031	0.014	82.223	100.757
Ursula_15_062909_TM	150.5	0.968	16.047	25.661	2.237	153.704	2.788	1.400	0.031	0.014	645.499	650.315
Ursula_16_101309_TM	151.5	0.567	19.297	6.274	1.903	160.826	0.960	1.409	0.031	0.014	41.458	96.354
Ursula_16_101309_TM	152.5	0.771	16.615	31.550	2.273	153.010	1.989	1.394	0.024	0.011	110.114	122.111
.Ursula_18_110509	153.5	2.539	17.064	29.731	1.910	125.171	0.946	1.374	0.032	0.011	32.126	68.963
Ursula_16_101309_TM	155.5	1.175	15.962	21.562	1.941	151.441	0.582	1.403	0.023	0.011	77.716	126.663
Ursula_16_101309_TM	156.5	1.015	16.754	33.593	1.859	140.599	0.758	1.394	0.016	0.009	177.405	78.753
Ursula_14_061509_TM	158.5	3.032	17.187	27.028	1.938	154.393	1.694	1.408	0.022	0.009	7.054	46.270
Ursula_16_101309_TM	159.5	0.402	16.971	4.627	2.013	168.484	5.708	1.397	0.047	0.011	24.055	82.194

run	mid depth	[Ca]	Li/Ca	B/Ca	Mg/Ca	Mn/Ca	Zn/Ca	Sr/Ca	Cd/Ca	U/Ca	Al/Ca	Fe/Ca
Ursula_16_101309_TM	160.5	1.034	17.125	23.186	1.772	160.821	0.703	1.407	0.024	0.011	60.027	100.065
Ursula_14_061509_TM	161.5	2.237	15.491	22.726	2.242	153.579	2.599	1.401	0.029	0.010	552.798	345.638
.Ursula_18_110509	162.5	1.367	16.081	25.063	2.220	177.644	3.139	1.388	0.030	0.012	310.340	242.595
Ursula_21_030310_TM	163.5	1.777	15.420	47.291	2.136	168.995	1.385	1.323	0.042	0.014	109.198	128.316
Ursula_15_062909_TM	164.5	0.288	15.567	38.322	2.219	173.994	3.548	1.413	0.038	0.011	419.998	255.840

Appendix 4: MD99-2246 Data

run	mid depth	# bugs	[Ca]	Li/Ca	B/Ca	Mg/Ca	Mn/Ca	Zn/Ca	Sr/Ca	Cd/Ca	U/Ca	Al/Ca	Fe/Ca
E2.Ursula_41_060413	3.75	38	0.761	16.252	30.458	1.910	5.167	3.876	1.410	0.033	0.011	1678.589	386.460
E2.Ursula_41_060413	4.5	66	2.197	15.811	28.096	1.827	20.546	2.862	1.384	0.037	0.014	1107.943	351.139
E2.Ursula_42_060513	5.5	54	0.541	17.295	24.018	3.031	18.348	8.708	1.384	0.029	0.021	4550.562	1225.112
E2.Ursula_41_060413	6.5	71	2.811	15.694	27.284	1.934	22.148	2.280	1.367	0.042	0.015	970.817	419.247
E2.Ursula_41_060413	7.5	57	3.937	15.589	29.337	2.339	15.143	3.092	1.380	0.040	0.012	1631.525	499.431
E2.Ursula_41_060413	8.5	38	1.036	16.703	38.110	3.416	26.240	3.493	1.389	0.024	0.013	2489.634	522.323
E2.Ursula_42_060513	9.5	61	3.047	15.192	25.420	1.619	25.990	3.081	1.374	0.039	0.013	996.712	164.133
E2.Ursula_42_060513	10.5	46	0.577	17.046	28.023	3.389	32.011	3.282	1.384	0.036	0.023	2160.361	561.783
E2.Ursula_42_060513	11.5	50	0.928	16.109	22.290	2.171	134.628	2.993	1.352	0.048	0.016	3053.766	712.090
E2.Ursula_42_060513	12.5	64	0.674	17.202	26.937	4.127	18.371	4.575	1.358	0.033	0.015	3006.592	1312.727
E2.Ursula_41_060413	13.5	45	1.561	17.800	32.768	2.009	154.818	4.961	1.371	0.043	0.034	1474.871	618.738
E2.Ursula_41_060413	14.5	45	1.221	15.682	23.783	3.351	17.408	118.531	1.387	0.026	0.018	4116.337	1193.779
E2.Ursula_41_060413	15.5	51	3.024	16.921	29.661	2.202	26.166	26.925	1.395	0.038	0.018	1381.827	348.035
E2.Ursula_41_060413	16.5	61	1.511	17.282	27.097	2.262	25.704	1.975	1.377	0.040	0.016	1196.369	270.241
E2.Ursula_42_060513	17.5	53	0.104	17.842	24.346	4.002	38.575	7.590	1.462	0.032	0.032	52713.207	2509.810
E2.Ursula_42_060513	18.5	70	1.524	16.902	24.387	2.183	10.775	2.163	1.370	0.041	0.016	1329.651	471.597
E2.Ursula_41_060413	19.5	63	1.068	17.629	26.742	4.805	16.827	2.755	1.388	0.034	0.028	4122.207	675.695
E2.Ursula_42_060513	20.5	53	0.185	14.814	27.901	8.292	76.630	6.284	1.374	0.022	0.015	13716.418	5363.262
E2.Ursula_42_060513	21.5	59	1.255	16.437	19.169	4.291	#VALUE!	#VALUE!	1.382	0.031	0.016	2597.155	1087.283
E2.Ursula_42_060513	22.5	31	0.411	17.414	32.428	2.505	20.027	4.682	1.396	0.039	0.022	13539.469	911.123
E2.Ursula_42_060513	23.5	55	1.163	16.960	24.243	3.570	20.329	4.080	1.377	0.026	0.016	4787.367	1773.089
E2.Ursula_42_060513	24.5	57	0.840	17.286	24.643	2.429	41.437	4.016	1.345	0.042	0.019	3598.839	657.278
E2.Ursula_42_060513	25.5	45	0.966	17.785	26.888	4.595	45.472	3.798	1.366	0.031	0.019	2957.213	877.298
E2.Ursula_42_060513	26.5	40	0.680	18.431	32.587	3.316	22.723	4.256	1.392	0.034	0.065	4326.396	902.002
E2.Ursula_42_060513	27.5	46	0.918	18.213	25.176	3.046	22.897	3.433	1.383	0.032	0.015	3134.068	1073.089
E2.Ursula_42_060513	28.5	36	1.063	16.913	30.774	2.024	9.923	3.592	1.382	0.039	0.012	1324.608	295.777

run	mid depth	# bugs	[Ca]	Li/Ca	B/Ca	Mg/Ca	Mn/Ca	Zn/Ca	Sr/Ca	Cd/Ca	U/Ca	Al/Ca	Fe/Ca
E2.Ursula_42_060513	29.5	37	0.163	27.448	10.566	4.551	70.289	11.052	1.394	0.031	0.016	4969.984	2693.679
E2.Ursula_41_060413	30.5	38	1.905	17.504	24.054	2.250	14.524	2.159	1.380	0.033	0.012	847.710	484.195
E2.Ursula_41_060413	31.5	41	1.700	17.911	29.899	2.641	#VALUE!	#VALUE!	1.381	0.032	0.015	2885.553	784.429
E2.Ursula_41_060413	32.5	26	0.143	20.840	49.082	5.611	95.002	11.380	1.381	0.030	0.284	16543.274	3592.001
E2.Ursula_41_060413	33.5	39	0.345	20.712	58.552	2.306	45.142	5.230	1.415	0.028	0.037	3730.183	810.207
E2.Ursula_41_060413	34.5	40	0.590	17.826	26.521	2.392	15.046	3.093	1.400	0.032	0.014	3270.245	346.215
E2.Kari_00_062112	35.5	42	0.342	33.252	279.827	17.701	143.874	-2.179	-0.002	0.730	0.075	13548.919	6203.732
E2.Ursula_41_060413	36.5	37	1.052	18.723	24.489	2.577	22.864	3.343	1.389	0.025	0.013	5043.148	892.005
E2.Kari_00_062112	37.5	44	1.111	17.287	21.470	2.560	47.232	4.121	1.404	0.027	0.019	3022.206	898.337
E2.Ursula_41_060413	38.5	53	2.336	17.468	27.936	1.952	26.943	7.060	1.388	0.041	0.013	527.179	203.225
E2.Ursula_42_060513	39.5	41	0.946	16.796	27.621	3.668	33.847	2.369	1.399	0.029	0.012	2896.732	435.495
E2.Ursula_41_060413	40.5	50	1.599	16.715	35.693	2.762	34.295	2.384	1.390	0.030	0.014	1834.712	499.408
E2.Ursula_41_060413	41.5	42	1.975	25.878	25.190	2.592	64.743	4.176	1.395	0.035	0.012	2561.452	878.020
E2.Kari_00_062112	43.5	44	1.212	18.004	21.415	3.278	44.095	4.376	1.397	0.031	0.015	2735.195	1271.256
E2.Ursula_41_060413	43.5	40	1.480	17.404	31.536	3.222	48.013	2.643	1.404	0.031	0.014	717.487	381.778
E2.Ursula_42_060513	44.5	39	1.209	18.505	25.657	2.718	60.594	9.114	1.399	0.038	0.013	1652.282	541.519
E2.Ursula_41_060413	45.5	40	1.938	17.232	35.565	2.733	27.418	12.400	1.385	0.030	0.021	2350.269	446.679
E2.Ursula_42_060513	46.5	50	1.017	17.661	30.998	2.257	132.613	3.441	1.388	0.030	0.018	2527.337	606.648
E2.Ursula_42_060513	47.5	61	2.851	16.819	24.066	3.721	54.986	3.807	1.400	0.032	0.014	1551.697	828.969
E2.Ursula_42_060513	48.5	47	1.405	17.481	33.358	4.852	83.855	3.810	1.395	0.030	0.016	916.932	526.963
E2.Ursula_41_060413	49.5	48	3.202	17.088	30.417	2.324	42.083	2.748	1.389	0.030	0.013	2995.959	530.798
E2_Ursula_39_082712	50.5	54	0.526	18.220	119.958	13.454	84.650	9.480	1.390	0.035	0.023	10503.547	5382.319
E2_Ursula_39_082712	51.5	56	1.150	17.639	69.574	5.676	83.935	6.444	1.369	0.031	0.013	5395.720	1758.578
E2_Ursula_39_082712	53.5	61	0.121	23.884	258.270	3.308	151.595	13.849	1.360	0.037	0.081	5750.627	2537.910
E2_Ursula_39_082712	54.5	55	0.567	16.764	78.771	1.921	94.431	6.715	1.409	0.033	0.027	589.786	238.535
E2_Ursula_39_082712	55.5	54	1.051	18.434	35.854	3.725	71.306	4.232	1.376	0.032	0.012	3597.391	678.472
E2_Ursula_39_082712	57.5	66	1.298	16.994	31.865	2.915	84.498	2.665	1.421	0.031	0.016	1368.991	320.141

run	mid depth	# bugs	[Ca]	Li/Ca	B/Ca	Mg/Ca	Mn/Ca	Zn/Ca	Sr/Ca	Cd/Ca	U/Ca	Al/Ca	Fe/Ca
E2_Ursula_39_082712	58.5	71	0.446	16.795	27.718	2.502	55.893	4.539	1.415	0.031	0.014	1818.400	393.890
E2_Ursula_39_082712	58.5	71	0.317	20.487	47.892	2.618	71.846	5.240	1.441	0.022	0.017	2557.889	1785.100
E2_Ursula_39_082712	59.5	52	1.090	17.104	26.678	2.425	83.704	3.162	1.375	0.031	0.018	2746.784	653.737
E2_Ursula_39_082712	59.5	52	1.686	16.800	30.498	2.976	68.051	4.494	1.390	0.035	0.013	1278.830	417.481
E2_Ursula_37_071812	60.5	56	0.158	16.822	-10.837	2.205	67.967	4.799	1.412	0.022	0.015	1753.676	692.236
E2.Ursula_40_090412	61.5	60	1.276	17.596	-10.287	2.814	74.660	2.416	1.371	0.024	0.013	1981.205	547.708
E2.Ursula_38_071912	62.5	58	0.675	16.213	22.900	3.084	56.290	3.771	1.398	0.020	0.018	5901.089	1463.078
E2_Ursula_39_082712	63.5	50	0.542	18.007	37.735	1.993	120.281	2.696	1.407	0.139	0.022	864.884	340.910
E2.Ursula_38_071912	64.5	60	0.188	17.682	24.399	4.296	126.925	6.345	1.487	0.020	0.018	12597.715	2461.696
E2.Ursula_38_071912	65.5	32	0.390	17.181	24.701	2.406	68.812	3.089	1.397	0.023	0.014	4026.790	617.647
E2.Ursula_38_071912	66.5	94	0.918	17.958	28.263	3.583	85.155	5.158	1.437	0.028	0.066	4490.237	2279.957
E2.Ursula_38_071912	66.5	94	0.594	18.518	30.759	4.149	64.297	4.866	1.398	0.027	0.015	1869.999	554.295
E2.Ursula_40_090412	67.5	72	1.622	18.750	13.016	2.198	64.591	2.616	1.405	0.024	0.019	2237.286	775.467
E2.Ursula_40_090412	68.5	59	1.630	17.006	25.065	3.263	80.538	5.341	1.369	0.063	0.081	1239.098	475.484
E2.Ursula_40_090412	69.5	59	0.584	19.618	12.410	2.896	78.073	4.778	1.394	0.025	0.017	4871.259	1418.171
E2_Ursula_39_082712	70.5	68	1.155	18.082	122.743	3.784	103.625	2.751	1.382	0.033	0.013	1338.016	804.879
E2.Ursula_38_071912	71.5	60	0.654	18.152	20.934	2.481	142.315	6.255	1.400	0.034	0.010	2910.355	840.365
E2.Ursula_40_090412	72.5	49	0.756	17.515	29.316	2.059	91.300	3.134	1.405	0.025	0.019	1122.705	571.219
E2.Ursula_40_090412	73.5	62	1.131	18.485	-12.721	2.857	86.233	2.977	1.380	0.032	0.013	2169.689	539.644
E2.Ursula_40_090412	73.5	65	1.270	18.506	21.998	2.918	#VALUE!	#VALUE!	1.418	0.030	0.015	4067.218	1044.512
E2.Ursula_40_090412	74.5	70	2.984	16.907	25.114	2.276	#VALUE!	#VALUE!	1.385	0.031	0.021	840.330	416.269
E2.Ursula_40_090412	75.5	87	1.049	18.594	-5.166	2.059	143.323	3.321	1.402	0.282	0.014	1653.656	454.105
E2.Ursula_40_090412	76.5	81	2.360	16.769	26.745	2.057	159.692	22.812	1.379	0.054	0.020	524.813	137.371
E2.Ursula_40_090412	77.5	69	1.953	16.089	23.947	2.161	152.290	1.832	1.400	0.044	0.023	712.123	384.196
E2.Kari_00_062112	79.5	52	1.136	16.000	22.306	3.944	117.083	2.413	1.436	0.027	0.039	3446.164	875.749
E2.Ursula_40_090412	80.5	63	1.958	18.811	15.087	2.713	139.661	5.550	1.397	0.037	0.021	1499.568	637.974
E2.Ursula_40_090412	83.5	70	3.558	17.878	22.104	1.926	129.579	2.294	1.382	0.044	0.033	974.810	131.156

run	mid depth	# bugs	[Ca]	Li/Ca	B/Ca	Mg/Ca	Mn/Ca	Zn/Ca	Sr/Ca	Cd/Ca	U/Ca	Al/Ca	Fe/Ca
E2.Ursula_40_090412	84.5	66	3.219	18.409	19.188	2.124	117.321	3.312	1.388	0.040	0.038	1345.424	513.428
E2.Ursula_40_090412	85.5	80	3.469	17.431	16.263	1.904	108.458	1.488	1.373	0.046	0.025	551.489	189.863
E2.Ursula_40_090412	86.5	65	1.080	18.314	3.034	1.864	104.310	5.729	1.381	0.049	0.025	1689.250	195.380
E2.Ursula_40_090412	87.5	61	1.422	18.670	6.613	2.228	#VALUE!	#VALUE!	1.363	0.043	0.027	1551.865	456.150
E2.Ursula_40_090412	88.5	62	3.222	18.668	13.265	2.355	110.528	3.534	1.371	0.035	0.028	1234.078	767.745
E2.Ursula_40_090412	89.5	57	1.940	18.570	6.230	2.858	96.076	2.957	1.373	0.037	0.023	978.275	539.827
E2.Ursula_40_090412	91.5	61	1.150	18.407	3.445	2.024	122.925	4.345	1.388	0.036	0.023	2550.859	729.102
E2_Ursula_39_082712	92.5	65	0.699	16.995	30.155	2.095	99.791	4.409	1.387	0.029	0.014	2682.754	540.022
E2_Ursula_39_082712	92.5	65	0.793	17.465	33.568	1.750	114.756	3.937	1.381	0.168	0.022	817.176	263.443
E2_Ursula_37_071812	93.5	33	3.940	17.460	24.583	1.627	137.776	1.726	1.393	0.044	0.021	678.018	151.213
E2_Ursula_37_071812	94.5	44	0.447	18.539	-16.221	1.919	153.373	2.027	1.394	0.043	0.030	505.569	204.823
E2_Ursula_37_071812	95.5	43	0.238	22.516	6.415	4.434	145.548	10.654	1.472	0.042	0.041	18835.878	3267.190
E2.Ursula_40_090412	96.5	71	2.293	16.499	21.667	1.812	108.728	2.586	1.419	0.042	0.026	808.080	127.774
E2_Ursula_37_071812	98.5	67	0.733	20.781	9.989	1.738	128.982	1.381	1.398	0.041	0.038	338.638	186.763
E2_Ursula_37_071812	98.5	67	0.225	17.028	-20.226	1.199	114.660	3.264	1.431	0.042	0.036	109.675	49.548
E2_Ursula_37_071812	99.5	61	0.662	18.778	24.519	1.825	160.353	1.729	1.385	0.049	0.049	2946.581	123.618
E2_Ursula_37_071812	99.5	61	1.501	18.488	19.684	2.102	160.942	1.641	1.409	0.061	0.050	1997.255	189.789
E2_Ursula_39_082712	100.5	87	1.059	17.444	33.823	1.963	165.473	1.518	1.446	0.074	0.096	682.355	299.371
E2_Ursula_39_082712	100.5	87	0.909	18.391	41.568	2.001	173.581	1.712	1.471	0.079	0.119	1725.313	239.400
E2_Ursula_39_082712	101.5	60	1.176	18.480	36.202	2.551	215.986	4.540	1.401	0.075	0.072	1336.291	231.773
E2_Ursula_37_071812	103.5	30	0.351	18.715	6.928	1.747	161.267	5.507	1.414	0.070	0.048	933.045	118.107
E2_Ursula_37_071812	105.5	24	0.274	17.424	12.777	2.050	136.565	3.287	1.453	0.032	0.026	484.615	321.203
E2.Kari_00_062112	112.5	42	1.464	16.929	24.084	2.001	177.881	2.573	1.399	0.027	0.023	2840.955	544.367
E2_Ursula_39_082712	113.5	48	1.237	16.273	129.034	1.977	252.540	23.450	1.398	0.048	0.043	2666.363	195.305
E2_Ursula_39_082712	115.5	29	2.235	17.943	25.638	2.687	316.630	3.265	1.373	0.041	0.042	1132.581	472.661

sample	species	mid depth	d13C PDB	d13C PDB st. dev.	d18O PDB	d18O PDB st. dev
MD99-2246	*G. bulloides*	3.75	-0.26	0.008	2.01	0.016
MD99-2246	*G. bulloides*	4.5	-0.21	0.010	2.02	0.025
MD99-2246	*G. bulloides*	6.5	0.02	0.029	1.69	0.028
MD99-2246	*G. bulloides*	8.5	-0.15	0.009	2.02	0.023
MD99-2246	*G. bulloides*	9.5	0.02	0.013	2.23	0.019
MD99-2246	*G. bulloides*	10.5	-0.02	0.012	2.19	0.025
MD99-2246	*G. bulloides*	11.5	-0.28	0.010	2.27	0.015
MD99-2246	*G. bulloides*	12.5	-0.08	0.009	2.11	0.022
MD99-2246	*G. bulloides*	13.5	-0.08	0.014	2.15	0.024
MD99-2246	*G. bulloides*	14.5	0.00	0.016	2.13	0.036
MD99-2246	*G. bulloides*	15.5	-0.14	0.011	2.08	0.027
MD99-2246	*G. bulloides*	16.5	0.09	0.043	1.81	0.054
MD99-2246	*G. bulloides*	17.5	-0.39	0.024	1.77	0.039
MD99-2246	*G. bulloides*	18.5	-0.06	0.019	1.91	0.028
MD99-2246	*G. bulloides*	19.5	-0.25	0.014	1.81	0.029
MD99-2246	*G. bulloides*	20.5	-0.27	0.011	2.11	0.015
MD99-2246	*G. bulloides*	21.5	-0.26	0.006	1.90	0.029
MD99-2246	*G. bulloides*	22.5	-0.26	0.012	1.85	0.021
MD99-2246	*G. bulloides*	23.5	-0.24	0.017	1.99	0.029
MD99-2246	*G. bulloides*	24.5	0.02	0.008	1.99	0.028
MD99-2246	*G. bulloides*	25.5	-0.29	0.009	2.09	0.023
MD99-2246	*G. bulloides*	26.5	0.01	0.010	1.99	0.021
MD99-2246	*G. bulloides*	27.5	-0.29	0.009	1.87	0.020
MD99-2246	*G. bulloides*	28.5	-0.23	0.016	2.07	0.025
MD99-2246	*G. bulloides*	29.5	-0.05	0.007	1.93	0.015
MD99-2246	*G. bulloides*	30.5	0.14	0.016	1.74	0.030
MD99-2246	*G. bulloides*	31.5	-0.36	0.009	2.05	0.031
MD99-2246	*G. bulloides*	32.5	-0.20	0.013	1.89	0.025
MD99-2246	*G. bulloides*	33.5	-0.39	0.010	2.09	0.030
MD99-2246	*G. bulloides*	34.5	-0.29	0.007	1.91	0.022

MD99-2246	*G. bulloides*	35.5	-0.14	0.018	2.05	0.014
sample	*species*	mid depth	d13C PDB	d13C PDB st. dev.	d18O PDB	d18O PDB st. dev
MD99-2246	*G. bulloides*	36.5	-0.59	0.011	1.99	0.044
MD99-2246	*G. bulloides*	37.5	-0.27	0.011	2.07	0.032
MD99-2246	*G. bulloides*	38.5	-0.21	0.030	1.59	0.063
MD99-2246	*G. bulloides*	40.5	-0.11	0.015	1.92	0.023
MD99-2246	*G. bulloides*	41.5	-0.12	0.014	2.10	0.035
MD99-2246	*G. bulloides*	42.5	0.13	0.014	2.25	0.026
MD99-2246	*G. bulloides*	43.5	-0.17	0.015	2.06	0.023
MD99-2246	*G. bulloides*	44.5	-0.10	0.012	1.80	0.023
MD99-2246	*G. bulloides*	45.5	-0.28	0.014	1.94	0.040
MD99-2246	*G. bulloides*	46.5	-0.32	0.010	1.86	0.021
MD99-2246	*G. bulloides*	47.5	-0.22	0.016	2.05	0.019
MD99-2246	*G. bulloides*	48.5	-0.18	0.017	1.83	0.025
MD99-2246	*G. bulloides*	49.5	-0.23	0.011	1.91	0.024
MD99-2246	*G. bulloides*	50.5	-0.24	0.015	1.94	0.023
MD99-2246	*G. bulloides*	51.5	-0.26	0.009	2.07	0.024
MD99-2259	*G. bulloides*	52.5	-0.05	0.008	1.97	0.022
MD99-2246	*G. bulloides*	54.5	-0.66	0.013	2.08	0.023
MD99-2246	*G. bulloides*	55.5	0.04	0.009	1.95	0.016
MD99-2246	*G. bulloides*	56.5	-0.09	0.023	1.44	0.054
MD99-2246	*G. bulloides*	57.5	-0.20	0.026	1.79	0.034
MD99-2246	*G. bulloides*	58.5	-0.06	0.015	1.73	0.020
MD99-2246	*G. bulloides*	59.5	-0.43	0.027	1.97	0.046
MD99-2246	*G. bulloides*	61.5	-0.25	0.014	2.01	0.030
MD99-2246	*G. bulloides*	62.5	-0.51	0.016	2.13	0.028
MD99-2246	*G. bulloides*	63.5	-0.27	0.019	2.01	0.024
MD99-2246	*G. bulloides*	64.5	-0.35	0.012	2.20	0.032
MD99-2246	*G. bulloides*	65.5	-0.02	0.018	2.20	0.019
MD99-2246	*G. bulloides*	66.5	-0.27	0.013	1.56	0.028
MD99-2246	*G. bulloides*	67.5	-0.01	0.007	1.96	0.027
MD99-2246	*G. bulloides*	68.5	-0.16	0.011	1.86	0.029

MD99-2246	*G. bulloides*	69.5	-0.33	0.010	1.97	0.027
sample	*species*	mid depth	d13C PDB	d13C PDB st. dev.	d18O PDB	d18O PDB st. dev
MD99-2246	*G. bulloides*	71.5	-0.46	0.022	2.07	0.036
MD99-2246	*G. bulloides*	72.5	-0.30	0.010	2.11	0.020
MD99-2246	*G. bulloides*	73.5	-0.45	0.018	1.88	0.051
MD99-2246	*G. bulloides*	74.5	-0.38	0.009	2.11	0.035
MD99-2246	*G. bulloides*	75.5	-0.45	0.019	1.75	0.041
MD99-2246	*G. bulloides*	76.5	-0.18	0.019	2.07	0.009
MD99-2246	*G. bulloides*	77.5	-0.12	0.014	1.88	0.021
MD99-2246	*G. bulloides*	79.5	-0.37	0.023	1.91	0.032
MD99-2246	*G. bulloides*	80.5	0.02	0.007	1.96	0.018
MD99-2246	*G. bulloides*	83.5	-0.01	0.014	2.12	0.019
MD99-2246	*G. bulloides*	84.5	-0.22	0.013	1.80	0.038
MD99-2246	*G. bulloides*	85.5	-0.66	0.010	1.89	0.035
MD99-2246	*G. bulloides*	86.5	-0.09	0.011	1.93	0.012
MD99-2246	*G. bulloides*	87.5	-0.25	0.011	2.01	0.022
MD99-2246	*G. bulloides*	88.5	-0.20	0.015	2.22	0.032
MD99-2246	*G. bulloides*	89.5	-0.36	0.016	2.12	0.020
MD99-2246	*G. bulloides*	91.5	-0.13	0.014	2.07	0.019
MD99-2246	*G. bulloides*	92.5	-0.20	0.014	2.03	0.028
MD99-2246	*G. bulloides*	93.5	-0.40	0.063	1.65	0.073
MD99-2246	*G. bulloides*	94.5	-0.38	0.015	2.10	0.015
MD99-2246	*G. bulloides*	95.5	-0.43	0.008	1.63	0.021
MD99-2246	*G. bulloides*	98.5	-0.17	0.006	1.99	0.023
MD99-2246	*G. bulloides*	99.5	-0.13	0.012	2.00	0.023
MD99-2246	*G. bulloides*	100.5	-0.53	0.015	1.76	0.036
MD99-2246	*G. bulloides*	101.5	-0.29	0.014	1.93	0.029
MD99-2246	*G. bulloides*	103.5	-0.46	0.035	1.75	0.025
MD99-2246	*G. bulloides*	106.5	-0.84	0.046	1.95	0.054
MD99-2246	*G. bulloides*	108.5	-1.35	0.025	1.26	0.058
MD99-2246	*G. bulloides*	110.5	-0.78	0.023	1.65	0.054
MD99-2246	*G. bulloides*	112.5	-0.50	0.022	2.22	0.023
MD99-2246	*G. bulloides*	113.5	-0.55	0.006	2.14	0.038